Grid Method Studies of the Geometrical Uncertainties in Free Form and Micro Processes

A thesis submitted to the

Cardiff University

for the degree of

Doctor of Philosophy

by

Ekaterin Minev

Cardiff School of Engineering

Cardiff University

United Kingdom

February 2012

ABSTRACT

This research is devoted to the engineering of a generic, reliable and cost-effective method for the investigation of accuracy in layer based fabrication technologies. It begins with a review of the causes of deviations and uncertainties in component parts, analyses of the existing approaches for accuracy investigation and their limitations and disadvantages.

The main focus of the research is the development of an original and convenient methodology capable of defining the dimensional uncertainties and accuracy of the technologies and the distribution of dimensional errors within the entire build area. The Grid Methodology is based on the discretisation of the object to allow the measurement, calculation, visualisation and analysis of part distortion in terms of linear and shear deviations from nominal. A single test piece and routine measurement procedure are utilised to estimate the distribution of the above entities; calculated in a similar way to the geometrical characteristics of strains in solid mechanics.

The methodology was applied to research the causes of inaccuracy in the vertical direction of SLS Polystyrene. The presence of a critical dimension in height from where the distortion changes from shrinkage to extension was revealed and explained. The methodology was also utilised to estimate the necessary scaling factors to improve part accuracy, based on the calculated distortions. Implementation of the Grid Method to Micro Projection Stereolithography resulted in the ability to describe and estimate curling distortion in terms of angular deviations from nominal and separate it from linear distortions.

Furthermore the application of the GM to the emerging micro-nano manufacturing sector has been shown to support the assessment of process capability. This provides a means of calculating process tolerances using results obtained from the single test piece. Investigation of the accuracy capabilities of three micro-processes was performed and their compatibility for designing process chains presented.

ACKNOWLEDGEMENTS

I would like to express my thanks to my supervisor Dr. Samuel Bigot for his support and supervision.

To the students John Heaven, Mickael, Quentin, Serkan, Isold, Dmitri, Gisay, Francois for the software support and experiments as well as for their inspiration.

To Paul Prickett for his voluble suggestions during manuscript preparation.

Special thanks to Dr. Krastimir Popov for the help, support and encouragement.

My deepest gratitude to Dr. Rusi Minev for his help and guidance, otherwise the thesis would never have been produced.

DECLARATION

This work has not previously been accepted in substance for any degree and is not being concurrently submitted in candidature for any degree.

Signed ……(Ekaterin Minev, candidate) Date……

STATEMENT 1

This thesis is being submitted in partial fulfilment of the requirements for the degree of PhD.

Signed ……(Ekaterin Minev, candidate) Date……

STATEMENT 2

This thesis is the result of my own independent work/investigation, except where otherwise stated. Other sources are acknowledged by explicit references.

Signed ……(Ekaterin Minev, candidate) Date……

STATEMENT 3

I hereby give consent for my thesis, if accepted, to be available for photocopying and for interlibrary loan, and for the title and summary to be made available outside organisations.

Signed ……(Ekaterin Minev, candidate) Date……

TABLE OF CONTENTS

ABSTRACT.....i

ACKNOWLEDGMENTS.....iii

DECLARATION.....iv

TABLE OF CONTENTS.....v

LIST OF TABLES.....ix

LIST OF FIGURES.....x

ABBREVIATIONS.....xv

NOMENCLATURE.....xviii

CHAPTER 1: INTRODUCTION 1

1.1 Motivation.....1

1.2 Aims and objectives of the research.....3

1.3 Outline of the thesis.....5

CHAPTER 2: A REVIEW OF ACCURACY PROBLEMS IN THE FREE-FORM (FF) FABRICATION 8

2.1 Sources of uncertainties in the FF manufacturing methods.....9

2.1.1 Errors caused by laser scanning system.....11

2.1.2 Errors caused by material shrinkage.....14

2.1.2.1 Photopolymerisation.....14

2.1.2.2 Temperature variations.....17

2.1.2.3 Phase transformation.....20

2.1.2.4 Curling.....24

2.1.3 Errors caused by laser beam spot size and Heat Affected Zone ……....32

2.1.4 CAD, tessellations and slicing errors.....41

2.1.5 Random errors.....49

2.2 Summary and conclusions.....52

CHAPTER 3: METHODS AND TEST PARTS FOR ACCURACY STUDY AND CALIBRATION OF THE RAPID PROTOTYPING TECHNIQUES 55

3.1 General approach and considerations.....56

3.2 Test parts for accuracy study – overview and classification.....61

3.2.1 Pyramids.....61

3.2.2 Specially designed test parts (benchmark test pieces).....65

3.2.3 Real part model.....71

3.2.4 Parts for surface quality investigation and mechanical testing.....73

3.3 Analysis of the disadvantages of the pyramids for shrinkage, scaling and accuracy determination.....75

3.4 Summary and conclusions.....84

CHAPTER 4: GRID METHOD AS A TECHNIQUE FOR INVESTIGATION OF THE DEVIATIONS IN SHAPE AND DIMENSION 88

4.1 Basic definitions of strains, linear and angular deviations from nominal.....89

4.2 The concept of the Grid Method for calculations of linear and angular deviations from nominal.....94

4.3 Methodology for Grid Method implementation in the study of the RP process...98

4.4 Test plate geometry considerations.....101

4.5 Non-process related errors.....103

4.6 Accuracy analyses and statistical validation of the plate measurement method106

4.7 Summary and conclusions.....111

CHAPTER 5: GRID METHOD ANALYSES AND MODELLING OF THE GEOMETRICAL DISTORTIONS IN SLS PROCESSES 113

5.1 Overview of Selective Laser Sintering of Polystyrene powder.....114

5.2 Analyses of the geometrical variations caused by the physical processes in SLS Castform.....117

5.2.1 Experimental set up.....118

5.2.2 Results and discussions.....120

5.3 Implementation of the GM calibration in the SLS RP practice and modelling of the distortions.....127

5.4 Implementation of the GM for studying other RP materials and processes.....137

5.4.1 SLS Polyamide (PA).....137

5.4.2 Process monitoring of the Multi-Jet modelling system (3D Systems 'ThermoJet') for investment casting wax atterns.....139

5.5 Conclusions.....140

CHAPTER 6: COMPARATIVE STUDIES OF MICRO PROCESSES AND CHAINS ACCURACY 142

6.1 Technological chains and the importance of the accuracy compatibility.....142

6.2 Micro-Stereolithography accuracy study by Grid Method.....143

6.2.1 Experimental set up and methodology.....145

6.2.2 Results from the Grid Method for accuracy study of micro-Stereolithography process.....148

6.3 Implementation of the Grid Method for accuracy analysis of micro milling 157

6.4 Conclusions.....161

CHAPTER 7: HOW TO USE GM DATA TO EVALUATE PROCESS CAPABILITIES? 163

7.1 Grid Method for capability studies of MNT.....163

7.2 Capability study of MNT processes.....170

7.3 Conclusions.....179

CHAPTER 8: CONTRIBUTIONS, CONCLUSIONS AND FURTHER WORK 180

Contributions.....180

Conclusions.....181

Further work.....184

APPENDIXES 186

Appendix 1 Program code for automatic CMM measurement control.....186

Appendix 2 Results for scaling calculations of SLS Castform.....194

REFERENCES 201

List of Tables

Table 3.1	Authors and parameters investigated for SLS	58
Table 3.2	Summary of geometric features and their purposes for benchmarking (Mahesh M., 2005)	67
Table 4.1	Illustrative example about similarity in values between true and engineering strains	91
Table 4.2	Statistical results for strain calculations	108
Table 6.1	Standard deviations and mean values of linear and angular deviations for μSLA process	156
Table 6.2	Accuracy and precision of: μSLA; Micro Milling; Micro milling + EDM	162
Table 7.1	Complementarity / Compatibility evaluation and „process spread" (μm) for a typical feature size (100μm)	176
Table 7.2	Recommended process tolerances for nominal dimensions L=10-500μm	179
Table 7.3	Calculated component tolerances corresponding to the expected quality standards	180

List of Figures

Figure 2.1 A typical SLS machine layout 11

Figure 2.2 Two galvano-mirrors laser scanning system 12

Figure 2.3 Focal plane obtained through f-θ lens 13

Figure 2.4 Barrel-shaped distortions due to laser scanning system 13

Figure 2.5 Vinyl-type monomer-polymer transformation (top) and cross-linked monomer-polymer transformation (bottom) 15

Figure 2.6 Scheme of photo polymerisation 16

Figure 2.7 Temperature distribution in the part bed 18

Figure 2.8 Change in specific volume due to phase transformation 22

Figure 2.9 Steps in curling formation in SLA 25

Figure 2.10 Curling developing in SLS process 25

Figure 2.11 Free shrinkage of a layer (left) and forces and bending moments when shrinkage is restricted due to the bond between layers (right) 27

Figure 2.12 Circular curl model 28

Figure 2.13 Measured profiles of the bottom surfaces of SLS polycarbonate blocks with thickness of 1, 2, 10, 20 and 50 layers 29

Figure 2.14 Curling, warping and associated deformation of an element from inside the part. 30

Figure 2.15 A scheme of the laser beam raster pattern during the scanning 33

Figure 2.16 Interaction of the laser irradiation and powder bed 35

Figure 2.17 Laser beam energy distribution 36

Figure 2.18 a) - Pyramid for beam offset calibration; b) - interpolation of the measurements and beam size determination by extrapolation of the line 37

Figure 2.19 Insetting the contour of a solid part according to the beam size and shape. 38

Figure 2.20 Comparison of the three offset methods 39

Figure 2.21 Potential beam compensation problems and their correction via structural scan paths 40

Figure 2.22 Faceted representation of a sphere 42

Figure 2.23 Pro/ENGINEER dialog box for .STL file tolerances setting 43

Figure 2.24 Stair-step effect as inaccuracy source due to the thickness of the build layers 44

Figure 2.25 Identical (a) and selective (b) approaches in adaptive layering 45

Figure 2.26 Reduced staircase effect by utilising adaptive layer slicing and variable nozzle diameter in FDM process 45

Figure 2.27 Simplifying the shape and sacrificing of small features 46

Figure 2.28 Reducing the accuracy after CAD modelling, STL tessellation and slicing in the cases of fine (a) and rough (b) tessellation 47

Figure 2.29 Steps and errors due to CAD, CAM, tessellation and slicing processes 48

Figure 2.30 Cause and effect diagram for accuracy of a part in the case of rapid tooling FF application 52

Figure 3.1 Common pyramids shapes 62

Figure 3.2 Modified pyramid test parts and their arrangement for investigations 65

Figure 3.3 Benchmark part for investigation of SLS/SLM processes 66

Figure 3.4 Examples of specifically designed benchmark parts 68

Figure 3.5 Possible causes of problems that can be investigated by benchmark test piece 69

Figure 3.6 Examples of real part used as a benchmark piece in RP 72

Figure 3.7 Examples of test parts for surface roughness and morphology study 74

Figure 3.8 Lengths and directions for measurements of pyramid shape test part 77

Figure 3.9 Illustrative picture for possible error distribution 79

Figure 3.10 Type of measurement and corresponding result for distortion. (i) - total lengths to the step; (ii) -change of the step length (delta) 82

Figure 4.1 Shear strain illustration 92

Figure 4.2 Plain strain involving small distortions (Mielnik E. M., 1991) 93

Figure 4.3 Square grid: a) - before processing and b) - after processing 95

Figure 4.4 Examples of plate orientation in the build platform for investigation of dimensional deviations from nominal in different directions 97

Figure 4.5 Picture of plate measuring process 99

Figure 4.6 Screen shot of the Mitotoyo QuickVision *Pro* software window 100

Figure 4.7 Method of averaging the coordinates of the problematic holes 104

Figure 4.8 Process flowchart for the GM methodology 105

Figure 4.9 Plate for statistical validation of measurements 108

Figure 5.1 a) Casting tree with infiltrated Castform pattern; b) final metal casting 115

Figure 5.2 Plate orientations for vertical accuracy investigation 119

Figure 5.3 3D visualisation of εz (vertical size deviations from nominal) distribution in the (*x, z*) plane produced by GM 121

Figure 5.4 Distribution of εz -vertical deviation of the sizes from nominal 122

Figure 5.5 Schematic distribution of εz in vertical direction and specific contributions to it 123

Figure 5.6 Scanning electron image of SLS Castform sintered layers 126

Figure 5.7 Layer thicknesses of SLS Castform depending on their *z* position 126

Figure 5.8 Picture of the plate for scaling verification 129

Figure 5.9 εz distribution in calibration plate 130

Figure 5.10 Scaling factor calculated by the average of Sc for the corresponding *z* 131

Figure 5.11 3D εz distribution in plate built without scaling 133

Figure 5.12 3D εz distribution in plate build with scaling 133

Figure 5.13 Side view of εz distribution surface in plate build without scaling 134

Figure 5.14 Side view of εz distribution in plate build with scaling 134

Figure 5.15 Four scenarios of accuracy and precession of a process 136

Figure 5.16 **a)** Distribution of horizontal deviations (εx) 138

Figure 5.15 **b)** distribution of vertical deviations (εz) in polyamide SLS plate 139

Figure 5.17 Distribution of εz in faulty Thermojet build"s volume 140

Figure 6.1 Neuro-medical insert produced in acrylic resin with PM-μSLA showing the curling effect 145

Figure 6.2 Plate orientation for μSLA accuracy experiment 147

Figure 6.3 Graph of hole diameter against plate thickness for acrylic based photo resins (Perfactory R11 material) 148

Figure 6.4 Test plate after the build completion on EnvisionTec Perfactory platform 149

Figure 6.5 Surface of εz distribution over the test plate 151

Figure 6.6 Surface showing the distribution of γ over the test plate 152

Figure 6.7 Distribution of shear strains (described as deviations from nominal) γ in *z* direction along different columns 152

Figure 6.8 Mean values and spread of γ represented by its Std+ and Std- along each line over the test plate from Figure 6.4 155

Figure 6.9 Distribution of vertical strains εz alongside a column in the middle of the plate 158

Figure 6.10 A punch produced by micro milling process 159

Figure 6.11 A die manufactured by micro drilling and micro wire EDM processes 160

Figure 6.12 Distribution of εy. Left – pins (punch tool) from Figure 6.10; Right-hols (die tool) from Figure 6.11 161

Figure 7.1 Specification limits and natural tolerances 167

Figure 7.2 Defining the process capability 168

Figure 7.3 Graphical representations of process precision and accuracy 169

Figure 7.4 Comparison of the process capabilities of two processes 170

Figure 7.5 Tolerance limits for the PM-μSLA 173

Figure 7.6 Tolerance limits for the μ-Milling process 174

Figure 7.7 Tolerance limits for the μ-Milling + μ-EDM process chain 174

Figure 7.8 Process spread of the investigated MNTs for determination of recommended tolerances 178

Abbreviations

BS – Beam speed

CAD – Computer Aided Design

CAM – Computer-aided manufacturing

CMM - Coordinate measuring machine

CNC Computer Numerical Control

Db – Laser beam diameter

DMD - Digital micro-mirror device

EDM - Electric Discharge Machining

FDM - Fused Deposition Modelling

FEA - Finite Element Analysis

FF - Free-form Fabrication

FIB - Focus Ion Beam

FLSI - Functional and Length Scale Integration

GM – Grid Method

HAZ – Heat Affected Zone

IC – Investment Casting

LNTL - Lower Natural Tolerance Limit

LP – Laser power

LSL - Lower Specification Limit

LSp – Laser scan speed

μEDM - Micro Electric Discharge Machining

μSLA - Micro Stereolithography

MEC – Manufacturing Engineering Centre

MNT - Micro/Nano Technology

MSA - Measurement System Analysis

NC – Numerical Control

PA - Polyamide

PDS - Product Design Specification

PM-μSLA - Projection Mask Micro-Stereolithography

PS - Polystyrene

RP - Rapid Prototyping

RP & M - Rapid Prototyping & Manufacturing

SCSP – Scan spacing

SEM - Scanning Electron Microscopy

SLA – Stereolithography

SLM – Selective Laser Melting

SLS – Selective Laser Sintering

SME - Small and Medium Enterprise

STL - Stereolithography File Format

Tb – Part bed temperature

Tg – Glass transition temperature

Tm – Melting temperature

Tp – Part piston temperature

UNTL - Upper Natural Tolerance Limit

USL - Upper Specification Limit

YAG - Yttrium Aluminium Garnet laser

Nomenclature

ε_E	[-]	engineering strain
C_f	[-]	curl factor
C_{pk}	[-]	process capability index
dl	[m]	change in length
dT	[K]	change in temperature
E	[m]	error
E	[Mpa]	Young's modulus
l	[m]	lenght
Lf	[m]	actual lenght
Ln	[m]	nominal lenght
LNTL		Lower Natural Tolerance Limit
S	[-]	linear shrinkage
Sc	[-]	scaling factor
S_{cz}	[-]	scaling factor in z
S_v	[-]	volumetric shrinkage
T_0	[K]	initial temperature
T_f	[K]	final temperature
T_g	[K]	glass transition temperature
T_m	[K]	melting temperature
UNTL		Upper Natural Tolerance Limit
$W_{1,2}$	[-]	weight factors
ΔT	[K]	change of temperature
α	[1/K]	linear coefficient of thermal expansion
ε	[-]	true strain

ε_T	[-]	thermal strains
ε_x	[-]	linear deviation in size from nominal per unit length in *x* = linear strain in x
ε_y	[-]	linear deviation in size from nominal per unit length in *y* = linear strain in y
ε_z	[-]	linear deviation in size from nominal per unit length in *z* = linear strain in z
γ	[rad]	angular deviation from nominal = shear strain
γ_x	[rad]	angular deviation from nominal in x= x shear strain
γ_y	[rad]	angular deviation from nominal in y= y shear strain
γ_z	[rad]	angular deviation from nominal in z= z shear strain
μ		mean value
σ		standard deviation
σ	[Mpa]	stress

CHAPTER 1 INTRODUCTION

1.1 Motivation

11 years ago a commercial project to produce a 1200 mm tall polystyrene pattern for investment metal casting by Selective Laser Sintering was assigned to our research centre. At that time Rapid Prototyping (RP) was a novel but less mature technology than it is today. Our knowledge and understanding of the accuracy issues of the process was also somewhat limited. Nevertheless the proposal was accepted, analysed, successfully completed and documented. The achievement was a major breakthrough for understanding the capabilities of the technology. Unfortunately, it was later found that upon casting, the metal components produced from the pattern were not to the correct specification. Although the total height was within tolerance, the sizes and distances between some important features along the length of the part were far from sufficiently accurate. It became clear that the distribution of the distortions inside the part was not uniform and that further examination of this distortion was required; as a result appropriate corrections and corresponding non-linear scaling would have to be applied. Furthermore the root causes of geometrical errors within the process had to be determined and investigated. From this process specification limits (tolerances) have to be defined and considered as well.

These were the initial stimuli to conduct the presented research.

After the research was completed the reasons for the inaccuracies mentioned above became clearer (Chapter 4), but this was not so at the time of producing the patterns. Many commonly used approaches for investigating accuracy (Section 2.2) were applied to reduce deviations from the nominal dimensions and yet the large components were rarely produced to the required tolerances. The limitations of the existing practice was analysed and the need to research and develop a new, holistic approach and a respective methodology for RP accuracy investigation emerged. During its development the methodology was progressively applied to various RP manufacturing processes, where significant improvements were achieved, as well as being successfully adopted to the Micro/Nano Technology (MNT) research area (including applications of micro mechanical milling, micro Stereolithography and Focus Ion Beam milling processes).

The experiments which were conducted using the newly developed methodology were analysed and validated in a research capacity, with a view for commercial approval and use. Apart from some of the practical aspects of this research, such as accuracy evaluation and process calibration, it was very important to study the causes of the process uncertainties as well as to evaluate the process capabilities in terms of determining feasible tolerance limits. It also became evident that expansion of the research to study the compatibility and complementarity of the processes within specific process chains (involving layer based technologies and MNTs) was possible. These particular aspects of the presented research were successfully implemented by the author in the EC FP7 Collaborative Project and Coordination and Support Action EUMINAfab (Integrating European Research Infrastructures for

Micro-nano Fabrication of Functional Structures and Devices out of a Knowledge-based Multi-materials' Repertoire).

1.2 Aims and objectives of the research

The presented research is focussed on the following general aims and objectives:

- Overview and *critical analysis of methodologies* for accuracy investigation in layering technologies. The study will look at the applicability and reliability of existing methods to: reflect and measure the part distortions and reveal their nature; estimate the geometrical uncertainties and their distributions; define the process deviations in different plains and directions. The ultimate outcome of this overview is to summarise the disadvantages of existing accuracy investigation practices and to motivate and *validate the necessity* of a new methodology that overcomes the present limitations.

- *Development and validation of an alternative methodology* suitable for studying the uncertainties and capabilities of various layering and other technologies. The methodology should provide a more generic approach in the research of the above characteristics and particularly investigate the *distribution* of process errors along any direction within the entire operational volume.

- *Study of SLS process* phenomena that affect the distortions of components, particularly in the critical vertical direction. The aim of this aspect of the research is to analyse the factors and their influence on process uncertainties and investigate the possible measures to reduce them. Improved knowledge of the process capabilities and limitations is to be gathered and concluded by analysing the results obtained by means of the new methodological approach for process study. *Implementation* of the developed methodology for *calibration of the platforms and accuracy improvement* of the SLS processes will be enabled.

- *Investigation of accuracy capabilities of various MNT processes* in terms of their compatibility and complementarities when designing process chains that enable production of complex MNT products encompassing functional and length scale integration features. Revealing and defining the process specification limits and related parts dimensional tolerances that can be achieved by specific advanced manufacturing processes as deployed in the micro-fabrication and micro-tooling domain.

1.3 Outline of the thesis

The thesis consists of 8 chapters inclusive of this chapter.

Chapter 2 describes the main sources of uncertainties regarding Freeform Fabrication processes, which are subsequently referred to in order to explain the observed part distortions phenomena. Measures for compensations to overcome deviations in sizes from the nominal are also reviewed.

Chapter 3 considers how the deviation in the sizes and shapes of components are investigated in the current practice. The chapter's literature review contains classification and analysis of the advantages and disadvantages of different types of test parts that are commonly used. Particular attention is focused on pyramid test parts, as these are the most popular and universally implemented. A critical approach is applied to reveal and motivate why a different methodology for accuracy investigation was essential. The conclusion that existing practices do not give correct distribution of uncertainties can be considered as a contribution to the studied area.

The Grid Methodology developed in this study with the aim of improving the reliability of the investigations to analyse the deviations in the shape and dimensions of components from the nominal, is described in Chapter 4. The developed methodology is claimed as one of the contributions of this research, being a new generic and more suitable approach that can be implemented for thorough process accuracy investigation.

The results and analysis of accuracy investigation in the Selective Laser Sintering process using the Grid Method – one of the main objectives and contributions of the research - are presented in Chapter 5. The specific vertical-direction build phenomena, which were revealed by the study, are discussed and explained in the chapter. On this basis the implementation of the developed methodology for the calibration of platforms and improving the accuracy of the process is also illustrated.

Chapter 6 deals with accuracy investigation and analysis of micro processes. The prominent curling phenomenon in Micro Stereolithography process is studied and the finding that the curling is best revealed, described and quantitatively measured by calculating the shear (angular) deviations considered. This is a contribution to the study of the process shrinkage phenomenon. The research is further extended to the micro milling plus micro electric discharge machining (μEDM) process chain. This constitutes the background research for the proposed process capabilities studies in the next chapter.

Chapter 7 proposes how the results obtained from the Grid Method for accuracy investigation (strains and their deviations) could be utilised for a process capability study. On the basis of the calculated results for strain values, the compatibility and complementarity of the processes in a process chain is assessed. The main outcome of this chapter is that the presented analysis provides a possible answer to the current difficulty associated with the comparison and selection of micro processes for compatible utilisation.

Chapter 8 presents summaries and contributions to the knowledge that are concluded in the presented research. It also looks at future work which could be conducted on 3D process accuracy modelling; comparison and investigations of the behaviour of different materials for free form fabrication; shape and size classification of the components based on the process ability by layering technologies.

CHAPTER 2 A REVIEW OF ACCURACY PROBLEMS IN THE FREE-FORM FABRICATION

As one of the main objectives of this study was to develop a generic method for accuracy investigation, it was essential to review the possible sources of uncertainties and their influences on the studied part characteristics. On that basis, when the methodology developed in this study was applied to evaluate RP and other advanced manufacturing and micro/nano technological (MNT) processes, some important practical conclusions about possible process improvements could be made. Analysis of the obtained results could be focussed on the determination of process capability with respect to part accuracy.

Many varieties of Free-form Fabrication (FF) processes have been introduced since the first rapid prototyping (RP) techniques became available in the late 1980s. Today some processes are fully established and proven, whilst some are in the early stages of implementation and others are still in the development phase.

The practical applications of RP processes are determined mainly by their technical capabilities and economical considerations. These can be summarised as follows (Masood and Soo 2002):

- Price of the RP machine and equipment;
- Range or type of build materials available;
- Maximum dimensions of the part building envelope;
- Dimensional accuracy and their consistency in the *x*, *y* and *z* directions;

- Surface finish of the built part;
- Speed of part building;
- Production cost of the part as a complex assessment of time, material, labour, success rate, etc.

In all cases the selection of FF process and the specific RP platform requires rigorous investigation especially with regard to part accuracy, repeatability and quality.

The dimensional and shape accuracy requirements in addition to part functionality play an important role in the creation of product design specifications (PDS), process control and the monitoring and planning of process chains. In the case of RP the final accuracy of the part is a function of many factors such as: the geometry of the part in question, the CAD model and slicing method, the build method, post processing methods and part finishing.

2.1 Sources of uncertainties in the Free-form Fabrication manufacturing methods

Although dozens of parameters contribute to the final accuracy, not all of them have equal effects in all RP process routes. For instance in Selective Laser Sintering (SLS) processes the laser system, especially the laser scanning system, will be one of the main sources of error formation from a hardware point of view (Tang et al. 2004). In addition to this the thermal nature of the process leads to

shrinkage, distortion and warping of the part; all of these phenomenon contribute to significant errors in the built parts. Therefore it is especially important to perform an accuracy analysis that systematically reveals the type of errors, their sources and magnitudes, so that improvements in the production practice can be implemented.

Diverse classifications about sources of errors in the RP domain exist. Some authors (Hopkinson and Sercombe 2008) consider build position and build height as error sources. However, although the dimensions of parts built in different bed positions differ considerably, the position itself is not a source of error; the reason for the error is usually temperature variations in the build chamber. A possible general classification of error sources common for most popular FF processes comprises the following (Tang et al. 2004):

- *Errors caused by laser scanning system*
- *Errors caused by material shrinkage*
- *Errors caused by laser beam spot size and heat effected zone (HAZ)*
- *Errors caused by Computer Aided Design (CAD), tessellation and slicing*
- *Random errors*

The above sources of errors are discussed in separate sections below mainly in regards to the two RP technologies - Selective Laser Sintering and Micro Stereolithography (μSLA). The accuracy of these processes was the subject of investigation in the presented research and the revealed uncertainties were

subsequently analysed (Chapters 5 and 6) by utilising the Grid Method (GM) developed in this research (Chapter 4).

2.1.1 Errors caused by laser scanning system

The nature of these errors may be illustrated in the case of Selective Laser Sintering RP processes. The laser sintering process builds a part by using a laser beam that scans and sinters powder material layer by layer. Figure 2.1 shows a schematic layout of an SLS system.

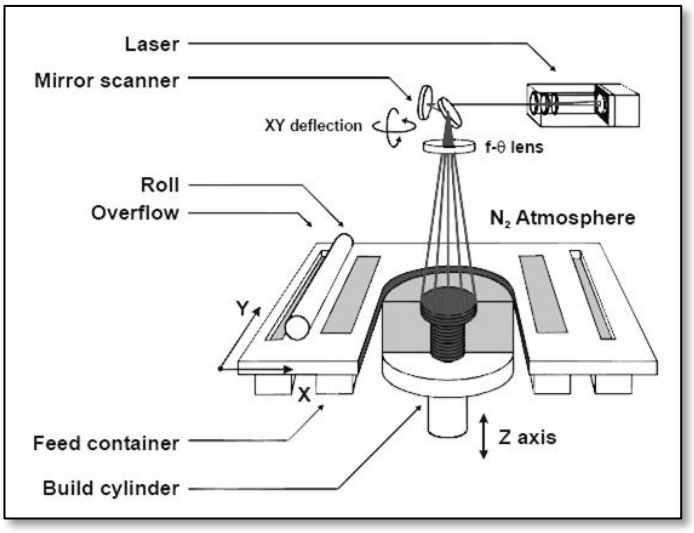

Figure 2.1 A typical SLS machine layout (Kruth et al. 2004)

Commercial SLS machines vary in many ways, for example: in the way the powder is deposited - by using roller (3D Systems DTM) or scraper recoat (EOS); by utilising different protective atmospheres (Ar or N_2) and by various types of laser (CO_2 laser, lamp or diode pumped Nd: YAG laser, disk or fibre

laser) (Kruth et al. 2004, 2003) . The scanning laser path is generated by reflecting a laser beam through two rotating galvano-mirrors in the X and Y directions. The configuration and mechanism of the two galvano-mirrors laser scanning system is shown in Figure 2.2.

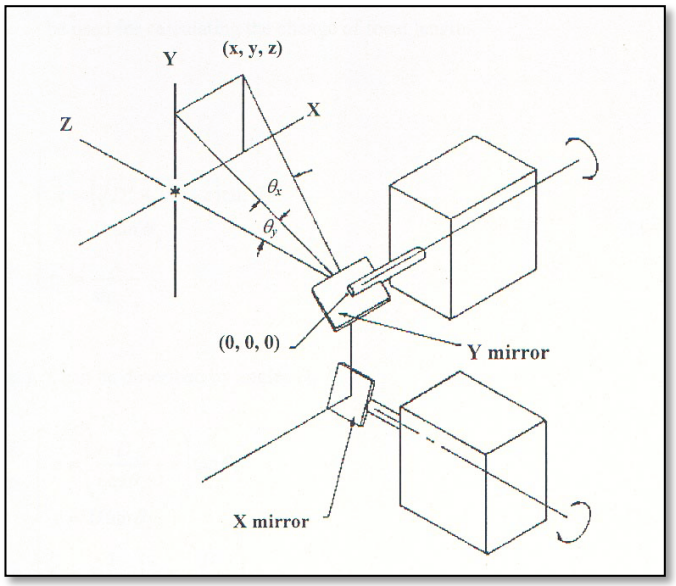

Figure 2.2 Two galvano-mirrors laser scanning system (Tang et al. 2004)

The rotating motion system of the two galvano-mirrors affects the accuracy laser scan path. The laser scanning spot movement realised by the two galvano-mirrors can be described by angles θ_x and θ_y (Shakeri et al. 2007). The focus distance f changes with variation in θ values. In order to get the laser beam focused on a horizontal plane, which represents the working surface (part bed), an f-θ lens is used. The f-θ lens has a special optical design, which allows the different parts of lens to have different focus distances according to the entry angle of the laser beam. This allows the laser beam spot to be focused on a plane as the mirror is rotated, albeit with a slight error. The role of the f-θ lens is shown in Figure 2.3.

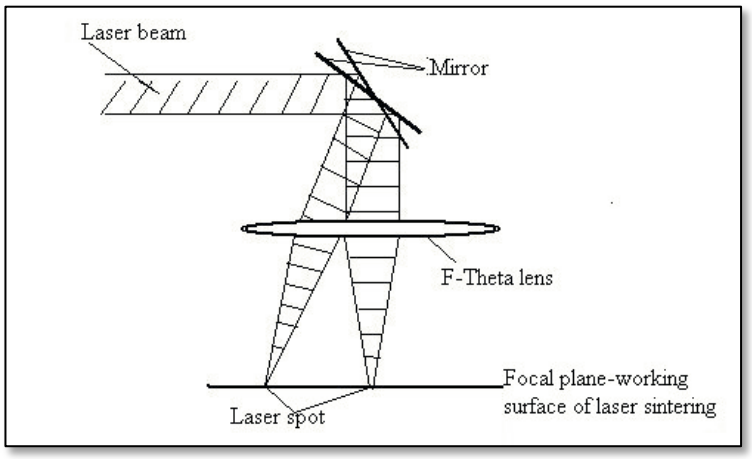

Figure 2.3 Focal plane obtained through f-θ lens (Tang et al. 2004)

The rotating motion of the two mirrors and the f-θ objective cause barrel-shaped distortions of the image field as shown in Figure 2.4.

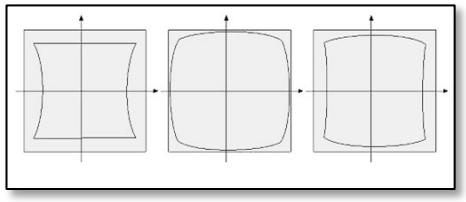

Figure 2.4 Barrel-shaped distortions due to laser scanning system (Tang et al. 2004)

This distortion will affect the shape and accuracy of built parts and correction and calibration are needed to eliminate this effect. Some additional distortions are caused by the mirror and lens due to their fabrication and configuration. Furthermore the inaccuracy of mechanical movement and inertia effects of moving parts can contribute to the total overall error.

These types of errors could be corrected and compensated at the platform design phase as well as during machine maintenance. Additional corrections by application CAM software or build preparation are possible although limited.

2.1.2 Errors caused by material shrinkage

Many RP processes are unavoidably subject to material shrinkage. The main reasons for shrinkage are *polymerisation (photopolymerisation)*, *temperature* changes during and after processing and *phase* transformations. Specific to layer based technology is a combined phenomenon caused by temperature shrinkage and residual stresses in the layers known as *curling*. These four factors are separately described in the following sub-sections in respect to their nature, influence on part accuracy and countermeasures that could be implemented to reduce their contribution to part geometry uncertainties.

2.1.2.1 Photopolymerisation

In the stereolithography (SLA) process the reaction that transforms liquid resin to solid is photopolymerisation. The polymerisation chemical reaction of a monomer allows each carbon atom in the carbon-carbon double bond to form a new bond, typically with a carbon atom from another monomer molecule. In the process the molecules undergo a transformation from loose Van der Waals interaction with neighbouring monomers to a network of covalent bonds, thus many bulk properties of the resin material change. The average distance between

groups decreases, resulting in an increase in density leading to shrinkage. Polymerisation of multifunctional monomers results in a cross-linked polymer with even higher density. Additionally, polymerisation of some materials, such as acrylate based resins undergoes an exothermal reaction associated further with increases in temperature. Cooling after process completion causes additional shrinkage. Theoretical analysis of polymerisation was given in (Jacobs 1992). Schematically the polymerisation of a vinyl-type monomer is illustrated on Figure 2.5.

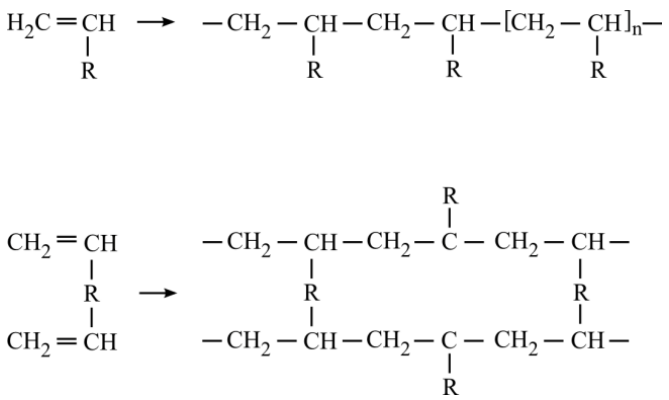

Figure 2.5 Vinyl-type monomer-polymer transformation (top) and cross-linked monomer-polymer transformation (bottom) (Jacobs 1992)

The photopolymerisation is a reaction where resins solidify by exposure to some electromagnetic radiation such as γ-rays; x-rays; UV light; visible light; e-beams. The UV-curable polymers, commonly used in RP consist of: reactive monomers; photo-initiators; fillers and/or modifiers. During photopolymerisation the photo-initiator absorbs some photons and transforms into its excited state P•, after undergoing several complex steps. These molecules then react with a monomer to form polymerisation, initiating molecules PM•, which later react and form longer

molecules PMMMM•. The process continues until a chain inhibition process terminates the polymerisation reaction. Schematicaly photopolymerisation is shown in the Figure 2.6.

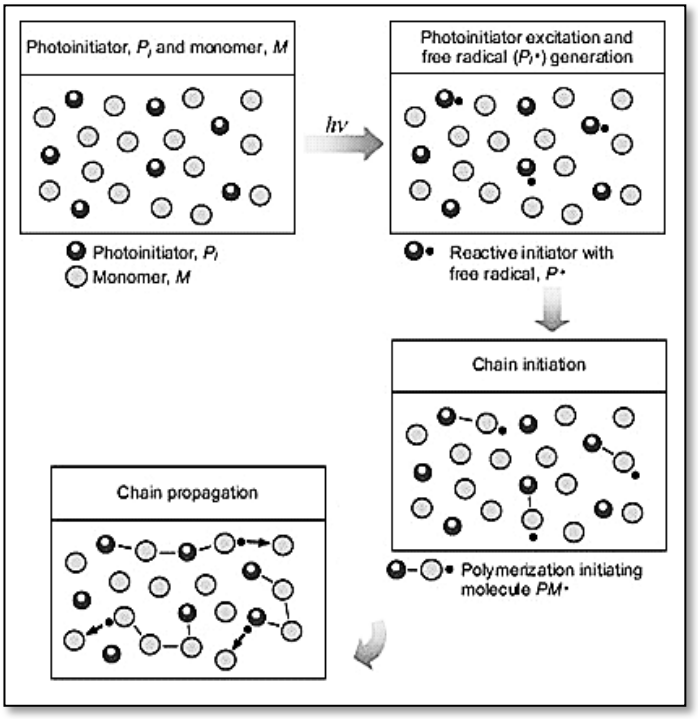

Figure 2.6 Scheme of photo polymerisation (Chua et al. 2010)

Polymerisation and more particularly photo-polymerisation is one of the main reasons for material shrinkage and curling and it has a significant influence on part accuracy in SLA processes. Chapter 6 of this thesis explores the uncertainties and curling phenomenon in the μSLA process domain due to photo-polymerisation; on the basis of the developed Grid Method, which is new for the RP domain. Specific attention was given to the assessment of the geometrical characteristics and their distribution that best described the magnitude and type of part distortions revealed by the proposed method.

2.1.2.2 Temperature variations

Most FF fabrication methods are accompanied with temperature change and some are thermally activated. In SLS significant changes in temperatures are intentionally induced during and after the building process. The desired temperatures are controlled and kept within a certain range depending on the material used. Process complexity can lead to non-uniform heating which together with differences in the mechanical and insulating systems in specific platform areas could lead to considerable temperature variations within the building chamber. Careful control of the thermal environment is critical to prevent undesirable growth of the part after sintering by the laser. Additionally, during the cooling process, thermal gradients in the part must be minimised to avoid geometric distortions resulting from thermally induced residual stresses (Diller et al. 2012).

The temperature control system works within certain tolerances and due to process speed requirements, not all variations and changes in temperature can be eliminated. As a consequence part shrinkage is uneven and difficult to predict. Measurements of temperature variations within the build volume chamber (Shen et al. 2000) and (Manetsberger et al. 2001) are shown in Figure 2.7.

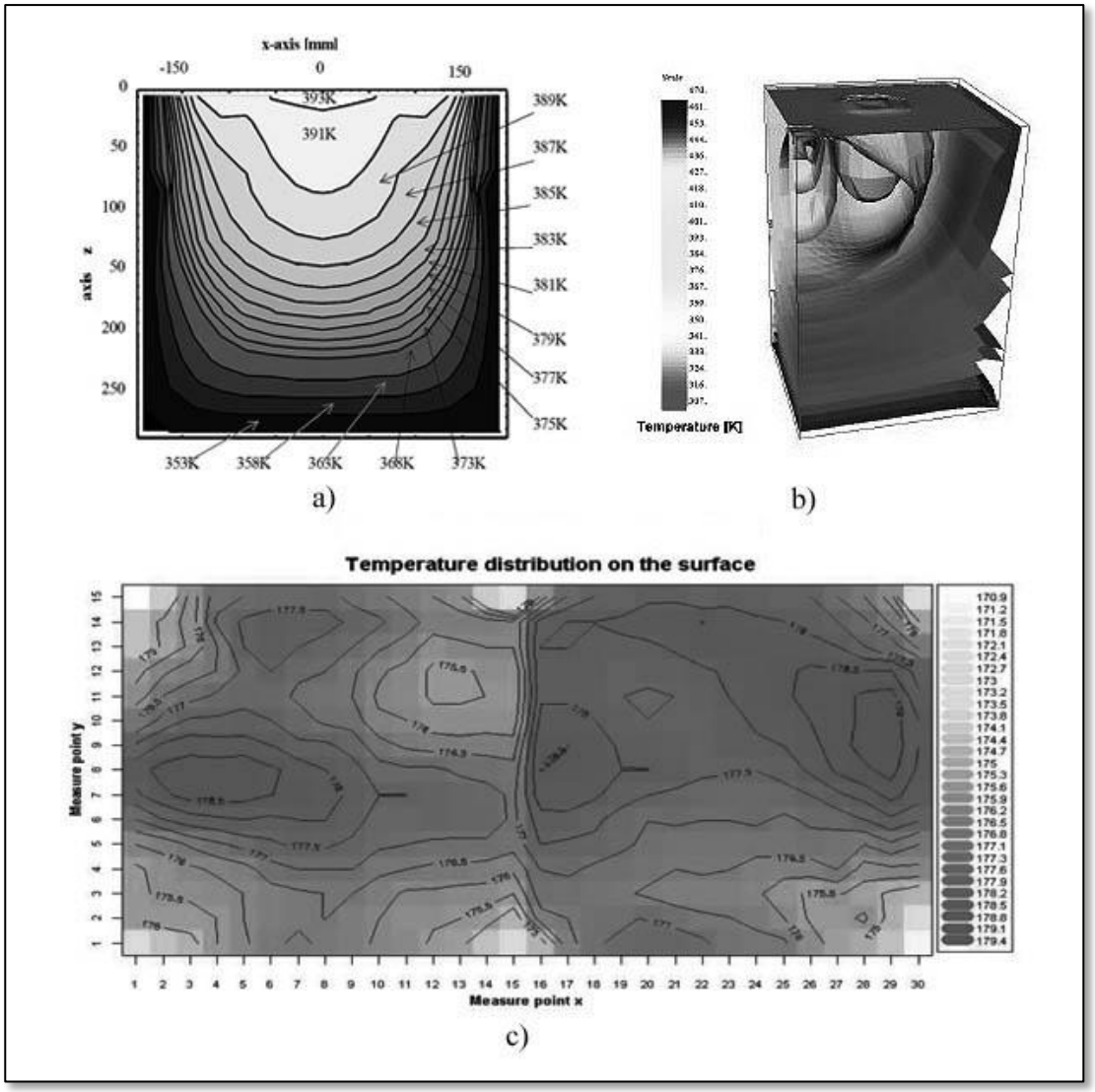

Figure 2.7 Temperature distribution in the part bed a) by (Shen et al. 2000), b) by (Manetsberger et al. 2001) c) courtesy of Dr. Shwe Soe, Cardiff School of Engineering

It can be seen that the differences in temperature in the vertical direction are from 150K to 40K depending on the sintered material and platform. The temperature gradients would influence the length of time for which the various sections of the part remain at high temperature. This leads to differences in the shrinkage caused by the pressure from the material above.

The temperature variation over the part bed in the horizontal plane is also highly important. The temperature isolines presented on Figure 2.7 show more than 35K difference. This temperature difference would dramatically influence the thermal shrinkage of sintered parts or different sections of them, in regard to their position in the part bed. A study in the RP laboratory at Cardiff School of Engineering conducted by Dr. Soe analysing non-uniform temperature distributions along the top of the part bed, using an EOS P700 Laser Sintering machine, showed that the differences in temperatures are 10K (Figure 2.7 c), which can lead to considerable variations in thermal shrinkage on parts. A recent study (Diller et al. 2012) based on the computer modelling of a build chamber temperature distribution shows similar variations of about 12K. Earlier studies (Childs and Tontowi 2001; Tontowi and Childs 2001) indicated experimentally and by simulation that a 4% decrease in density can be expected when the temperature is decreased by 4K. In the same research it was found that uncertainties in sizes of approximately 0.5% can be expected with a 4K temperature change. On that basis the authors concluded that a machine design target with temperature consistency of 4K could be established. Other research (Hopkinson and Sercombe 2008; Sercombe and Hopkinson 2006) also shows that in the case of indirect SLS of aluminium, the dimensions vary in the range of 1% depending on build position. The non-uniform temperature distribution in the part-bed, which is generally hotter in the centre than the edge was deemed the root cause for this variance.

A common approach in RP practice is the application of an appropriate scaling to the part geometry that can compensate for the shrinkage of parts produced by FF

fabrication due to the temperature variations. This compensation can be applied using the CAD software or the machine CAM software.

The important consideration in the scaling procedure is the quantitative knowledge about distortions and most importantly their distribution and nature. The methods that are used to collect and analyse the data for uncertainties in the current practice are not always effective and accurate enough. The reasons for this are clarified in Section 3.3 of this thesis. The thesis is later focused on developing a methodology for accuracy assessment that gives a comprehensive valuation of the distribution of distortions. As a result of such research it will be shown that the part size, part shape and orientation as well as horizontal and vertical position of the parts in the building chamber must be taken in consideration for effective part scaling.

2.1.2.3 Phase transformation

When the material temperature is altered sufficiently, phase transformations can occur. Distinctively, a material may be transformed from a liquid to a solid, or in some cases from a solid to a liquid and then back to a solid again. Within the field of Rapid Prototyping & Manufacturing (RP&M) phase change phenomena specifically occur in the following processes:

- Stereolithography (SLA),
- Selective Laser Sintering (SLS) and Selective Laser Melting (SLM),
- Fused Deposition Modelling (FDM),

- Thermal Phase Change Inkjets (ThermoJet, Pattern Master),
- Rapid Investment Casting.

Such transformations are accompanied by changes in physical and chemical properties of the material (Callister 2010, William and Hashemi 2009, Edwards and Endean 1995). From an accuracy viewpoint the important issue is the change in volume due to the phase transformation that manifest as shrinkage when the part is cooled down. Volumetric shrinkage S_v, and linear shrinkage S are related in the case of isotropic shrinkage, by the expression (Jacobs 2000):

$$S = 1 - (1 - S_v)^{1/3} \quad (2.1)$$

or by the more common relationship:

$$S \approx {S_v}/{3} \quad (2.1\text{ a})$$

The phase transformation involves a change in the specific volume and the resulting shrinkage. The total volumetric shrinkage varies from process-to-process, and from material-to-material, for a given process (Jacobs 2000).

The critical temperatures for polymeric materials to change phase are melting temperature (Tm) and glass transition temperature (Tg). The typical behaviour of volume changes in polymers when the Tg and Tm have been exceeded is schematically illustrated in Figure 2.8.

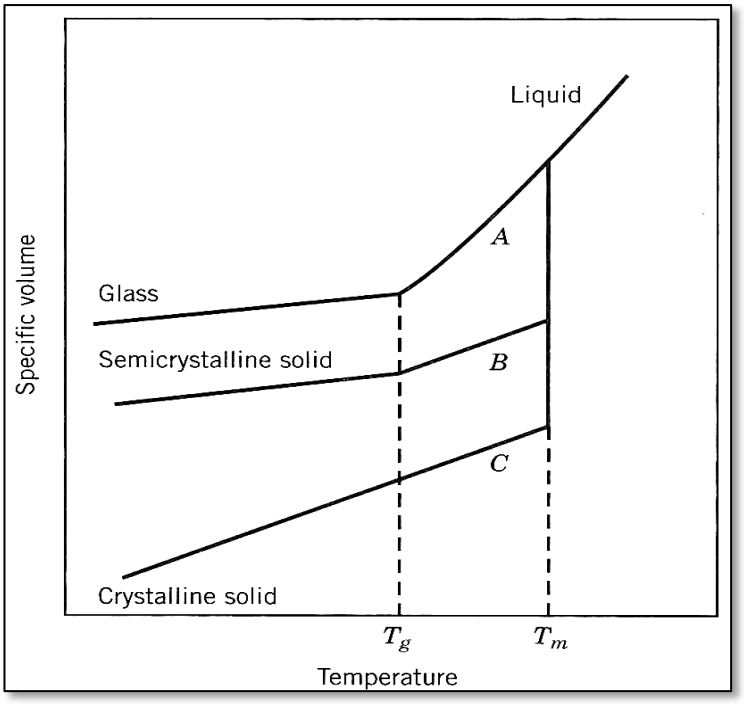

Figure 2.8 Change in specific volume due to phase transformation (Callister 2010)

In SLS processes amorphous, crystalline and semicrystalline materials can be used. The powder changes from solid phase to liquid phase and then back to solid phase in a three-dimensional unsteady heat transfer process. These phase change processes are accompanied by both the absorption and release of thermal energy. A moving boundary exists that separates the phases; at this boundary some thermal energy is either absorbed or liberated. The superheat in the melting powder and the latent heat liberated at the solid/liquid boundary are transferred across the solidified RP part and across the boundaries. In some cases, the powder is partly solid and partly liquid and resembles a porous medium.

Tg and Tm are also important factors for determining part bed temperature and laser power. Above Tg the amorphous phase has a “rubbery” character. As the powder becomes sticky at such temperatures, which leads to aggravated layering

and material growth on the part surface. The part bed temperature must not exceed Tg for amorphous polymers. On the other hand to reduce the temperature differences between the sintering and after-sintering period, the part bed temperature must be close to Tg (Gibson and Shi 1997). In all cases the temperature of sintered material (after the laser beam power has been applied) exceeds Tg and hence the material undergoes phase transformation during the cooling down stage. For similar reasons, the part bed temperature should be set a few degrees below its melting temperature Tm for semi-crystalline polymers and again subsequently phase transformation will occur when cooling the melted polymer.

In the case of sintering semicrystalline material, the part bed temperature should be set close to Tg. The Tg for a semicrystalline mixture can be calculated by the following formula (Tobolsky 1967):

$$\frac{1}{T_g} = \frac{W_1}{T_g'} + \frac{W_2}{T_g''} \qquad (2.2)$$

where,

W_1 and W_2 are the weight fractions of each component in the mixture,

T_g' and T_g'' are glass transition temperatures of each component in the mixture.

The common practice for shrinkage compensation due to phase transformation is scaling the CAD model in similar way as for the temperature shrinkage. The limited consolidation obtained with amorphous systems results in relatively low shrinkage (typically about 1%), but the relatively high laser powers which are used to make the parts can cause considerable growth. Crystalline or

semicrystalline materials exhibit high shrinkage (typically 3-4%) associated with both the material phase change and the high degree of consolidation obtained during processing, but the amount of growth is usually limited by the relatively low laser powers which are required to completely melt the material (Nelson et al. 1995(a)).

2.1.2.4 Curling

Curl distortion or *curling* can occur in all RP processes that build parts by fabrication of successive layers where the solidifying material undergoes shrinkage. Curling is one of the major sources of error even in the processes which are otherwise considered accurate. For instance Micro Stereolithography (μSLA) technologies can operate with layer thickness and voxel resolution of less than 25μm. On that basis such manufacturing systems can be associated with capabilities to build parts with feature sizes of a similar dimensional range (Envisiontec, http://www.envisiontec.de, accessed October 2011). However due to the curling dimensional errors for parts particularly in lower sections, are substantially higher and can reach relative values of 10%.

Figure 2.9 shows sequentially the steps leading to curling in SLA. A single layer of a cantilever will not display upward deformation but will tend to deform slightly downward. The second successive and subsequent layers are each bonded to the layer below. As the layers shrink this introduces a bending moment which causes upward displacement (curling) at the unsupported layers ends above the

liquid surface. As additional layers of liquid resin are applied, a self-correcting effect occurs. The build-up of layers creates a thicker section, which better resists the distortion, and less resin is applied to upwards-deflected regions.

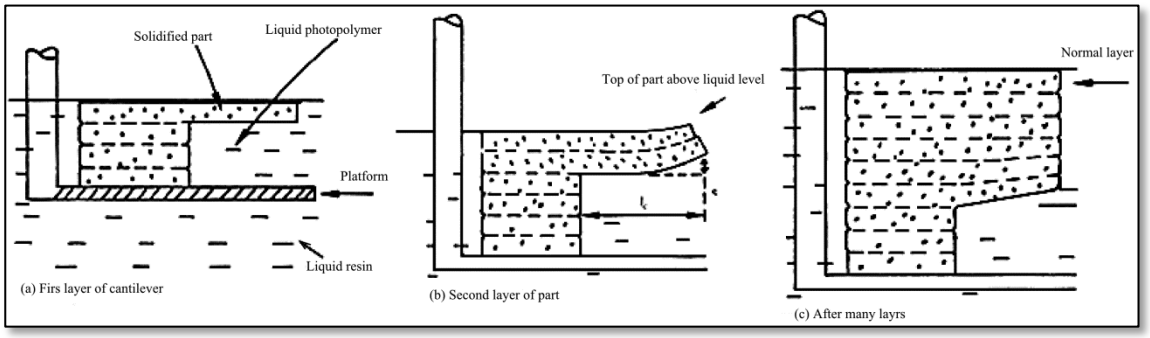

Figure 2.9 Steps in curling formation in SLA (Jacobs 1992)

In the case of SLS, the recently sintered upper region layers will additionally experience a large drop in temperature after the cooler powder is spread across the top of the layer. This leads to the upper most regions of the layer undergoing more shrinkage than other regions in the build, causing the build to curl (Jamal 2001) as shown on Figure 2.10.

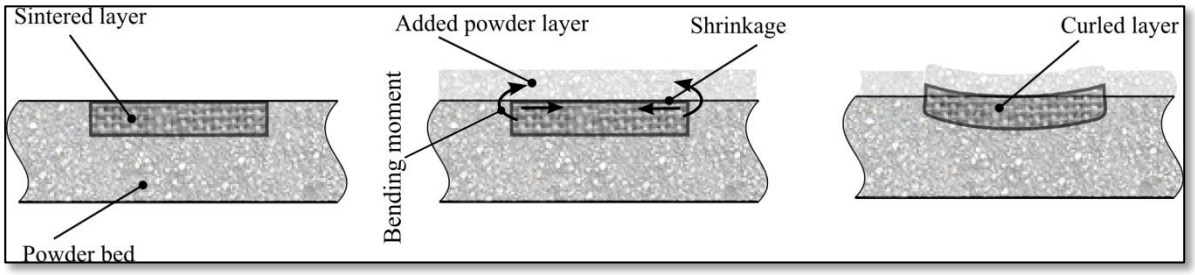

Figure 2.10 Curling developing in SLS process

If the top and the bottom layers are not bonded together, cooling down and shrinking of the top layer is not restricted and thermal stresses are negligible. The

thermal strains caused by cooling down from temperature T_0 to T_f can be expressed by formula as:

$\varepsilon_T = \alpha(T_0 - T_f)$, where (2.3)

α is the linear coefficient of thermal expansion (1/K), as defined by:

$$\alpha = \frac{dl}{l.dT}\,,$$ where (2.4)

dl is the change in length of the material in the direction being measured,

l is overall length of material in the direction being measured,

dT is the change in temperature over which *dl* is measured.

In case of proper sintering both layers are supposed to be bonded together. In this case the thermal strains from formula (2.3) on the top layer are restricted, which leads to thermal stresses. If a full restriction is applied then the resulting stresses are:

$$\sigma = E.\alpha.\Delta T,$$ where (2.5)

E - Young's modulus,

ΔT - change of temperature.

As the operational temperature in SLS process is close to the glass transition temperature, the material strength is reduced to levels lower than needed to resist the thermal stress, which leads to permanent curling distortion. This behaviour is analogous to a classic bimetal strip, where the top metal of the strip shrinks more than the bottom metal upon cooling, resulting in upward curling of the entire

strip. Schematically the resulting forces and bending moments are shown in Figure 2.11.

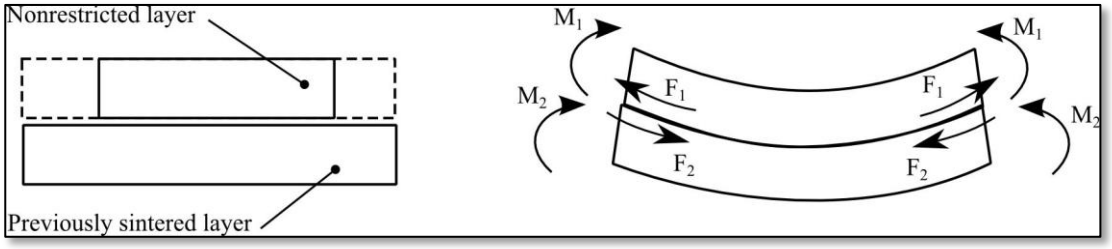

Figure 2.11 Free shrinkage of a layer (left) and forces and bending moments when shrinkage is restricted due to the bond between layers (right) (adapted from Jamal 2001)

Detailed analysis of the calculations of the elastic and plastic interaction between layers has been reported (Townsend et al. 1987, Nickel et al. 1999, Mercelis and Kruth 2006) and specifically in the case of Fused Deposition Modelling (FDM) (Wang et al. 2007).

Finite element analysis is another method capable of curling modelling (Jamal 2001). The results from finite element analysis can be effectively and conveniently compared and experimentally verified by the method developed in this thesis; the Grid Method (GM) for accuracy investigation (Chapter 3). The GM uses a grid in similar way to finite element methods, which provides experimental data about the continuous distribution of distortions calculated for each individual cell. In this way the obtained values from both methods can be compared and analysed.

The commonly used experimental technique for curling investigation is a linear measurement of the lifting of the base from the horizontal level. The curled layers can be simplified as an arc with radius R as shown in Figure 2.12.

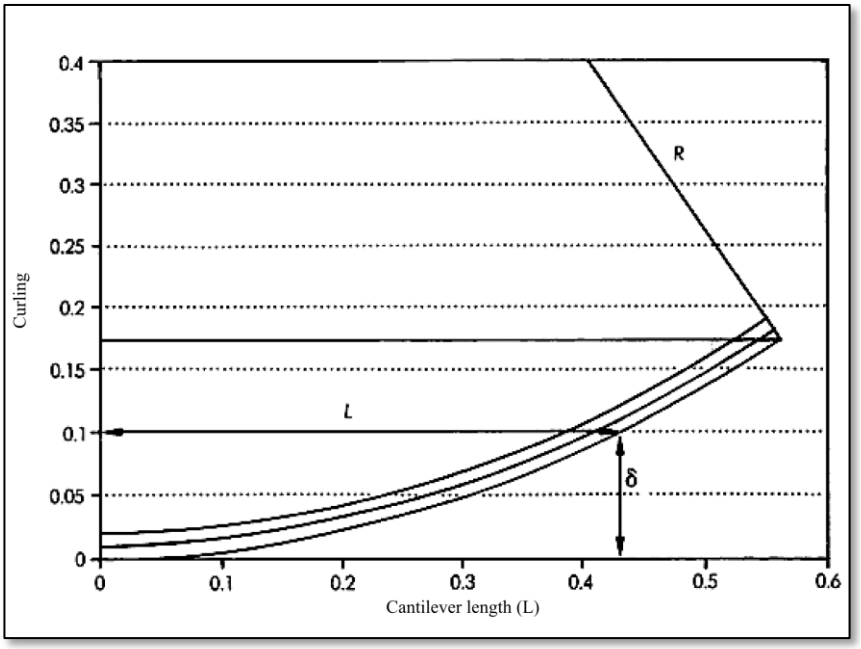

Figure 2.12 Circular curl model (Jacobs 1992)

From Figure 2.12, the curl factor, C_f, can be calculated as a percentage by formula (2.6):

$$C_f = \frac{\delta}{L} * 100, \% \qquad (2.6)$$

where:

δ is the lifting from the base,

L is the distance from the centre of the part.

Investigation of curl factor variation with respect to thickness for SLS polycarbonate was conducted by manufacturing a series of blocks with different

thicknesses. Subsequently the curled bottom surface with respect to its vertical lift was measured (Berzin 1995). The resulting profiles are shown in Figure 2.13.

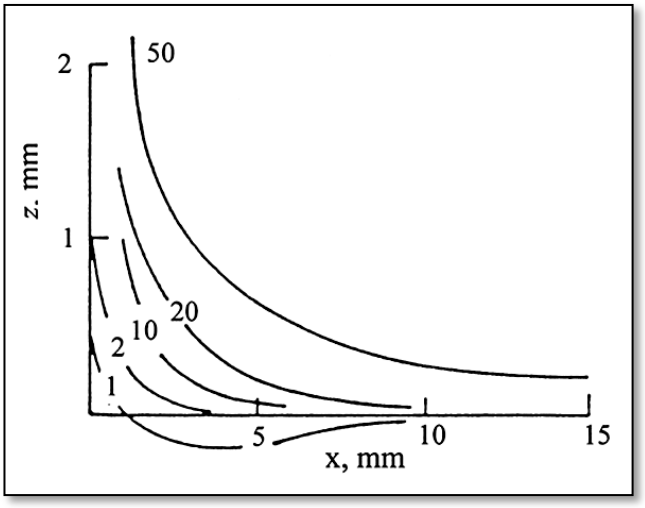

Figure 2.13 Measured profiles of the bottom surfaces of SLS polycarbonate blocks with thickness of 1, 2, 10, 20 and 50 layers (Berzin 1995)

Such an approach is not very informative and is not a comprehensive experimental study of the curling phenomenon, since the deviations and their distributions inside the part are not measured.

The illustration in Figure 2.14 shows curling and warping distortions. Another terminology for the same phenomenon is *in-build curling* and *post-build curling* respectively (DTM Corp. 1999, 1998, 1997). It can be seen that these kinds of deformations are not only linear in character, but also consist of significant amounts of angular/shear strain components that could be even predominant. The strain distribution inside the part is complex and it is not possible to distinguish curling, warping or shrinkage by measurement of deflection in the z direction only, from the reference surface or any other linear dimensional variations.

Warping itself can be associated to a great extent with part section bending, thus in some cases it could be reduced or eliminated by part straightening after building.

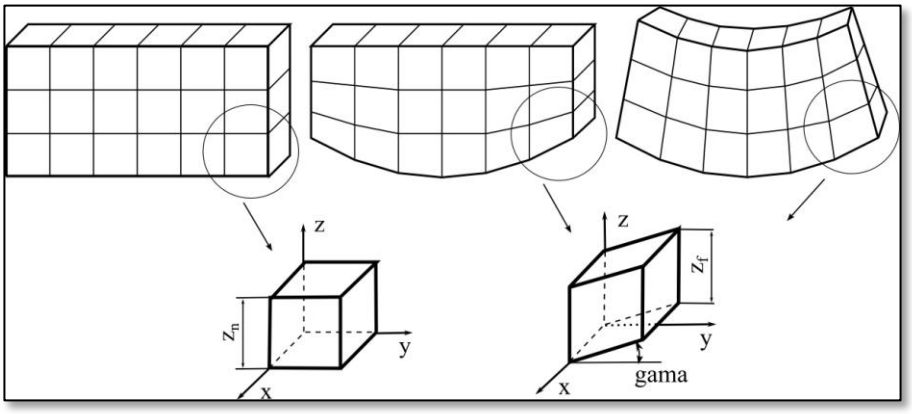

Figure 2.14 Curling, warping and associated deformation of an element from inside the part

Depending on the process utilised there are several measures that can be applied to reduce final part curling. Curling can be reduced by developing new materials and altering materials properties, by process parameter optimisation and by geometrical compensation in the CAD model.

In the resin based SLA process, the material properties responsible for curling such as polymerisation rate may be separated from other process parameters and tested by building a cantilever diagnostic test (Jacobs 1992).

In the powder based SLS process the material deterioration (e.g. polyamide) after repeated exposures at high temperature has a significant effect on part curling and other quality factors such as strength, accuracy and surface finish. In spite of

this only a certain amount of fresh powder is mixed with the used powder for economic reasons. Investigation into the influence of powder-recycling rate on curling in the case of polyamide material has been was conducted (Jain et al. 2008). In a separate study the ratio of virgin powder to used powder was found to have significant effect on curling (Senthilkumaran et al. 2009).

The process parameters and their influence over the curling in different RP technologies have been discussed by several researchers. For SLA this shows that laser power and scan speed are responsible for cure depth, which influences the amount of curling (Jacobs 1992 and Patri 2004). Some measures to prevent curling include applying suitable support structures, choosing a favourable part orientation and hatch and scanning strategies.

For SLS the influence of process parameters on curling has been investigated (Jamal 2001, DTM 1997, 1998, 1999, Nelson et al. 1995, Senthilkumaran et al. 2009). The complexity and interdependence of process parameters used to solve curling problems usually leads to contradictions in the final results. Measures to decrease curling sometimes worsen other properties of the part. For instance reducing cure depth in SLA has a positive effect on the curling, however it could lead to weak bonds between layers and delamination of the material.

The reduction of curling distortions by applying compensations to CAD models requires numerical data of curling considering the part size and shape, which makes the task rather complex. Finite Element Analysis (FEA) of curling

phenomenon is a possible tool to model curling and applying measures to reduce it (Jamal 2001).

The real strain condition in complex distortions such as curling is usually a result of a combination of several phenomenon that manifest by linear and angular deviations from the nominal. These phenomenon impose the need for a generic method of experimental investigation to analyse the geometrical uncertainties that are capable of describing complex part distortions in general terms of linear and shear strains. The development and validation of such a method (referred to as the Grid method) was a major objective of this research and is described in Chapter 4. Implementation of the method and the results of curling investigation of μSLA process are presented in Chapter 6. The data obtained by implementation of the proposed approach provide a mathematical model of curling distribution in the horizontal and vertical directions as well as across total part thickness. In this way the data acquired from the proposed experimental Grid Method could be used for scaling and compensation of the digital CAD part.

2.1.3 Errors caused by laser beam spot size and Heat Affected Zone (HAZ)

The errors caused by the laser beam spot must be considered when using SLA and SLS processes. This section describes laser spot issues and laser beam interaction with the powder material. Most of the paradigms regarding the laser spot influence on the build errors are also applicable for SLA processes.

The laser sintering process builds up three-dimensional shapes by consecutively sintering powder layers; the bottom of the layer *n* is sintered to the top of the layer *n-1*. Raster-scanning the powder surface with the laser beam, as shown in Figure 2.15, sinters individual layers. The raster pattern is comprised of individual scan lines, each overlapping the previous to form a continuous layer. The fundamental process unit of the laser sintering process is a single scan line formed by a laser beam spot (Schultz 2003).

The beam size influences the *delivered power* P per surface unit and therefore the energy of the process as well as the *geometry* of the sintered layer. Schematically the beam and corresponding raster parameters are shown in Figure 2.15.

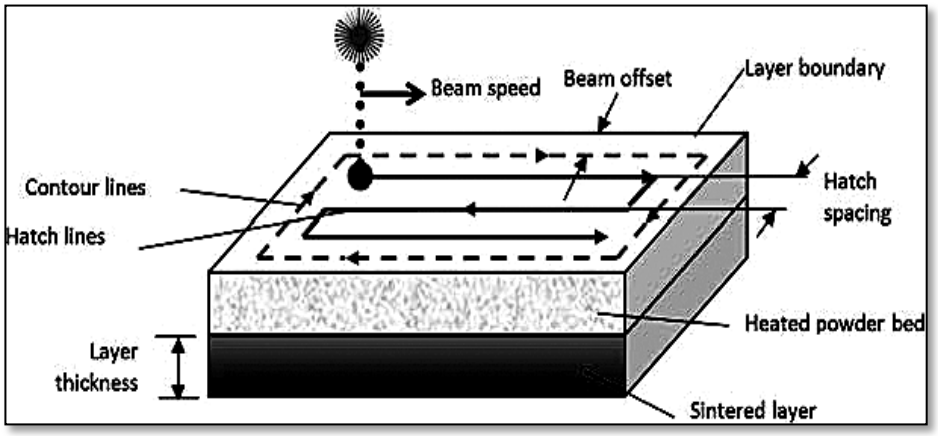

Figure 2.15 A scheme of the laser beam raster pattern during the scanning (Senthilkumaran et al. 2009)

The *delivered power* P can be expressed empirically as a function of the following parameters (Gibson and Shi 1997):

$$P = f(Db, BS, \rho, h, C, Tm, Tb, l_f, R) \quad (2.7)$$

where:

Db is the laser beam diameter on the part bed, BS is the beam speed, ρ is the density of the powder, h is the layer thickness, C is the specific heat, Tm is the melting temperature, Tb is the part bed temperature, l_f is the latent melting heat, R is the surface reflectivity.

The energy density delivered to the image plane is defined by Andrew Number A_N (Nelson 1993 and Nelson et al. 1993):

$$A_N = \frac{P}{V.HS} \quad \text{in } [J/m^2] \tag{2.8}$$

where:

P is the laser power delivered to the surface [W],

V - laser beam velocity [m/s],

HS - hatch spacing [m].

Formula (2.8) is known to be useful for relating physical properties of parts built by SLS to the three independent process parameters - P, V, HS (Vail 1993). Furthermore, the delivered laser power P in the formula (2.8) depends on the size of laser beam Db. The influence of variable laser diameter and build speed to the part quality has been investigated (Deckard and Miller 1995; Williams et al. 1996; Miller et al. 1997; Bae et al. 2007). Changing the laser beam diameter would require changing other sintering parameters in order to deliver the energy needed for successful sintering. Furthermore varying the laser spot would vary

the heat affected zone (HAZ) size. For that reason controlling the sintering process via the beam spot size is impeded and the modern SLS platforms still operate with a fixed laser beam diameter.

The interaction of laser irradiation, the powder bed and the consecutive energy division is depicted in Figure 2.16 where q-rad and q-conv are radiation and convection energy losses; q-cond is the energy conducted into the powder bed. The proportion of energy q-cond is the fraction of energy responsible for the temperature rise in the powder and the sintering of particles (Williams and Deckard 1998).

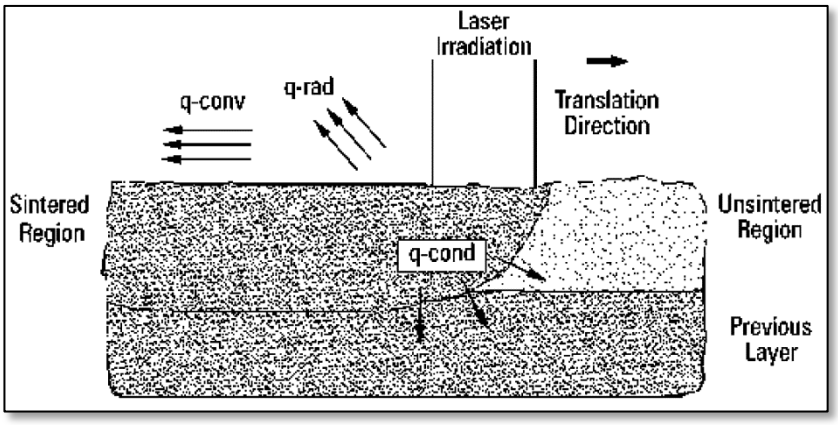

Figure 2.16 Interaction of the laser irradiation and powder bed (Williams and Deckard 1998)

The distribution of beam energy is assumed to be a Gaussian distribution that can be approximated by the square shape, as shown in Figure 2.17.

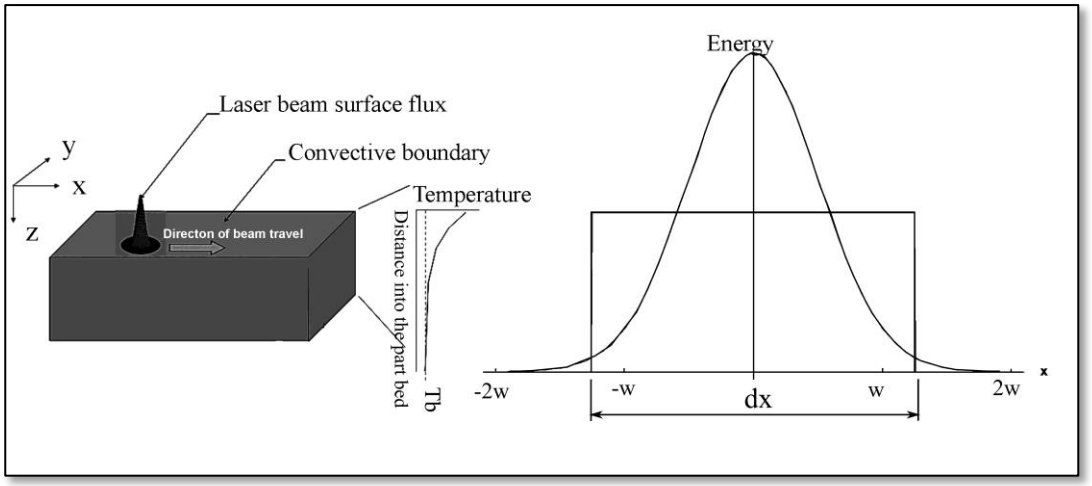

Figure 2.17 Laser beam energy distribution (Schultz 2003)

The beam spot shape is rarely circular, thus a further assumption is that the Gaussian beam has two normal spatial components x and y which can be considered separate with regard to their effect on heating the powder-bed (Schultz 2003). Hence, the laser beam *geometry* is defined by two diameters d_x and d_y.

In the case of the SLS process the beam spot size varies from the centre to the periphery of the build area due to optical parallax. Geometrical assumption (Wang 1999) shows that the difference between the beam diameter in the part bed centre and that at the periphery is no more than 50 μm. As this value is in the powder particles size range it can be ignored. The delivered energy also affects the area that surrounds the beam spot. Thus a bigger HAZ with an irregular and unspecified shape is formed that needs to be determined experimentally in order to apply correct beam offset compensation. In the case of the SLA process, the parallax effect also could be considered as negligible (Jacobs 1992).

Experimentally the beam offset is calculated on the basis of results obtained by building a standard pyramid as shown in Figure 2.18(a). The lengths of each step x_i and y_i are measured and each difference from the nominal $\Delta x_i = x_{in} - x_i$ and $\Delta y_i = y_{in} - y_i$ is calculated. The results can be graphically and numerically approximated. The extrapolated value of Δx and Δy when the pyramid step size is zero is interpreted as beam offsets d_x and d_y. The method for beam offset and shrinkage calculation has been described in detail (Wang 1999 and DTM 1999). Schematically the calculation of the beam offset is graphically depicted in Figure 2.18(b).

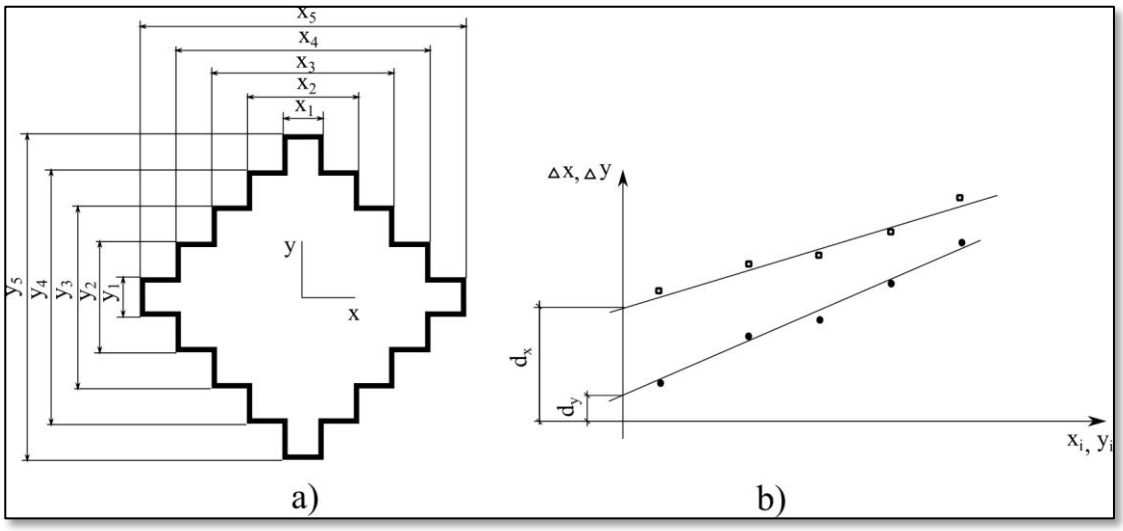

Figure 2.18 a) - Pyramid for beam offset calibration; b) - interpolation of the measurements and beam size determination by extrapolation of the line

Measures to reduce uncertainties caused by laser beam spot size have been introduced for by machine manufacturers. Today's software for laser-based additive manufacturing compensates for the finite laser spot dimensions by

insetting the contours of a solid part (Moesen et al. 2011). An offset of $b_{x(y)}/2$ should be considered as beam compensation so the edge of the beam follows the required CAD contour. The beam-offset value is a common parameter of modern applied CAM software. Schematically the compensation is illustrated in Figure 2.19.

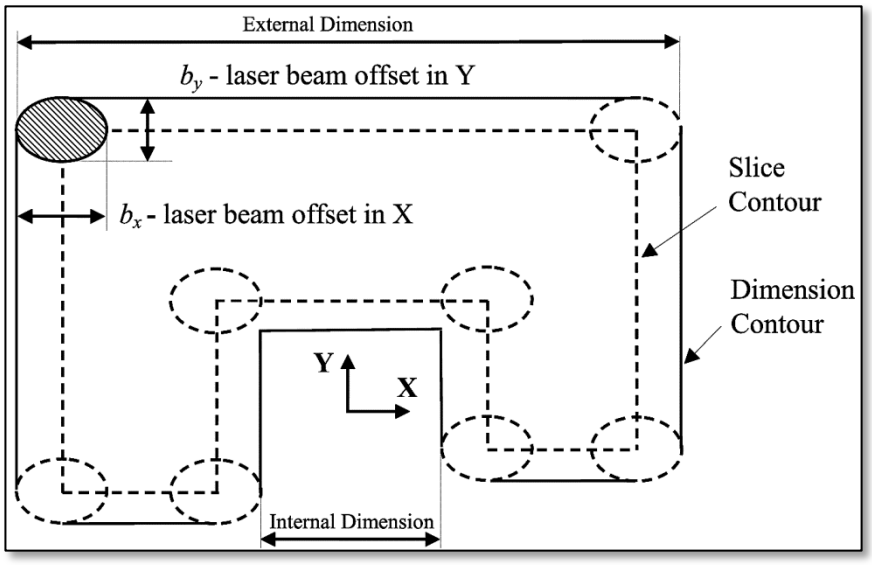

Figure 2.19 Insetting the contour of a solid part according to the beam size and shape. (Dothev and Soe 2007)

The three methods for beam compensation are *normal*, *constant* and *dihedral* (Nelson et al. 1995). In the *normal* offset method, a vector normal is calculated at each vertex based on the normals of the adjacent surfaces. The vertex is moved along the vertex normal to the new offset position. The normal offset method works best for geometries that have circular and flat surfaces because the angle between surfaces is large. As the angle between the facets decreases, the distance that the vertex is moved by the normal offset method is not sufficient to move the surface geometries by the desired amount. The *constant* offset method works best

for square features. In this method the vertex is offset by moving first in the *x* direction, then in the *y* direction, by corresponding beam offset values. An example of the *Dihedral* offset, is used by DTM (3D System) geometry tools software. The method uses the dihedral angle between connecting facets to calculate the new offset vertex position. This method adjusts for part geometry, making the dihedral offset method more accurate than the normal offset and constant offset methods. The three offset methods are graphically represented, in Figure 2.20.

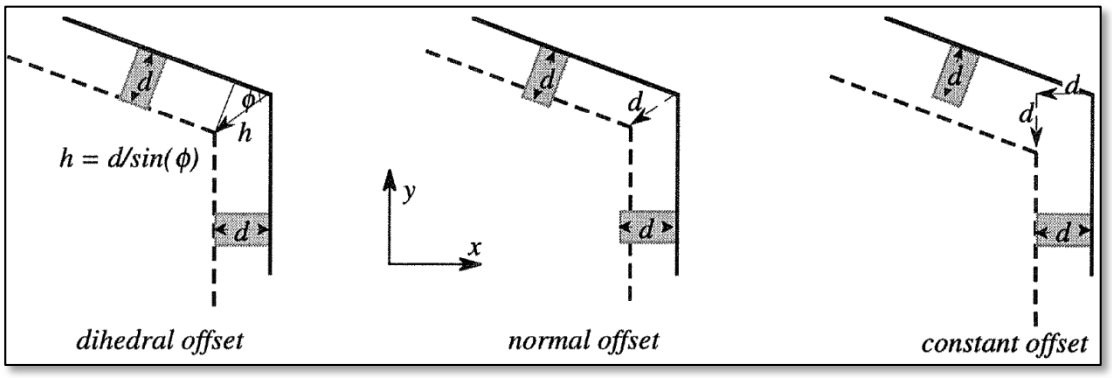

Figure 2.20 Comparison of the three offset methods (Nelson et al. 1995)

An expected consequence of insetting the contour is that features having smaller dimensions could be removed. This operation may also significantly alter the structure of thin-walled parts as well as being a source of potential production errors. For that reason a development of a new algorithmic framework was proposed (Moesen et al. 2011). The goal is to minimise the small features loss at reasonable computational cost and time. Schematically the problems and corrections are illustrated in Figure 2.21.

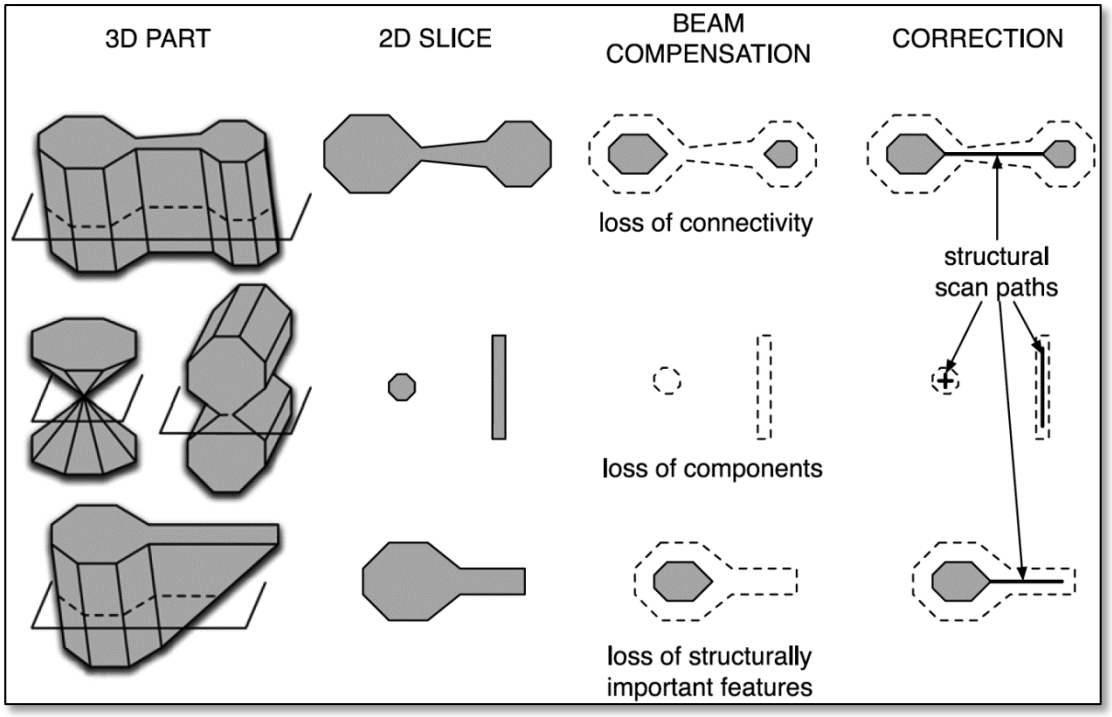

Figure 2.21 Potential beam compensation problems and their correction via structural scan paths (Moesen et al. 2011)

The melting and softening of material during powder sintering outside the desired part boundaries is known as *"growth"*. From a practical point of view, the result of growth and finite beam diameter on part accuracy are indistinguishable since they both cause a definite increase in part dimensions. Part growth dimensions are adjusted for using software compensation in the same way as they are for beam diameter. The difference is that in the *z* direction, z-growth is set as a separate parameter. One manufacturer DTM/3D Systems calls it "bonus-z".

The sources of uncertainties described in paragraph 2.1.3 above were not subject for investigation in this research. However they had to be considered when the test part geometry and features for measurement were designed. The analysis

presented in Chapter 3 showed that their influence on the measured parameters when the Grid Method was applied appeared negligible and could be ignored.

2.1.4 CAD, tessellation and slicing errors

Layer manufacturing considers the use of additive processes in which the geometry of the object to be manufactured is obtained from a CAD file. The geometry must be processed through several steps. First it is usually converted into the industry standard file format ".STL" (STL is derived from the word *stereolithography* or is taken by some authors as *Standard Tessellation Language*). It is then transformed into a series of cross-sectional layers. This process is known as "slicing". These layers are then used to generate the numerical control (NC) code required by the platform to build the corresponding physical layers and stack them into the final part. Some inaccuracies through the steps of converting the CAD file to sliced file have been analysed by (Banerjee 2004).

The CAD file geometry can be created from model data, for an existing object through reverse engineering, or using mathematical data such as surface equations. Regardless of the source, the process can generate errors particularly in the case of reverse engineering or surface approximation.

All current commercial RP systems require the part geometry to be prescribed in the .STL file format. This format has become the industry standard for two reasons (Tyberg 1998). First, 3D Systems, Inc. introduced the format three years

prior to any other company for use with their Stereolithography Apparatus. Second, its simplistic format for describing CAD models minimizes the cost of providing one-way translation. As a result, most CAD vendors have developed software that is capable of translating data to this format. The .STL file format consists of a triangular surface mesh that approximates the actual surfaces of the original CAD model. It is a boundary representation of 3D geometry, which in the case of a sphere is depicted in Figure 2.22.

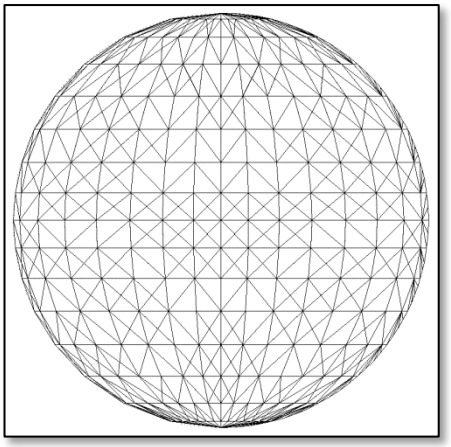

Figure 2.22 Faceted representation of a sphere (Tyberg 1998)

Conversion to .STL can be done through a number means; some CAD software programs allow for the direct export of .STL files, whilst others require "add-ins" within the CAD software. Conversion can also be achieved by specialised .STL file converters. When converting to .STL files, the user is given several options for resolution, sometimes called chord height or triangle tolerance, etc. as shown in Figure 2.23. Depending upon the size of the model, the geometry of small details, and the overall curvature of the part, the tolerance can typically be set to 0.0254*mm* for average models. Small parts or models with fine details may

require a tighter tolerance (Bastech Inc. 2011). In addition, the translation of CAD models to the .STL file format often produces errors such as missing and intersecting surfaces. Repairing these models is an imperfect task and could also be a source of errors.

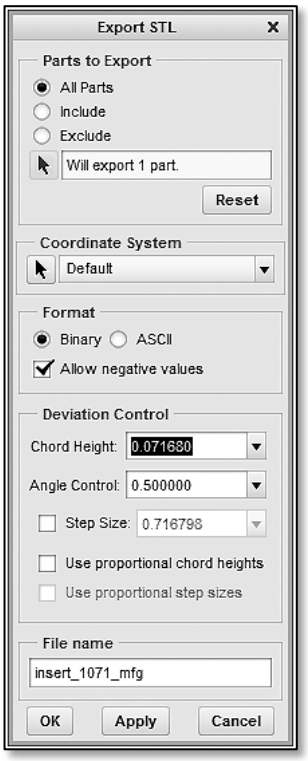

Figure 2.23 Pro/ENGINEER dialog box for .STL file tolerances setting

In the next step .STL model is a subject of the slicing procedure. In this process, the model is intersected with a set of horizontal planes to create a series of cross sections, or slices, comprised of contours that represent the material boundaries of the part to be built. Constructing a freeform sculptured 3D geometry by a series of $2\frac{1}{2}$ D layers will inherently produce an approximate representation of the original surface geometry. This is commonly referred to as the stair-stepping effect and it influences all non-horizontal surfaces. Figure 2.24 illustrates how

the layer thickness affects the stair-stepping effect and resulting inaccuracy. It appears that, by varying the layer thickness different accuracies can be achieved, however this is always a compromise with build time. In addition the layer thickness is not only a software factor for geometry approximation, it is an important parameter during the physical building of parts. It is connected to the process, material, platform and is closely related to other build parameters in a multifaceted manufacturing system.

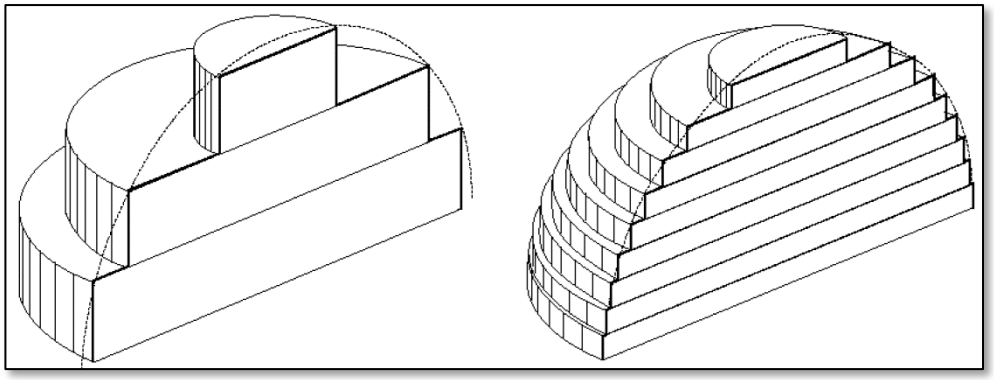

Figure 2.24 Stair-step effect as inaccuracy source due to the thickness of the build layers (Sabourin et al. 1997)

Research carried out on adaptive slicing shows that a compromise between accuracy and build time can be achieved (Danjou et al. 2010; Nezhad et al. 2010; Shakeri et al. 2007; Byun and Lee 2006; Pandey et al. 2003; Weiyin and Peiren 1999; Tyberg and Bøhn 1998; Tyberg 1998). In adaptive slicing the geometry is first analysed and the layer thickness is applied based on the vertical slope of the surface. Depending on the process a variable layer thickness can be implemented uniformly over the total part bed or selectively to each individual part as shown in Figure 2.25. The second approach is possible only for processes such as FDM where the material is deposited by a nozzle merely over the part.

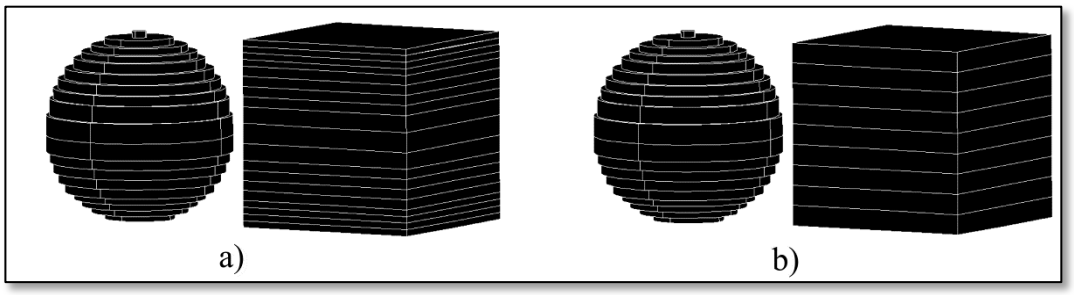

Figure 2.25 Identical (a) and selective (b) approaches in adaptive layering (Tyberg and Bøhn 1998)

Another possible way to increase the resolution and accuracy in FDM is to apply variable nozzle The combination of adaptive layer slicing and variable nozzle diameter is illustrated on Figure 2.26.

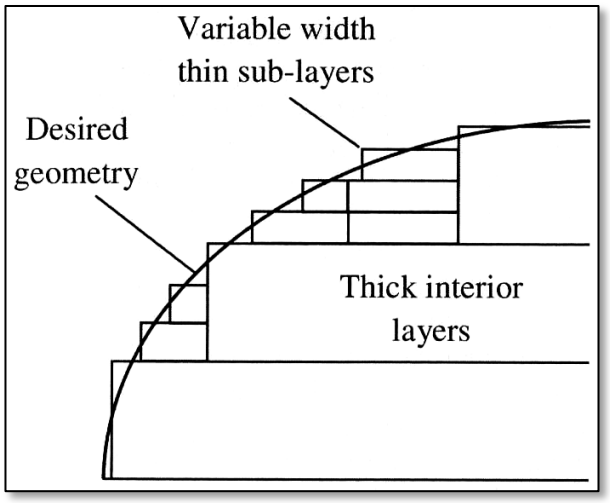

Figure 2.26 Reduced staircase effect by utilising adaptive layer slicing and variable nozzle diameter in FDM process (Brooks et al. 2012)

Theoretical analysis about improvement in horizontal accuracy and vertical resolution and build time when variable diameter nozzle is implemented for the fused deposition of polymers is described in (Brooks et al. 2012).

The layer thickness influences mostly the quality and roughness of sloping surfaces, but in some cases important features can be lost after slicing, this is shown in Figure 2.27.

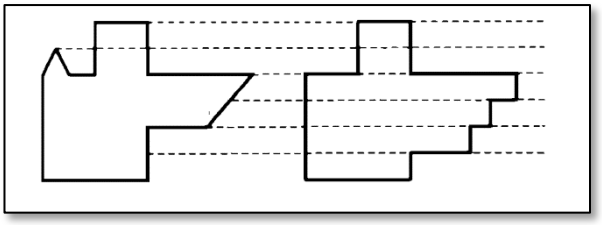

Figure 2.27 Simplifying the shape and sacrificing of small features (Dolenc and Mäkelä 1994)

Due to technological reasons variable slicing has not found a convenient application in RP practice so far. The slicing layer thickness is determined mostly by the requirements of a successful build process. It is usually an element of building parameters and is set by the CAM software of the hardware platform on which the part is to be built.

Some errors are inevitable due to the slicing algorithm itself. For example, using a curve-fitting algorithm (interpolation and smoothing) may cause Chordal deviation. A staircase error in the x and y directions may occur for curved contours when a large scan spacing is used; these errors can be reduced by improving the slicing algorithm. In addition to slicing, the quality of the .STL file

is also important in determination of the final accuracy that can be achieved since a surface made of smaller triangles (i.e. greater mesh density) provide greater accuracy in the slicing process (Figure 2.28).

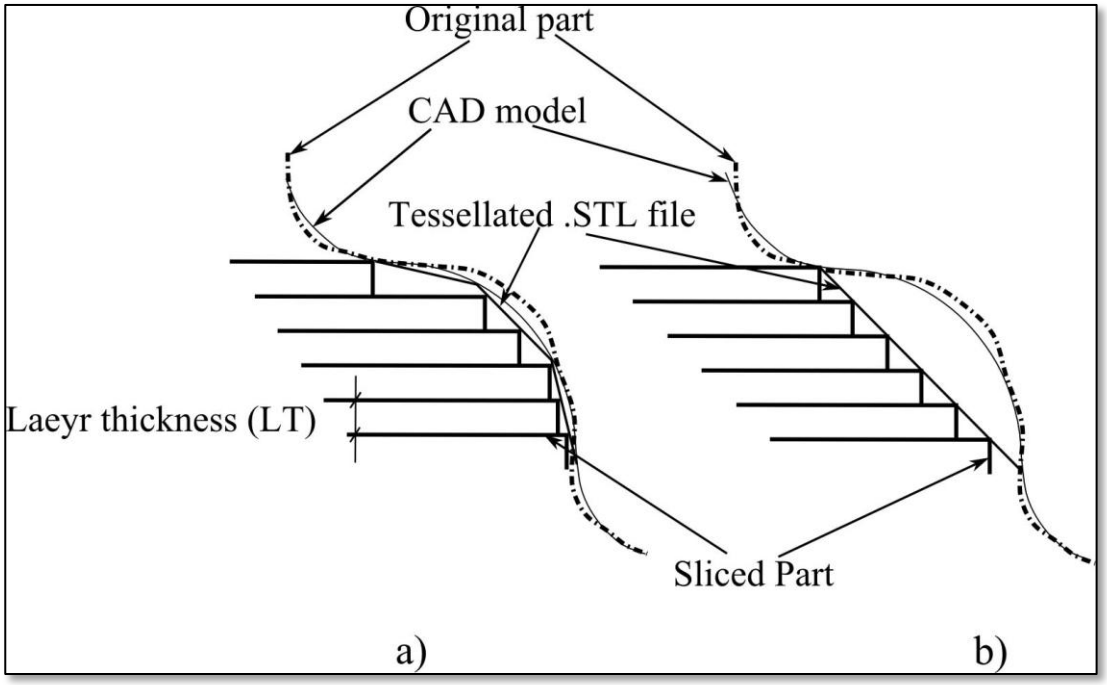

Figure 2.28 Reducing the accuracy after CAD modelling, STL tessellation and slicing in the cases of fine (a) and rough (b) tessellation

The uncertainties in the manufactured component introduced by sources that were subject of observation in this section were related to the RP software development domain and as such were not targeted for investigation by the GM in this study. In order to eliminate the influence of uncertainties due to the CAD tessellation and slicing, the resolution of STL files of the test parts were kept higher than the hardware resolution of the specific technological platform, which is usually limited by the layer thickness.

A summary based on the review from Section 2.1.4 is given as a flow diagram in Figure 2.29.

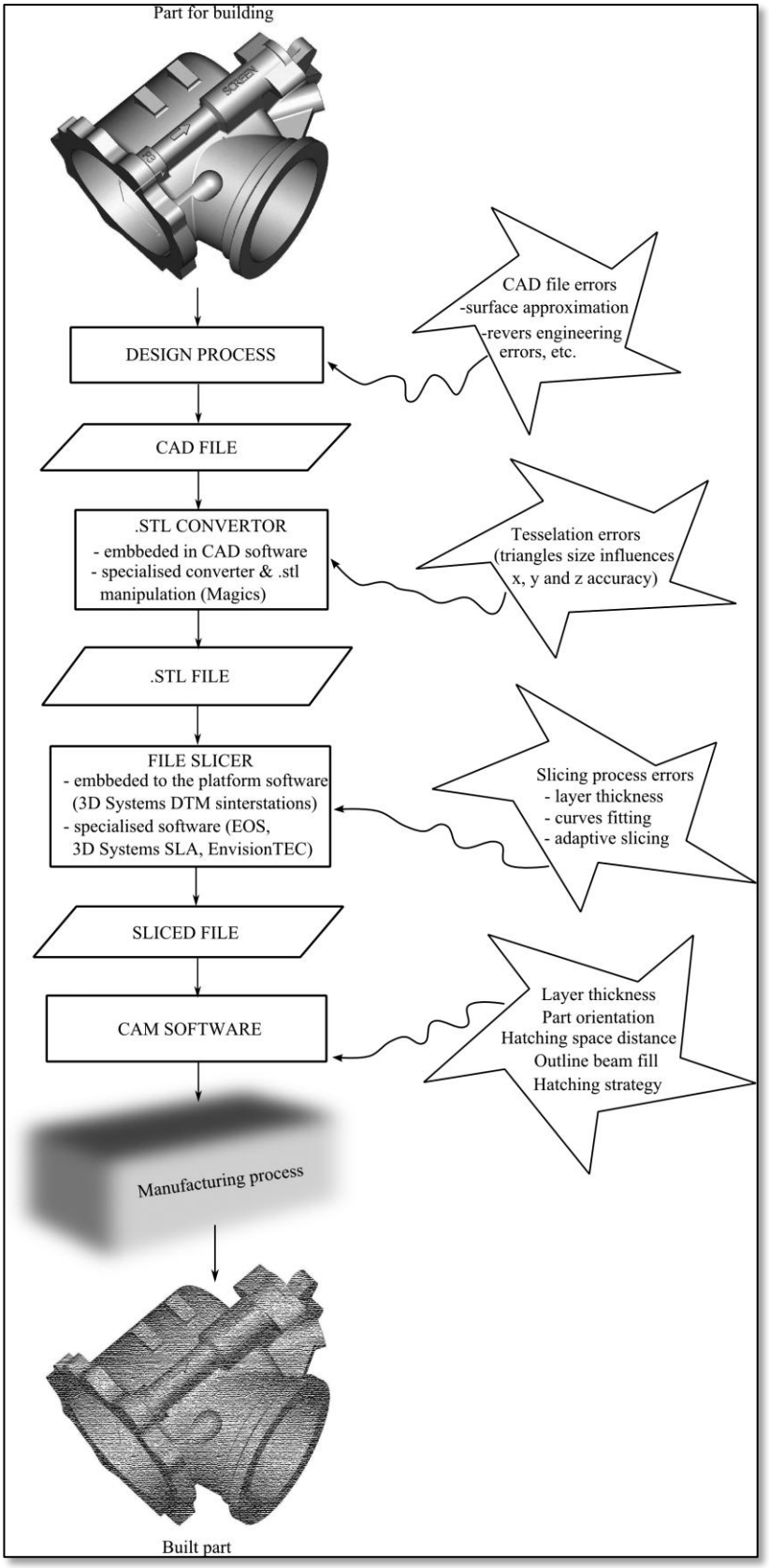

Figure 2.29 Steps and errors due to CAD, CAM, tessellation and slicing processes

2.1.5 Random errors

From the inauguration of the RP industry it was clear that for some processes consistent accuracy was not always achievable. Differences in shrinkage was observed between otherwise identical sections, of otherwise identical parts, prepared by the same people, in an identical manner, on the same equipment, using identical materials, under nearly identical environments (Jacobs 2000). Although no two parts and no two experiments and no two measurements within a given experiment are truly identical, such deviations of results which are caused by unknown and unpredictable changes in the experiments are known as *random errors*.

Since the most important validation experiments of the Grid Methodology presented in this work are carried out on SLS processes, this section summarises some of the most obvious sources of random errors in the powder based laser sintering process:

- variation in temperatures due to unpredictable dimming or manual cleaning of IR sensors;
- protective gas flow instability;
- variation in humidity and hence moisture of the powder or other types of build material;
- variation in material composition and structure e.g. particle size, distribution and shape of the powder;
- mixing and the density of the powder and liquid materials;
- unpredictable variations in cooling down or post curing procedures;

- part handling after building;
- variation in accuracy of mechanical systems such as part bed screw-thread mechanism;

While these kinds of errors are difficult to predict due to the fact that the causes and sources are not immediately obvious, they can be represented by statistical means because of their random nature. Random errors often have a normal statistical distribution. In such cases statistical methods for data analysis are relatively simple. Random errors influence the precision of the process or how the same dimensions are equal or close to each other when they are built repeatedly.

It was experimentally found (Jacobs 2000) that in SLA the resulting random shrinkage is directly proportional to the mean process shrinkage and can be expressed by the formula:

$$\sigma_s = K\bar{S} \qquad (2.9)$$

where,

σ_s is the standard deviation of the random noise, K is proportionality constant for a given process (for SLA it is found to be 0.095) and $\bar{S}$ is the mean process shrinkage.

2.2 Summary and conclusions

If the finished component produced by Free-form Fabrication methods is a part of a process chain then the final accuracy could be a function of the accuracy of many processes within the chain such as CAD, RP, casting, finishing, machining etc. The common variables that contribute to the final part accuracy could be represented in the form of a cause and effect diagram (also known as a Fishbone or Ishikawa Diapgram) proposed by (Nagahanumaiah and Mukherjee 2004), shown in Figure 2.30. The total number of parameters that influence the accuracy could not be defined but consideration of the most obvious accuracy influencing parameters total more than thirty. They might be further clustered in the five groups discussed in the above sections.

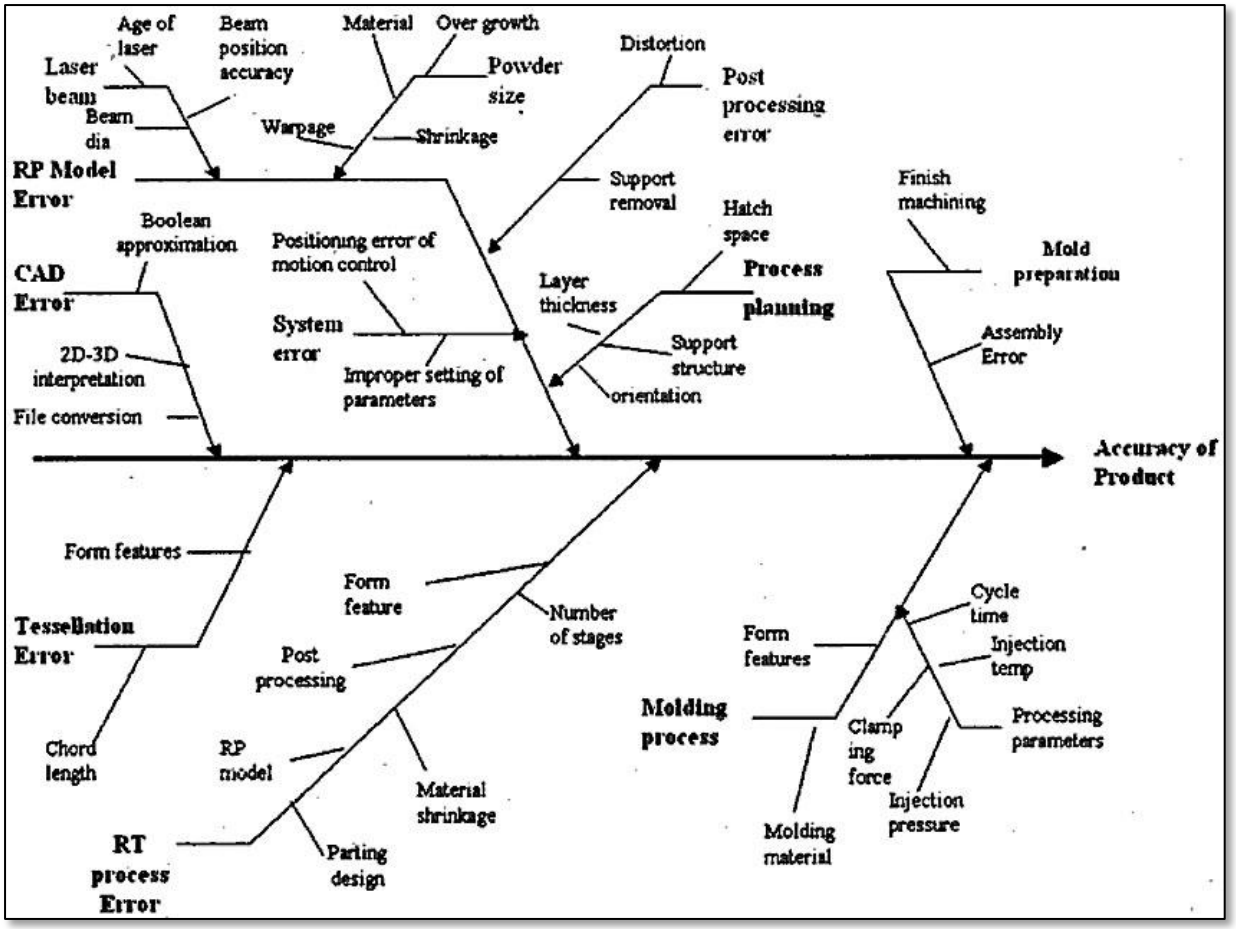

Figure 2.30 Cause and effect diagram for accuracy of a part in the case of rapid tooling FF application (Nagahanumaiah and Mukherjee 2004)

The common RP practice deals with the uncertainties manifested as a whole, by applying combined compensation (that reflect all of the listed factors) through the CAD model. Furthermore, by setting up appropriate build parameters and by applying some specific practices, such as support structure, temporary additional structures, part orientation, etc., an acceptable accuracy for an affordable price and build time could be achieved.

The following general conclusions can be made:

i) The sources of uncertainties are diverse. Their origin can be found in one of the following domains:

- material behaviour and properties;
- software - programs and data;
- manufacturer hardware (platform);
- human and random factors.

ii) Appropriate measures for compensations to overcome deviations in sizes from the nominal, is possible if the sources of errors are determined correctly and accurately.

iii) Distribution, magnitude and character of the uncertainties are not uniform within the build area of the manufacturing platforms and can vary significantly with part position, size and shape. This is due to the influences of various sources of errors. Hence the reliable and generic method for quantitative investigation of uncertainties and particularly their distribution is important.

Based on the analysis of inaccuracy sources described above, the following objectives were set:

1) To review the methods that are used for accuracy investigation and to evaluate their capabilities to reveal the distribution, magnitude and type of distortions that a FF process can cause to the final part. This was the subject of the next Chapter 3.

2) To develop an accuracy investigation methodology that would be able to reflect the process shortcomings described above and to provide sufficient

information to analyse them and improve the process performance. The methodology should be able to overcome the limitations in the existing testing methods and could be utilised as a generic and reliable approach for studying the FF processes. This objective was the subject of Chapter 4.

3) To study some 'critical' accuracy aspects of the SLS process (particularly in the vertical direction) in regard of polystyrene material; curling phenomenon in μSLA and other manufacturing processes in the MNT domain, by implementation of the developed method. This objective was the subject of Chapter 5 and 6.

4) To suggest and implement a GM based approach to study the capabilities and tolerance limitations of the FF and MNT processes and process chains. This objective was targeted in Chapter 7.

CHAPTER 3 METHODS AND TEST PARTS FOR ACCURACY STUDY AND CALIBRATION OF THE RAPID PROTOTYPING TECHNIQUES

3.1 General approach and considerations

The parts produced by FF techniques contain a variety of dimensional and shape deviations from the original design. The sources of deviations (errors) were described in Chapter 2. These errors could occur during the building stage or after the process is completed, e.g. during the cooling down stage. In some cases post processing and material aging can additionally change the part size. The accumulation of uncertainties influences final part accuracy.

Part accuracy is a major quality characteristic and thus is in constant consideration by RP research and development, especially during launching and implementation of new platform materials or processes into industrial practice. For that reason reliable generic methods for the investigation of geometrical deviation from the nominal are necessary. Some of the applications of these methods include: evaluation of process capability; setting dimensional/shape tolerances; process benchmarking and comparison; process chain design and investigation.

Achieving sufficient part accuracy is a complex and challenging task since the size and shape of the final part depends on numerous technological parameters specific to the RP process in question. The optimum build, depends on process

parameters including the material, part shape and size, section geometry of the manufactured part and many other issues.

For each RP process there are common manufacturing parameters affecting accuracy and these have to be investigated and taken into consideration. As an example the list of parameters for SLS (one of the main processes considered in this study) includes:

- laser power (*LP*);
- laser scan speed (LS_p);
- scan spacing (*SCSP*) or scanning hatch step;
- part bed temperature (T_b);
- part piston temperature (T_p);
- feed cartridges temperatures (T_l – left feed and T_r – right feed);
- scanning strategy (cross-hatch or non cross-hatch);
- sorted or unsorted scanning fill;
- layer thickness δ_l;
- warm-up and cool-down times;
- scan count number (the number of times that a layer is scanned);
- outline scanning;
- beam offset;
- bonus z compensation;
- scaling factors in *x*, *y* and *z* direction;
- worm-up part bed thickness;
- left and right feed distance;

- part heater inner/outer ratio.

By changing the above parameters one can change the energy delivered to the material, the warm-up/cooling-down conditions, and the structure of the built part or surface appearance with the ultimate purpose of producing a successful and good quality build.

The manufacturing parameters listed above have great significance on the part integrity, strength, density, surface quality and shrinkage for different processes and materials. The analysis of process parameters is therefore one of the main streams of RP research. For SLS the key process elements that affect part quality are the beam delivery and thermal control system (Nelson et al. 1995(a)). An overview of the research and corresponding investigated key parameters of the process are given in Table 3.1. Specific laser parameters - pulse duration, pulse frequency and number of pulse strikes, for sintering metallic powder, are optimised by Liao and Shie 2007. Some authors (Cooke et al. 2011) consider the process parameters as commercially sensitive, and do not provide their values.

Table 3.1 Authors and parameters investigated for SLS

	T_b	LP	LS_p	SCSP	δ_l	beam spot size	delay period	X or Y hatch pattern
Gibson and Shi 1997		✓	✓	✓				
Ho et al. 1999, 2003		✓						
Williams and Deckard 1998		✓	✓	✓		✓	✓	
Miller et al. 1997		✓	✓	✓		✓	✓	
Nelson et al. 1995(b)		✓	✓	✓	✓	✓		
Wang et al. 2005	✓	✓	✓	✓				
Zhu et al. 2006		✓	✓	✓	✓			
Jain et al. 2008	✓	✓	✓	✓	✓			✓
Raghunath and Pandey 2007	✓	✓	✓	✓				
Tontowi and Childs 2001	✓	✓						
Clijsters et al. 2012		✓	✓					

For the SLA domain the influence of process parameters over the part quality is given in (Jiang 2011; Lee and Cho 2003; Patri and Venuvinod - Weiyin Ma 2004; Mahesh et al. 2004) and for FDM (Pennington et al. 2005; Lee et al. 2005; Panda et al. 2009; Giannatsis et al. 2012; Clijsters et al. 2012).

Once an optimum set of parameters are established they are kept as a material's "profile". In particular cases of unexpected changes to part quality, adjustments to the parameters can be made according to the experience of the machine operator or platform manufacturer recommendations. Some platform manufacturers allow greater user input over the build parameters. For example

3D Systems/DTM provides access to more than 20 parameters although the three most influential process parameters in SLS are the laser power, laser scan speed and the temperatures. Other technology suppliers (EOS) prefer to limit the user input to the choice of "build style". In SLA and 3D printing domains the control of parameters from the end user is usually more constrained.

In most cases of RP fabrication it is practical to set the build parameters for optimum part strength, surface quality and build time. On this basis the accuracy in size and shape of the part can be targeted by applying scaling factors, beam offset compensation, part orientation and arrangement in the building chamber. This has been described (Yang et al. 2002) in two approaches to minimise shape distortion: adjusting the build conditions, and assigning some allowances to compensate for the distortions.

Essentially the practice of accuracy research in FF requires the building of various test parts or series of parts and evaluating the differences between their nominal and actual dimensions and shapes. Linear and angular dimensions, point's coordinates and surface roughness are the basic entities that are used to assess part geometry. Based on the results from measurements the dimensional compensation and geometrical tolerances can be calculated. In each process, the achieved tolerance is related to a number of variables, such as machine precision, the build material, the process parameters and the skill of the operator.

A methodology for accuracy investigation of FF (RP) processes can be evaluated by the following elements:

- choice of test part;
- type and range of geometrical entity for investigation;
- measurement instruments;
- measurement procedures;
- representation of the data;
- analysis and interpretation of the results;
- accuracy evaluation and statistical validation of the results.

The elements that distinguish between different methodologies for accuracy studies of RP processes are test parts and the related measured geometrical entity. The remaining elements are similar for most methodologies since they all predominantly follow similar metrology approaches. For this reason the presented research is focused our attention on collecting information and the subsequent classification of existing methodologies for the assessment and evaluation of RP accuracy according to specifically designed and implemented test parts and measured entities.

3.2 Test parts for accuracy study – overview and classification

The accuracy aspects to be investigated (e.g. deviations in linear or angular dimensions; evaluation of tolerances etc) and the purpose of the investigation itself (e.g. evaluation of the scaling characteristics; benchmarking etc) usually determines the test part geometry to be analysed. The most common types of test pieces can be classified in the following 4 groups:

- *simplified geometry akin to a **pyramid** or staircase;*
- ***specifically** designed test parts with variety of geometrical features on it;*
- ***real** part models established as a benchmark part;*
- *parts for surface quality investigation and/or mechanical **testing**.*

The above four groups of test parts and the methods they support are considered in the sections below, using the following structure: *overview* of the test piece; *examples and literature sources*; *applications* of the test piece; *advantages* of the methodology; *limitations/disadvantages* of the methodology.

3.2.1 Pyramids

Overview

These are test parts purposely designed with simple geometry. Easy handling and straightforward measurement dictate the shape, which inevitably consists of steps. The steps allow for convenient measurement landings. Most platform manufacturers implemented their own pyramids for calibration and recommend them to the end-users. The typical pyramid shapes are very common and are broadly spread but some modifications could also be found.

Examples and literature sources

Figure 3.1 shows typical examples of pyramid. Step shifting of the measurement landings is a typical feature that distinguishes the configuration of a test part as a pyramid.

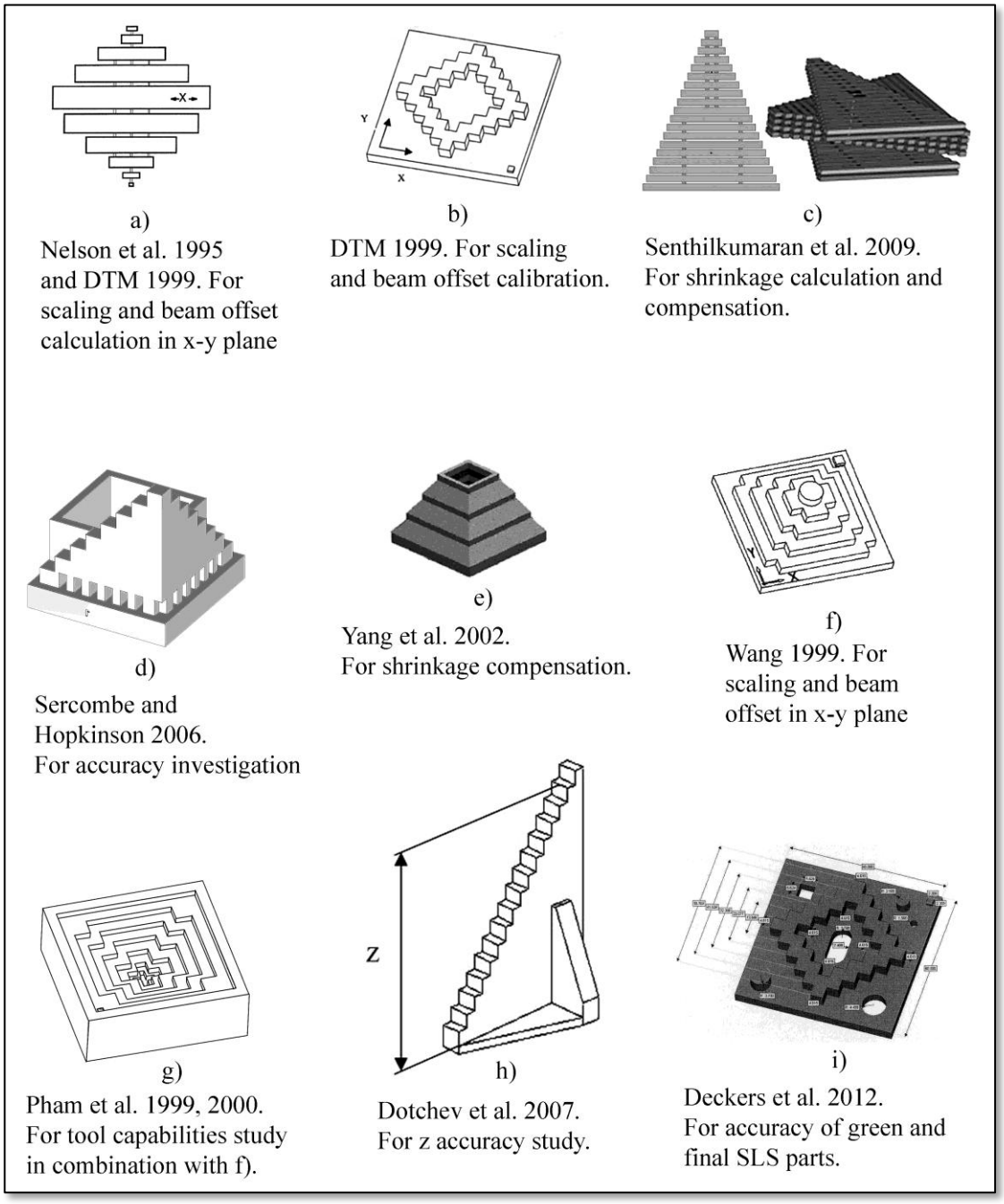

Figure 3.1 – Common pyramids shapes

Applications

The usual application of pyramids is basic scaling and beam offset calibration. In some cases pyramids are used for complex accuracy investigations including 3D study of shrinkage (Dotchev et al. 2007). Pyramids have been utilised for process capabilities studies for rapid tooling (RT) (Pham et al. 1999, 2000).

Advantages

The main advantages of pyramids are that they are a simple clear shape that can be easy standardised. They allow convenient and accurate measurements with basic equipment, and trouble-free handling and storing. For quick checking and machine calibration these parts have proven their practicality.

Limitations/Disadvantages

The steps of pyramids that are used for measurement are never collinear with the investigated direction - usually x, y or z. In fact each step gives a deviation value in a parallel direction but always in different position in the build chamber. For that reason the calculated inaccuracy is not for x, y and z-axis only, although it is interpreted as such.

The discrete change in dimensions (caused by the step effect) has a significant influence over the obtained results and chances of misleading results increases when the process inaccuracy increases. Particularly the consequences of uneven material shrinkage due to existing temperature gradients in the build chamber can be misinterpreted using a pyramid. More detailed analysis about the weakness of step effect geometries is given in Section 3.3.

Another limitation of pyramidal geometry is that, although the patterns for measurement are simple regular steps, automated measurement is not a straightforward procedure. This geometry often requires manual measurements, which can be laborious in the case of experiments that require many test parts in order to cover large build areas and reliability and repeatability of test results.

Detailed analysis of the pyramid test parts and possible incorrect results that could be obtained was one of the objectives of this study. The analysis is presented in section 3.3 below.

A variation of pyramidal test piece approach is the utilisation of specific single or multiple test pieces in form of a bar or block with some additional features on it (Figure 3.2). The lack of steps in such a configuration is an important advantage over the pyramid. However for investigation of a large area multiple test pieces are built, thus the price and labour required for the test is not justifiable.

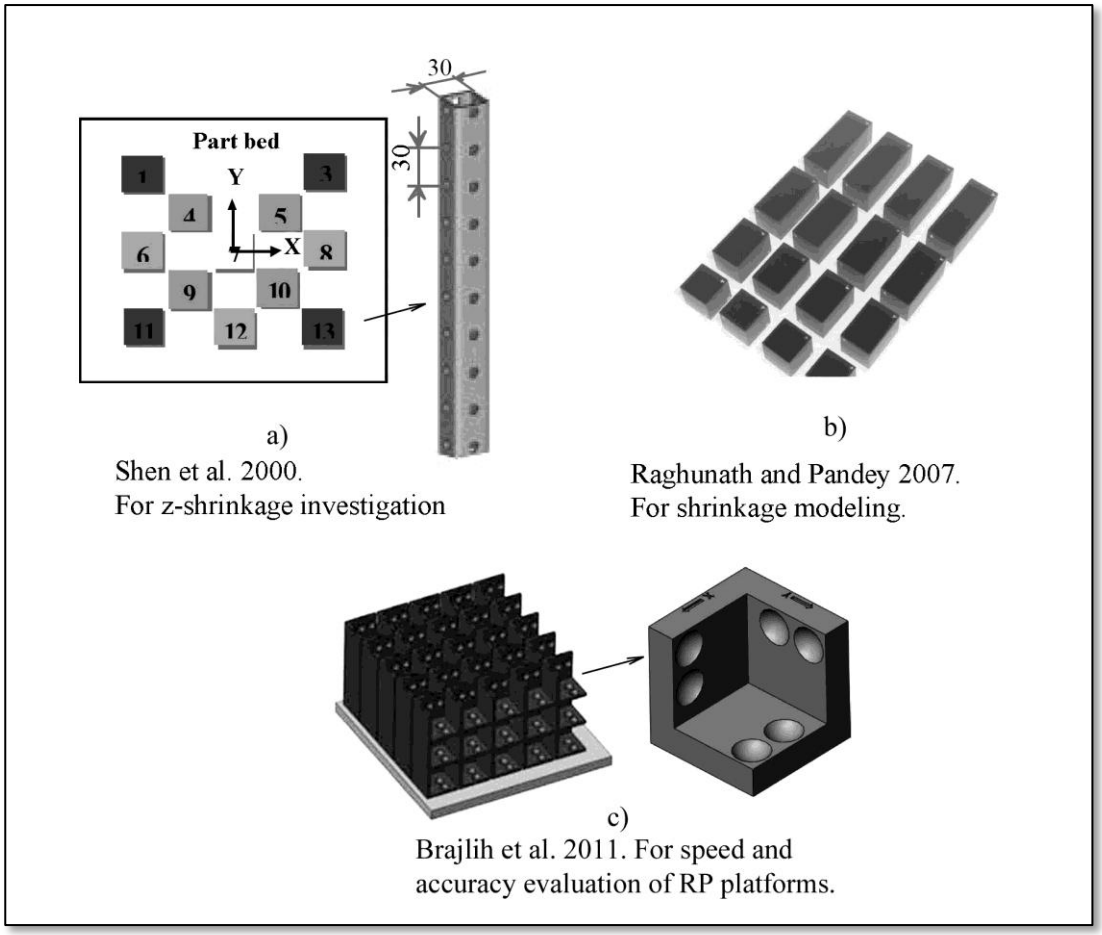

Figure 3.2 Modified pyramid test parts and their arrangement for investigations

3.2.2 Specifically designed test parts (benchmark test pieces)

Overview

These parts feature a variety of simple geometrical elements such as cones, cylinders, ribs, holes, etc. that are designed according to the specific requirements of the research. Investigations are conducted by measurement of the distances and angles between reference points, surface finish, as well as overall appearance.

Examples and literature sources

A typical example of a specifically designed test part is shown in Figure 3.3 (Kruth et al. 2005). The considerations that determine test part configuration are:

- The sloping plane and the rounded corner - to verify the stair effect;
- The presence of the thin plane - to indicate warping and curling;
- Small holes, cylinders and thin walls - for testing the feasible precision and resolution of the process;
- Sharp edges with different angles - to check the influence of heat accumulation at the angle tips and to discover scanning errors;
- The integrated circular and rectangular overhanging surfaces - to prove the possibility of producing overhangs without the need for support structures;
- All geometrical features can be used to measure process accuracy in x, y and z-direction.

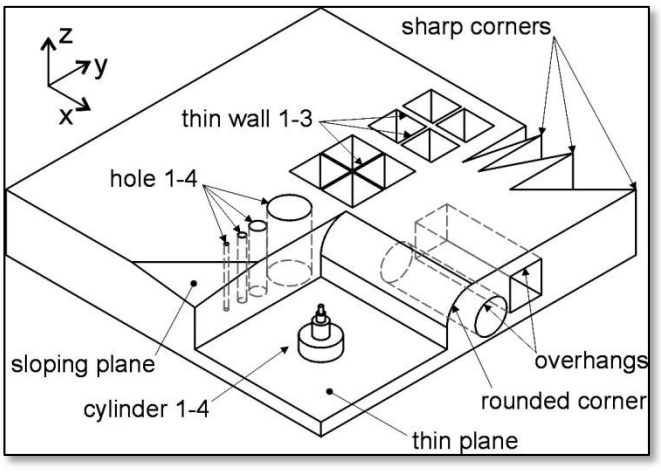

Figure 3.3 Benchmark part for investigation of SLS/SLM processes (Kruth et al. 2005)

A summary of frequently used geometrical features on the benchmark parts and their functions is given in Table 3.2.

Table 3.2 Summary of geometric features and their purposes for benchmarking (Mahesh 2005)

Features	Purpose
Square base [SB]	Flatness and straightness (A base for the other features)
Cube [CB]	Flatness, straightness, linear accuracy, parallelism and repeatability
Flat beam [FB]	Overhang, straightness and flatness
Cylindrical holes (z-direction)[CH]	Accuracy, roundness, cylindricity and repeatability of radius.
Cylindrical holes [CH]	Accuracy, roundness and concentricity
Spheres [SP]	Relative accuracy, symmetry and repeatability of a continuously changing sloping surface
Solid cylinders [SC]	Roundness cylindricity and repeatability
Hollow cylinders [HC]	Accuracy, roundness, cylindricity and repeatability of radius
Cones [CN]	Sloping profile and taper.
Slots [SL]	Accuracy of slots, straightness and flatness
Hollow squares [HS]	Straightness and linear accuracy, also thin wall built.
Brackets [BR]	Linear accuracy, straightness and angle built
Circular holes [CR]	Cylindricity, relative position, roundness and repeatability.
Mechanical features	Efficiency of machine to build special features
Fine features	Ability of machine to build certain features

Benchmarking case studies done by various researches are listed in (Chua et al. 2010). Some examples of benchmark parts that have been used for variety of RP processes and applications are given in Figure 3.4.

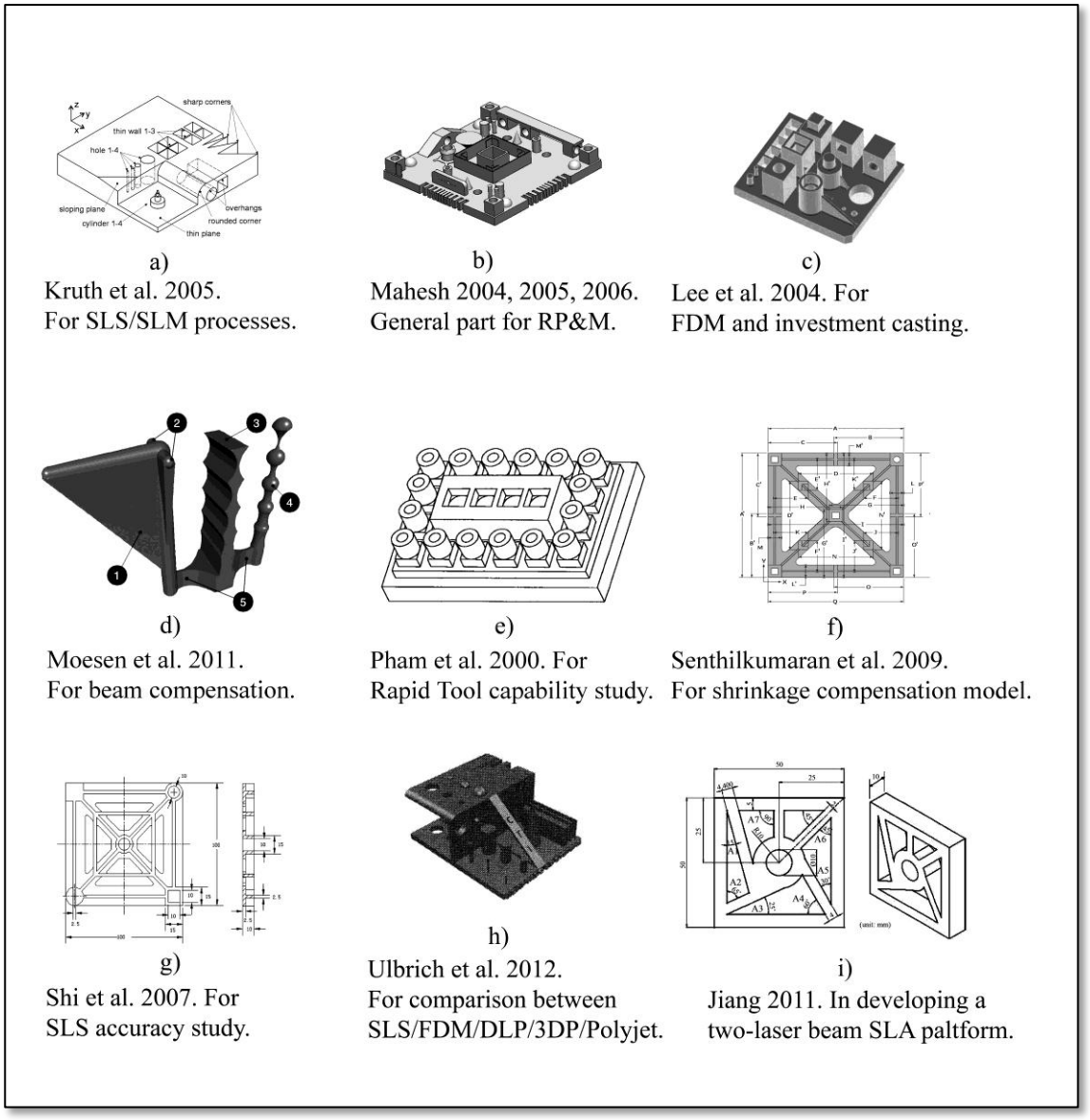

Figure 3.4 Examples of specifically designed benchmark parts

Applications

Benchmark test parts can be used for process limitations analysis, process parameter optimisation, accuracy investigation, staircase effect study, analysis of curling, delamination, surface roughness, orange peel phenomenon, warping, resolution for holes and walls etc. Additionally mechanical tests can be performed on specimens taken from the benchmark parts.

A summary of areas for investigation, by specifically designed benchmark parts is provided in the cause and effect diagram in the Figure 3.5.

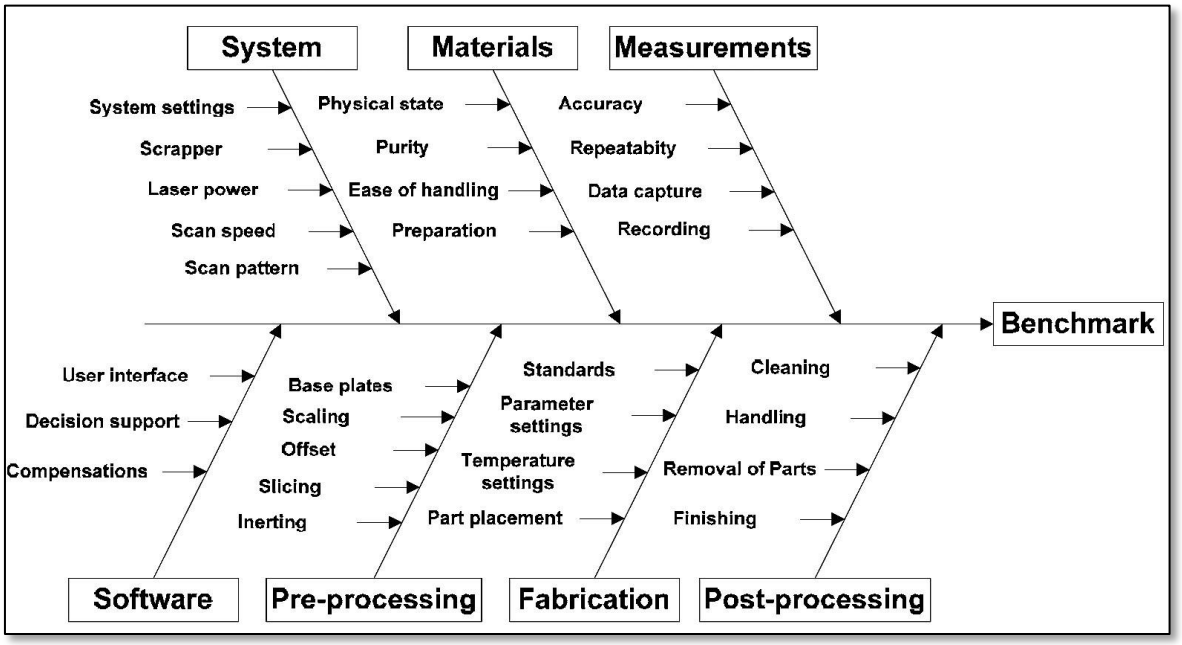

Figure 3.5 Possible causes of problems that can be investigated by benchmark test piece (Mahesh 2004)

Advantages

Benchmark parts allow for more universal applications than other kinds of test piece. They can be designed either for general-purpose investigation, or for investigation of a particular problem; thus one part can be used to study a wide variety of process and/or material phenomenon. The shape and sizes of the features on the part can be flexibly adapted to the process and materials. If a standard test part for RP evaluation is ever to be established it is most likely to be in some form of benchmark part.

Limitations/Disadvantages

A good benchmark part has to be designed according to carefully chosen considerations with respect to the manufacturing process utilised, material and aim of the study. The procedure of part configuration design could be subjective, which limits the possibility of creating a benchmark part with universal applications.

Even though some benchmark parts have been used for comparison of a number of processes, they are not universal with regard to material. For instance the part in Figure 3.4 h) is used for investigation of 5 different processes including SLS (Ulbrich et al. 2012), however it would be unsuitable for polystyrene SLS as overhanging surfaces are problematic for post processing wax infiltration.

Distortions of a particular shape could be considered as a special case rather than as a general characteristic of the material/process combination. For instance curling and warping of the benchmark parts in Figure 3.4 b) were used to "fine-tune" the parameters until the best attainable features on that particular part can be built (Mahesh 2004, 2005, 2006).

The measurement of complex benchmark features can be difficult and exposed to errors; the setting up the reference points and datum(s) for measurement can be a source of errors also and due to complex geometries automation of measurement is also impeded.

The shape of the benchmark parts is usually not simple, thus building and working with many parts for investigation of the entire build chamber is a costly procedure and not always justifiable.

3.2.3 Real part model

Overview

As this approach is the closest to the actual use of the RP platforms it is probably the best approach for general observation but not for complex analysis of different phenomenon and revealing all possible sources of errors. Case studies and illustrations about improvements and developments are usually made using real parts as a test piece. Using a real part can initiate the beginning of a study, as well as a final proofing stage. However all analysis and modifications between these two manufacturing stages is best conducted on a specialised test part. In some specific applications a real part replica is essential to estimate the process accuracy and build time etc. Such bespoke prototypes are typical for medical use. In other medical applications, such as soft tissue facial prosthetics, where aesthetic appearance is more important, the judgement of accuracy and surface quality can be done more successfully by qualitative assessment rather than a quantitative one on a real part test.

Examples and literature sources (Figure 3.6)

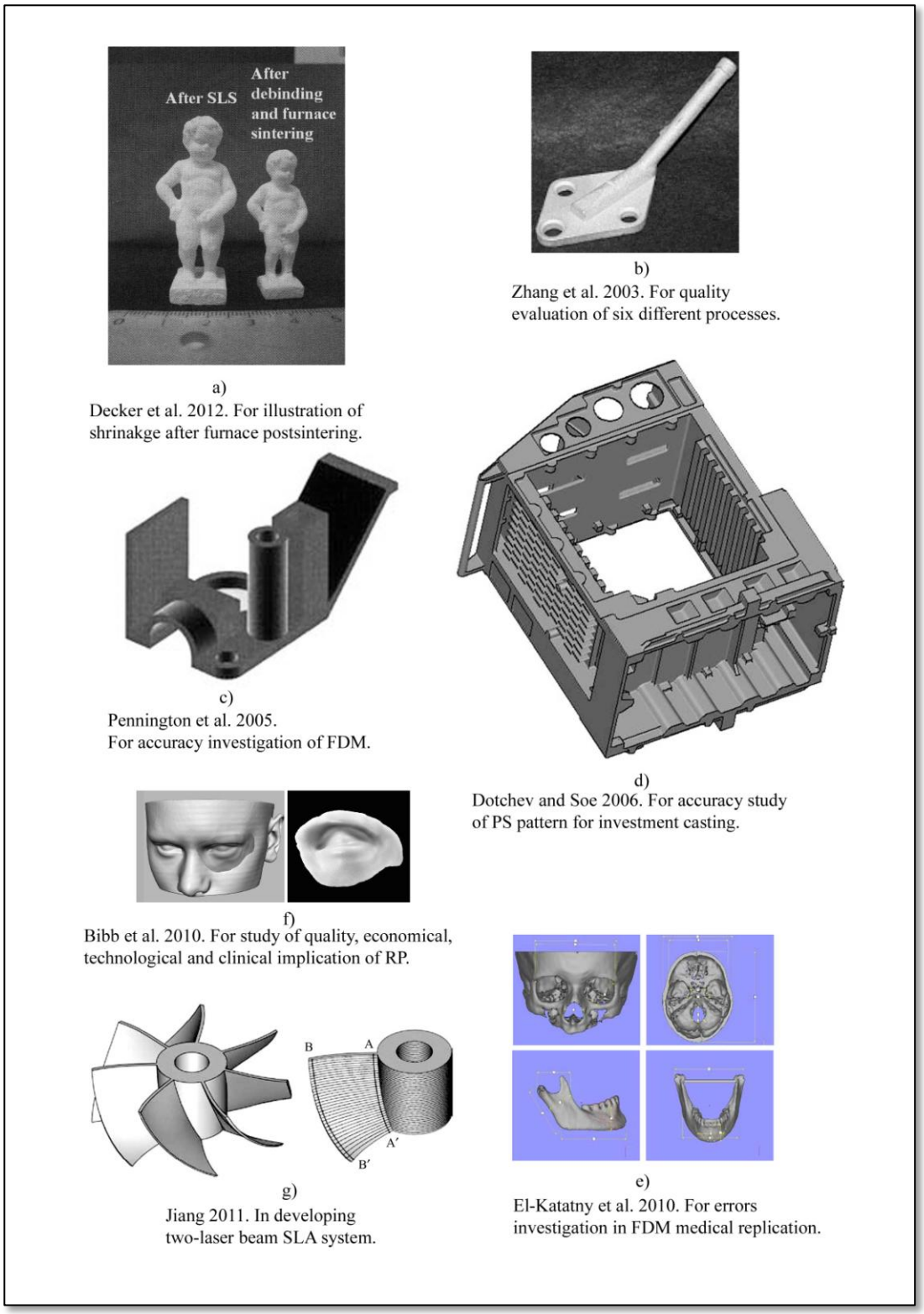

Figure 3.6 Examples of real part used as a benchmark piece in RP

Applications

Study of the process, material or machine using a real part could be a preferable approach, especially if the particular industry targeted is new to the RP domain. Typical examples are medical, jewellery and art applications of RP processes.

Advantages

Results from such attribute tests are fast and easy for interpretation and if a quick conclusion or presentation is required this is the most effective approach. If a big production batch is needed, as in case of rapid manufacturing, the process/material/shape combination is best to be evaluated with a real part test.

Limitations/Disadvantages

General conclusions about the process cannot be made as the results have only a limited validation for the specific test part. Phenomenon that cause inaccuracies are difficult to reveal and analyse. Most real parts are suitable mainly for general observation and important errors could be omitted. Spatial orientation of the part for datum settings before measurement could be awkward.

3.2.4 Parts for surface quality investigation and mechanical testing

This is a variation of specifically designed benchmark parts for surface finish investigation and mechanical properties investigation. For surface study it is important that the test piece allows investigation on planes with different angles

and 3D orientation. Parts for mechanical properties testing usually follow the standard configurations and could also be performed along specific angles of orientation.

Examples and literature sources (Figure 3.7)

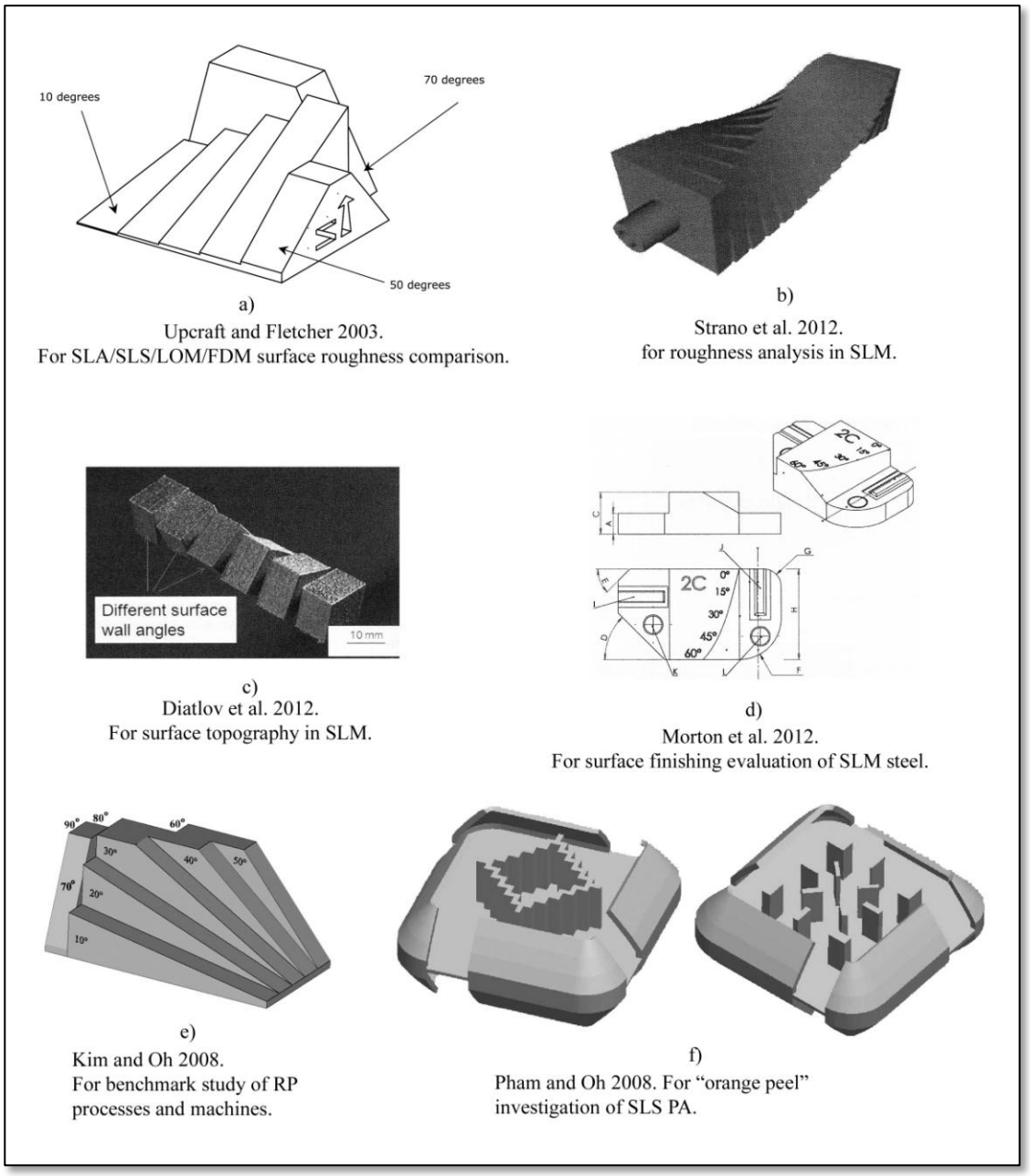

a) Upcraft and Fletcher 2003. For SLA/SLS/LOM/FDM surface roughness comparison.

b) Strano et al. 2012. for roughness analysis in SLM.

c) Diatlov et al. 2012. For surface topography in SLM.

d) Morton et al. 2012. For surface finishing evaluation of SLM steel.

e) Kim and Oh 2008. For benchmark study of RP processes and machines.

f) Pham and Oh 2008. For "orange peel" investigation of SLS PA.

Figure 3.7 Examples of test parts for surface roughness and morphology study

3.3 Analysis of the disadvantages of the pyramids for shrinkage, scaling and accuracy study

As mentioned in the previous paragraphs one of the main objectives of this research is to study the important drawbacks when pyramid test parts are used for process accuracy investigation and geometrical component compensation. These drawbacks require a more detailed analysis which is presented in this section.

Pyramidal (staircase) style test parts (Figure 3.1) have been utilised in a large number of experimental studies on RP process accuracy. They are the most universal and widely used test parts in the FF domain as was proven by the literature review as well as the observed in house commercial practise. They are also recommended by equipment manufacturers and followed by other RP bureaus, SMEs and research organisations. These practices were also implemented worldwide by numerous industrial and research partners of the author who were involved in EU research networks such as SARE, FASTFAB, 4M, EUMINAFAB, COTECH etc. The methodologies that utilise this type of test piece are based on measurements of the staircase dimensions and calculation of the material shrinkage and corresponding x, y, and z scaling factors. The results are sometimes used for research purposes to evaluate the distribution of part distortion along the build volume. The practice shows that significant errors in the manufactured part could occur if the scaling values obtained from pyramid test are incorrect. The potential sources of such incorrect data and misleading data interpretations are described below.

Analysis of the directional errors when using pyramid type of test parts

The measurement of lengths between pyramid steps in the *y*-direction is shown in Figure 3.8. The idea of such measurements is usually to determine the difference between the nominal dimension l_n and the final dimension l_f (produced by the machine) usually called the error (*E*). It can be expressed by:

$$E = L_f - L_n \qquad (3.1)$$

Where:

E– error,

L_f – actual length,

L_n - nominal length

As discussed in Chapter 2 there are substantial variations in accuracy over the part bed (or build chamber), which is the reason for changing the position of the features and feature lengths to be measured. It means that the ***distribution*** of errors *E* varies over the part bed defined as a plane (*x, y*). In other words the error is a function of two variables (*x* and *y*):

$$E = f(x, y) \qquad (3.2)$$

If the shrinkage were homogeneous, then relative error would be constant and only one length measurement for *x*, *y* or *z* would be sufficient for investigation. In general practice it is important to know the length changes either in all directions (producing a map of entire field of distortions) or in some particular directions.

The pyramidal shape can only be used for an unidirectional investigation and does not allow for a choice of direction; it is constrained according to a pre-set shape, which is an inconvenient restriction.

As illustrated in Figure 3.8, the direction in which the pyramid stairs advance is the "**actual** direction" that is investigated for error distribution, which may not necessarily be the "**desired** direction" for investigation. Failure to observe this correctly can result in misleading directional results. When the lengths m_i are measured, each step is shifted in a direction defined by the angle α:

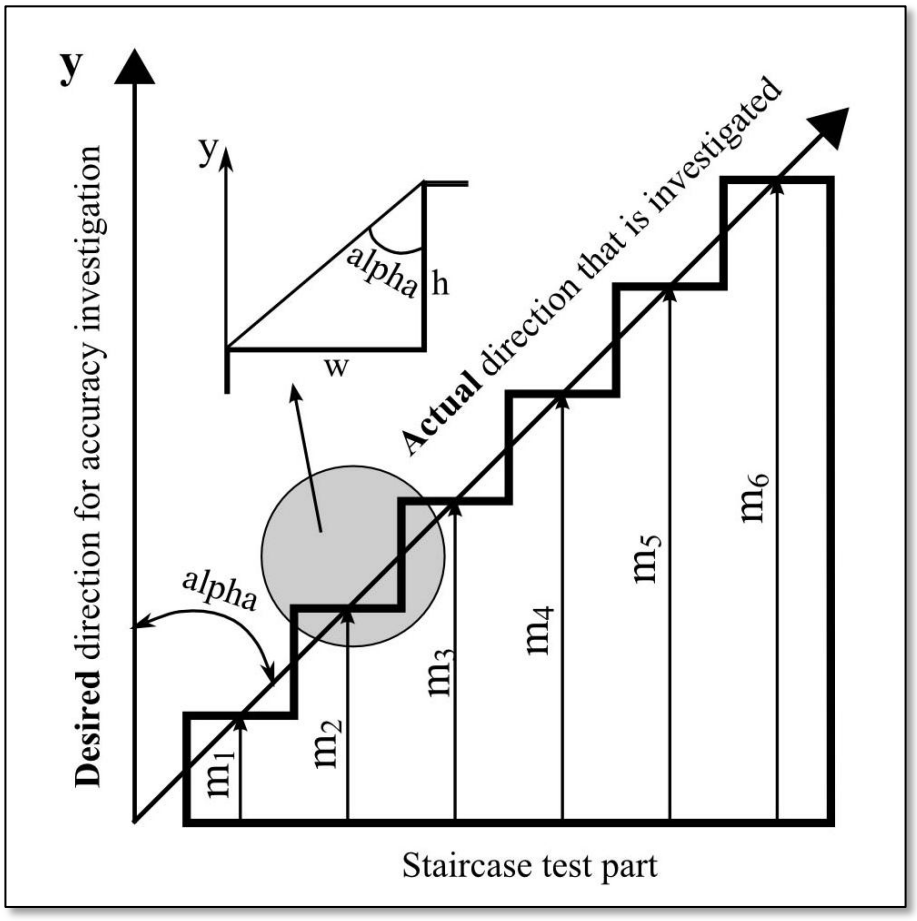

Figure 3.8 Lengths and directions for measurements of pyramid shape test part

$$\alpha = \tan^{-1}\left(\frac{w}{h}\right) \quad (3.3)$$

where:

w - width of the step,

h – height of the step.

The measured lengths m_i are step-arranged in the same α direction. As a result instead of analysing distribution of *y* direction inaccuracy, the measurements give data along the "**actual** direction" inclined by the angle 'alpha'. The "actual direction" is determined from the ratio of the pyramid step *w/h*. In a similar manner, using the perpendicular landings of each step, the pyramid can be used for the calculation of inaccuracies in the *x* direction. Again the obtained results have to be assigned to the "**actual** direction" instead of the "desired direction" (*x*).

The total rate of change of the function (3.2) that describes the error distribution in the part bed plane is given by:

$$dE_{xy} = \frac{\partial E}{\partial x}dx + \frac{\partial E}{\partial y}dy \quad (3.4)$$

A length change in *y* direction only of the error function (3.2), when *x = const*, can be expressed as partial differential. In an engineering case, a change of length in *y* direction of a final element with size (Δx x Δy) can be expressed by:

$$\Delta E_y \cong \frac{\partial E}{\partial y}\Delta y \quad (3.5)$$

For illustration purposes the geometrical interpretation of ΔE_y is depicted by the line "1" on the Figure 3.9.

Similarly a length change in *x* direction only of the error function (3.2), when *y* = *const*, can be expressed by equation (3.6) and depicted by line "2" on Figure 3.9:

$$\Delta E_x \cong \frac{\partial E}{\partial x}\Delta x \qquad (3.6)$$

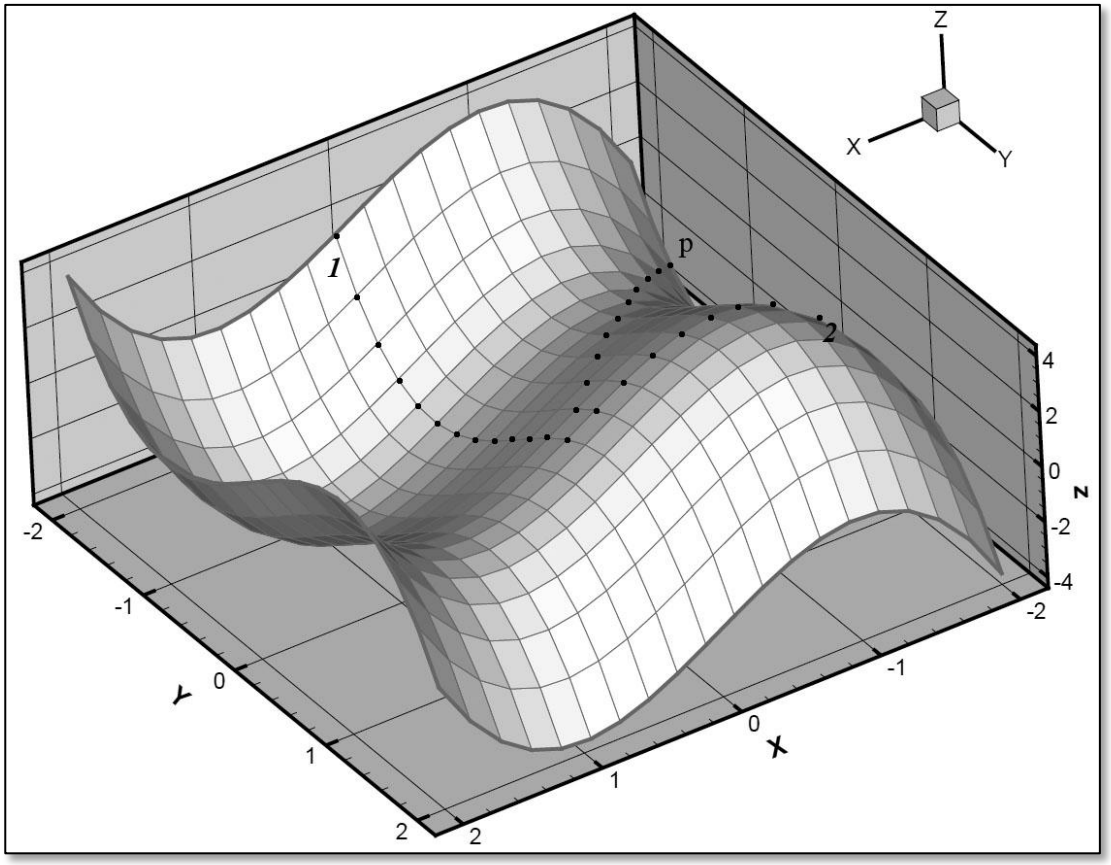

Figure 3.9 Illustrative picture for possible error distribution

When a pyramid test-part is used, the distribution of length changes calculated as described above, are in a direction depicted by the line "*p*" on the Figure 3.9. The trend of the changes in this direction could be significantly different from the

trend in *x* or *y* direction. Hence any conclusions about trend of length changes in direction *x* and *y* are not valid.

In the case of the most popular pyramid shapes (a, b, i) on Figure 3.1 the extent of misleading results is increased. The results of measurements from such pyramids give an error distribution along a direction perpendicular to the investigated direction as the angle defined by the pyramid is $\alpha = 90^{o}$.

Most notably, should the misleading directional results be used for scaling parts in order to compensate shrinkage, there is still the potential for error. The scaling results and accuracy is improved by implementation the more reliable, proposed methodology is described in details in Chapter 5.

The only way to eliminate the issue of misleading directional results is to make the angle $\alpha = 0$ (formula 3.3) this could be achieved by the use of a modified pyramid test part (such as that depicted in Figure 3.2 a). However this approach does not eliminate the next disadvantage - limited scope of the investigation.

Limited scope of investigation.

Both the pyramid and the 'pole/bar' type test parts (as shown in Figure 3.2 a) give results that analyse inaccuracy along a single direction only. The test piece in this respect is ineffective as it occupies a large area giving limited output data. If a bigger part or bed/chamber area has to be investigated, then modified pyramids are a better choice (Figure 3.2). Using this type of test piece and methodology design provides a more holistic picture for strain distribution, since

multiple test pieces are built over the entire part bed. Additional disadvantages of such a testing approach are the required time, price and labour for the experiment. These may not be justifiable and reliability would not be satisfactory.

Measurement and calculation issues.

In all cases of accuracy investigations on RP processes considered by the author the application of specific test pieces stipulates a specific metrology approach to the measurement of dimensional deviations. The types of entity that can be calculated on the bases of pyramid measurements are either: the total error of a given length or the error within the step increment. This is illustrated in Figure 3.10.

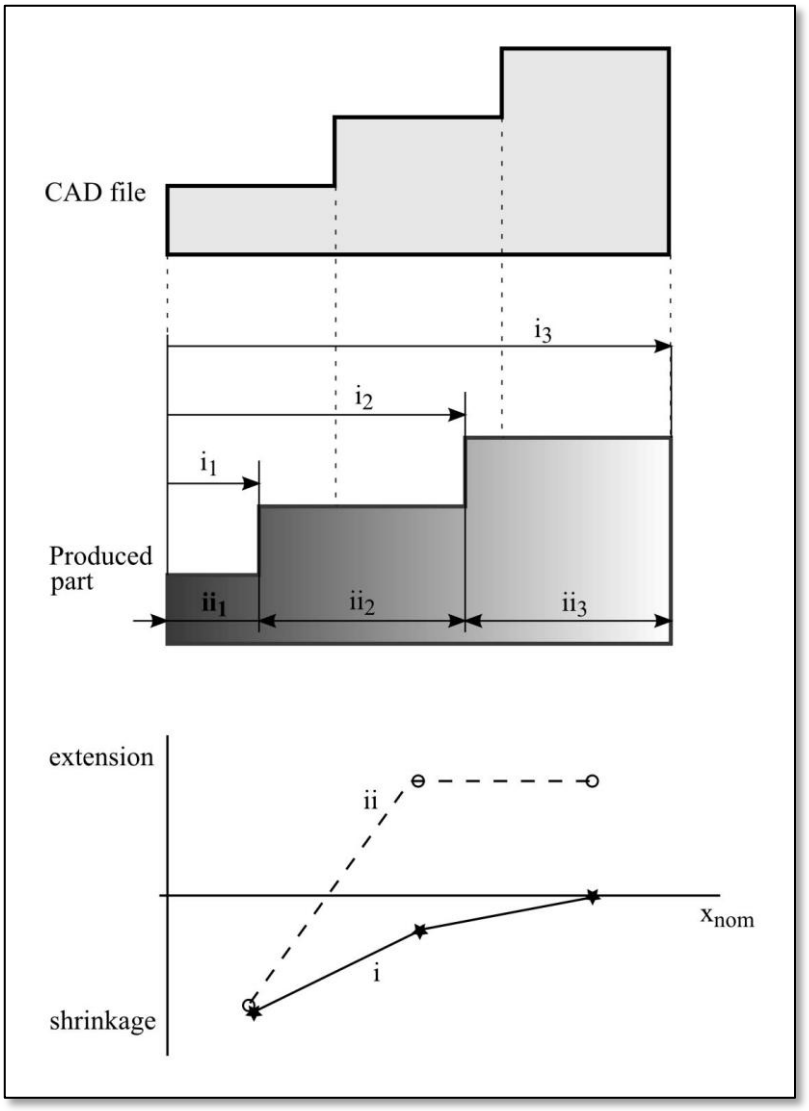

Figure 3.10 Type of measurement and corresponding result for distortion. (i) - total lengths to the step; (ii) change of the step length (delta)

The measured error of a given length (i) is widely used and this is justifiable in the cases when simple factors (or one single factor) are (is) affecting the accuracy besides acting in the same direction (e.g. shrinking). A typical example is the study of thermal (or phase transformation) effects of many RP processes where the error in x and y directions are studied, taking into account only the shrinkage error-causing factor.

If more complex factors (for example acting in different directions – shrinking and extension) are involved in part distortion (e.g. z-build or curling, laser parallax error or tessellation problems etc.) and the research is done according to (i) then the important error distribution can be concealed and hence the proper analysis of the error source(s) is not possible. An example of this situation is the accuracy study in *z* direction of SLS processes, which is a subject of more detailed analysis in Chapter 5 of this thesis.

Assuming that the distortion of different parts of the test piece, built in different areas of the part bed are different (shrinkage and extension) then the measurements of the change in step lengths (ii) is more informative. An illustration of this is depicted in Figure 3.10 where all results from (i) are shrinkages although only the foremost left segment shrinks while the second and third segments are equally extended. For this reason misinformed decisions about scaling and achievable accuracy could be made. Obviously the more uneven the distortion of the part the more prominent the difference between the two kinds of measurements would be.

The general conclusion from the information and analysis presented in Section 3.3 and Section 3.2.1 could be summarised in the following statement:

Although pyramids are very useful in daily and express practices, the inherent limitations and drawbacks of pyramidal geometries could be a source of significant misleading, if a comprehensive accuracy investigation relies on the results from pyramid test parts only.

3.4 Summary and conclusions

The test parts illustrated in Section 3.2 have their specific advantages such as the capability of analysing all three axial dimensions simultaneously and simplicity in handling and post-processing, but could also encompass several limitations and disadvantages that need to be targeted for improvement. These disadvantages may be summarised as follows:

(i) Investigating accuracy by measuring the lengths on step shaped parts introduces inaccuracy, as the land measured on each step requires a directional shift. This approach can therefore give a misleading distribution of results along the desired direction, since the data obtained actually varies with the angle of inclination for the required directional shift, which in most practical cases is of no use. Examples of test parts manufactured with a pyramidal or stepped geometry are shown in Figure 3.1;

(ii) The popular test pieces analysed in this chapter do not present continuous distribution of the distortions over the entire part bed or build chamber as the area covered by test part is usually limited or the number of reference points for measurement is small;

(iii) If the described methodologies are used the study of process accuracy within the entire build volume would require a great number of test pieces;

(iv) The results from measurements performed on the studied test pieces are not generic and relate to a specific part size or shape;

(v) The routine acquisition of automatic measurements and data processing are not always possible due to the complex geometry of the samples;

(vi) The initial settings of the coordinate system and datum for part measurement are complicated and the results could be sensitive to the settings.

The question arises: 'Does a test part and methodology for accuracy investigation that overcomes all existing disadvantages exist?' The current answer to the proposed question is that a test part does not exist. Thus it is evident that there is scope and a necessary requirement for improvement.

Problems due to improper scaling caused by pyramid test parts have been encountered a number of times, particularly in regard to the z direction. The most typical examples in this study were associated with tall SLS polystyrene parts that were manufactured (with regards to industrial practice) at the Manufacturing Engineering Centre at Cardiff University.

Similarly a significant amount of curling inaccuracy effects was observed in RP processes such as SLA, SLS, FDM and μSLA. The extent, magnitude and distribution of this phenomenon in both the vertical and horizontal directions were also not easy to quantify. A number of questions regarding dimensional accuracy exist concerning process chain tolerances and capabilities that can be solved if

reliable and consistent accuracy investigations are performed for each process in the chain.

Inaccuracies in components can be caused by various complex factors such as the method of manufacture, specific build platform used, the material type, component size and post-processing procedures including handling etc. These factors lead to different distortion phenomenon such as shrinkage, elongation, bending and curling. On that basis it can be concluded that a more generic description of deviations in dimension and shear displacements of the manufactured part compared to the CAD model that can reveal size and shape inaccuracy is needed. The value and sign (+/-) of such deviations and their distribution in different directions could be conveniently used for accuracy studies as well as for part tolerancing at the design stage and component realisation. The pyramid shape test part cannot be used effectively for this purpose.

Based on the presented analysis of sources of uncertainties and limitations of test parts, the conclusion can be made that a generic and reliable method for accuracy study is needed. The method should overcome the drawbacks of the most popular pyramid test parts and provide data about the type of distortions that parts could exhibit after FF manufacturing. The method should also provide comprehensive information about the distribution of errors of the process for investigation and along the entire working (build) volume of a platform.

The development and implementation of a Grid Method (GM) for accuracy investigation in RP and other manufacturing processes is presented in this research (next Chapter 4). It was initiated from the issues mentioned above.

A more detailed analysis of inaccuracy distributions and the causes of uncertainties are given in the following chapters after the development, adaptation and specific implementations of GM for studying RP and MNT (micro & nano technology) processes.

CHAPTER 4 GRID METHOD AS A TECHNIQUE FOR INVESTIGATION OF THE DEVIATIONS IN SHAPE AND DIMENSION

The need for better analysis of component manufactured using FF resulted in the formation of the GM. The initiation of this method in the area of RP accuracy investigations is a new approach and its development was a main objective of the presented research. Its aim was to give more generic and accurate descriptions of inaccuracies of RP processes and produced components. This is one of the contributions of this research.

This chapter describes the basic concepts and main components of the GM methodology and the steps required for its implementation. The definitions of the formulae used to describe the deviations in terms of strains (both linear and angular) are given and the methodology of measurements and the calculations applied are presented. All descriptions and particularities are concisely presented in Figure 4.8 considering the process steps in form of flow diagram, from design of the test part to the application of the GM method and utilising the obtained data for manufacturing parts with improved quality.

As shown in Chapter 2 the inaccuracies in produced components can be caused by various complex factors such as the method of manufacture, specific build platform used, the material type, component size and post-processing procedures including handling etc. These factors lead to various types of distortions, such as shrinkage, elongation, bending and curling, all of which influence final part

accuracy. The existing geometrical deviations from the nominal dimensions and shape can be classified as linear and angular. They are characterised by the following attributes:

- *sign:* plus or minus (+/-), that identifies an increase or decrease of the entity of interest (length or angle);
- *direction:* along which the deviation is calculated;
- *magnitude of deviations:* calculated by defined formula.

In general terms the manufactured part can be considered as 'deformed' in relation to the nominal design. The term 'deformed' here is used only figuratively since the stresses are only one of the various factors that influence the resulting inaccuracy, however the final strains (relative to the nominal dimensions) can be measured and considered as a geometrical representation of the dimensional and angular deviations from nominal. They could be calculated by the same formula as the traditional strains but will be referenced in this research as linear and angular deviations. The next section specifies the formulas and the characteristics that are used elsewhere in the research for process accuracy characterisation.

4.1 Basic definitions of strains as linear and angular deviations from nominal

A *Geometrical* definition and calculation of the term *strain* was adopted in this research to support a geometrical description of part distortion. Other terms that are used elsewhere in RP domain in reference to part inaccuracies are shrinkage, error, percentage deviations per unit length and rarely the angular deviations are mentioned. To provide greater clarity of the distortions the part is

undergoing, linear and angular deviations from nominal in small areas can be calculated the same way as strain calculations would be in mechanics of solids. The aim of this Section is to clarify that the term strain is used for more generic descriptions of size and shape deviations, of a part or a section of a part.

Regardless of the cause, it can be assumed that the change of dimensions or shape of a body manifests itself in the same geometrical appearance as strain. Pure body motions such as translation or rotation do not cause the body to change its shape and thus no strain is encountered. (Mielnik 1991). Strain is defined as being *linear* or *shear (angular)*.

The linear strains can be defined and calculated as *engineering strains* (ε_E) or as *true strains* (ε). True strains can also be called *logarithmic* or *natural* and engineering strain can be called *nominal* strains (Hosford and Caddell 1983). The linear true strain ε is defined as the ratio of change in linear dimension to the instantaneous value of the dimension:

$$\partial\varepsilon = \frac{\partial l}{l} \tag{4.1}$$

$$\varepsilon = \int_{l_0}^{l} \frac{\partial l}{l} = ln\frac{l}{l_0} \tag{4.2}$$

Where l is the instantaneous length and l_0 is the initial (nominal) length.

The linear engineering strain ε_E is defined as the ratio of the change in length to the original length of the same dimension:

$$\varepsilon_E = \frac{\delta}{l_0} = \frac{\Delta l}{l_0} = \frac{l - l_0}{l_0} \tag{4.3}$$

Where l is the final length and l_0 is the original length. l_0 later refers to the nominal length.

Engineering strains often provide more meaningful results, by representing results as percentages.

Although there are mathematical differences in calculation between the two types of strains it should be noted that for strains of small magnitude the two definitions give identical values (Dieter 1988). The example from Table 4.1 gives ratios of the true to engineering strains (Hosford and Caddell 1983):

Table 4.1 Illustrative example about similarity in values between true and engineering strains

Engineering strain in %	Ratio of true to engineering strain
$\varepsilon = 0.001 = 0.1\%$	$\frac{\varepsilon_E}{\varepsilon} = 0.9995$
$\varepsilon = 0.01 = 1\%$	$\frac{\varepsilon_E}{\varepsilon} = 0.995$
$\varepsilon = 0.02 = 2\%$	$\frac{\varepsilon_E}{\varepsilon} = 0.990$
$\varepsilon = 0.05 = 5\%$	$\frac{\varepsilon_E}{\varepsilon} = 0.976$
$\varepsilon = 0.1 = 10\%$	$\frac{\varepsilon_E}{\varepsilon} = 0.953$

The values from the Table 4.1 illustrate that the two definitions of strain give nearly identical values for relatively small strains. For up to 5% engineering strain the ratio is still very close to 1 and the approximation $\varepsilon_E \approx \varepsilon$ can be

considered acceptable. 5% is the maximum range of relative errors in size for parts produced by most RP technologies and on that basis both calculations of strains are equally suitable.

An advantage of describing the inaccuracy of parts manufactured by FF processes, in terms of strains, is the possibility it allows to combine analysis of linear and angular deviation from nominal. The angular change in a right angle is known as *shear strain* (γ) and is defined as the change in angle between two line segments which were previously mutually perpendicular. Engineering shear strain is the total shear strain. Figure 4.1 illustrates the shear (angular) strains in case of *pure* shear which is defined as:

$$\gamma = 2\tan\theta \tag{4.4}$$

In the general case of shear deformation γ_x and γ_y can be calculated separately by the segments a, b, c and d (Figure 4.1).

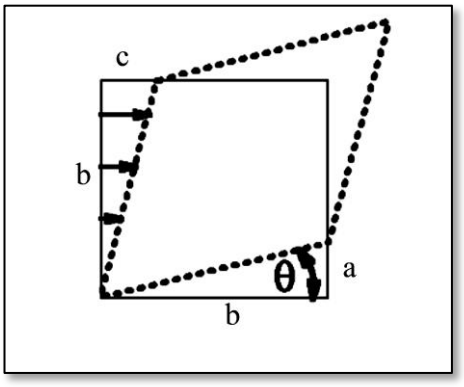

Figure 4.1 Shear strain illustration

The Grid Method (GM) described in the next Section 4.2 gives approximated calculations of true strain at an area so small that it could be considered as a

point. The strain concept of extension and shear strain at a point is illustrated on Figure 4.2. The geometrical relations show strains at the point "A" if the nodes "ABCD" transform to "abcd". Linear and shear strain at a point are calculated by formulas:

$$\gamma = \frac{\partial u_y}{\partial x} + \frac{\partial u_x}{\partial y} = \gamma_x + \gamma_y \tag{4.5}$$

$$\varepsilon_x = \frac{\partial u_x}{\partial x} \tag{4.6}$$

$$\varepsilon_y = \frac{\partial u_y}{\partial y} \tag{4.7}$$

Where: ε_x is linear strain in direction *x*; ε_y is linear strain in direction *y* and γ is shear strain.

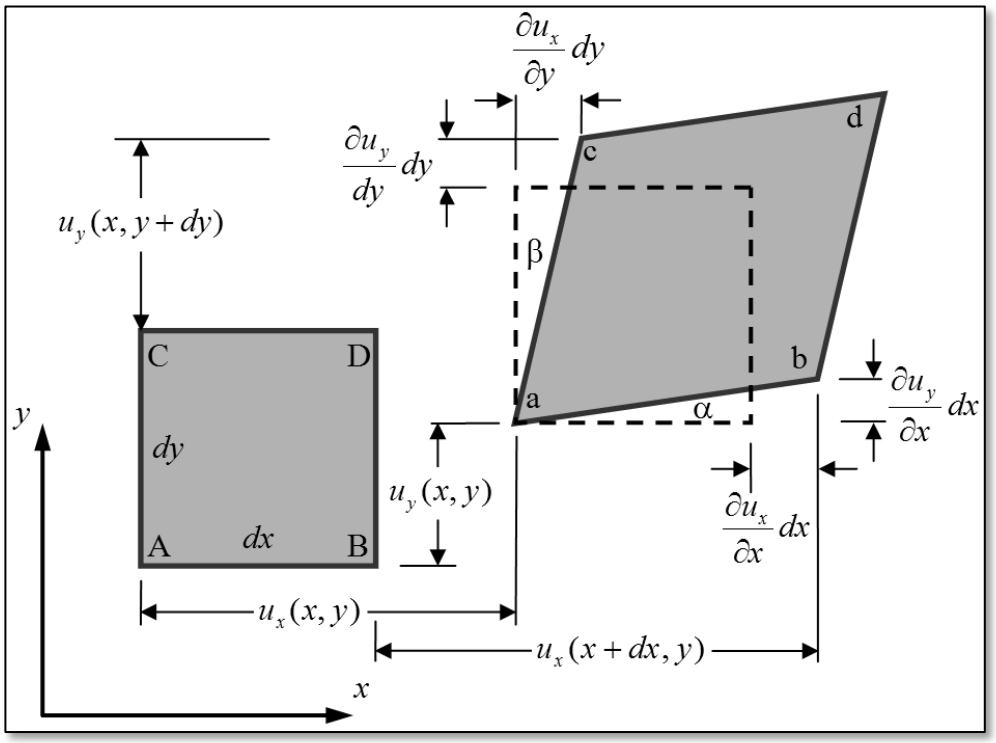

Figure 4.2 Plain strain involving small distortions (Mielnik 1991)

4.2 The concept of the Grid Method for calculations of linear and angular deviations from nominal

The analysis methodology is based on examining linear and shear strains at many points throughout a test piece - in the form of a flat plate. To expose the strains, a square grid is applied to the CAD model of the test piece beforehand. After the plate is manufactured the actual grid is measured and compared with the CAD model. As the produced grid differs from the nominal CAD grid it can be considered as deformed and therefore the strains calculated. Several ways to estimate the strains of a deformed object are known, however the Coefficient or Square Grid Method is utilised here since it has been proven as the most effective (Dankert and Wanheim 1979; Gagov et al. 1995). This method was introduced by Bredendick in (Bredendick 1967, 1969) and has been implemented in metal forming analysis but not in the FF sector.

The initial vectors $\vec{1}$ and $\vec{2}$ in Figure 4.3 represent the nominal part (i.e. the CAD model) and upon part realisation these become vectors $\vec{1}'$ and $\vec{2}'$. The strains due to the manufacturing process in the region of each intersection point "P" of the grid can be calculated from the coordinates of these vectors, which are denoted as follows:

$$\vec{1} = (x_1, y_1) \quad \text{after processing becomes} \quad \overrightarrow{1'} = (x_1', y_1'); \tag{4.8}$$

$$\vec{2} = (x_2, y_2) \quad \text{after processing becomes} \quad \overrightarrow{2'} = (x_2', y_2'). \tag{4.9}$$

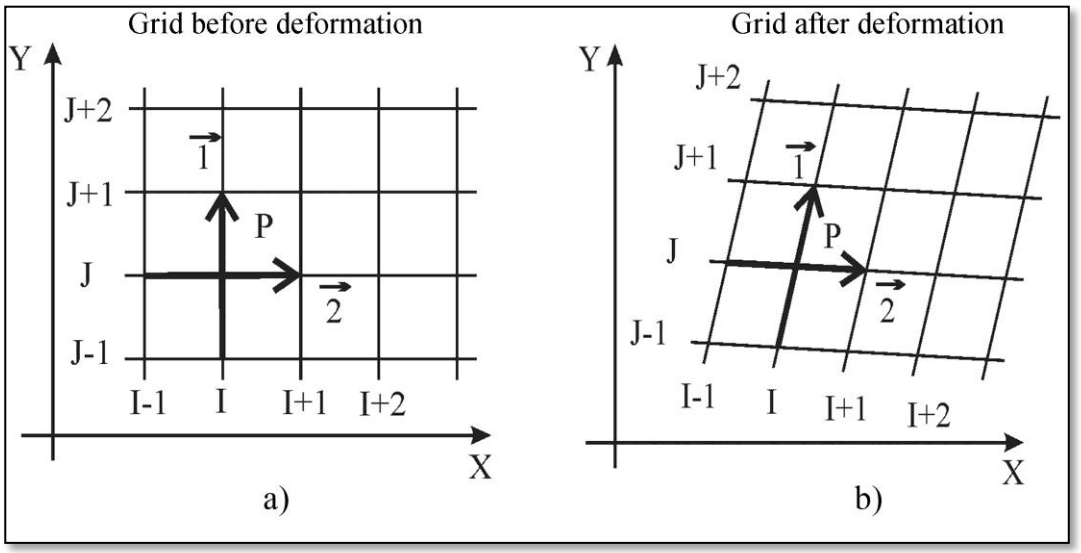

Figure 4.3 Square grid: a) - before processing and b) - after processing

The linear strains ε calculated by the method are true (logarithmic) strains. The agreement with engineering strains is pointed in Table 4.1 and Section 4.1.

The shear strains γ are defined as the change in angle between two initially perpendicular lines through a point. In the case of described method this is the angle between the vectors $\vec{1}$ and $\vec{2}$.

The strains at point P after the processing are given by the following relations (Bredendick 1967, 1969):

$$\varepsilon_x = \ln f + (c_{11} - c_{22})/2fq \quad (4.10)$$

$$\varepsilon_y = \ln f - (c_{11} - c_{22})/2fq \quad (4.11)$$

$$\gamma_x = c_{12}/fq \quad (4.12)$$

$$\gamma_y = c_{21}/fq \quad (4.13)$$

Where:

$$c_{11} = (x_1' y_2 - x_2' y_1)/D \quad (4.14)$$

$$c_{21} = (y_1' y_2 - y_2' y_1)/D \quad (4.15)$$

$$c_{12} = (x_1 x_2' - x_2 x_1')/D \quad (4.16)$$

$$c_{22} = (x_1 y_2' - x_2 y_1')/D \quad (4.17)$$

$$D = x_1 y_2 - x_2 y_1 \quad (4.18)$$

$$f = \sqrt{c_{11}c_{22} - c_{12}c_{21}} \quad (4.19)$$

$$B = (c_{11} + c_{22})/2f \quad (4.20)$$

$$q = \frac{\sqrt{B^2 - 1}}{\cosh^{-1}(B)} \quad \text{when } B > 1; \quad (4.21)$$

$$q = 1 \quad \text{when } B = 1; \quad (4.22)$$

$$q = \frac{\sqrt{1 - B^2}}{\cosh^{-1}(B)} \quad \text{when } B < 1; \quad (4.23)$$

The calculated strains could be any pair of ε_x, ε_y, and ε_z depending on the test plate orientation during processing (Figure 4.4).

One advantage of such a methodology is the simple geometry of the test-part - a plate with square grid. The plate can be arbitrary in size and location within the build chamber (Figure 4.4). It is also suitable for handling and automatic measuring as well as being representative of various engineering parts.

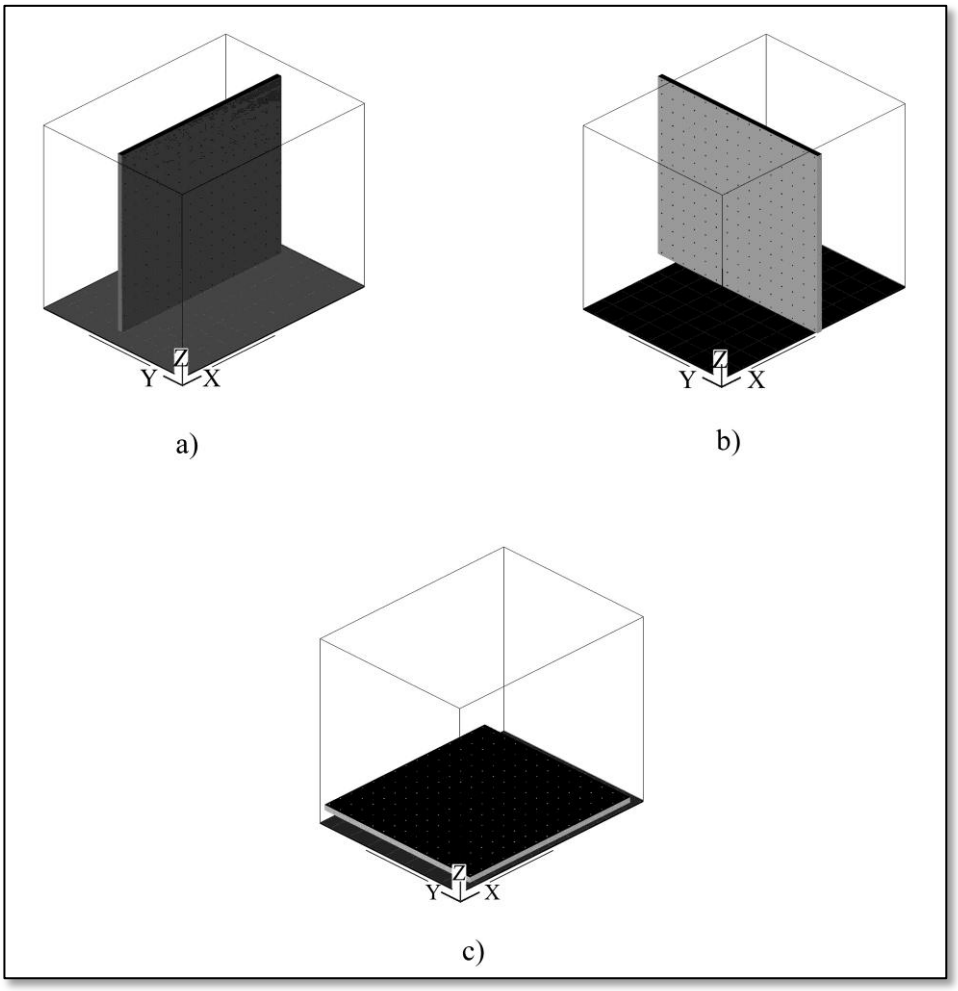

Figure 4.4 Examples of plate orientation in the build platform for investigation of dimensional deviations from nominals in different directions

4.3. Methodology for Grid Method implementation in the study of the RP processes

Depending on the direction(s) of the dimensional and angular deviations to be investigated, the rectangle plate test part can be oriented vertically, horizontally or in any other direction as well as being positioned in different areas of the build chamber (Figure 4.4). If the plate is built horizontally the deviations ε_x and ε_y (Figure 4.4c) can be determined, if positioned vertically then either ε_z and ε_x (Figure 4.4a) or ε_z and ε_y (Figure 4.4b) can be calculated. By building a set of plates with a given orientation and in different positions in the build chamber, a three dimensional concept and model of the distribution of dimensional deviations over the entire build envelope can be created.

The test plate geometry consists of through holes, which represent the grid intersection points as illustrated in Figure 4.3. The plate has to be built with no scaling in x, y and z directions if the possible inaccuracy of the process without correction is to be investigated. After building the test part, it has to be cleaned and the holes cleared of material following the procedure recommended by the platform producer and associated operator experience.

A coordinate measuring machine (CMM) can be used to automatically measure each hole centre coordinates with an optical probe (Figures 4.5 and 4.6). For the purpose of this research, specialised software was developed to set the datum, coordinate axis and to control the objective measurement movements of the CMM (the program code is given in Appendix 1).

The measuring procedure follows these steps:

- adjustment the optical parameters (lens magnification, brightness, contrast, focus);
- set the datum point;
- align the axis;
- start automated measurement of the reference points;
- save the data.

One advantage of such a methodology is that the hole centres can be measured routinely, within minutes, after the initial datum point and axis are set. The setting and the screenshot of the measuring software window are shown in Figure 4.5 and 4.6.

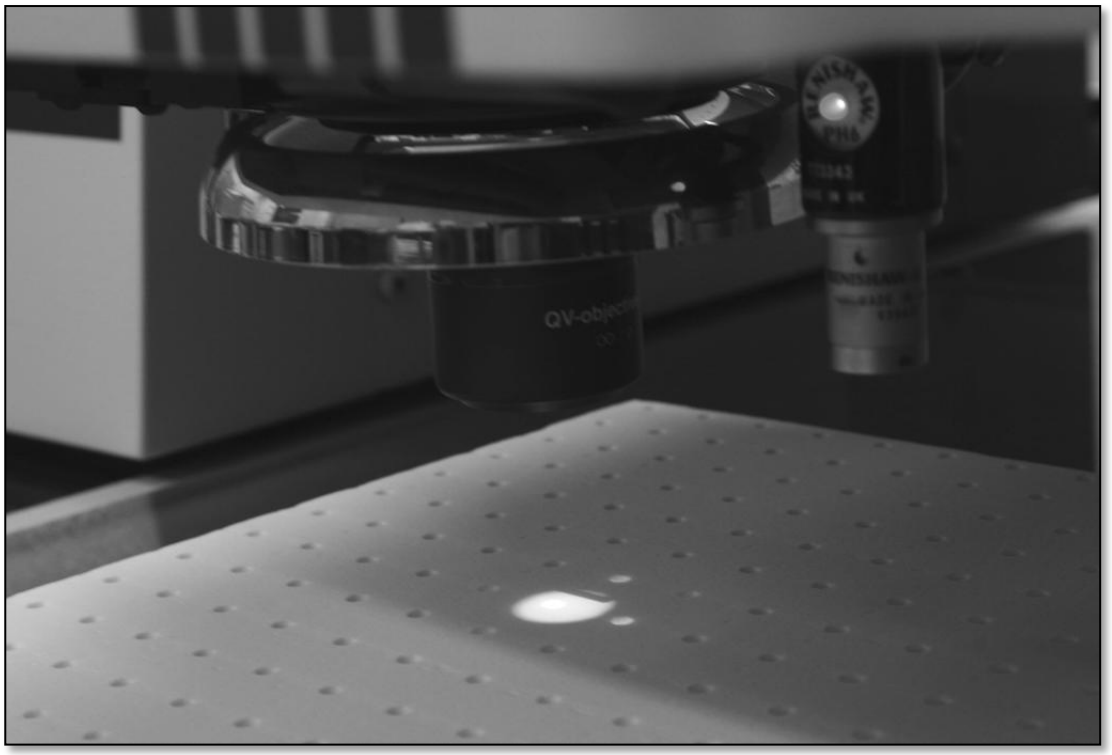

Figure 4.5 Picture of plate measuring process

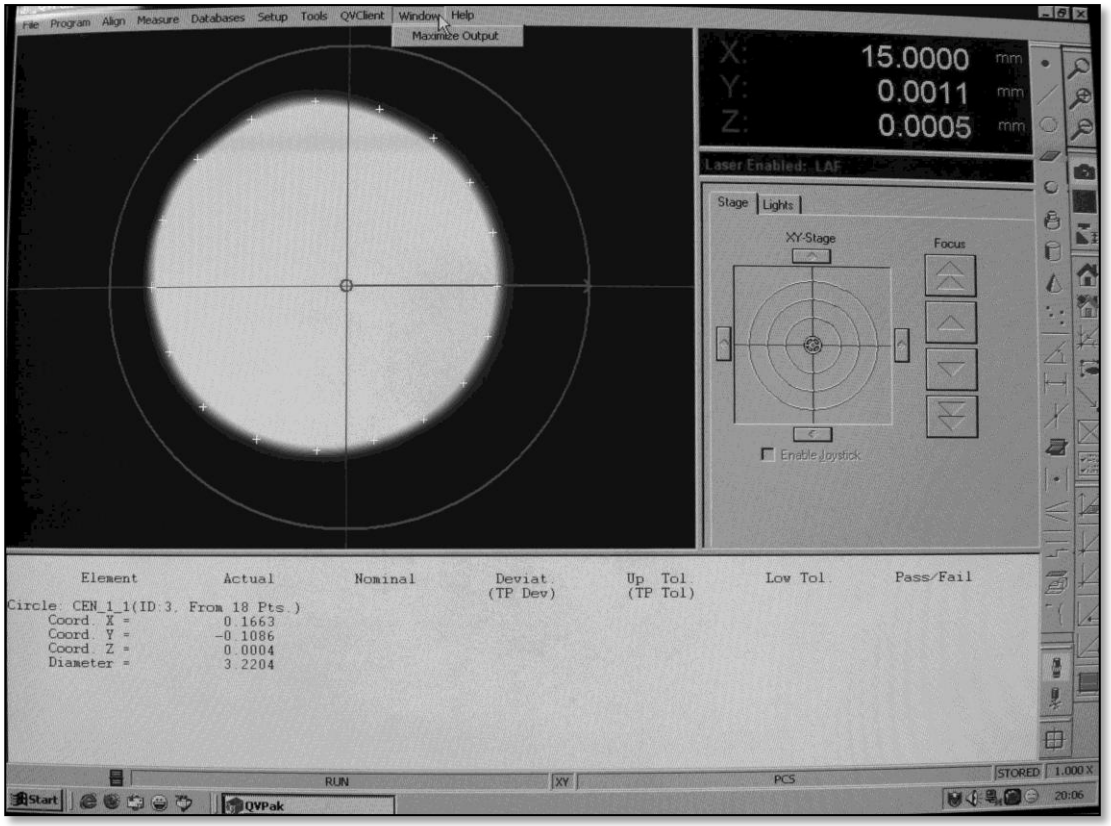

Figure 4.6 Screen shot of the Mitotoyo QuickVision *Pro* software window

The measured *x* and *y* coordinates of all hole centres, which represent a grid point after processing, are saved as a file together with their nominal values from the CAD file. This data is used as input data for linear and angular deviations from nominal calculations in a specially created MS Excel spreadsheet program. Calculations of linear ε and shear γ deviations are carried out according to the formulas for strain calculations described in Section 4.2. The next step in data processing includes a specialised MatLab program that was also created in this research. The role of the MatLab software is to analyse the results and generate a 3D visualisation of the distributions of linear and shear deviations over the part surface. The next step of the software route is to correct part geometry by applying some compensation value for process distortion. This could involve

either CAD software, specialised RP software (Magics RP) or the CAM software of the platform. The main components and steps sequences of the methodology are depicted on Figure 4.8.

4.4 Test plate geometry considerations

An important element of the methodology was the determination of test plate dimensions and geometry of the grid features used as reference points. This was the first step in methodology implementation as depicted on Figure 4.8 in the block "Design of the test plate". The overall sizes of the test part were determined by the area and volume that were the subject of accuracy investigation as well as the objectives and desired precision of the study. All test plate dimensions are governed by three critical parameters:

- the grid *density* (step or cell size),
- the hole *diameter* and,
- the plate *thickness*.

Determination of an optimal plate configuration may require some preliminary experiments and trials using the previous experience as a starting point. The above parameters could depend on:

- the process to be examined,
- equipment used,
- build material,
- area of building chamber for investigation,
- aim of research etc.

The appropriate grid *density* can be established by taking into account:

- the specific application of the methodology,
- the total build size,
- the technical specification of the platform,
- the chosen strain deviation between the neighbouring cells,
- additional specific to the investigated process considerations, e.g. material properties (viscosity, strength etc.)

A test piece for studying the SLS processing of Polystyrene (PS) is given below as an example for practical determination of the critical plate characteristics.
The grid *steps* were determined to be 15 mm between hole centres, for investigation of the total build chamber. This step size gave a continuous graphical representation of the process accuracy and a practical, usable data set.

The most appropriate hole *diameter*, for the same PS material and process as above, was found to be 2.2 mm. Larger hole sizes do not correspond to the circular measuring tool shown in Figure 4.6 as it exceeds the viewfinder range. Conversely, if the hole is too small then cleaning and opening of the holes is impeded as the powder inside the hole partially sinters due to the increased temperature of the enclosure and consequently some damaging of the hole edge may take place, potentially increasing the error of the measurement.

Trials with different plate *thicknesses* showed that the thinner the plate, the easier it was to clean and open the holes. However SLS polystyrene is a weak, porous

material (to allow for wax infiltration) as its main purpose is for investment casting patterns. For the large overall plate size of (x = 225mm; z = 330mm) the manageable thickness was found to be at least 8 mm. This thickness is also representative for the purpose of PS SLS components as sacrificial patterns for large body type investment casting parts.

The implementation of this method for other materials and RP technologies such as Micro Stereolithography (μSLA) would require different dimensions to the above. However the considerations and underlying theory would remain the same. The details for the test plate geometry applied to study other processes and materials are given in Chapter 6.

4.5 Non-process related errors

Some unpredictable sources of errors can contribute to excessively large deviations of strains at a particular point on the grid. In common consideration, such sources can be regarded as not typical of general process accuracy. Examples of such sources are:

- local contamination of the build material;
- temporary halt of the build process;
- software interpolation error;
- damaged holes due to cleaning and holding etc.

In such cases the values of strains can be averaged to the strains in the neighbouring grid points. To implement this, any problematic hole was detected and its coordinates changed according to the adjacent hole coordinates, as shown in Figure 4.7. The assumption is that the hole initially lay on the intersection point of the diagonals will remain on the intersection point of the same diagonals after the approximation.

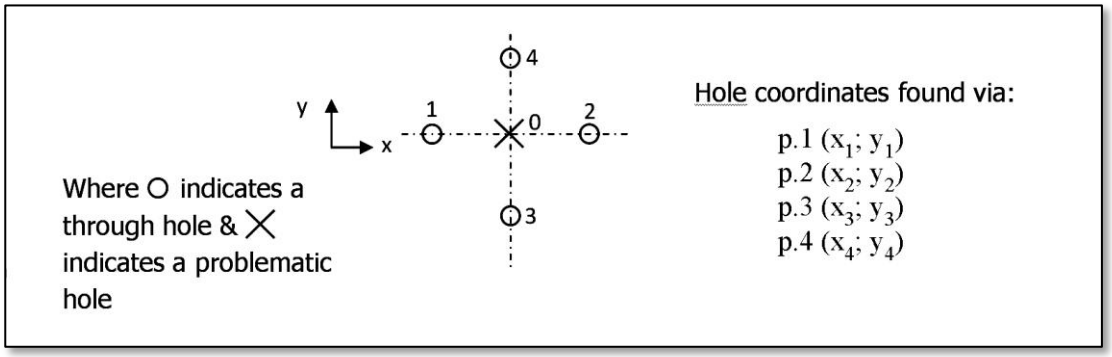

Figure 4.7 Method of averaging the coordinates of the problematic holes

The number of the reference points on the test-plate could be very large in order to produce smooth representation of strain distribution. This increases the probability of non-process related errors occurring.

A typical example of non-process related errors is damaged grid features for measurements on the test-plate (hole, pin, cross). The hole for instance may not be formed concentrically or blocked by the post process cleansing. In these cases the above-described procedure for averaging could be applied.

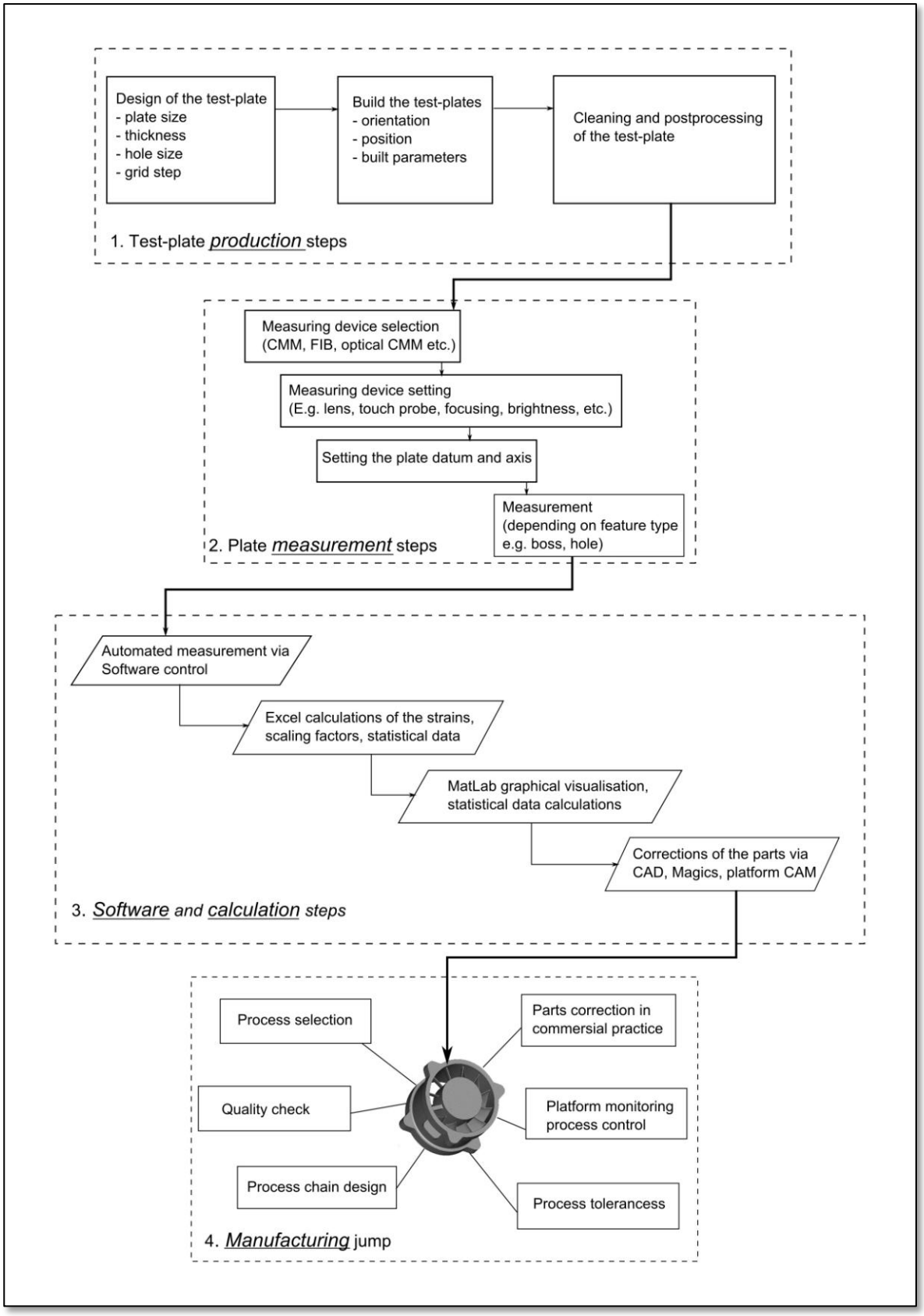

Figure 4.8 Process flowchart for the GM methodology

4.6 Accuracy analyses and statistical validation of the plate measurement method

A statistical approach was applied to validate and analyse the uncertainty of the proposed experimental methodology and the cause of potential errors. The main objective was to estimate the uncertainty in the plate measurement and to compare it with the uncertainty in the strains of a studied process.

Initial tests were conducted to determine the sufficient number of measurements required to obtain acceptable consistency of the results. After conducting five measurements an adequately small standard deviation of 0.0005 (confidence level less than 0.05) and a confidence interval of 0.0003 for strain calculation in a randomly selected cell were achieved. On that basis five measurements was considered sufficient to determine the measurement variations in all validation experiments described below. In addition these five experiments proved that the results obtained for measurement were normally distributed.

The variability of the measurements in this methodology manifests itself in a number of ways. The Measurement System Analysis (MSA) will address the following issues (Bicheno and Catherwood, 2005):

(i) The *accuracy* of the measurement system (optical or other) that was used to measure the grid. The absolute error in the utilised optical CMM measurement equipment (optical + mechanical systems) according to the manufacturer (Mitotoyo Quick Vision *Pro*) specification was 1.5 µm which is negligible (<

0.05%) compared to the measured distances, which was in the range of 2.5 to 15 mm.

(ii) The *repeatability* of the measurements of the distance between the centres of the holes. The repeatability of the measuring system depends on the CMM equipment and the software that approximates the hole contours. Since the errors from CMM are negligible compared to the measured values it will be salient to investigate only the repeatability of the software to determine if the contour of hole is consistently measured each time. If there are significant deviations in the approximations of the hole contours this will lead to errors in estimation of the positions of their centres and unreliable strain calculations.

A plate with overall dimensions of (x=165mm; z=225mm) mm was used for the validation process. This plate generated a matrix of 165 through holes (ϕ=2.2mm), at a centre distance (also referred to as step size) of 15mm apart (Figure 4.9). The plate was measured 5 times after it had been positioned and oriented without further movement. ε_x and ε_z were then calculated for the existing 140 grid cells after each subsequent measurement. In order to apply a conservative approach (the worse accuracy scenario) the cell with the highest value of variations in calculated strains was chosen for repeatability evaluation of measurements. The results of measurements without part movement are shown in Table 4.2 in the columns “no move”.

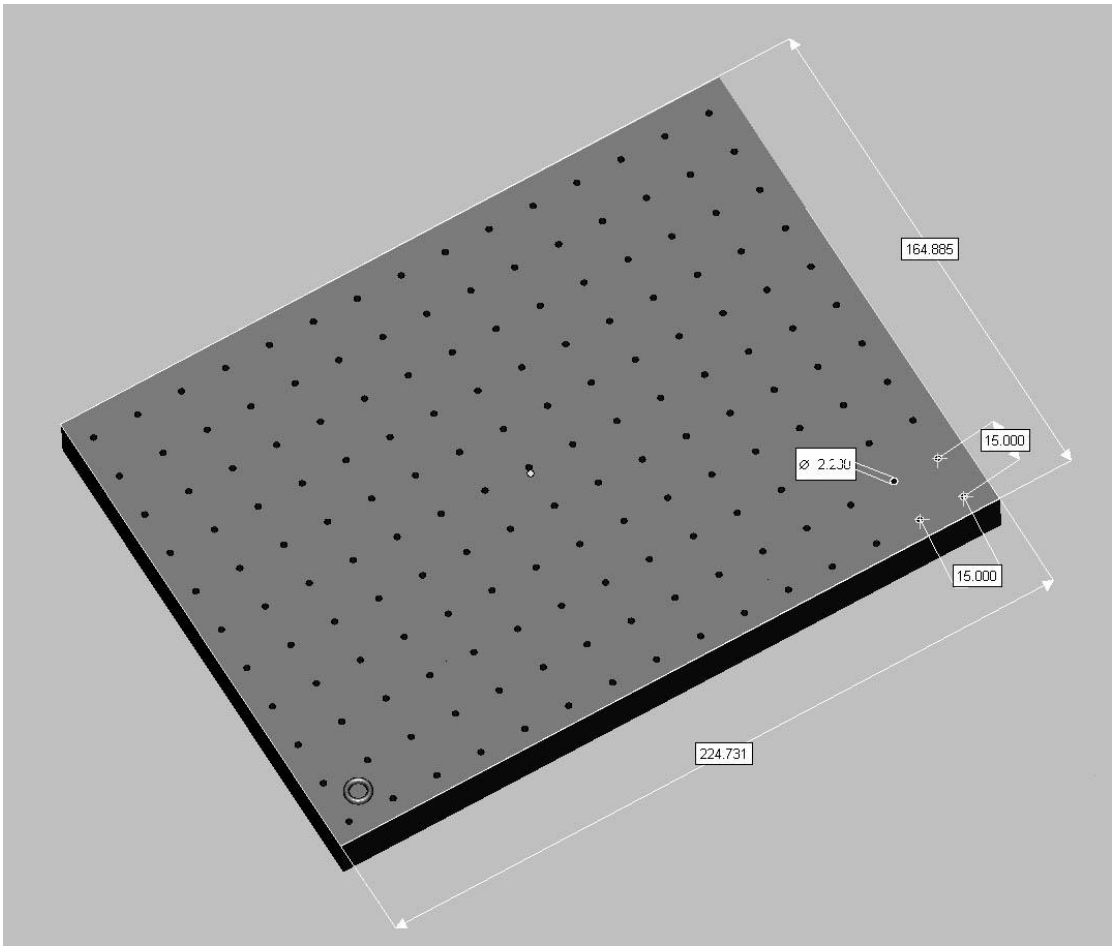

Figure 4.9 Plate for statistical validation of measurements

Table 4.2 Statistical results for strain calculations

	ε_x no move	ε_z no move	ε_x with move	ε_z with move
Number of measurement:	5	5	5	5
Average strains:	0.018	0.024	-0.014	0.021
Standard Deviations (σ):	0.00057	0.00018	0.00067	0.00049
Range:	3.3E-07	3.1E-08	4.5E-07	2.5E-07
Prediction:	0.0011	0.00063	0.00095	0.00063
Error in %:	6.3	2.6	6.9	2.9

(iii) ***Reproducibility*** of the system. The orientation and location (plate positioning and initial settings) of the plate before measurement required validation since the CMM requires a manual setup to define a datum point and coordinate axis orientation before beginning the automatic measurement process. The consequence of these procedures would define the sum of the repeatability and reproducibility (total) variations of the system especially when different operators perform measurements. The variation of the calculated data was estimated after each setting and measurement performed by a different operator and they were considered as *total measurement variations*.

A similar statistical approach as in the repeatability evaluation was carried out, this time moving the plate and setting it up each time before it is measured. The results of measurements taken after part movement are shown in Table 4.2 in the columns "with move".

To calculate the reproducibility component ($\sigma_{reproducibility}$) of the measurement deviations the following formula was applied:

$$\sigma^2_{measurement} = \sigma^2_{repeatability} + \sigma^2_{reproducibility} \quad (4.24)$$

Where:

$\sigma_{repeatability}$ is the standard deviation when the plate is not moved,

$\sigma_{measurement}$ is the "total" standard deviation when the plate is moved.

If the maximum deviations for strains ε_x ($\sigma_{repeatability}$ = 0.00057 and $\sigma_{measurement}$ = 0.00067) are taken from Table 4.2 the overall value of the deviation due to the reproducibility factor would be $\sigma_{reproducibility}$ = 0.00035. This proves that the reproducibility component in the measurement deviation is significantly smaller than the repeatability component of the measuring process deviation, proving that the methodology is relatively independent from a measurement set up context. More over the total variation of the measurement system was proved to be very low. Furthermore the confidence interval calculated by $\sigma_{measurement}$ (confidence level 0.05) would be 0.00059 which is two orders of magnitude smaller than the absolute values of the average strains, presented in Table 4.2 (strains could be positive or negative).

The values of the strains determined in all experiments conducted in this study do not exceed 0.03 (3% engineering strain). From Table 4.2 and presented estimations it can be seen that the variations in the measurements are at least two orders of magnitude smaller than the measured quantities, which in turn makes the errors acceptable compared to the total errors of the examined processes.

Therefore, it can be concluded that the measurements are reliable and the dependability of the methodology is proved.

4.7 Summary and conclusions

1. This work has shown that a single GM test piece and routine measurement procedure can be utilised to estimate the distribution of linear and angular deviations from the nominal sizes of FF fabricated parts. The calculations of the above entities can be done in a similar way to the geometrical characteristics of the strains developed in solid mechanics.

2. The geometry of the utilised test piece has advantages over the stair case (pyramid) type test pieces since it gives correct data about inaccuracy distribution along a particular direction or particular axes. This is in contrast to the stair case where each measuring landing is located in different places of the part bed.

3. When compared to the popular test pieces analysed in Chapter 3 the GM methodology can present the continuous distribution of distortions over the entire part or build chamber. Furthermore these results can be achieved with a single test piece.

4. Statistical validation of the methodology has been completed, showing that the variations in the measurements are at least two orders of magnitude smaller than the measured quantities. This is considered to mean that the errors are acceptable compared to the total errors of the examined processes. Therefore, it can be concluded that the measurements are reliable and the dependability of the methodology is approved.

5. The routine automatic measurements and data processing are easily achieved due to the simple geometry of the samples. The initial settings of the coordinate system and datum for part measurement are not complicated and the test results are less sensitive to the settings compared to the conventional test-piece approach. The fundamental reason for this advantageous of GM is that the strains are estimated on measurement of the difference in distances or angles rather than measurements of their absolute values. This also means that the methodology is less sensitive to the systematic errors of measurement equipment.

CHAPTER 5 GRID METHOD ANALYSES AND MODELLING OF THE GEOMETRICAL DISTORTIONS IN THE SLS PROCESSES

The need to understand the SLS process phenomena that can result in distortions of manufactured components and implementation of the GM for calibration and process accuracy improvement were the main motivations behind the development of the presented methodology.

For many years the SLS processes were studied and attempts were made to improve the consistency of the quality in produced parts. This improvement is imperative for the efficiency of SLS as a mature manufacturing process. Therefore the investigation of the process by means of the developed GM methodology was one of the main objectives of this research.

Polystyrene (PS) SLS material was chosen as a target for accuracy investigation because it is one of the most commonly used materials in RP practices, despite the numerous problems attributed to the complexity of the production process chain. With regards to commercial interest in this material during the last 10 years, the total share of orders received by the Manufacturing Engineering Centre (MEC) for PS SLS produced parts ranged from 15% to 30%-35% of the total number of orders; proving the significant commercial interest to this material. Moreover there are many studies on this technology that provide a basis to compare the effectiveness of the developed GM methodology. It is intended that the GM method, once shown to be effective, can be applied to other processes.

5.1 Overview of Selective Laser Sintering of Polystyrene powder

Polystyrene material for SLS processing is best known by its trade name Castform. The material is used to crate patterns for investment metal casting - Figure 5.1. 'Green' parts produced by SLS are low density with approximately 45% of the density of the solid material. Users then infiltrate the green patterns with foundry wax. Wax fills the pores of the parts, making them strong enough for handling, finishing, shipping, casting tree preparation and embedding. The material does not require significant modifications to the foundry equipment and procedures in respect to the common foundry practice of burning the wax patterns. It also has very low residual ash content (<0.02%). All this makes polystyrene SLS patterns behave much like the most desired investment casting material - wax. The material is amorphous and during the sintering process is subject to rheological deformations due to high temperature and weight pressure.

In selective laser sintering of the polystyrene powder there are numerous unsolved accuracy problems; notably the problem of dimensional accuracy along the lengthwise vertical (or *z*) direction. In this direction the component dimensions are nonlinearly distorted and distributions of dimensional deviations within the total build volume are not always clear. This impedes proper part scaling for dimensional compensation, which is crucial for final accuracy. Since this task is rather challenging some researchers find that the only possible way around the problem is to produce a preliminary mock part and measure it, correcting the machine scaling parameters accordingly for the next trial (Dotchev et al. 2007). Such an approach could easily double the lead time and cost.

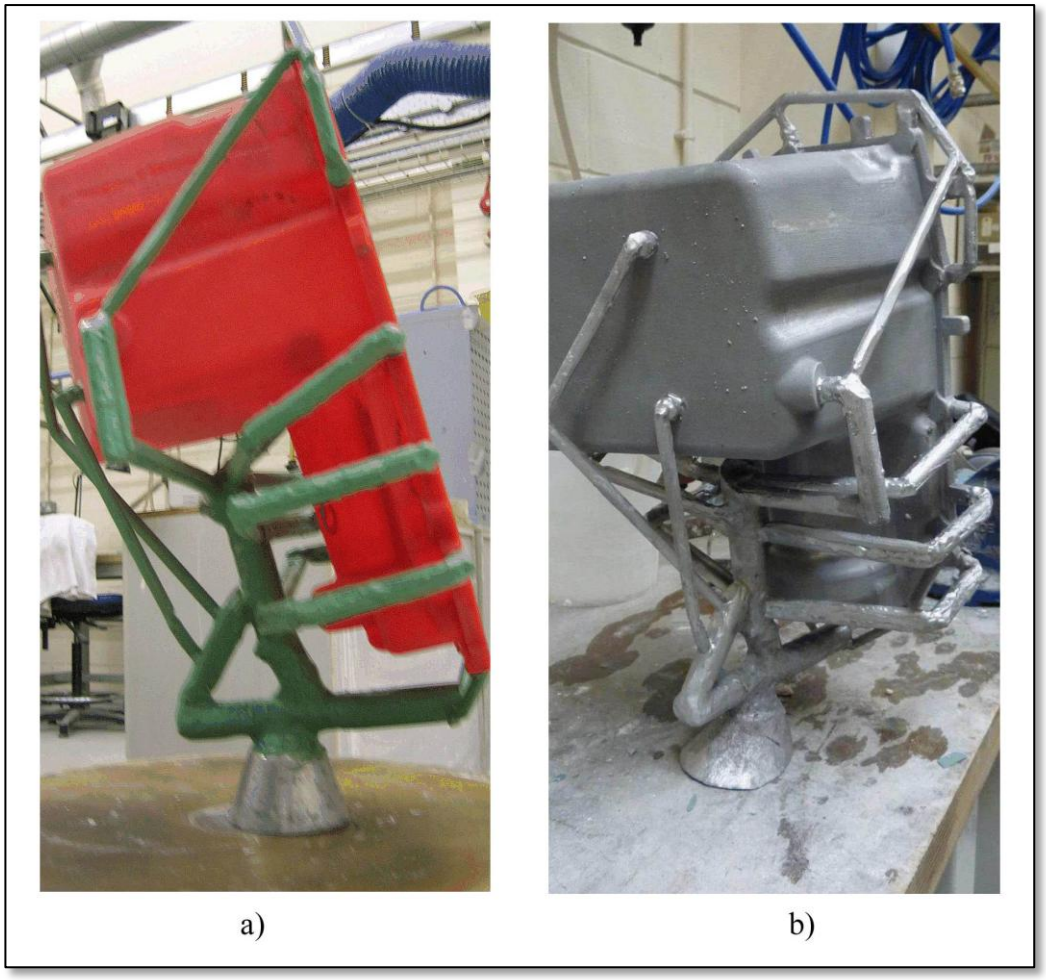

Figure 5.1 a) Casting tree with infiltrated Castform pattern; b) final metal casting

The distortions induced in the RP parts in the vertical direction of the building process are caused by various sources analysed in paragraph 2.1. More specifically in the context of SLS of PS, the most influential source of error is shrinkage. The variations in shrinkage depend of factors such as:

- total build height;
- part height;
- part shape and wall thickness;
- part arrangement in the build;
- sintering parameters and variation in temperature.

The final part might be correct in overall height, yet usually exhibits more shrinkage in lower sections, less or none at some levels, and may even show, paradoxically at first glance, elongation in upper sections as the author's experience suggests.

In general, as considered in this chapter, the term shrinkage does not accurately reflect the complexity of the expected part inaccuracies. The prediction and determination of part distortion and taking into consideration of wax infiltration post-processing additionally complicates achieving the desired accuracy. Some versions of RP machine software allow users to apply nonlinear scaling as a formula with *x, y* and *z* as variables. This option cannot be utilised effectively until the type of distortions and their directional distribution are investigated and quantitatively measured.

The aim of the research described in this chapter is to investigate dimensional and shape inaccuracies in SLS PS by calculating the linear and angular dimensional deviations from nominal by means of calculating the respective strains using the GM.

The GM method for studying the above RP material and manufacturing method, can be implemented in analysing the following suggested areas:

(i) process accuracy and precision study;

(ii) analysing of sources of errors;

(iii) scaling factors calculation;

(iv) assessment of curling and other distortion phenomena;

(v) comparative studies of different processes;

(vi) facilitating process chains integration;

(vii) developing mathematical models of inaccuracy distribution;

(viii) monitoring the specific equipment for technical problems or maintenance requirements.

The GM methodology is comprehensively applied not only to the SLS of Polystyrene but also for other materials and processes with similar applications and corresponding accuracy problems such as SLS of Polyamide (PA) and the Thermojet 3D wax printer. An example of the latter is given in the end of this chapter.

5.2 Analyses of the geometrical variations caused by the physical processes in Selective Laser Sintering Castform

The ultimate aim of the described methodology is to characterize and analyse the 3D distribution of geometrical deviations from the nominal over the entire region of interest. In the case of SLS processes the values of the deviations vary considerably within the build volume. The factors that determine the plate distortion in the various directions could be summarised as follows:

(i) **Along the x and y directions** – The central part of the test plate would retain residual heat for a longer period than the part extremities, thus the cooling rate and shrinkage of the material positioned in the middle of the part bed would be slower than that of the material which is close to the wall.

(ii) **Along z direction** – the sintered sections of the part shrink whilst the part bed piston moves down with constant increments. Each new layer of fresh powder compensates to a greater extent the z shrinkage of the previous layers. The factors described in point (i) are applicable for z direction also.

The most challenging direction to maintain accurate sizes in the SLS process is the vertical one. In this direction the accuracy is influenced by both factors (i) and (ii). For this reason the grid methodology is applied to study mainly ε_z distribution.

Apart from the major factors described above other issues, which are discussed later in the chapter, may play significant and somewhat complicated role in the plate distortion.

5.2.1 Experimental set up

Machine

The main sintering machine used for the experiments described below was 3D Systems CI 2500. Complimentary experiments on DTM 2000 and 2500 *Plus* were also conducted in order to support the general conclusions from the observations regarding the process and material behaviour.

Material

Castform PS. This is the 3D trade name of polystyrene powder material for SLS process.

Test piece design and orientation

To examine the most of the build area vertical plates with orientations shown in Figure 5.2 were produced. The sizes of the test plate were x=235mm; z=310mm. The grid step was 15mm. This provides grid of 15 columns and 20 rows on the plate. The reference hole diameter was 2.2mm.

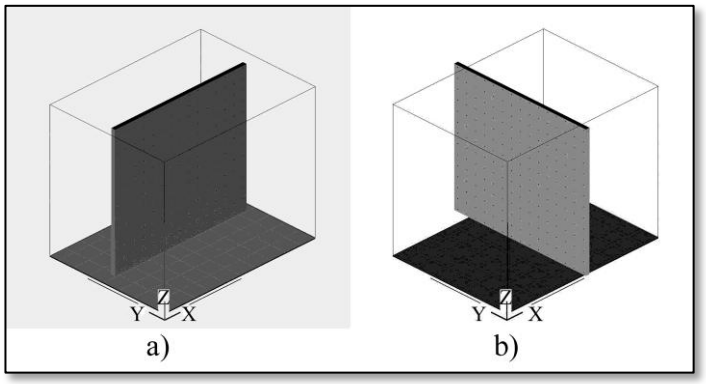

Figure 5.2 Plate orientations for vertical accuracy investigation

Sintering parameters

The sintering parameters were kept at their optimum values for the Castform material. These parameters were established during the commercial practice in order to fulfil requirements for part surface quality, strength and integrity with acceptable building time taking into consideration the platform manufacturer recommendations. The values of main process parameters were:

Laser power = 7W;

Outline power = 0W/(no);

Slicer Fill Scan Spacing = 0.10mm;

Cross Fill Scan = 1/(yes);

Warm-up = 25mm;

Cool-down = 2mm;

Sorted Enable = 1/(yes);

Left/Right feed distance = 0.254mm;

Powder Layer Thickness = 0.15mm;

Left/Right Feed Set Point = 40°C;

Part Cylinder Heater Enable = 1/(yes);

Part Cylinder Heater Set Point = 60°C;

Part Heater Set Point = 85°C;

In/Out ratio = 1;

Scan speed = 5080mm/s (200in/s);

Piston Heater Enable = 1/(yes);

Piston Heater Set Point = 60°C;

Beam offset x = 0.112;

Beam offset y = 0.196.

These set of parameters were stored for use as "material default settings" in platform CAM software. As the objective of the study was to reveal the distortions in the part due to the process no scaling factors were applied.

5.2.2 Results and discussions

It was found that ε_z distributions in both test plates orientation shown on Fig. 5.2 were similar regardless of their position. The results from plate oriented according Figure 5.2(a) are depicted in Figures 5.3 and 5.4 and analysed bellow. The similarity

in the shapes of ε_z surfaces obtained from various plates built vertically suggested common causes for the distortions.

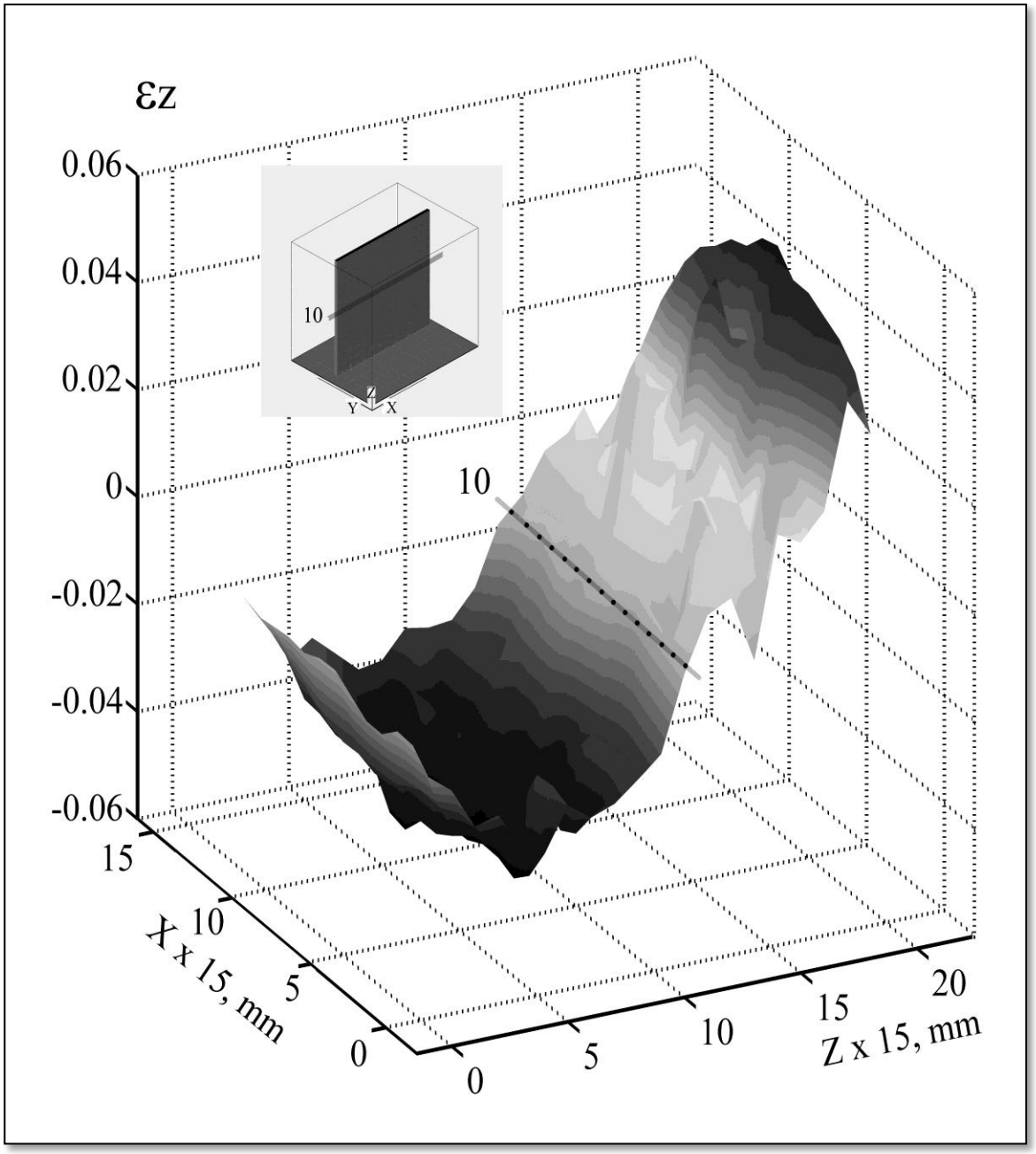

Figure 5.3 3D visualisation of ε_z (vertical size deviations from nominal) distribution in the (x, z) plane produced by GM

The mean value of the 15 reference points along each row of the plate gives a point of the line shown on Figure 5.4. As an example the highlighted *row* "10" from Figure 5.3 gives the position of the *point* "10" on the Figure 5.4.

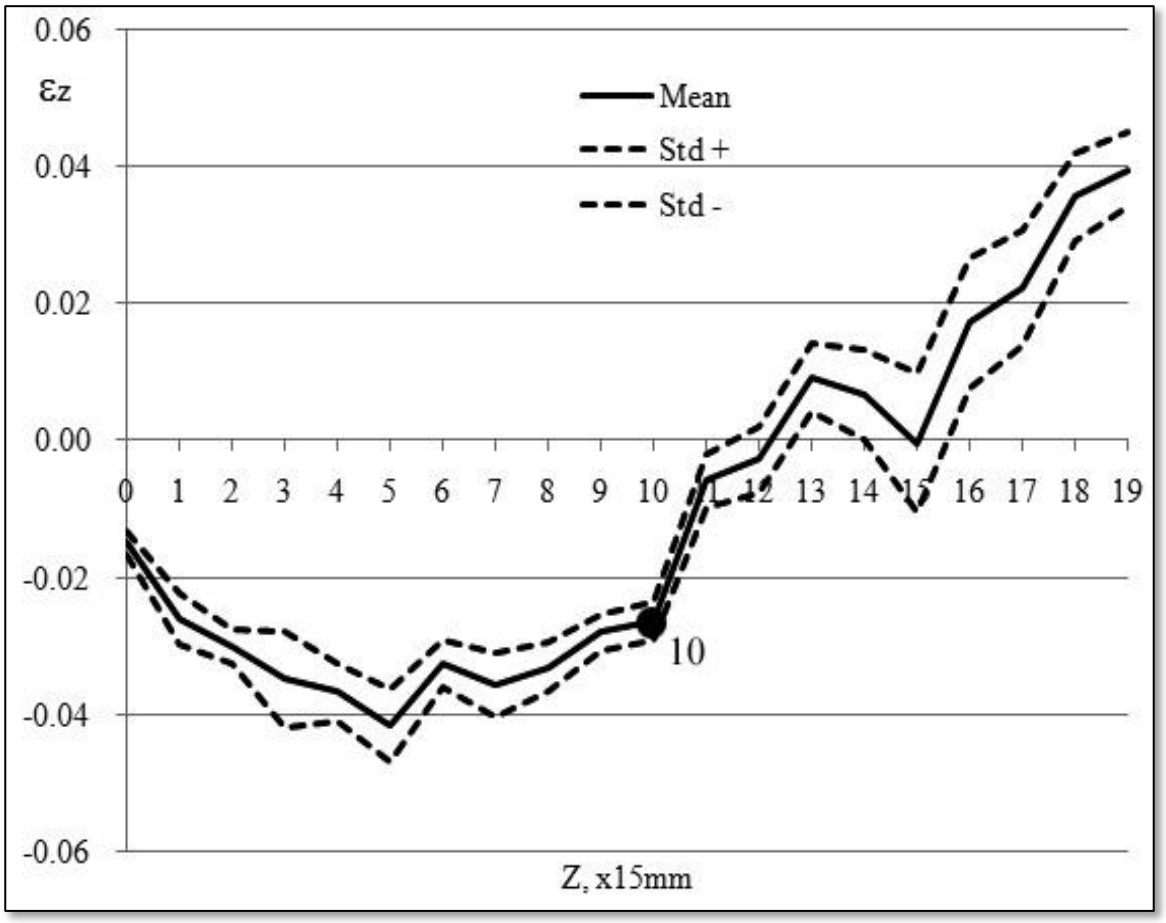

Figure 5.4 Distribution of ε_z -vertical deviation of the sizes from nominal

The line "Mean" on the Figure 5.4 is obtained by calculation of the mean value of ε_z along each row from the test plate. The lines "Std+" and "Std-" show standard deviation of ε_z along horizontal direction.

The shape of the curves in Figure 5.4 reinforces the requirement for further attempts to establish a general mathematical model of the material's behaviour along the z direction and to suggest a polynomial formula which could be utilised in the supporting computer-aided manufacturing **(**CAM) software for dimensional compensation.

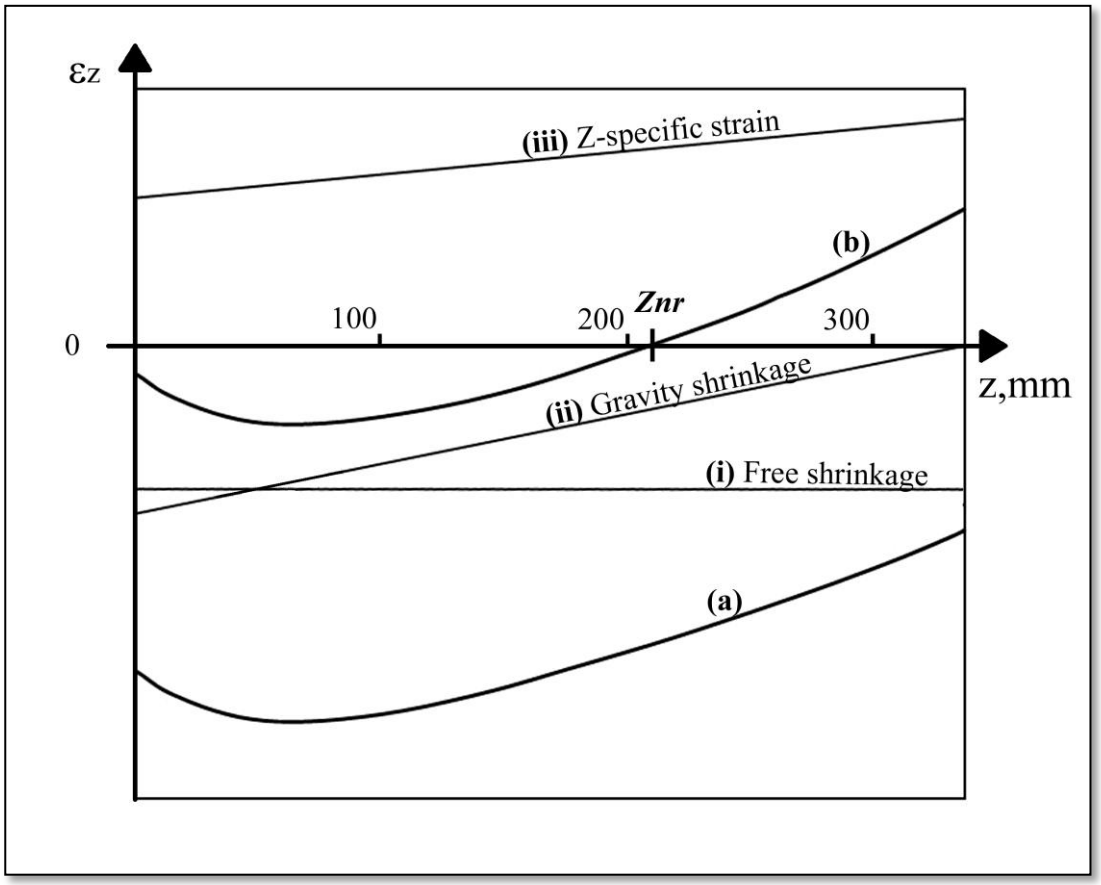

Figure 5.5 Schematic distribution of ε_z in vertical direction and specific contributions to it

In Figure 5.5 the ε_z axis represents the elongation or shrinkage of the sintered part along the *z*-direction. Schematically the curve **(b)** corresponds to the real distortion curve calculated by GM as illustrated in Figure 5.4. Up to approximately $z \approx$

80 mm the shrinkage in the part slightly increase. After this extremity the shrinkage decreases and becomes zero at $z \approx 210\,mm$ i.e. at this height the part is most accurate. The volumes above this 'neutral' level ($\mathbf{z_{nr}}$) exhibit elongation rather than shrinkage. Two immediate conclusions could be made from the above observations:

1. Parts shorter than the 'neutral' height ($\mathbf{z_{nr}}$) will always exhibit shorter *z* dimensions between features, and the overall size will be smaller than the nominal.
2. Parts higher than $\mathbf{z_{nr}}$ have elongated features in *z* direction above the neutral line although overall part size may be shorter.

This means that in SLS of PS, features along the z axis and vertical distances between functional surfaces may have either positive or negative dimensional changes.

Three major factors contributing to the material shrinkage could be suggested with reference to Figure 5.5 to explain the shape of the ε_z distribution (Figure 5.3 and 5.4) repeatedly observed in this research as well as author's experience in the Castform SLS commercial practise:

(i) Thermal shrinkage of the material. This shrinkage is constant and depends on the linear coefficient of thermal expansion α according the equation (2.3). It is usually averaged by a horizontal pyramid test part and constant shrinkage compensation is applied to the x and y dimensions of the part;

(ii) Gravity induced shrinkage This deformation is associated with the fact that upper layers press the lower layers under temperature above glass transition (T_g)

whereas the viscosity of the material is elevated and rheological behaviour is more prominent;

(iii) *Z*-specific deviation This deviation is associated with the mechanics of the layering process. As the volume below the currently sintered layer shrinks thermally, the part bed also moves down simultaneously to allow for new layer fabrication. A new layer of powder is spread across the uppermost layer and compensate for this *z*-direction sinking. The upper the layer is, the greater the sinking effect is and thus a greater amount of new powder is applied for the next layer by the recoating system.

The superposition of factors **(i)** and **(ii)** (both causing shrinkage) will result in a curve, which is schematically depicted as **(a)** on Figure 5.5. If the factor **(iii)** is superimposed onto the curve **(a)** it will be translated and twisted towards + ε_z. The resulting curve **(b)** is the type of curve observed in all parts of the building area as shown in Figure 5.4 irrespective of their *x* and *y* position. The variations in shape and curvature can be explained by the different 'temperature history' of build area.

The distribution of z dimensional deviation from nominal in the vertical direction revealed by GM suggests that the actual layer thickness is not constant and equal to the value set by build profile parameters. Variations in layer thickness matching the dimensional deviation were confirmed by a Scanning Electron Microscopy (SEM) study. Samples at heights of 15 mm, 60 mm, 105 mm, 150 mm and 195 mm were taken from the test plate. The samples were sputter coated with Gold/Palladium (Au/Pd) in order to prevent electron-charging effects during SEM imaging. The layer thicknesses have been measured from the SEM image using specialised micro imaging software. As can be seen from the typical sample picture on Figure 5.6 the

layers are distinguished, although not sharply defined. To increase the reliability of measurement, ten layers of each sample were measured and the mean values of layer thickness were then calculated. The maximum standard deviation in measurement of the layer thicknesses was found to be 11.5 μm. The plotted results of layer thickness against corresponding *z* position in the build are presented on Figure 5.7. Noticeably the shape and trend of the curve shows change of layer thickness with *z* that confirmed the shape of deviation curves obtained by GM (Figure 5.4). This is another illustration of complex nonlinear distribution of deviations in the *z*-direction revealed by implementing the SEM imaging.

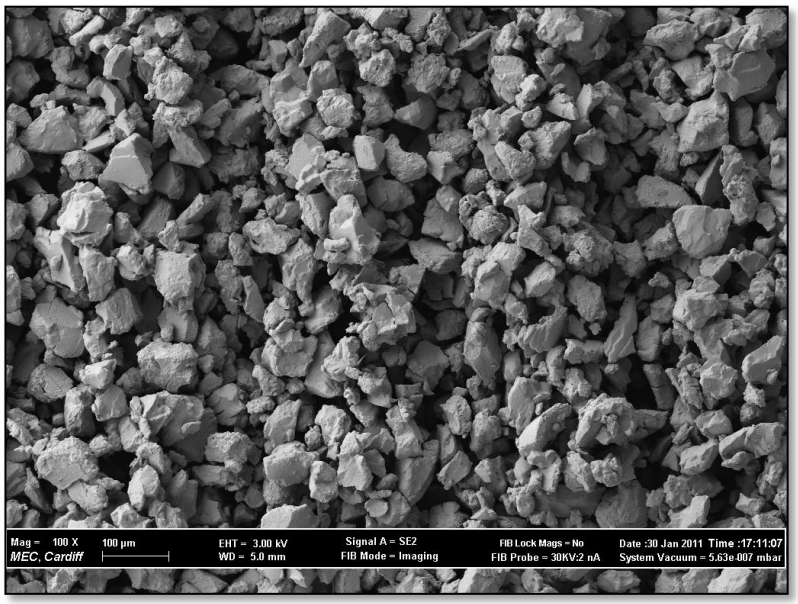

Figure 5.6 Scanning electron image of SLS Castform sintered layers

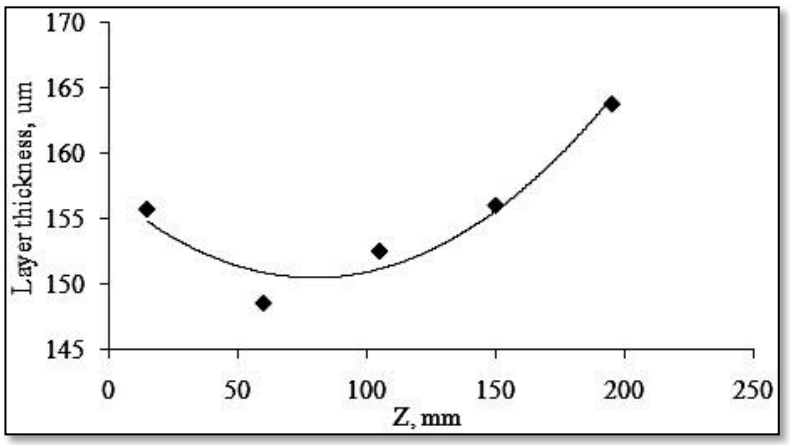

Figure 5.7 Layer thicknesses of SLS Castform depending on their *z* position

Experiments and calculations that were conducted on horizontal plates (built in *x, y* plane) showed less deviation in sizes. This conformed to the results of ε_x given in Appendix 2. Distributions of ε_x and ε_y can be explained by the influence of thermal factors on the shrinkage and part distortions that are described in section 2.1.2.2.

5.3 Implementation of the GM calibration in the SLS RP practice and modelling of the distortions

To compensate for the distortions after the manufacturing process, the nominal sizes from the CAD file are scaled accordingly. The possibility for accurate calculation of scaling factors that will compensate the specific and complex part distortions that occur in RP manufacturing processes is an important application of GM. In common RP practice the scaling factors are determined experimentally (DTM 1999), (Wang 1999), (EOS 2003) and calculated by the formula:

$$S_{cz} = \frac{z_0}{z} \qquad (5.1)$$

where

z_0 - is the nominal size from the CAD model,

z - is the measured size achieve from the process.

From equation (4.3) and (5.1) the scaling factor can be expressed in terms of strains as:

$$S_{cz} = \frac{1}{\varepsilon_{E_Z} + 1} \quad (5.2)$$

The above calculation of scaling by formula for engineering strains that was used to determine the dimensional deviations from nominal, introduces a negligible error as per the practice described in Paragraph 4.1 and is in the range illustrated in Table 4.1.

The results of GM accuracy investigation, allows the scaling factors to be calculated as a function of the *x, y, z* coordinates and an approximation formula applied to the CAD model compensating the distortions. Thus it is possible for part sizes to be compensated with greater correctness according to their position in the build chamber and also their location within the manufactured part itself. Furthermore instead of average scaling formulae, distribution of deviations along a specific direction can be used for formula scaling approximation. Separate experiments were conducted to verify the reliability of the GM for part scaling.

Experimental set up

The sizes and grid parameters of the plates were:

x = 235mm;

z = 175mm;

Grid step = 15mm;

Number of rows = 11;

Number of columns = 15;

Thickness = 8mm;

Holes diameter = 2.2mm.

Picture of a test piece (plate) for process scaling is shown in Figure 5.8.

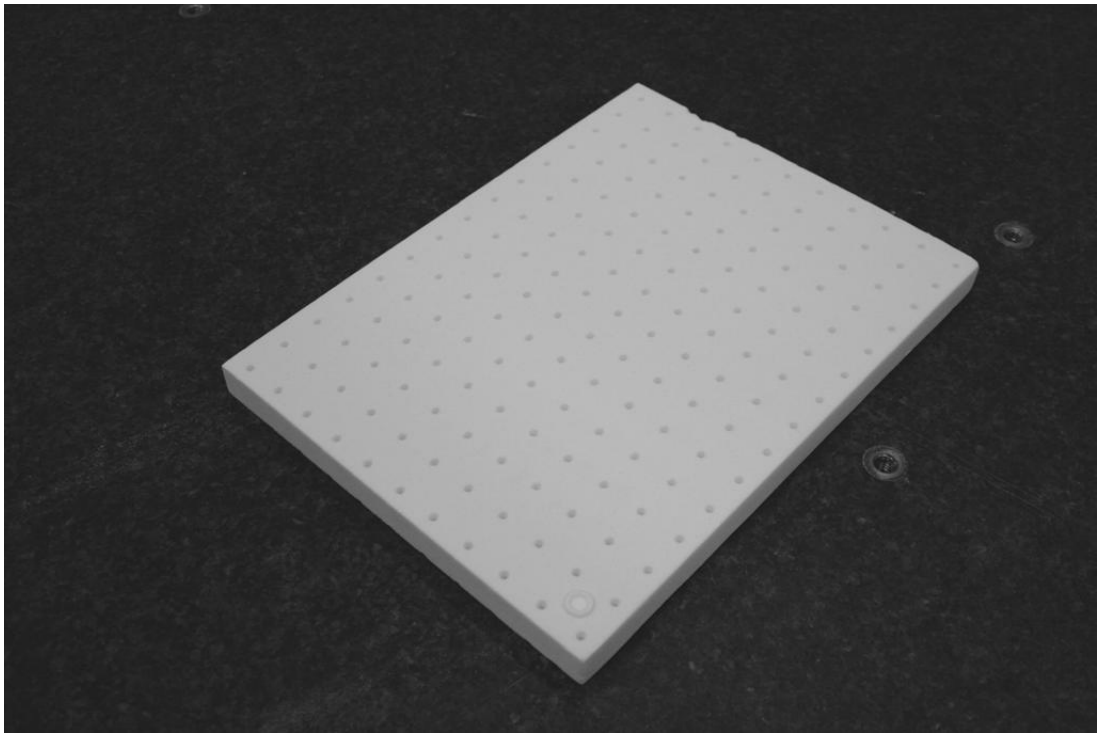

Figure 5.8 Picture of the plate for scaling verification

Plate shown on Figure 5.8 was built in the centre of the part bed and it was oriented as shown in Figure 5.2(a).

Results

Distribution of ε_z which was used for scaling calculations is depicted in Figure 5.9. Detailed results are given in Appendix 2. The abnormal deviation along Row 4 can be classified as accidental as described in Section 2.1.5. No further abnormalities of

such a character were observed in this experiment and its influence was negligible after applying the approximation formula for scaling.

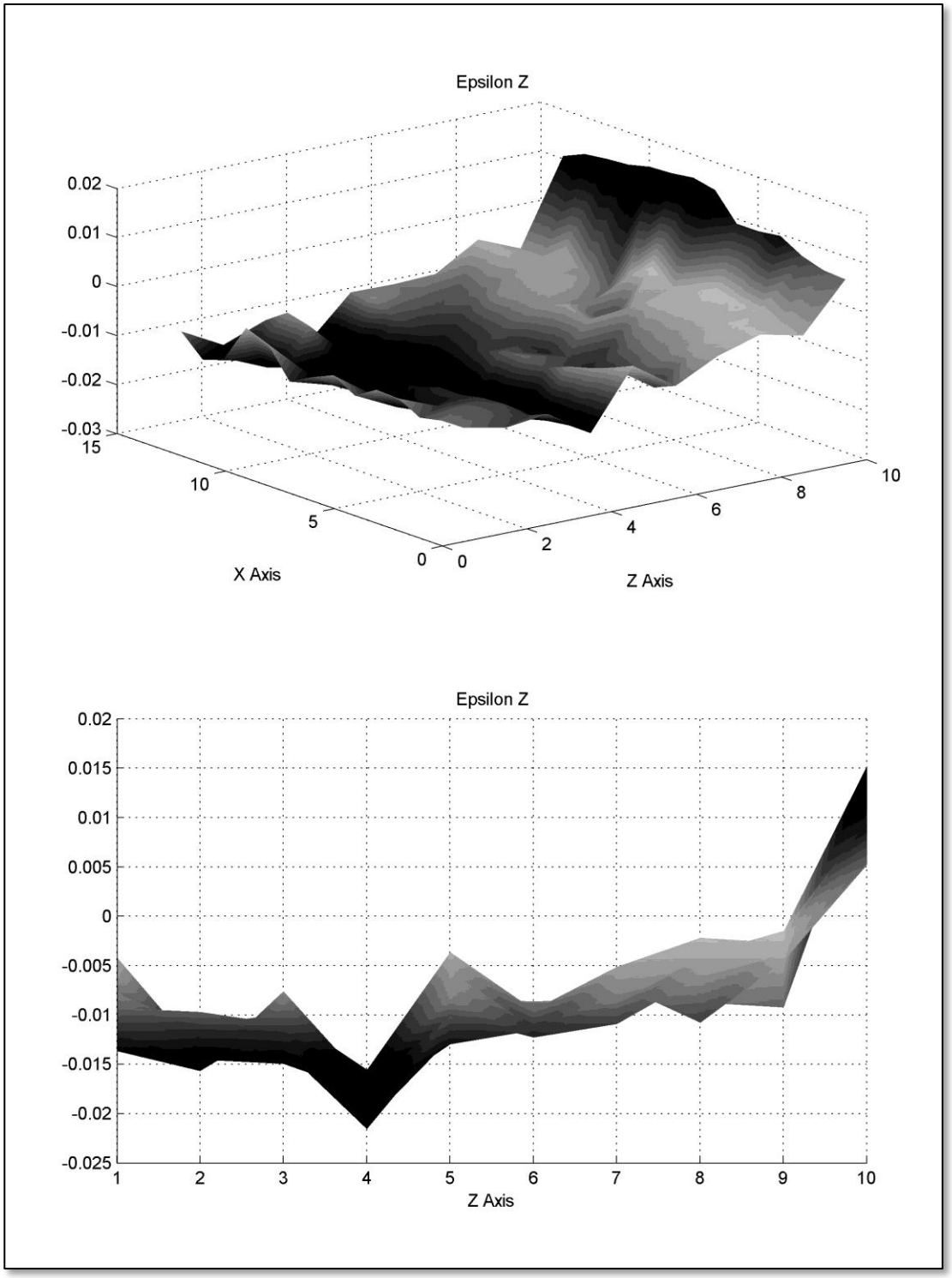

Figure 5.9 ε_Z distribution in calibration plate

Scaling factors can be calculated either on the basis of the data from particular set of columns or by averaging the scaling over all columns (Figure 5.10). First approach would be more applicable if a specific build area of the platform is targeted for calibration. For overall calibration and for large parts the 'averaging' approach is more suitable; it was applied in this research.

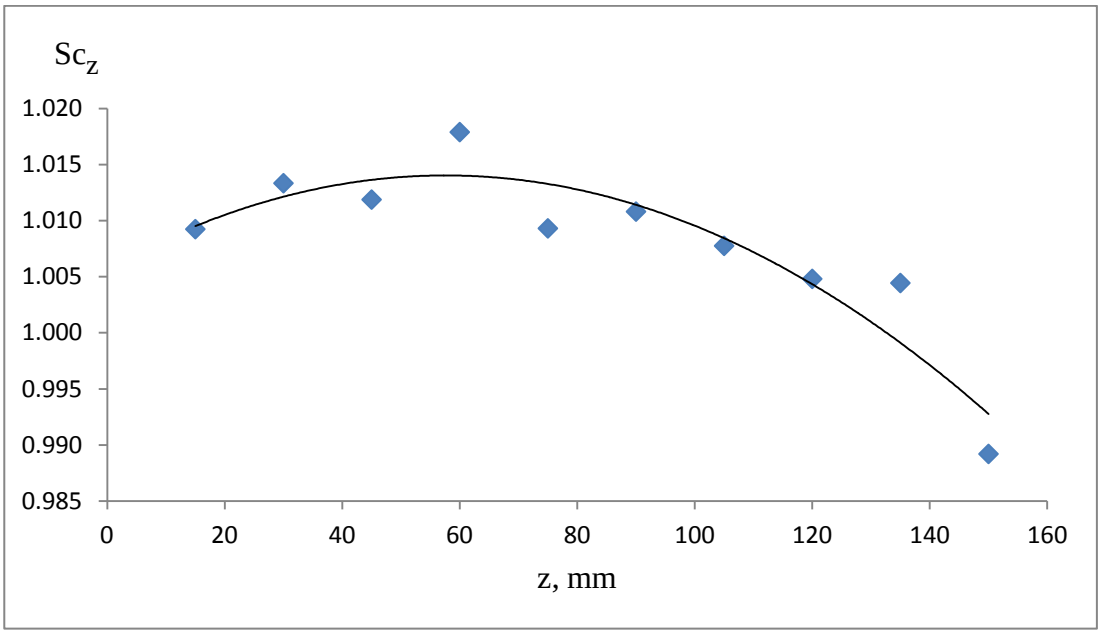

Figure 5.10 Scaling factor calculated by the average of Sc for the corresponding *z*

Application

For this research two plates were built simultaneously side by side - one without scaling and another with applied scaling factors according to the analytical formula (scaling as a function of *z* height) obtained from the test-plate described above (Figure 5.10):

$$S_{cz} = -2.10^{-6}z^2 + 3.10^{-4}z + 1.058 \qquad (5.3)$$

Where:

S_{cz} is scaling factor in *z* (vertical) direction.

Comparison of ε_z (dimensional deviations from nominal per unit length) distribution in the SLS plate before and after correction following the GM scaling calculations is illustrated in Figure 5.11, Figure 5.12, Figure 5.13 and 5.14. It can be seen that the variation of ε_z in the part without scaling is from -0.018 (-1.8%) to 0.013 (1.3%) depending on z. After scaling by formula, the values of ε_z are substantially reduced (up to 3 times) within the range of +/- 0.006 (0.6%) and are symmetrically distributed around zero for the entire height of the part.

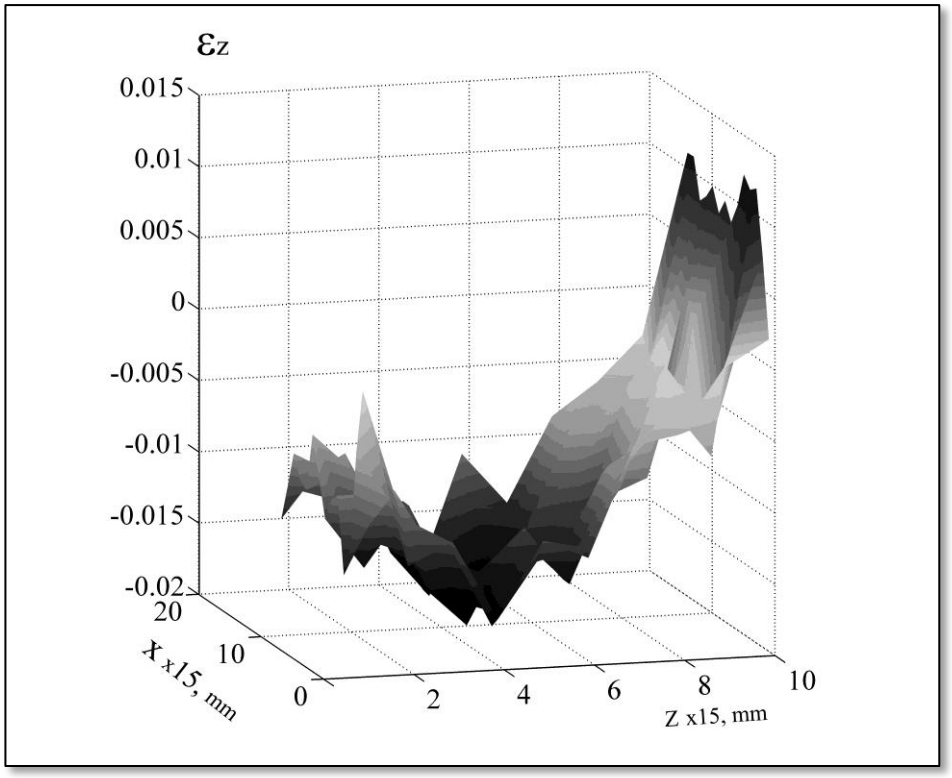

Figure 5.11 3D ε_z distribution in plate built without scaling

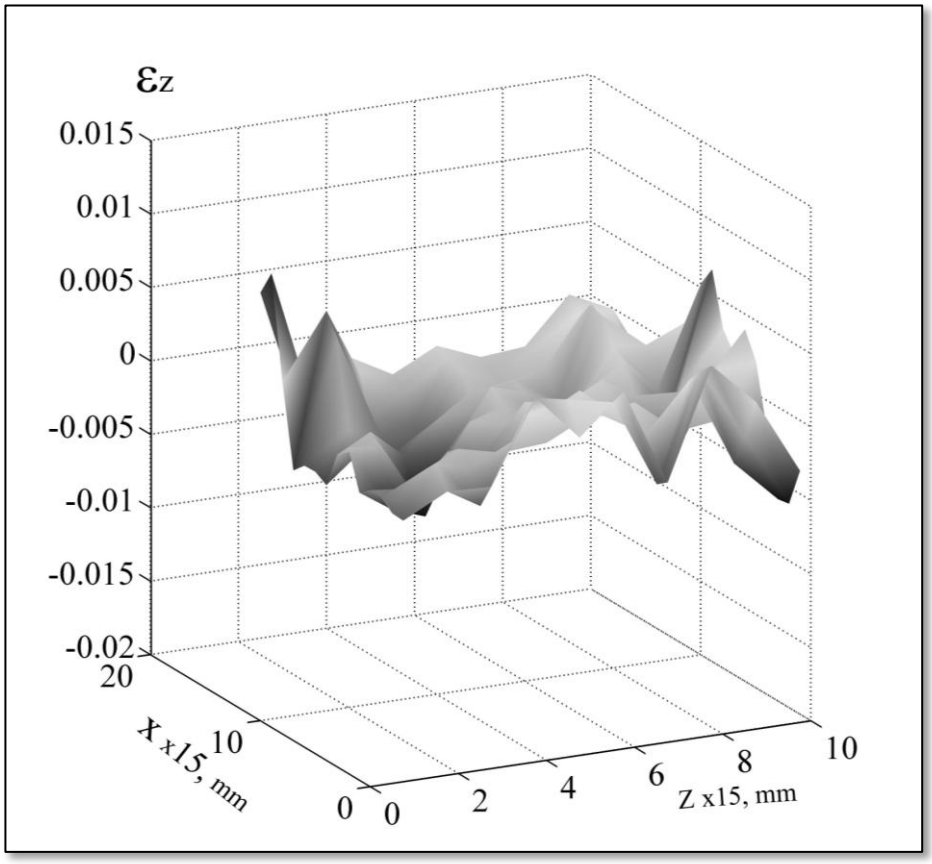

Figure 5.12 3D ε_z distribution in plate build with scaling

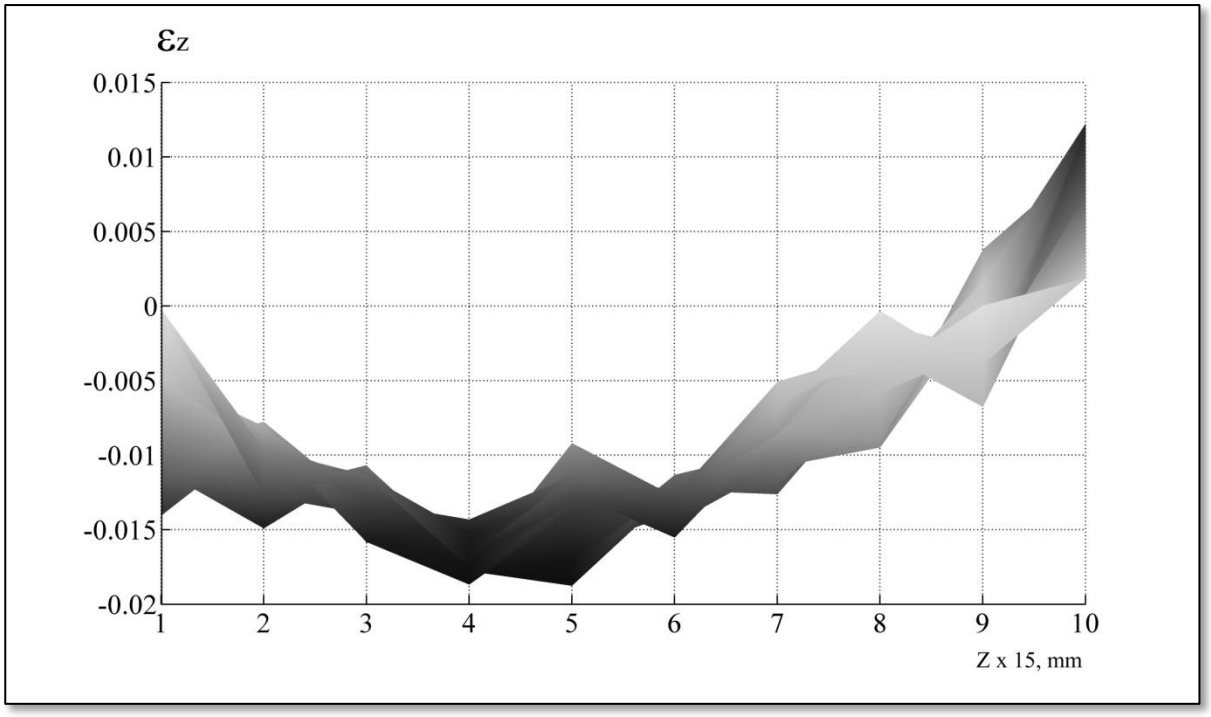

Figure 5.13 Side view of ε_z distribution surface in plate build without scaling

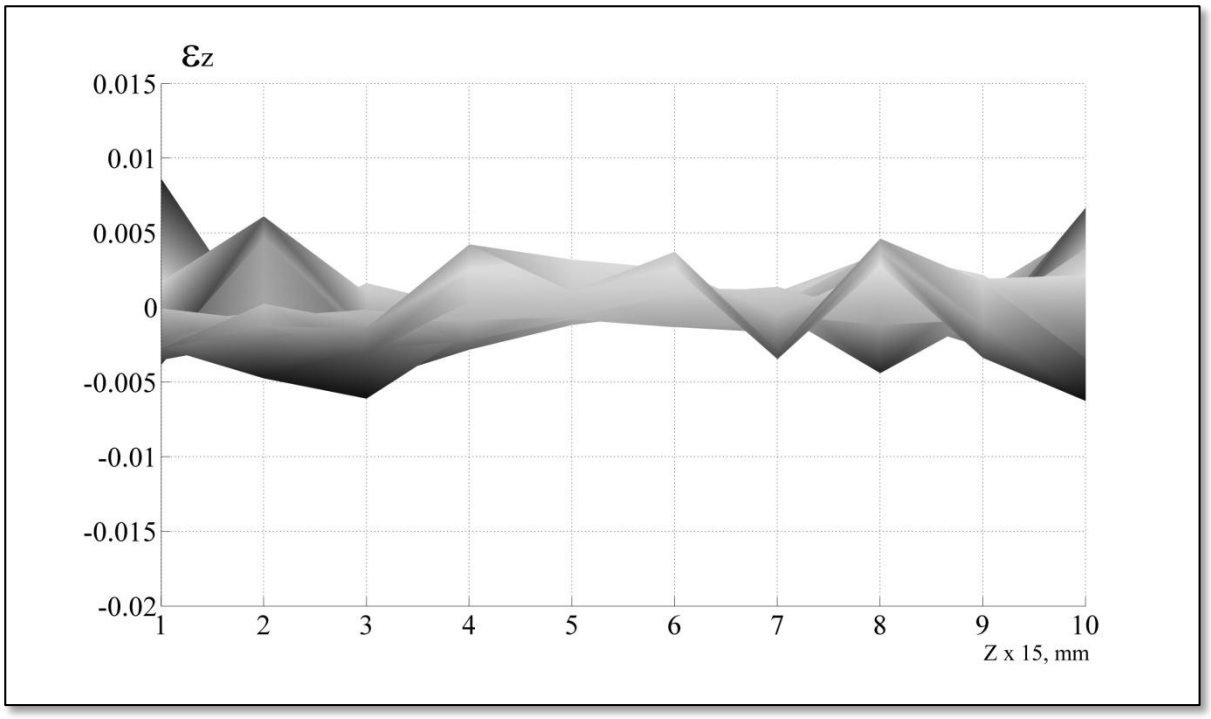

Figure 5.14 Side view of ε_z distribution in plate build with scaling

Conclusions about process accuracy and precision can be made from GM investigation and can be used for scaling by analysis of the shape and position of the 3-D distribution surface of ε. The application of the GM for accuracy study and calibration of different RP platforms (including SLS, micro SLA, micro-CNC milling, ion beam ablation) (Minev et al. 2011, Minev et al. 2010) revealed several types of strain distribution surfaces. They are summarised and illustrated schematically on Figure 5.15 where the bold lines represent the mean values of a deviations in certain direction. The results from the real experiment that was conducted for scaling calculations of SLS Castform demonstrated scenario a) and d). They are given in Appendix 2.

Accuracy is presented by the deviation of the mean value from 0, while the precision is measured by standard deviation as a criterion for a spread of deviations at certain line (dotted lines). The process (a) is 'accurate' but not 'precise' while process (b) is 'precise' but not 'accurate'. In case (b) simple scaling by a constant scaling factor can be applied to correct the inaccuracy. Processes (c) and (d) require scaling calculated by formula (linear and non-linear respectively) as illustrated in the case of SLS polystyrene parts described above.

The 3-D distribution of ε surfaces could also be used for:

- comparative studies of different processes,
- evaluating the processes in terms of their integration in process chains and
- developing mathematical models of inaccuracy distribution.

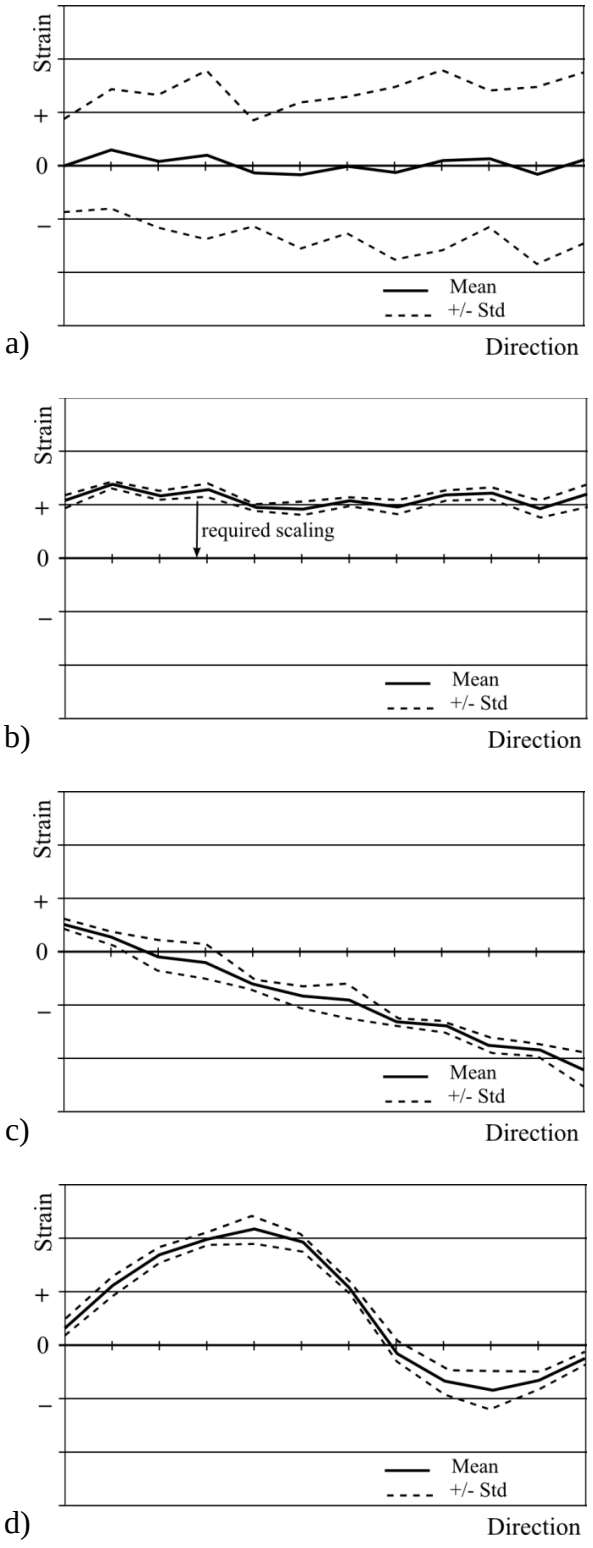

Figure 5.15 Four scenarios of accuracy and precession of a process

5.4 Implementation of the GM for studying other RP materials and processes

5.4.1 SLS Polyamide (PA)

As stated in Chapter 3 one of the strongest aspects of the GM methodology is its ability to illustrate distributions of ε in various sections of the test parts. For example the method can be used to evaluate the changes in distortions at different levels of the build as well as to compare and evaluate these changes in different directions.

This is illustrated by the study of ε in SLS Polyamide (PA) material. For this study a plate with sizes z = 510mm and x = 225 mm and orientation as shown on Figure 5.2(a) was built using EOS P700 machine. This platform is highly utilised to produce large, functional polyamide prototypes and is of particular interest for RP in the automotive industry.

The results are depicted on Figure 5.16. The ε_x deviations are smaller compared to the CastForm Polystyrene (PS) material. In contrast with the same material the distribution of ε_z in the most critical (vertical) direction is uniform. One reason for that is due to SLS Polyamide material sintering to a much higher density than CastForm material (approx. 95% for PA vs. 45% for PS) and therefore is not influenced by gravity induced shrinkage (factor (ii) described in Section 5.2.2). As two different machines were used for PA and PS, the conclusions about accuracy comparison between these materials are not conformed.

Considerable values of ε_Z (Figure 5.16 b) are observed only in the beginning of the build and are due to the unsettled temperatures leading to a severe curling. (The other randomly scattered peaks observed in this experiment are non-process related accidental measurement errors, see Section 4.5).

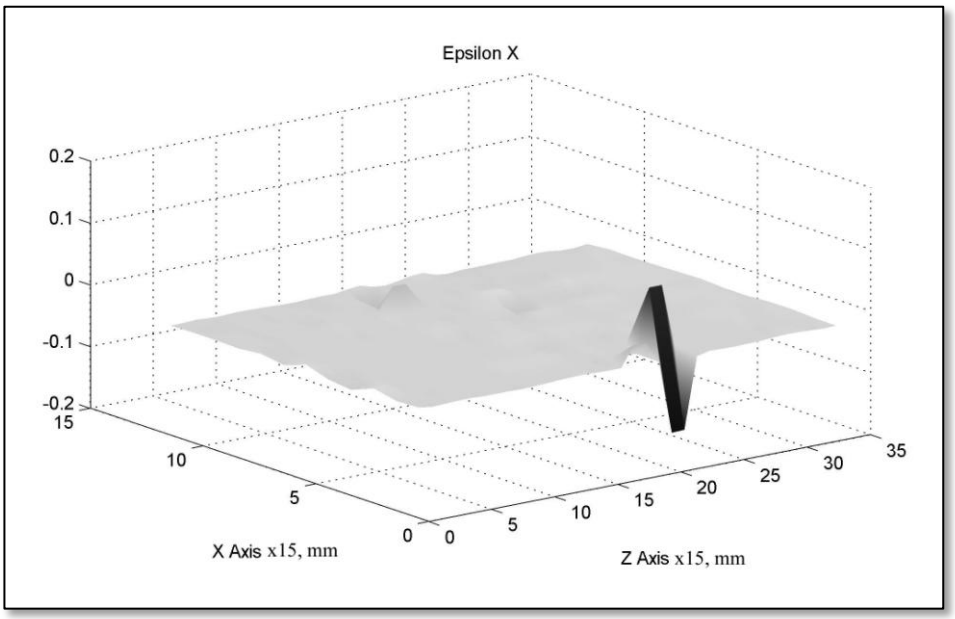

a)

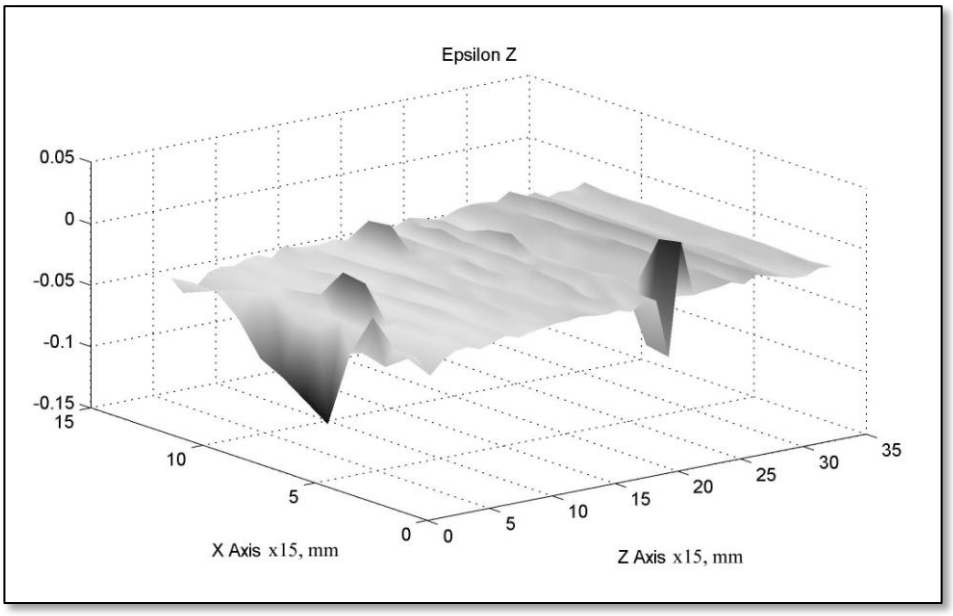

b)

Figure 5.16 a) Distribution of horizontal deviations (ε_X) and **b)** distribution of vertical deviations (ε_Z) in polyamide SLS plate

As a final conclusion it can be stated that the deformations and corresponding deviations in the PA material are more uniformly distributed than those in PS and could be easier compensated by applying an appropriate constant scaling factor.

5.4.2 Process monitoring of the Multi-Jet modelling system (3D Systems 'ThermoJet' for investment casting wax patterns)

Process and equipment monitoring and fault diagnosis can be done efficiently using GM by building a plate over the build volume. This is illustrated in this section for the case of a faulty Thermojet machine. The distortions in RP Thermojet parts (Figure 5.17) are more uniformly distributed and less scattered compared to SLS. The material that undergoes fused deposition on the build surface cools down rapidly below the Tg and is not subjected to viscous flow over the entire building period. Therefore the positive (elongation) changes of the upper layers due to factors (ii) and (iii) (Paragraph 5.2.2) are avoided. However as it can be seen from Figure 5.17 the deviations (strains) at high *z* volumes in this particular platform are dramatically scattered. Subsequent investigations discovered that the reason for this was mechanical problems with the machine. This is a convincing demonstration of the potential ability for the suggested methodology to monitor and flag-up specific platforms with technical problems or in need of maintenance attention.

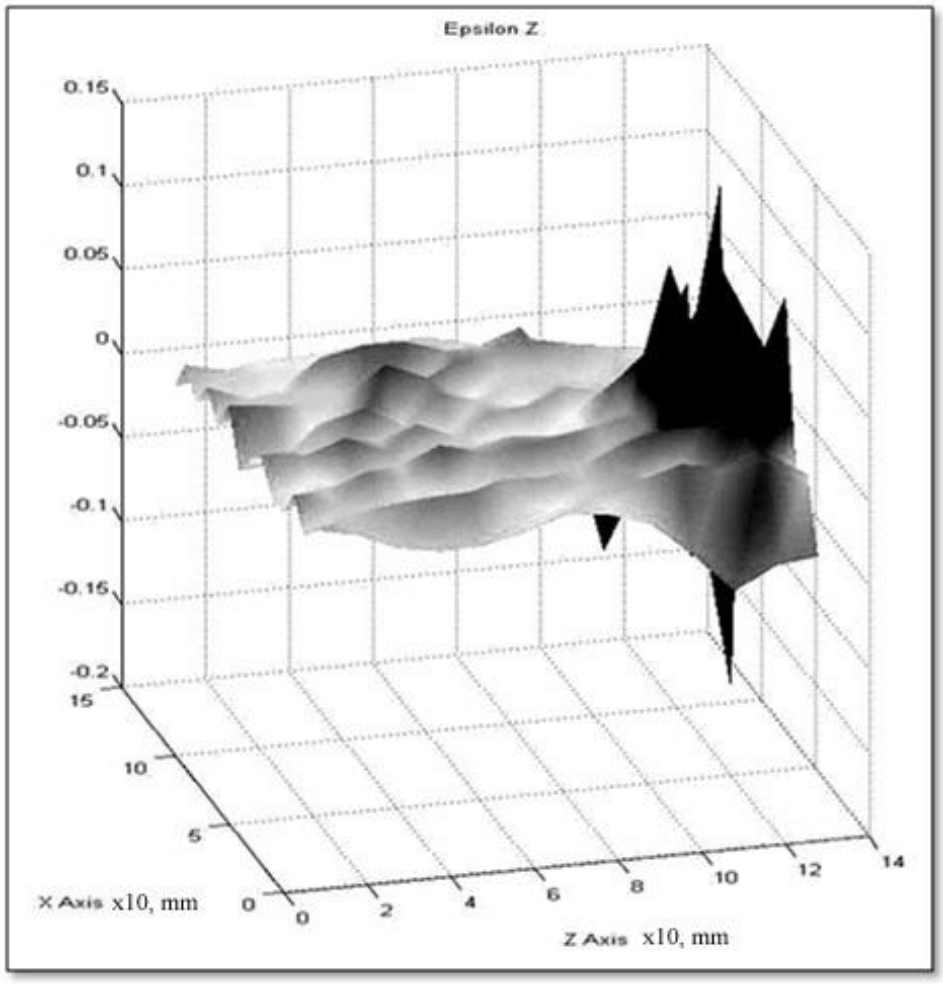

Figure 5.17 Distribution of ε_z in faulty Thermojet build's volume

5.5 Conclusions

This investigation has shown that GM can be easily and cost effectively applied to generate and analyse the distribution of dimensional deviations in the RP build process throughout the entire build envelope. It is a powerful means to obtain valuable information for analysing the different build phenomena. The data could be interpreted and analysed from a point of view of accuracy and precession of the parts.

It proposes that a single GM test piece and routine measurement procedure could be utilised to estimate the scaling factors throughout the entire part build and to improve part accuracy. In particular it was demonstrated that the dimensional deviation in parts could be reduced by up to three times when the scaling formula was applied. The dimensional error in the *z* direction of the SLS polystyrene part was reduced from 1.8% to 0.6%. This was a convincing verification of the important practical application to CAD model scaling for process uncertainties compensation.

In this research the GM was applied to study the causes of dimensional inaccuracy in the z-direction of SLS polystyrene process. A critical dimension in height was found from where the part size distortion changes from shrinkage to extension. The reason for this was proved to be the layer thickness variations in the process. Future investigation of the factors affecting part accuracy in different RP methods is possible. More specifically it is important to study and distinguish the influence of the factors affecting part deformation such as: gravity induced shrinkage; overcompensation of the layers; temperature distribution; energy delivered for processing.

CHAPTER 6 COMPARATIVE STUDIES OF MICRO PROCESSES AND CHAINS ACCURACY

To make the processing sequence efficient there is a need to address challenges related to micro-strains and distortions. The installations must be verified during machine setup with respect to the accuracy issues identified below. The verification process will lead to development of process specifications and will also involve the development of common approaches for evaluating and setting up alternative and complementary installations.

6.1 Technological chains and the importance of the accuracy compatibility

In the process of horizontal integration of micro- and nano-technologies (MNT) installations there is a particular need for keeping accurate dimensional control throughout the entire manufacturing process (Bigot et al. 2010; Hansen 2007). As an example a micro structured surface could be produced by a Projection Mask Micro-Stereolithography (PM-μSLA) apparatus at one installation, then it could be laser treated and nano-structured at a second and/or third installation and finally it could be transferred by electroforming in Ni-shim for high throughput polymer thermal replication. Therefore the equipment must operate within its specifications to facilitate its integration in process chains (EUMINAfab 2010; Kautt 2009).

This chapter describes a method for performing a comparative investigation with reference to PM-μSLA and micro milling processes using the GM. These processes

are investigated as they are promising technology in various master-making chains (Kennedy 2009; Imahori et al. 2005).

6.2 Micro-Stereolithography accuracy study by Grid Method

In Projection Mask Micro-Stereolithography (PM-μSLA) processes the digital part model is converted into a series of layers of bitmap images. These are then transferred to a dynamic pattern generator, which controls a digital micro-mirror device (DMD). The DMD projects the pattern (a mask) of the layer profile onto the photo curable polymer to allow for exposure and thus layer curing (Yang et al. 2009; Sun et al. 2005; Zhang et al. 1999). Advantages of the method are that no structure recoating is required. The surface being illuminated is always smooth, the illuminated layer is not subjected to the atmosphere and thus inhibitions caused by oxygen are reduced (Melchels et al. 2010). One μSLA material that has been developed for commercial utilisation is acrylic based photo resin polymer. This material could be used for creation of meso-micro prototype parts or patterns for precision Investment Casting (Dean Al 2004). This outlines a new potential process chain candidate, namely μSLA → Investment Casting (IC) → Injection moulding.

Achieving good accuracy of parts fabricated by additive layer based processes (such as μSLA) is a complex task that is constantly under consideration by process planners. A common issue with Stereolithography systems and especially important in μSLA is the uncontrolled penetration of the ultraviolet light source into the photo-cross-linkable resin when fabricating down-facing surfaces (Choi et al. 2009). The horizontal resolution is governed by the pattern generator pixel size and the

reduction factor of the optical components used to focus the mask profile on the photo-reactor surface. The vertical resolution is limited by the absorption of the chemical medium and the current recoating strategy (Bertsch et al. 2000). Post processing and handling of μSLA parts is an additional factor contributing to the overall resolution and accuracy. One common distortion phenomenon that has been observed in our research and commercial practice in MEC was curling (Figure 6.1).

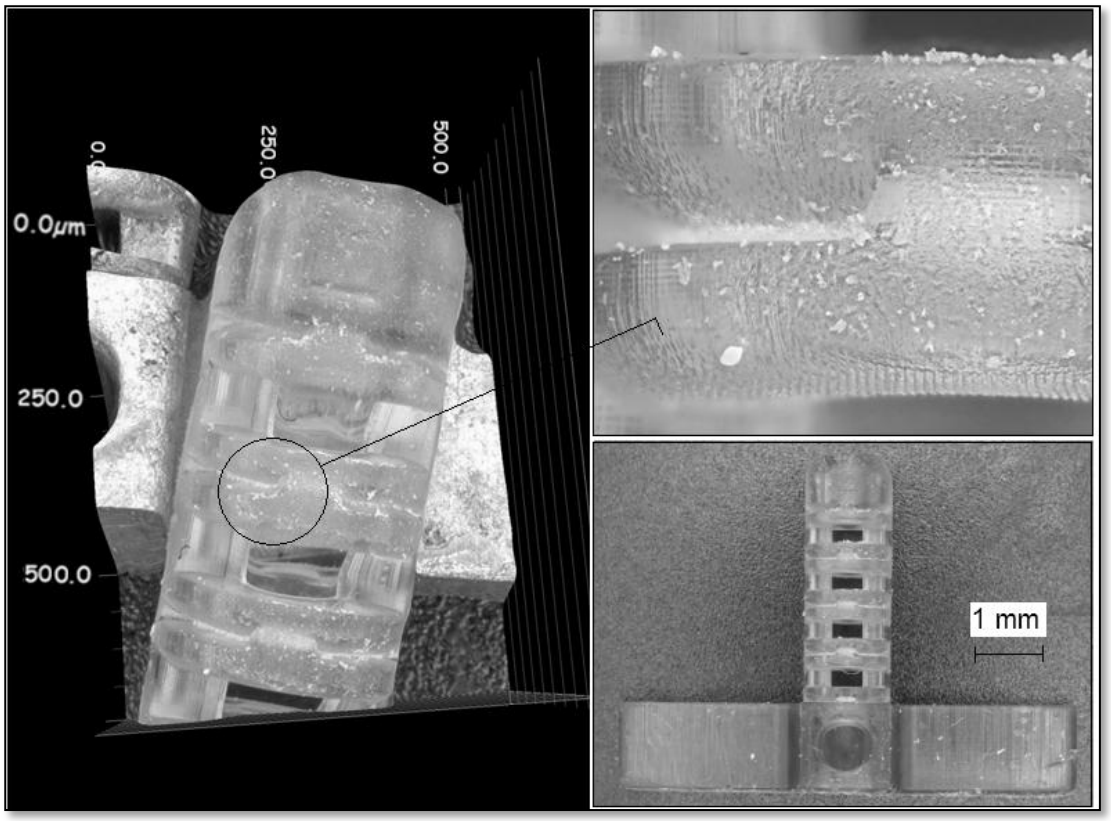

Figure 6.1 Neuro-medical insert produced in acrylic resin with PM-μSLA showing the curling effect

In this chapter the accuracy issues above are addressed by implementation of GM. Some of the data has been previously published (Minev et al. 2011). The results enabled better 3D model scaling and tailoring by assigning dimensional

compensations, which is a crucial prerequisite for final part accuracy and MNT process compatibility.

6.2.1 Experimental set up and methodology

Machine

The platform used for the experiments was the EnvisionTec Perfactory® using R11 material (an acrylic based photo resin polymer), that is recommended for investment casting patterns. The machine was specifically acquired to extend the micro manufacturing capabilities of MEC. Its specifications allowed producing components with small and intricate features in plastic or metal (after investment casting of the plastic patterns) which were difficult or not achievable by other processes.

Test piece design and orientation

To examine the most of the build area vertical plate with orientation shown in Figure 6.2 was produced. The sizes of the plate were x=40; z=62.5mm and thickness 1mm. The grid step was 2.5 mm, and the reference holes diameter was 0.5mm. The test plate sizes and grid step were determined following the general considerations described in Section 4.4.

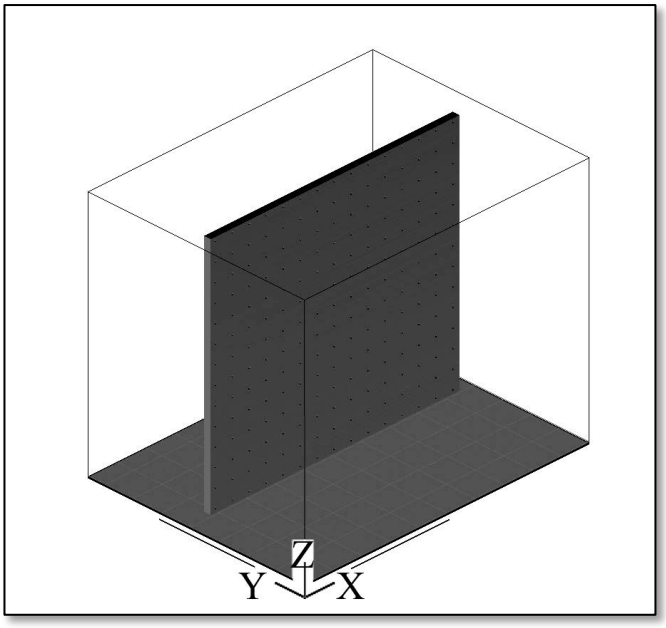

Figure 6.2 Plate orientation for μSLA accuracy experiment

The hole diameter needed to be large enough for correct cleaning (i.e. to prevent holes becoming congested with uncured material) The minimum through-hole diameters that can be built and cleaned-out effectively (in order to be accurately measured by the CMM system) are interrelated with the plate thickness; the thinner the plate is the smaller the diameter of the achievable holes. Figure 6.3 shows the minimum hole diameter achievable reference to the plate thickness. The trendline (regression line) “diameter of all holes to breakthrough” shows the minimum hole size that should form without problem. The line “diameter of one hole to breakthrough” shows the minimum hole size that can be achieved, but without confidence (i.e. experimentation would be required prior to part build to ensure that a hole can be formed sufficiently well).

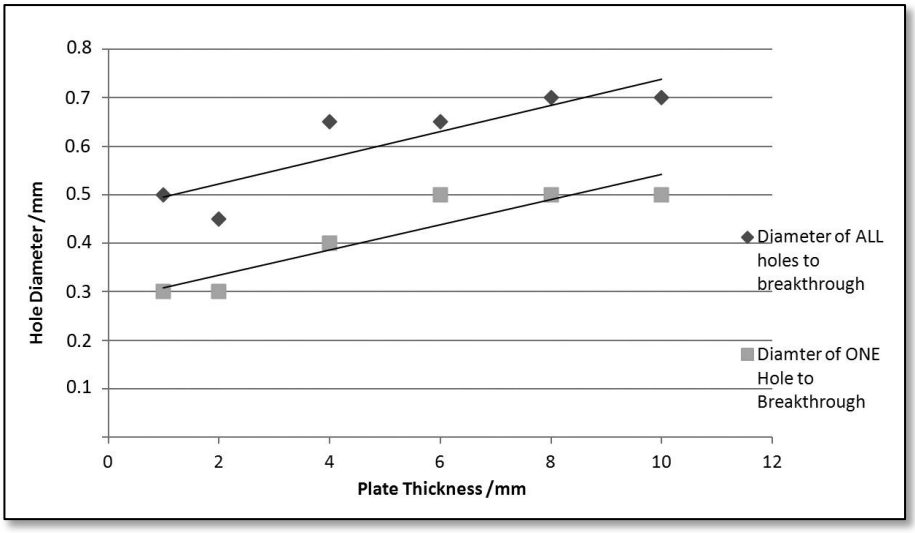

Figure 6.3 Graph of hole diameter against plate thickness for acrylic based photo resins (Perfactory R11 material)

From these results it was decided that a plate thickness of 1mm and a hole diameter of 0.5 mm should be used. This ensured that all holes should form and breakthrough correctly and the plate thickness is representative for length scale applications of μSLA, as well as strong enough to withstand processing. It should be noted that the freshness and the quality of the resin are important factors for build resolution and hence the achievable hole sizing. Further decrease of the hole size was not practical because cleaning would be impeded and relative error of automatic contour approximation would increase. The appropriate grid density was established taking into account the considerations described in Section 4.4 "Test plate geometry considerations". In the case of studying acrylic based photo resins along the whole building chamber the grid cell size was 2.5 mm.

After completion of the building process (Figure 6.4) the plate was cleaned and post-cured in accordance with the material supplier recommendations.

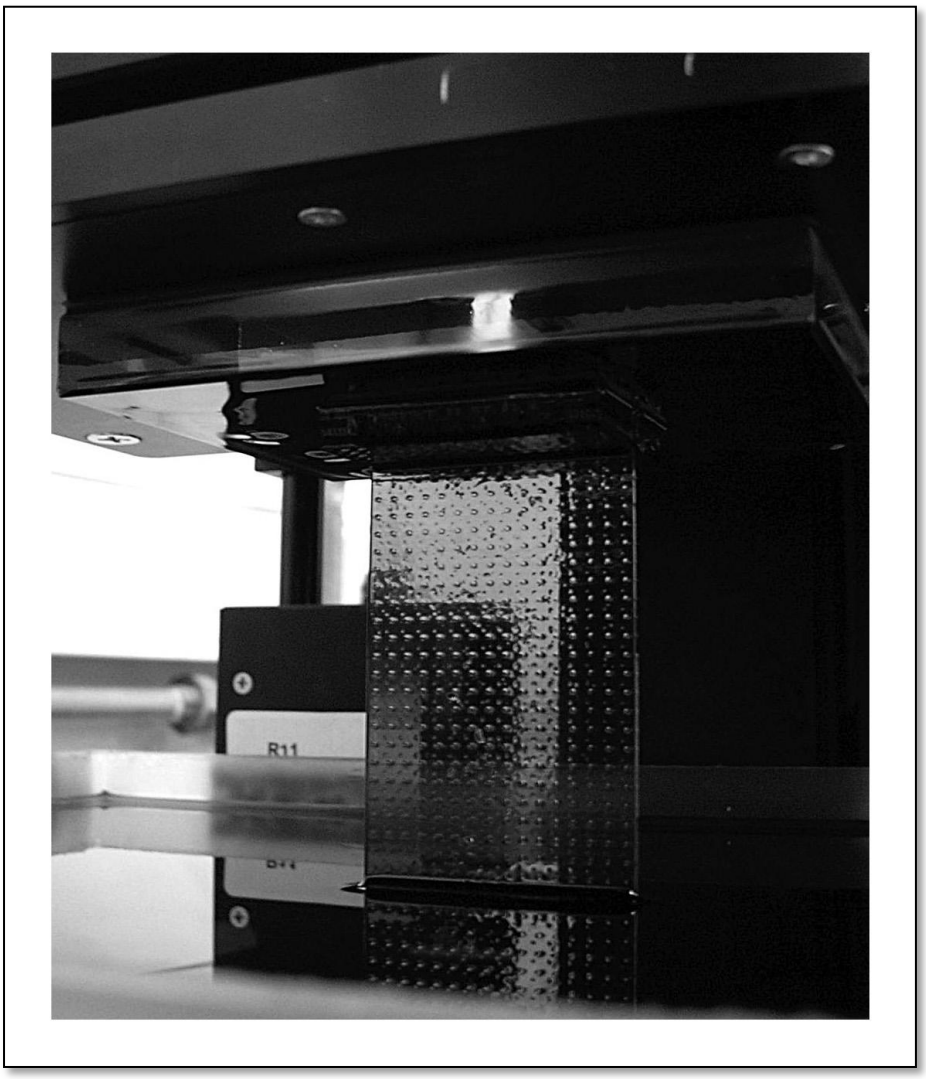

Figure 6.4 Test plate after the build completion on EnvisionTec Perfactory platform

6.2.2 Results from the Grid Method for accuracy study of micro-Stereolithography process

The described methodology provides the possibility to represent and analyse the 3D strain distribution in the built object over the large build space. In this study the focus was on determination and analysis of the usually most problematic vertical

accuracy and the associated linear (ε) and angular (γ) dimensional deviations from nominal. In this direction the accuracy is linked to numerous factors such as the mechanical movement of the platform, light scattering during curing, cure depth and curling phenomenon. The linear and angular geometrical characteristics of accuracy are calculated in terms strains by the definitions provided in Section 4.1.

The 3D distribution of ε_z (deviation of length from nominal in z direction) over the plate depicted on Figure 6.4 is shown on Figure 6.5. If a few significantly scattered points are ignored (non process related errors considered paragraph 4.5) ε_Z are within the interval +/- 0.01 (1%) and relatively small for RP processes. From the "front view" of the ε_Z surface (Figure 6.5b) it can be seen that the material is predominantly shrinking (ε_Z are negative) in nature.

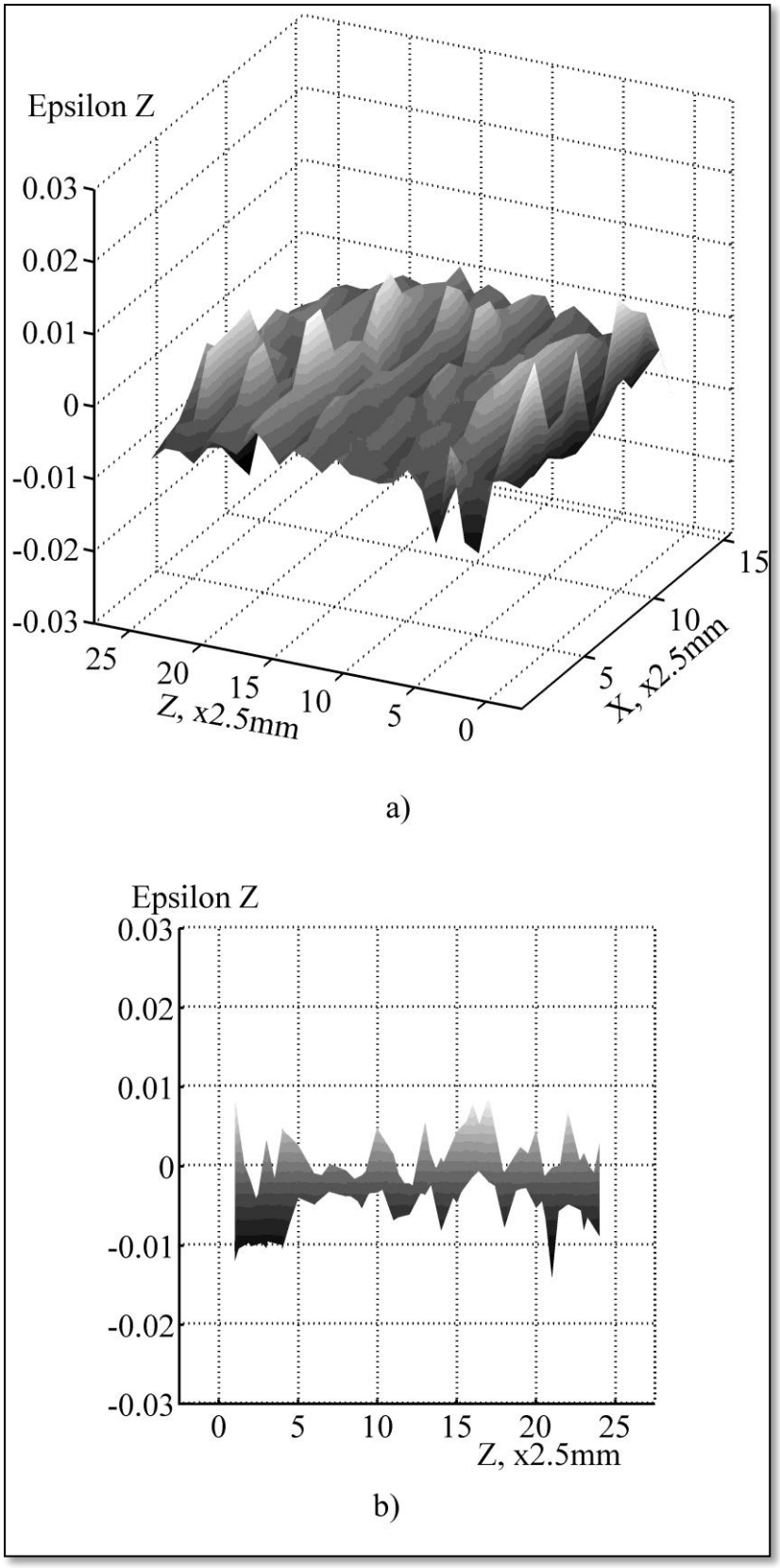

Figure 6.5 Distribution of ε_z over the test plate. a) 3D representation, b) front view of the same surface

The observations of parts produced by μSLA show that the curling has a significant impact on the part quality. As described on Figure 2.14 (Section 2.1.2.4) curling manifests more obviously by shear (angular) deviations from nominal (or strains γ), which can be analysed from the same test-plate. The results are shown on Figure 6.6 and Figure 6.7.

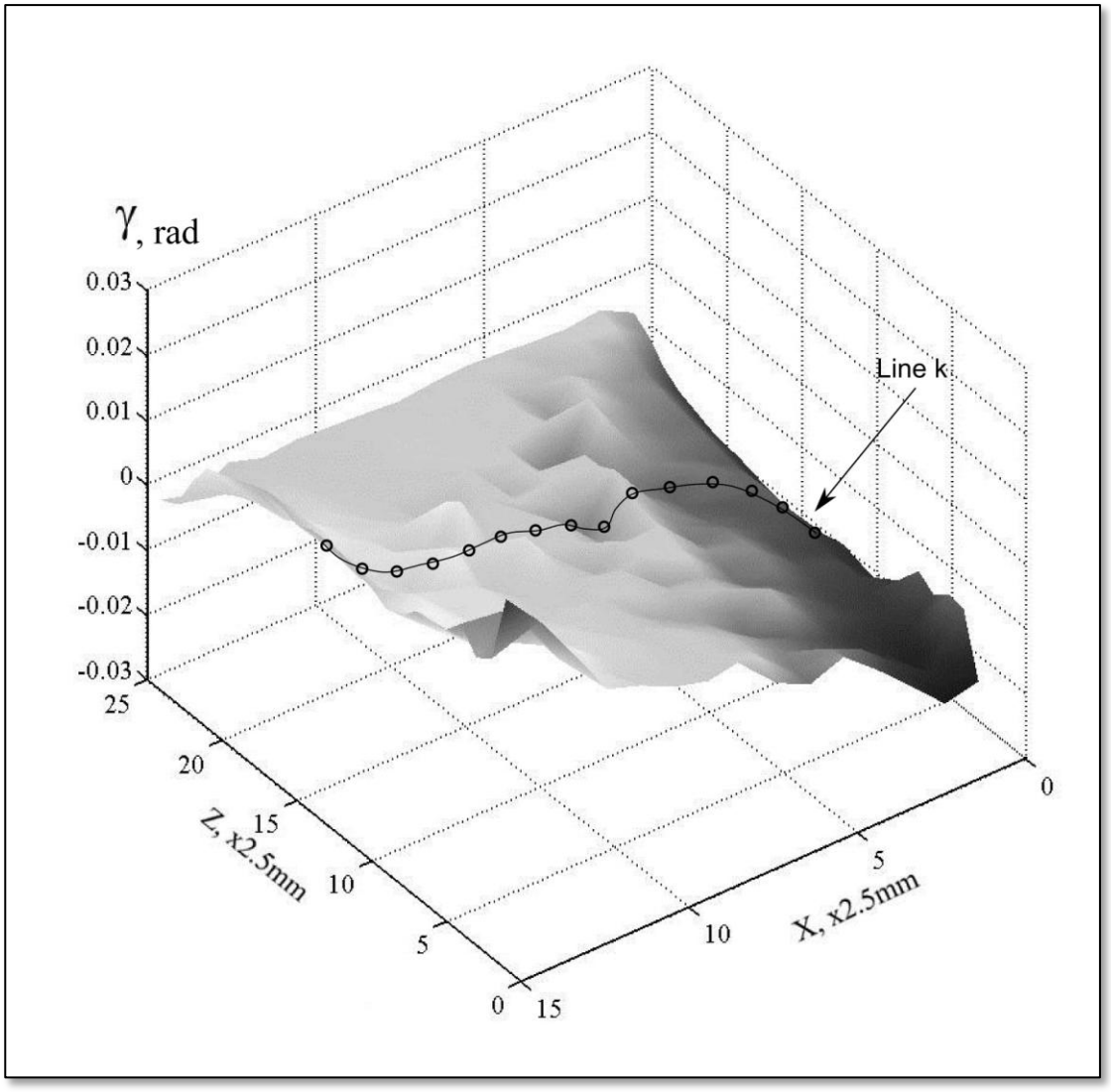

Figure 6.6 Surface showing the distribution of γ over the test plate

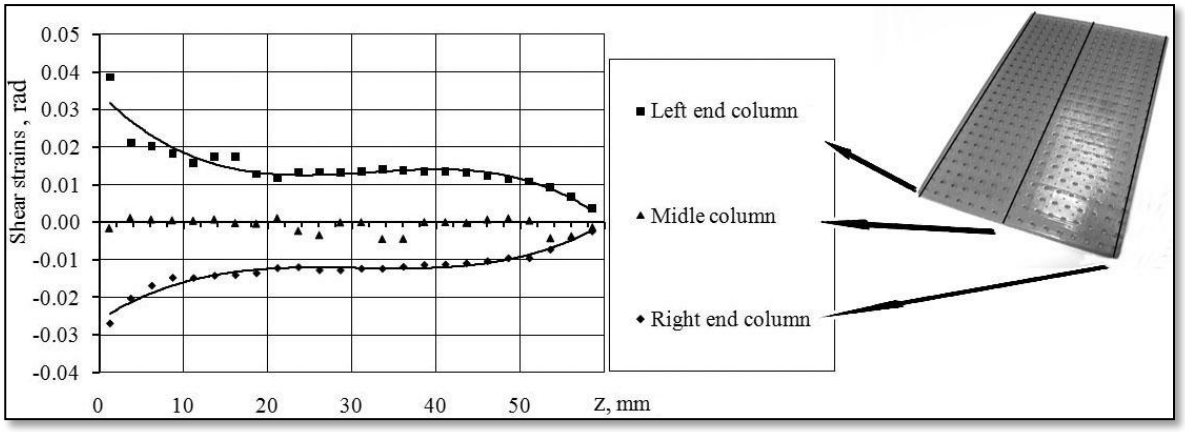

Figure 6.7 Distribution of shear strains (described as deviations from nominal) γ in *z* direction along different columns

In the case of the considered μSLA, the curling is identical on the left and on the right side of the part. This is illustrated by the symmetrical curves presented on Figure 6.7. From the graphs it can be seen that curling close to the edges is significant in the lower area of the part, it then drops off steeply (three times in value), after the height of 20 mm the distortion remains constant and become marginal at the top. This must be taken into consideration for real part builds. The typical curling phenomenon is due to the shrinkage effects after lightening up and curing of the resin, which is described in Chapter 1.

Some cross-sections of the presented surface on Fig. 6.6 could be derived in order to evaluate the distortions in the test plate along different directions and more particularly in horizontal and vertical directions. This would reveal the important differences of component inaccuracy distribution.

The line ‘k’ on Figure 6.6 represents the distribution of γ along the horizontal (*x*) direction. It can be seen clearly that γ are at a maximum close to the left and right

sides of the build (positive and negative respectively). They are at a minimum in the centre. In order to assess the changes in γ along the vertical direction it is useful to compare the values along *z*-axis. Since they are different in the centre and close to the edges of the build (see distribution alongside x) it is beneficial to compare their mean values for given z. The mean value of strain along each line "k" from Figure 6.6 generates the point "k" on the graph depicted on Figure 6.8. From this figure it is clear that this point has similar and very low (close to zero) values alongside z because the positive and negative deviations at left and right side of the build (close to the edges) are compensated giving nearly zero deviation at any height of the build. This could be interpreted as high average accuracy of the process.

The Standard Deviation of strains at each point "k" was also calculated. It represents the scatter of the γ values (lines "Std+" and "Std-"). The values of the Standard Deviations vary significantly and depend on the *z* position. This could indicate that the process precision at a given z is different and is much lower at the beginning of the build due to the considerable curling.

Total process precision over the entire plate can be evaluated by value of total standard deviations (throughout the whole build). At the same time the accuracy of the process could be evaluated by the mean value of the strains throughout the whole build. The results from calculations are:

μ = -0.00095 rad,

Std = 0.0086 rad,

and are included in Table 6.1.

To summarise the above observations, we can say that the process accuracy is high and process precision is relatively low and is dependent on the height of the build.

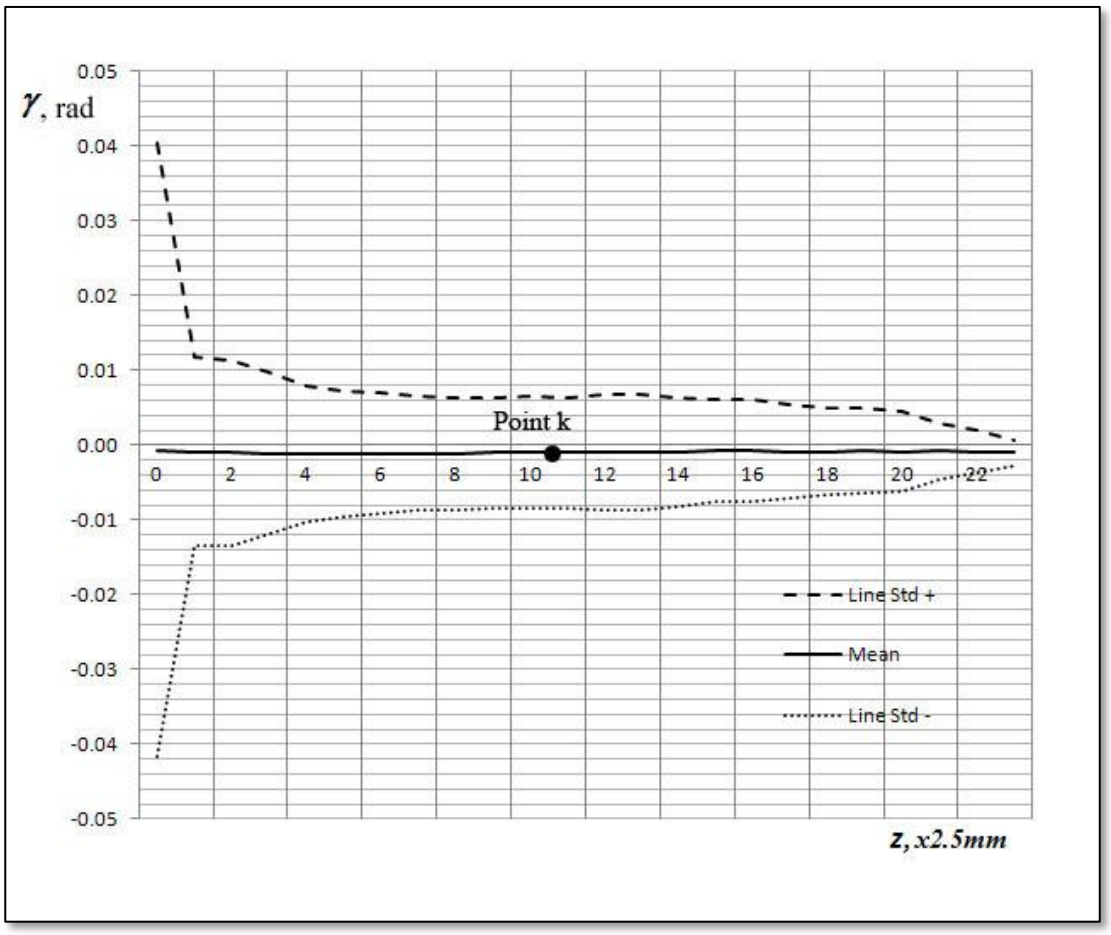

Figure 6.8 Mean values and spread of γ represented by its Std+ and Std- along each line over the test plate from Figure 6.4

As stated above γ can be considered as a general measure of curling distortion. The symmetrical nature of the curling phenomenon, which was shown above, gives the process high accuracy. However the spread of angular deviations γ is significant. The lines “Std +” and “Std -” (Figure 6.8) show considerable curling from the start of the build that can be expected (up to approximately 10 mm from the base). After this

level the curling is reduced and remains consistent to the end of the part build where it becomes negligible.

Test plate (Figure 6.4) was utilised to calculate ε_Z and ε_X along with their spread and mean values in a similar way to γ. The results of both linear (ε) and shear (γ) inaccuracies of the process are summarised in Table 6.1.

Table 6.1 Standard deviations and mean values of linear and angular deviations for μSLA process calculated over the total test plate

	Standard Deviation	Mean value
Angular deviations γ, rad	0.0086	-0.00095
Vertical deviations ε_Z	0.0039	-0.0028
Horizontal deviations ε_X	0.0049	-0.0071

Because of the complexity in strain distribution along the vertical and horizontal directions caused by the curling, it cannot be reduced easily by scaling only. Other measures such as changing the support structure are usually implemented to reduce the curling impact on total process accuracy (as described in Section 2.1.2.4).

Linear deviations have to be used to calculate the scaling factors of the part. In this case the linear strains are not uniform due to the curling effect. To exclude the curling influence, vertical scaling of a part is best done on the basis of results from

the *centre area* of the test plate (where the curling is zero). ε_z in the middle area of the plate is depicted on Figure 6.9. On this graph ε_z are interpolated with a line whose position illustrates the process accuracy. The gradient of the interpolated line and the mean value of the ε_z can be used as an evaluation of the process accuracy within the total build chamber. From the obtained statistical data it can be concluded that the process exhibits good accuracy with the mean value ε_{zmean} = -0.00119 (see Figure 6.9). Although the distribution of the strains within the total build volume is the main objective of the study using this method, some results with practical importance for scaling the parts can also be made. The mean value of ε_z could be interpreted as the total height of the plate being -0.119% shorter than nominal. The inclination of the interpolated line is small which demonstrates an absence of an undesirable trend in the vertical inaccuracy. It means that for this particular platform the CAD models of the real parts can be scaled by a constant scaling factor calculated by formula

$$Sc = 1/(\varepsilon_{zmean}+1) = 1.0012 \qquad (6.2)$$

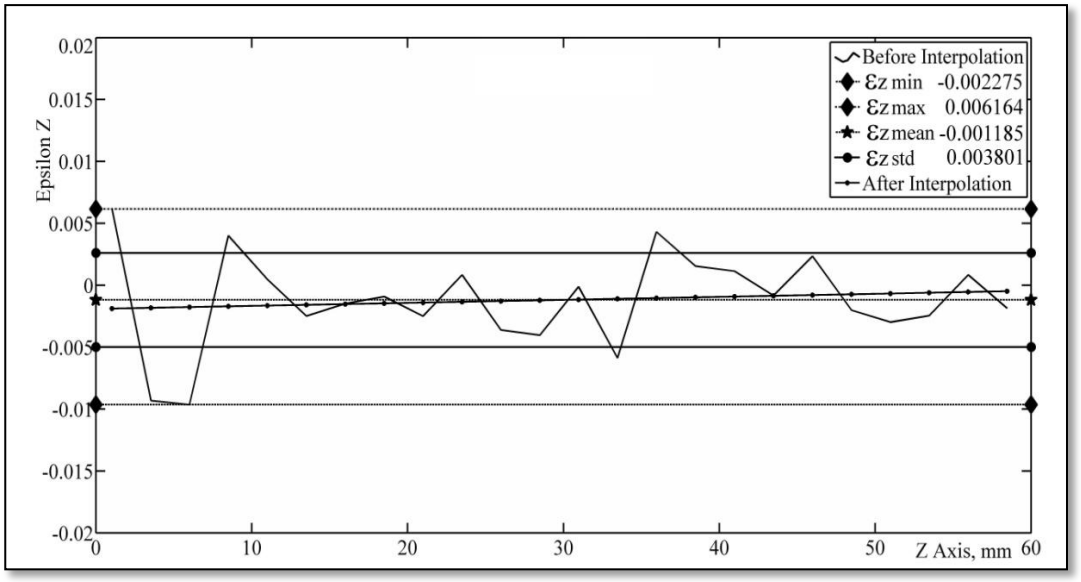

Figure 6.9 Distribution of strains ε_z alongside a column in the middle of the plate

It must be noted that applying a constant scaling factor for RP processes *is not always possible* as was illustrated in Section 5.3. These are the cases in which either the gradient of the approximation line is significant or the approximation is non-linear and can be applied only by a curve. Figure 6.9 also depicts the value of the Standard Deviation ($\varepsilon_z$std = 0.0038) which characterises the precision of the process in the *z*-direction. It shows that the spread of the mean value of ε_z (-0.00119) is significant and indicates the necessity of improvement if small features are to be produced.

6.3 Implementation of the Grid Method for accuracy analysis of micro machining

This section describes a comparative investigation with reference to micro drilling and micro wire electric discharge machining (μEDM) using the GM. Together with PM-μSLA these processes are promising technology in various master-making chains.

As a generic approach for accuracy investigation GM can be used *not only* for Free Form Fabrication processes but also for a variety of conventional processes or advanced micro manufacturing processes. Applications of such an approach have been reported recently (Minev et al. 2011).

The punching tool for green ceramic tapes (used for complex multilayer assemblies for microelectronic applications (Bredeaua and Bancillon 2011)) was targeted for accuracy investigation. The tools are shown on Figure 6.10 and Figure 6.11.

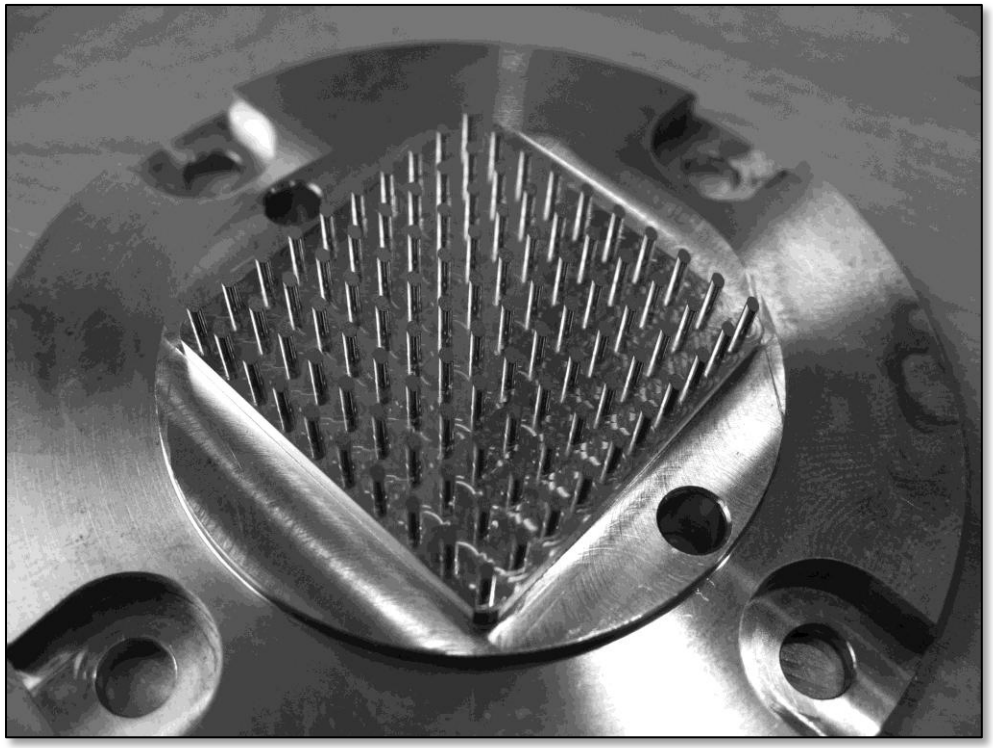

Figure 6.10 A punch produced by micro milling process

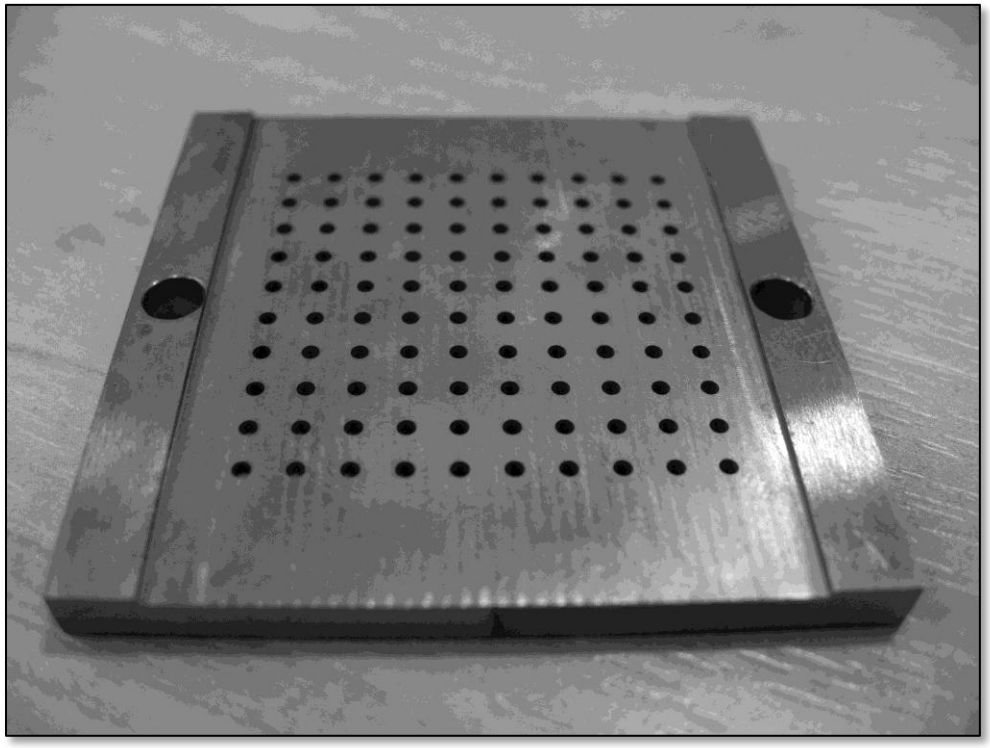

Figure 6.11 A die manufactured by micro drilling and micro wire EDM processes

Since both these parts mate, accuracy of both parts is imperative for tool functionality. The punch (Figure 6.10) is produced by one micro milling process which requires one machine setup operation. The die (Figure 6.11) manufacture requires two different processes (micro drilling and micro wire electric discharge machining (μEDM)) and thus two machine setting operations.

In this case, due to their geometry, the actual components can be used directly for strain calculations instead of producing a test plate with a grid. The key features, the pins and the holes act as reference points of the grid for measurement. Their positions were measured directly in the same way as those of the test plate described in Chapter 4. The results are illustrated on Figure 6.12. Values for ε_x and ε_y are statistically identical and only ε_y are shown for illustration.

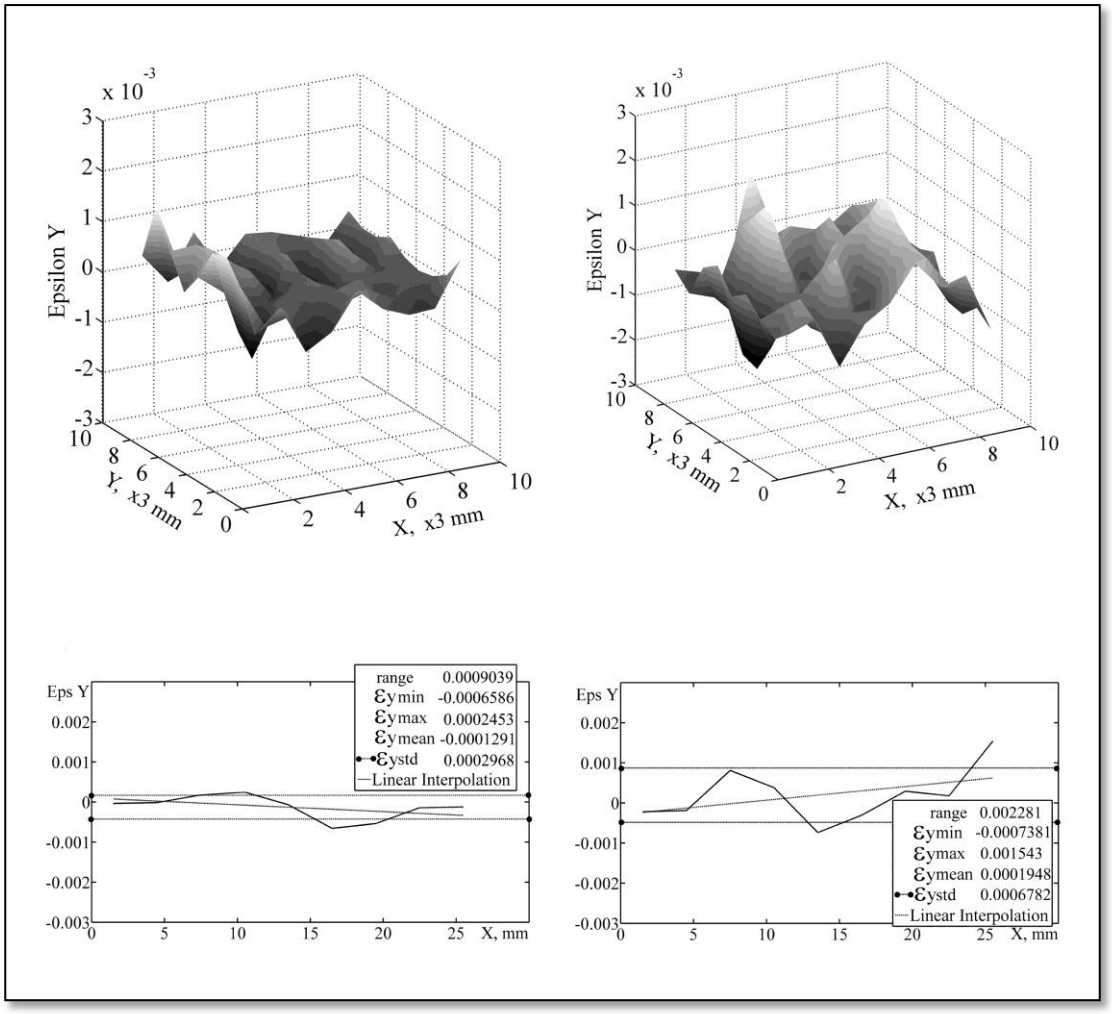

Figure 6.12 Distribution of ε_y. Left – pins (punch tool) from Figure 6.10; Right – hols (die tool) from Figure 6.11

The study of the inaccuracies by GM reveals that in the case of one machine setting operation, ε_y distribution is in the range of 0.1% and approximately 0.2% in the case of two setting operations. The results show well-matched accuracy between the two consecutive processes. The final errors after the second process of EDM are no more than twice the errors of the initial micro machining process which means that the contributing inaccuracies from each process are equal and the cumulative inaccuracy is acceptable.

It is important to note (Figure 6.12 and Table 6.2) that the accuracy and the precision of the micro-milling process (measured by the mean value of strains and the Standard Deviation) is 10 times higher than that of the μSLA and the micro-milling + micro EDM process chain is 5 times more precise and accurate than the micro SLA.

Table 6.2 Accuracy and precision of: μSLA; Micro Milling; Micro milling + micro EDM

	Micro SLA	Micro Milling	Micro milling + EDM
Mean value of ε_y (accuracy)	-0.00119	-0.000129	0.000195
Standard Deviation of ε_y (precision)	0.0038	0.00030	0.00068

6.4 Conclusions

This chapter has shown that, in terms of geometrical uncertainties, curling can be best described as a rotation of the line segments manifested in the same way as shear strains. The utilised GM methodology can be used to clearly reveal and estimate the curling magnitude and distribution within the part. In layer based RP processes such as μSLA the curling effect on the lower layers and close to the part edges is significant and *must* be taken into consideration.

It has also shown that GM could be utilised not only to evaluate the accuracy of RP but also is applicable for characterisation of the geometrical uncertainties of other advanced manufacturing technologies.

In particular the study of Micro-Stereolithography (μSLA) process shows that curling is the most typical source of inaccuracy of micro-parts. The deviations from the nominal are within 1% and the edge curling of the parts significantly contributes to the vertical inaccuracy. As an example the holes close to the part edge would have an angular displacement of 2 degrees when compared to holes at the centre.

Overall the work indicates that GM can be applied successfully to study the accuracy of process chains and analysing accumulated errors from each consecutive process. Furthermore in this study it was shown that the process chains for producing a punch tool are capable of achieving good matching accuracy (0.2% cumulative positional error).

It has been proven that the measurement and the calculating technique of GM for accuracy investigation can be used on real components without producing a dedicated test part, this depends upon the geometry of the real part to be produced.

CHAPTER 7 HOW TO USE GM DATA TO EVALUATE PROCESS CAPABILITIES?

7.1 Grid Method for capability studies of MNT

This chapter is focused on outlining a methodology, based on the Grid Method, to evaluate the process capability and rational determination of tolerance bands for the studied processes. The process benchmark criteria in this study, as well as the ways to define the process compatibility (namely the ability of the processes to be combined in pairs and chains) are also determined. In the process of designing micro parts it is necessary to know the specified tolerances based on the functional requirements of the part and those required by the customer. However, for a realistic assignment of tolerances the knowledge of the capabilities of process or process chains is of paramount importance.

The tolerance capability of the processes and process chains could be effectively studied with the Grid Methodology taking into account the following specifics:

1) There is no shape and size contextualisation when the method is applied to evaluate the uncertainties. Therefore the achieved results could be implemented in the design specification and process evaluation for different geometries.

2) The results obtained by applying the Grid Methodology are achieved on a plate geometry type and should be used with some precaution when tolerancing special

and more complex shapes. However this 'disadvantage' is even more acute and results are less transferable when specific test pieces are used (such as 'stair cases' samples, shafts, holes etc.) to evaluate process variances.

3) The variations in the dimensions calculated with the Grid Method are complex by their nature. They encompass and take into account the deviations throughout the whole build envelop of the FF or/and MNT process and could be interpreted as a holistic measurement of the process capability. These results could be used for benchmarking and evaluating process compatibility and complementarity, with regards to both single process and process chains.

In engineering design the Upper Specification Limit (USL) and Lower Specification Limit (LSL) are defined by the designer/manager as boundaries within which the system must operate. When those limits are not yet known they can be obtained and adjusted by the process statistics for the particular sample size. They are defined as natural tolerance limits (Chandrupatla et al. 2009), (Krajewski et al. 2010): Upper Natural Tolerance Limit - UNTL and Lower Natural Tolerance Limit – LNTL (Figure 7.1):

$$UNTL = \mu + 3\sigma; \qquad LNTL = \mu - 3\sigma \tag{7.1}$$

Where μ is the population mean, σ is the population standard deviation of sample size *n* of the measured parameter *X*.

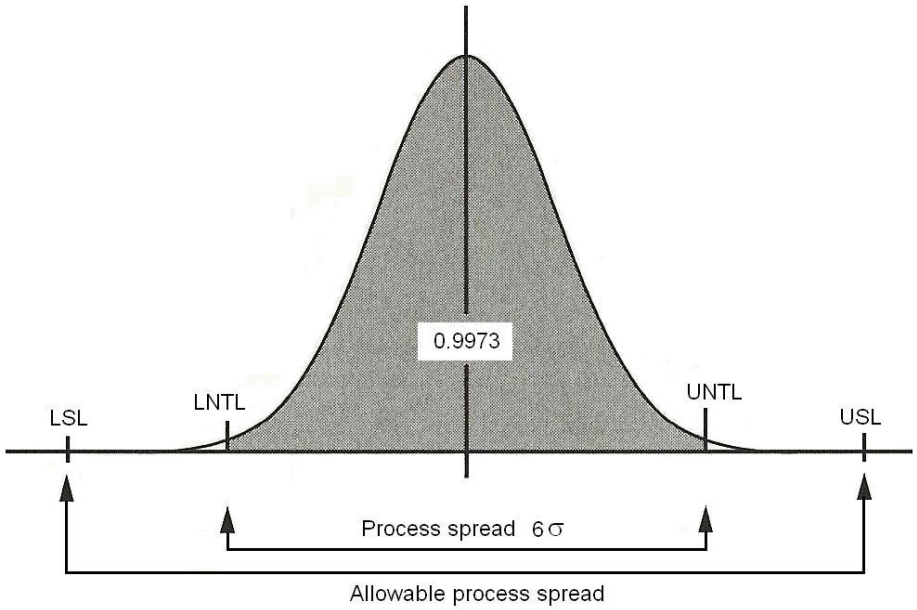

Figure 7.1 Specification limits and natural tolerances (Chandrupatla et al. 2009)

If the uncertainties are normally distributed then 99.73% of the samples will fall in this interval and the 'process spread' is defined as:

$$\text{UNTL} - \text{LNTL} = 6\sigma \tag{7.2}$$

If the process is skewed 'off-centred' (Figure 7.2) with $b=|\mu-T|$, where T is the target value of X then:

$$UNTL = T + b + 3\sigma \tag{7.3}$$

$$LNTL = T + b - 3\sigma \tag{7.4}$$

If the above approach is applied to the dimensionless deviation from nominal per unit length ($\varepsilon = \frac{\Delta L}{L_0}$) calculated by the Grid Method then the target value is:

$\varepsilon = T = 0$

and the equations for the UNTL and LNTL will be transformed as follows:

$$\left(\frac{\Delta L}{L}\right)_{UNTL} = T + b + 3\sigma = \mu + 3\sigma$$

$$\left(\frac{\Delta L}{L}\right)_{LNTL} = T + b - 3\sigma = \mu - 3\sigma \qquad (7.5)$$

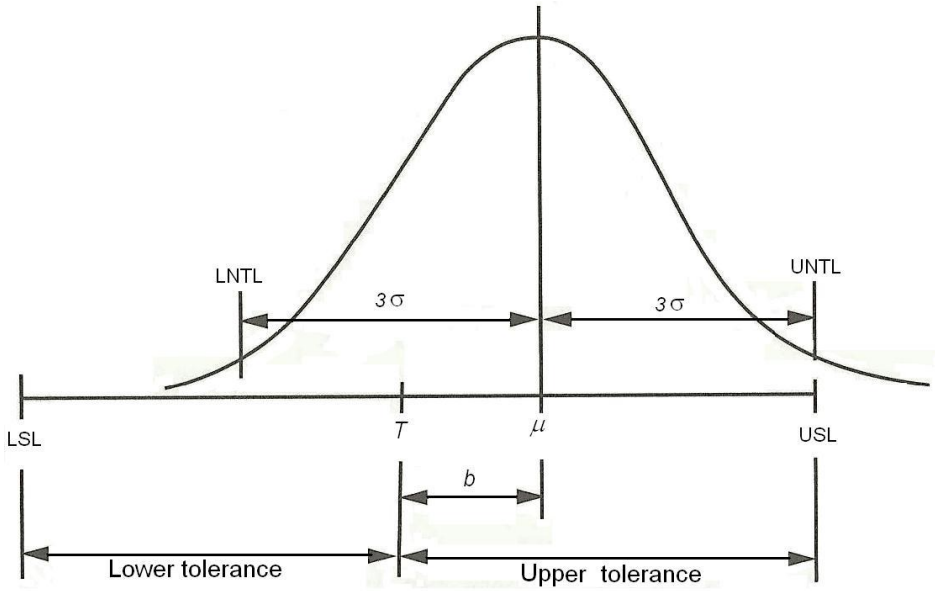

Figure 7.2 Defining the process capability (Chandrupatla et al. 2009)

In the Grid Method the variance could be estimated for any particular area within the process build envelop. The root cause of variance could differ according to the process specifics and the physical phenomenon (thermal, mechanical, rheological, chemical) behind each process. In Chapter 5 the particularities in the SLS process were studied and the implications they may have on the accuracy of the build part in accordance of their size, geometry and position within the built part were considered. It is clear that the process capabilities could be determined (and tolerances assigned) separately for any particular area of the build envelop. The process capability will differ according to the size of the part and its position in the part bed. In MNT processes such differentiation is not always possible or practically feasible. In this case an integrated capability variance reference to the entire operational envelops could be estimated and the '3σ' tolerances for any

dimension could be calculated based on the natural tolerance limits following equations (7.5) as follows:

$$\Delta L_{USL} = \mu L + 3\sigma L$$

$$\Delta L_{LSL} = \mu L - 3\sigma L \qquad (7.6)$$

The benchmarking of the studied MNTs based on their capabilities is presented in the following sections and is conducted using the following parameters:

Process offset ($b=\mu$) - accuracy indicator

Process spread (6σ) - precision indicator

The graphical representations and the interpretations used later in this Chapter for studying the MNT process 'capabilities' are shown on Figure 7.3 and Figure 7.4. Ideally, after calibration (for instance following the procedure described in Chapter 5), the process offsets will be zero.

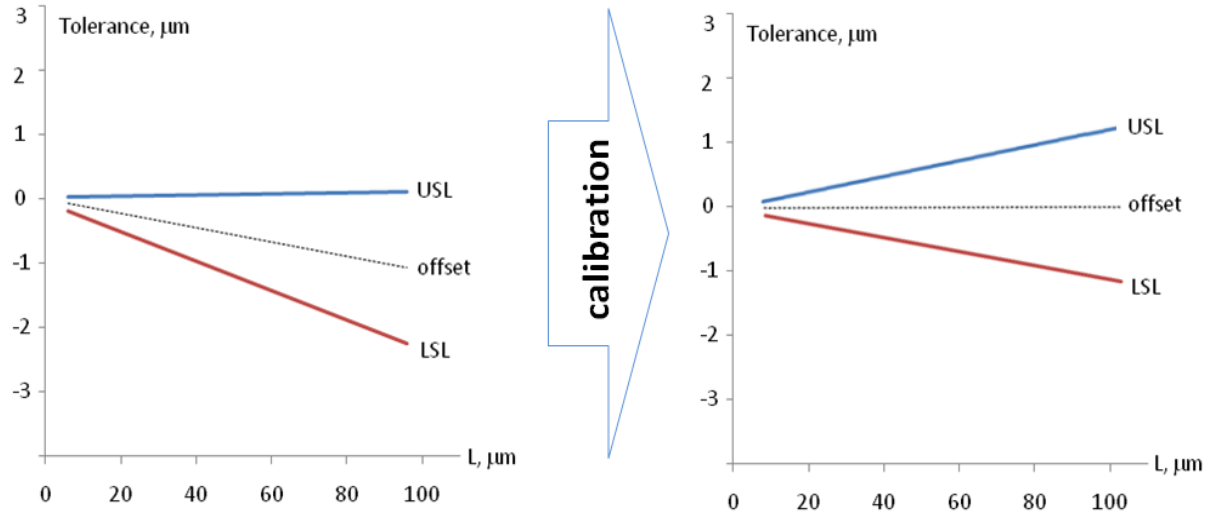

Figure 7.3 Graphical representations of process precision and accuracy

The evaluation of the process compatibility to form a pair (chain) and the estimation of the tolerance of the process pair is described on Figure 7.4. Process

1 is more accurate and precise than Process 2 but their tolerances are of the same order of magnitude and they are compatible from a dimensional accuracy point of view, these could be deemed complementary if used as a adjacent processes (i.e. a pair) on different materials.

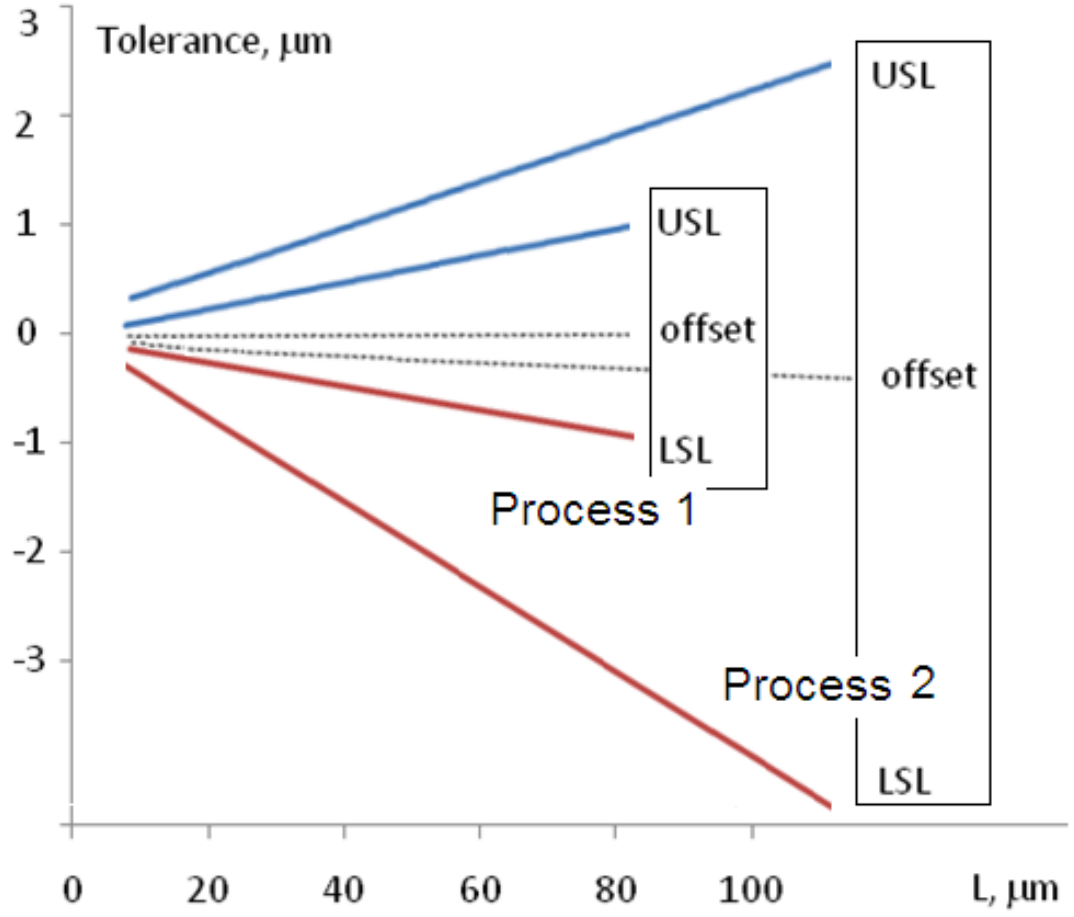

Figure 7.4 Comparison of the process capabilities of two processes

The following definitions apply when discussing here and later the process compatibility and complementarity (Vella et al. 2010; Bigot et al. 2010):

Complementarity is an overall measure of how much two processes are perceived to be able to complement or enhance each other's capabilities so that the

combined application of the processes should have a value added (or synergetic) effect on the capabilities.

Compatibility is an overall measure of how much two processes are perceived to be able to work successfully together or to perform to the same level of the capability parameters. In the ultimate case of complete compatibility the processes are competing alternatives rather than a complementary section of a process chain.

We suggest the following imperatives when defining the process compatibility/complementarity based on the assessment of the dimensional accuracy of the processes (Minev et al. 2010(a), (b)):

- **IF** process capability parameters **ARE** of the same order of magnitude, then the parameters and the corresponding processes are **Compatible**.
- **IF** process capability parameters **ARE NOT** of the same order of magnitude, then the parameters and the corresponding processes are **Complimentary**.

Usually when defining the capability of a process the capability index (C_{pk}) is used:

$$c_{pk} = min\left[\frac{\mu - LSL}{3\sigma}, \frac{USL - \mu}{3\sigma}\right] \qquad (7.7)$$

The user of a particular technology targeting a quality of three, four, five, or six sigma will use C_{pk} = 1; 1.33; 1.67 or 2 respectively (Krajewski et al. 2010). Some recommended values of the LSL and USL for selected dimensions produced with μSLA have been calculated utilising the described Grid Method approach and presented in specific Figures and Tables in the following section.

Since the measurement procedure shows very good reproducibility and repeatability (Paragraph 4.6) the methodology (an hence results) could be applied quickly (i.e. an "express mode") using a single test piece. However the repeatability of the process itself is not considered if a single test piece is produced.

7.2 Capability study of MNT processes

Since the Grid Method utilised in this study enabled the collection of a large amount of data from a single test piece (sample size of more than 150) the 'express' option provides reliable and satisfactory results. This allows for a comprehensive study of capabilities and tolerances of several processes to be stored for reference (i.e. it creates a "toolbox" of data) for producing different MNT tools and components with specific length scale integration features or multi-material utilisation (Bigot et al. 2010, 2009).

Ultimately this section presents a practical guideline for defining the design tolerances and control limits of the studied processes (PM-SLA; μ-Milling; μ-

EDM; Focused Ion Beam Milling). All calculations are based on the results of μ and σ from relevant GM experiments. To compare the processes capabilities for other dimensions it has been assumed that the deviations depend linearly on the nominal. This approach is suggested as express and rough method for process comparison and estimation of predicted tolerances. By excluding rows and columns of the grid it is possible from the same test part easily to obtain data for estimating tolerances for larger nominal dimensions.

The tolerance window for the PM-μSLA process calculated according to the equation (7.6) is presented in Figure 7.5. The recommended tolerances in this process are nearly 10 times higher than the corresponding values for the μ-Milling process and μEDM processes (Figure 7.6 and Figure 7.7).

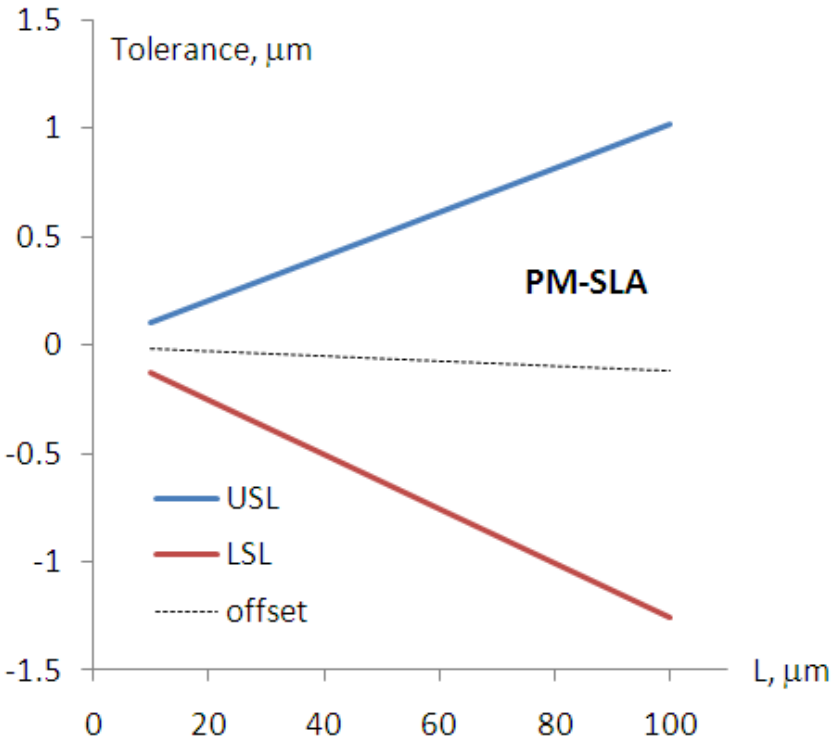

Figure 7.5 Tolerance limits for the PM-μSLA

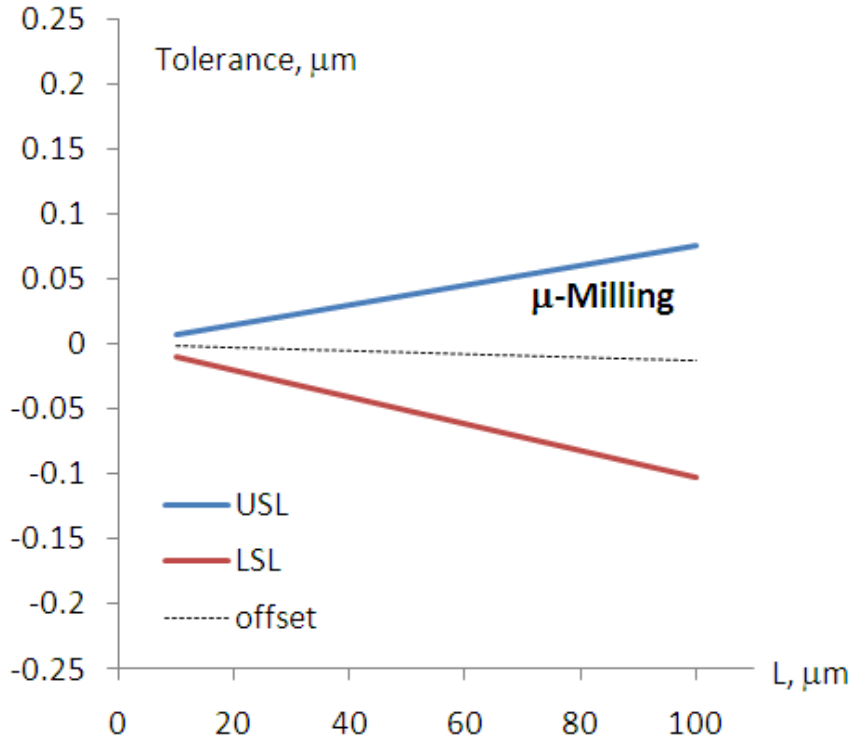

Figure 7.6 Tolerance limits for the µ-Milling process

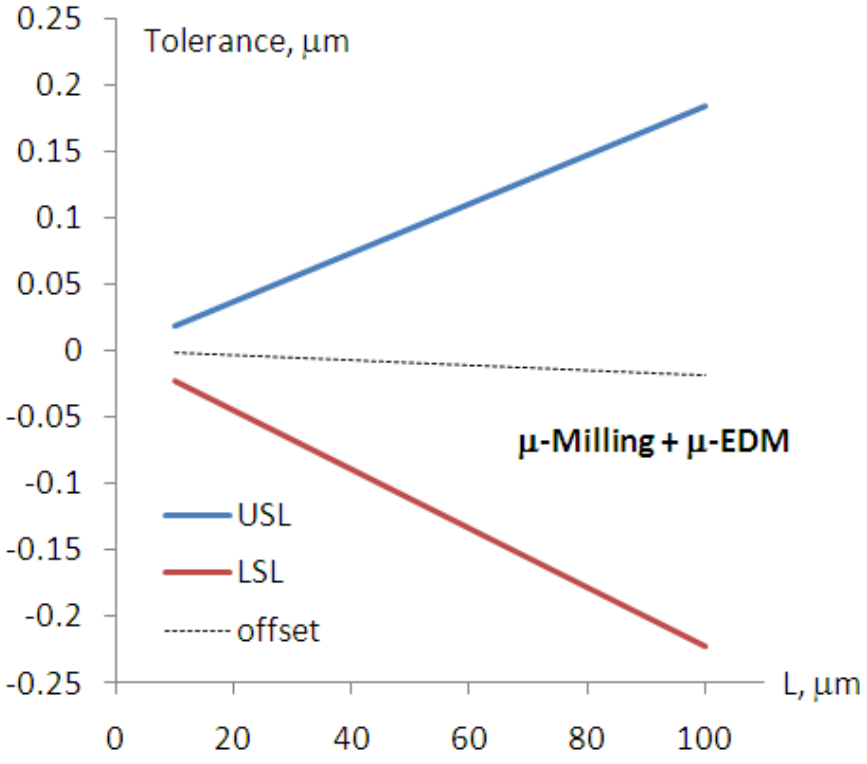

Figure 7.7 Tolerance limits for the µ-Milling + µ-EDM process chain

The evaluation of the compatibility/complementarity nature of the processes according to the methodology described in section 7.1 is summarised in Table 7.1.

Table 7.1 Complementarity / Compatibility evaluation and 'process spread' (μm) for a typical feature size (100μm)

μ-Milling	μ-Milling + μ-EDM	FIB	
Complementary PM-SLA: 3 μm μ-Milling: 0.2 μm **(*)**	***Complementary*** PM-SLA: 3 μm μ-M/EDM: 0.5 μm **(*)**	***Compatible*** PM-SLA: 3 μm FIB: 2 μm **(**)**	PM-SLA
	Compatible μ-Milling: 0.2 μm μ-M/EDM: 0.5 μm	***Complementary*** μ-Milling: 0.2 μm FIB: 2 μm **(***)**	μ-Milling
		Complementary μ-M/EDM: 0.5 μm FIB: 2 μm **(***)**	μ-Milling + μ-EDM

It can be seen that the tolerances for the process chain μ-Milling + μ-EDM are higher than the tolerances for the μ-Milling alone. The major contribution for the uncertainty in this case is the second process - μ-EDM. The EDM was used to calibrate the holes size to the design specification of the tool. The estimated

tolerances for this process are presented in Table 7.2. The use of a less accurate process (μ-EDM) after a more accurate process (μ-Milling) is usually not recommended but in this particular case it was a necessary compromise of the rule, in order to achieve the specific non-standard size of the holes.

A comparison of the studied processes that this approach enables in terms of their achievable accuracy tolerance is presented in Figure.7.8, which together with Table 7.2 could be used as a reference tool to estimate the indicative specification limits (USL and LSL). μ-Milling, μ-EDM and FIB processes are clustered together (Process cluster I) according to their accuracy in the range of < 0.5% error, while μSLA (due to the implemented thermal and photo curing processes) is less accurate with an error range of > 2% (Process cluster II). As shown in the Table 7.1 the differences in the accuracy range does not create an obstacle to form various process chains on the ground of either compatibility or complementarity nature.

Most of the indicative process chains designed and evaluated in this work through the Grid Method included accuracy evaluation, process phenomenon research and calibration. Typically they included multi-material objects (tools and parts) and Functional and Length Scale Integration (FLSI) features (Bigot S. et al., 2009). The examples cited with (*), (**) and (***) in Table 7.1 are briefly outlined below:

(*)

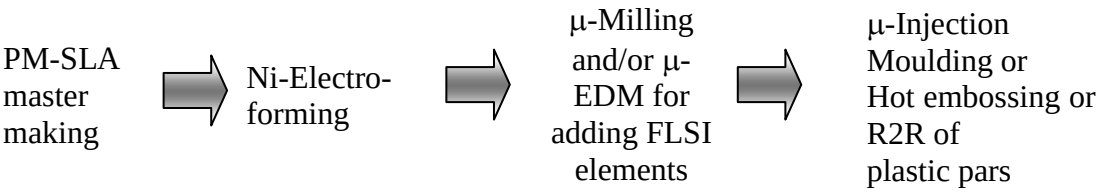

Product examples: Neuro-medical electrodes

(**)

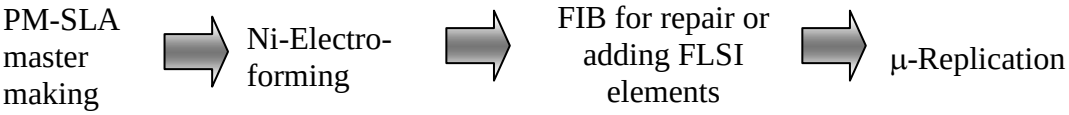

Product Examples: Shark skin or other bio-mimetic surfaces; Neuro-medical electrodes

(***)

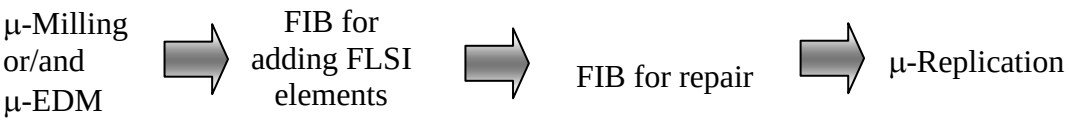

Product Examples: Diffractive optical devices

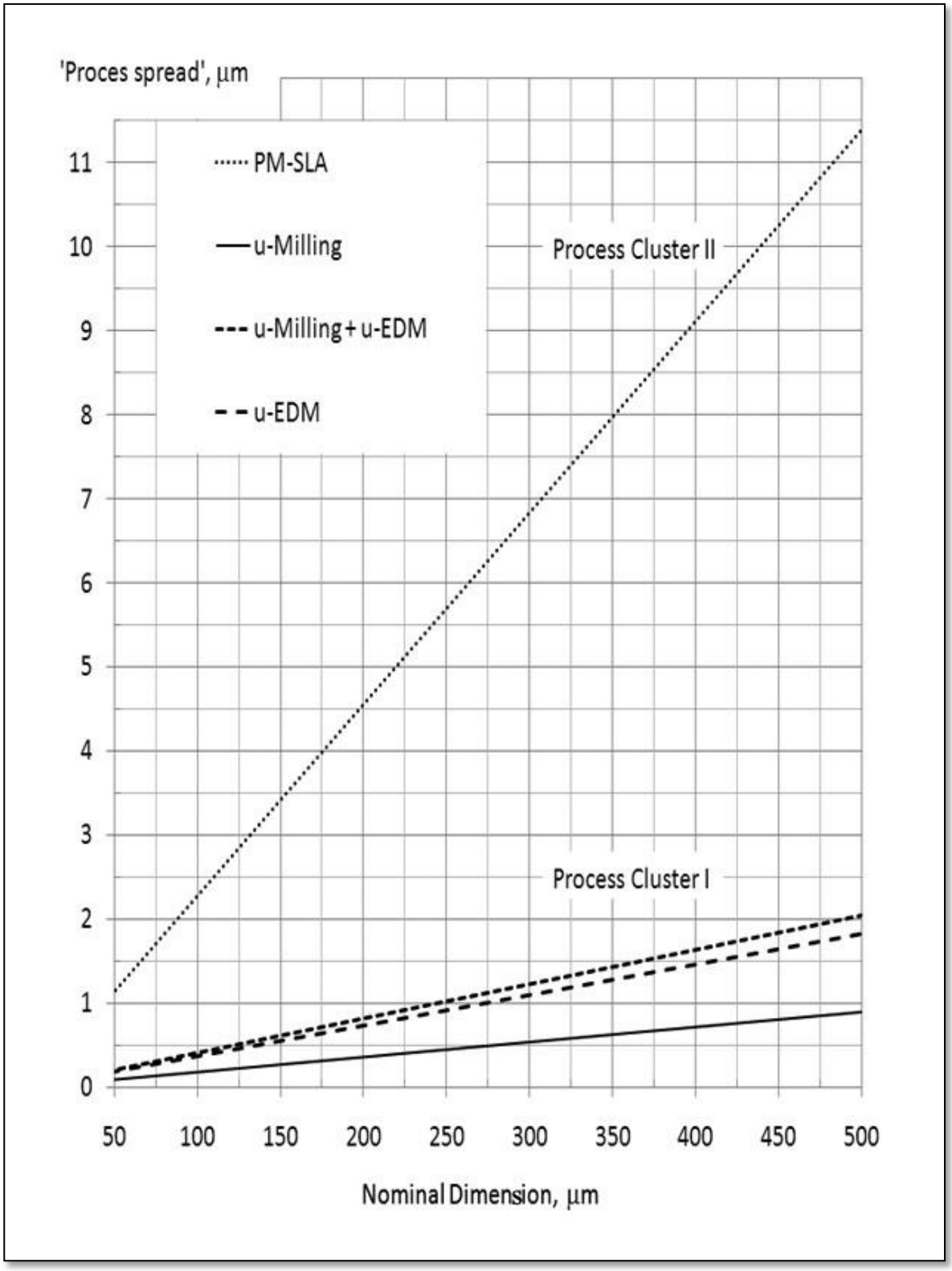

Figure 7.8 Process spread of the investigated MNTs for determination of recommended tolerances

Table 7.2 Recommended process tolerances for nominal dimensions L=10-500 μm

	PM-SLA			μ-Milling			μ-Milling + μ-EDM			μ-EDM		
L, μm	USL, μm	LSL, μm	spread, μm	USL, μm	LSL, μm	spread, μm	USL, μm	LSL, μm	spread, μm	USL, μm	LSL, μm	spread, μm
10							0.02	-0.02	0.04	0.02	-0.02	0.04
20				0.02	-0.02	0.04	0.04	-0.04	0.08	0.04	-0.04	0.07
30				0.02	-0.03	0.05	0.06	-0.07	0.12	0.05	-0.06	0.11
40				0.03	-0.04	0.07	0.07	-0.09	0.16	0.07	-0.08	0.15
50				0.04	-0.05	0.09	0.09	-0.11	0.20	0.09	-0.09	0.18
60	0.61	-0.76	1.37	0.05	-0.06	0.11	0.11	-0.13	0.24	0.11	-0.11	0.22
70	0.72	-0.88	1.60	0.05	-0.07	0.12	0.13	-0.16	0.28	0.12	-0.13	0.26
80	0.82	-1.01	1.82	0.06	-0.08	0.14	0.15	-0.18	0.33	0.14	-0.15	0.29
90	0.92	-1.13	2.05	0.07	-0.09	0.16	0.17	-0.20	0.37	0.16	-0.17	0.33
100	1.02	-1.26	2.28	0.08	-0.10	0.18	0.18	-0.22	0.41	0.18	-0.19	0.37
110	1.12	-1.38	2.51	0.08	-0.11	0.20	0.20	-0.24	0.45	0.19	-0.21	0.40
120	1.23	-1.51	2.74	0.09	-0.12	0.21	0.22	-0.27	0.49	0.21	-0.23	0.44
130	1.33	-1.64	2.96	0.10	-0.13	0.23	0.24	-0.29	0.53	0.23	-0.25	0.48
140	1.43	-1.76	3.19	0.11	-0.14	0.25	0.26	-0.31	0.57	0.25	-0.26	0.51
150	1.53	-1.89	3.42	0.11	-0.15	0.27	0.28	-0.33	0.61	0.27	-0.28	0.55
160	1.63	-2.01	3.65	0.12	-0.16	0.28	0.30	-0.36	0.65	0.28	-0.30	0.59
170	1.74	-2.14	3.88	0.13	-0.17	0.30	0.31	-0.38	0.69	0.30	-0.32	0.62
180	1.84	-2.27	4.10	0.14	-0.18	0.32	0.33	-0.40	0.73	0.32	-0.34	0.66
190	1.94	-2.39	4.33	0.14	-0.19	0.34	0.35	-0.42	0.77	0.34	-0.36	0.70
200	2.04	-2.52	4.56	0.15	-0.20	0.36	0.37	-0.44	0.81	0.35	-0.38	0.73
210	2.15	-2.64	4.79	0.16	-0.21	0.37	0.39	-0.47	0.85	0.37	-0.40	0.77
220	2.25	-2.77	5.02	0.17	-0.22	0.39	0.41	-0.49	0.90	0.39	-0.42	0.80
230	2.35	-2.89	5.24	0.18	-0.23	0.41	0.42	-0.51	0.94	0.41	-0.43	0.84
240	2.45	-3.02	5.47	0.18	-0.24	0.43	0.44	-0.53	0.98	0.42	-0.45	0.88
250	2.55	-3.15	5.70	0.19	-0.25	0.45	0.46	-0.56	1.02	0.44	-0.47	0.91
260	2.66	-3.27	5.93	0.20	-0.27	0.46	0.48	-0.58	1.06	0.46	-0.49	0.95
270	2.76	-3.40	6.16	0.21	-0.28	0.48	0.50	-0.60	1.10	0.48	-0.51	0.99
280	2.86	-3.52	6.38	0.21	-0.29	0.50	0.52	-0.62	1.14	0.50	-0.53	1.02
290	2.96	-3.65	6.61	0.22	-0.30	0.52	0.53	-0.65	1.18	0.51	-0.55	1.06
300	3.06	-3.78	6.84	0.23	-0.31	0.53	0.55	-0.67	1.22	0.53	-0.57	1.10
310	3.17	-3.90	7.07	0.24	-0.32	0.55	0.57	-0.69	1.26	0.55	-0.59	1.13
320	3.27	-4.03	7.30	0.24	-0.33	0.57	0.59	-0.71	1.30	0.57	-0.60	1.17
330	3.37	-4.15	7.52	0.25	-0.34	0.59	0.61	-0.73	1.34	0.58	-0.62	1.21
340	3.47	-4.28	7.75	0.26	-0.35	0.61	0.63	-0.76	1.38	0.60	-0.64	1.24
350	3.58	-4.40	7.98	0.27	-0.36	0.62	0.65	-0.78	1.42	0.62	-0.66	1.28
360	3.68	-4.53	8.21	0.27	-0.37	0.64	0.66	-0.80	1.46	0.64	-0.68	1.32
370	3.78	-4.66	8.44	0.28	-0.38	0.66	0.68	-0.82	1.51	0.65	-0.70	1.35
380	3.88	-4.78	8.66	0.29	-0.39	0.68	0.70	-0.85	1.55	0.67	-0.72	1.39
390	3.98	-4.91	8.89	0.30	-0.40	0.69	0.72	-0.87	1.59	0.69	-0.74	1.43
400	4.09	-5.03	9.12	0.30	-0.41	0.71	0.74	-0.89	1.63	0.71	-0.76	1.46
410	4.19	-5.16	9.35	0.31	-0.42	0.73	0.76	-0.91	1.67	0.73	-0.78	1.50
420	4.29	-5.29	9.58	0.32	-0.43	0.75	0.77	-0.93	1.71	0.74	-0.79	1.54
430	4.39	-5.41	9.80	0.33	-0.44	0.77	0.79	-0.96	1.75	0.76	-0.81	1.57
440	4.49	-5.54	10.03	0.33	-0.45	0.78	0.81	-0.98	1.79	0.78	-0.83	1.61
450	4.60	-5.66	10.26	0.34	-0.46	0.80	0.83	-1.00	1.83	0.80	-0.85	1.65
460	4.70	-5.79	10.49	0.35	-0.47	0.82	0.85	-1.02	1.87	0.81	-0.87	1.68
470	4.80	-5.91	10.72	0.36	-0.48	0.84	0.87	-1.05	1.91	0.83	-0.89	1.72
480	4.90	-6.04	10.94	0.37	-0.49	0.85	0.89	-1.07	1.95	0.85	-0.91	1.76
490	5.01	-6.17	11.17	0.37	-0.50	0.87	0.90	-1.09	1.99	0.87	-0.93	1.79
500	5.11	-6.29	11.40	0.38	-0.51	0.89	0.92	-1.11	2.03	0.88	-0.95	1.83

An illustaration of the process tolerances in accordance with the quality level (Krajewski et al. 2010), (Craig et al. 2005), (Montgomery 2004) and the value of

the capability index (C_{pk}) as described in section 7.1 are presented in Table 7.3. Two processes were compared (μSLA and μ-Milling), as they are representative of less and more accurate clusters of the studied processes.

Table 7.3 Calculated component tolerances corresponding to the expected quality standards

C_{pk}	Quality standard	Process yeld, %	**PM-SLA**		**μ-Milling**	
			Nominal size, μm	Tolerance, μm	Nominal size, μm	Tolerance
1	‘3σ‘	99.73 %	100	+1.0	100	+0.1
				-1.3		-0.1
			300	+3.1	300	+0.2
				-3.8		-0.3
			500	+5.1	500	+0.4
				-6.3		-0.5
1.33	‘4σ‘	99.99 %	100	+1.4	100	+0.1
				-1.7		-0.1
			300	+4.2	300	+0.3
				-4.9		-0.4
			500	+7.0	500	+0.5
				-8.2		-0.7
2	‘6σ‘	99.9999998 %	100	+2.2	100	+0.2
				-2.4		-0.2
			300	+6.5	300	+0.5
				-7.2		-0.6
			500	+10.8	500	+0.8
				-12.0		-1.0

7.3 Conclusions

The implementation of the Grid Method in combination with the basic concept of calculating the specification limits of processes provides a fast, economical and effective way to calculate and assign the design tolerances and quality control parameters in processes and process chains. This approach was implemented for benchmarking some MNT processes and to evaluate and predict possible process chains.

CHAPTER 8 CONTRIBUTIONS, CONCLUSIONS AND FURTHER WORK

CONTRIBUTIONS TO KNOWLEDGE

The main contributions to knowledge from the presented research can be summarised as:

The engineering of a new and original methodology for establishing the accuracy of components built by FF fabrication processes. This GM methodology is based on the descretisation of the object to allow the measurement, calculation, visualisation and analysis of the part distortion in terms of linear and shear deviations from nominal. The method overcomes limitations and disadvantages of currently used approaches for assessing the accuracy of RP processes.

The investigation of specific distortions in SLS polystyrene components using the GM revealed the presence of local extensions of the parts. This was not previously confirmed and clearly demonstrates the limitations of the commonly accepted model that assumed all over shrinkage. Proof that this effect can result in the distribution of inaccuracies is of a major significance. Proper process calibration and part compensation can now be undertaken using the data derived from the application of GM.

The important cause of part distortion known as curling was described in terms of angular (shear) deviations from nominal. This allows to separately analyse such kind of distortions from linear distortions and corresponding compensation measures to be implemented to improve product quality.

The application of the GM to the emerging micro-nano manufacturing sector has been shown to support the assessment of process capability. This provides a means of calculating process tolerances using results obtained from the single test piece. This demonstrated that, using the GM method, process compatibility and complimentarity can be more accurately calculated and process chains can thus be designed.

CONCLUSIONS

The review of current practice undertaken during this research indicated that there were sources of uncertainties arising in the performance of FF processes. It suggested that the distribution, magnitude and character of the uncertainties are not uniform within the build area of the manufacturing platforms and can vary significantly with part position, size and shape. This indicated that a reliable and generic method for the quantitative investigation of uncertainties and particularly their distribution was important.

The research considered the analysis of the methods and test parts used for these accuracy studies and concluded that the current investigation practices in the area

of Free Form (FF) fabrication were not always sufficient. In particular the approaches which utilise pyramid test parts were shown to be unable to provide reliable data regarding the distribution and type of uncertainties observed in build components. This was taken as justification for the engineering of a more generic and accurate methodology.

A new methodology was engineered to support the investigation of the distribution of linear and angular geometrical deviations in components. The methodology was named the Grid Method (GM). The adopted methodology utilises a test part in form of plate with grid formed across the part. The research then provided an automatic measurement procedure which enabled the calculation and presentation of geometrical characteristics that were designed for incorporation into software to enable a complete accuracy investigation.

Through the presented research it has been demonstrated that GM can be successfully applied to investigate and analyse the inaccuracy distribution in the RP process over the entire build envelope. Linear and angular deviations from nominal and their distributions were the geometrical characteristic used to describe the complex part distortions after building. These characteristics were calculated by adapting the concepts of strain used in solid mechanics. A single test piece that overcomes the disadvantages of pyramid test parts was utilised. This, in combination with automated measuring, makes the GM a powerful means for obtaining valuable information for analysing different build phenomena.

The GM was applied in order to research the causes of dimensional inaccuracy in the vertical direction of SLS polystyrene process. On the basis of the obtained results, the factors affecting part deformation such as gravity, induced shrinkage, overcompensation of the layers, temperature distribution and material behaviour were analysed. The existence of a critical dimension in height was revealed from where the part size distortion changes from shrinkage to extension. Layer thickness variations confirmed the complex causes for the nonlinear distortions of the built part.

It was demonstrated that the deviation of the sizes from nominal could be reduced by up to three times when the scaling formula was applied. The dimensional error in the *z* direction of SLS polystyrene part was reduced by applying GM from 1.8% to 0.6%.

The utilised methodology was shown to be capable of measuring and analysing the shear strain distribution to clearly reveal and estimate the magnitude of curling arising in any given line segment within the part. Interpretation of the strains as a measure of the dimensional uncertainties is clearly a very informative and easy to implement analysis tool. Its application to other manufacturing process was considered in the research; the study of µSLA processes indicated that curling is the most typical source of vertical inaccuracy in micro parts and that overall, the edge curling in µSLA parts significantly contributes to the vertical inaccuracy.

The GM was also applied to investigate the accuracy in advanced manufacturing technologies when they are deployed to form process chains by analysing

accumulated errors from each consecutive process. In this context it was shown that the process chains for producing a punch tool are capable of achieving good matching accuracy (less than 0.2% cumulative positional error).

The research indicated that, in some cases the measurement and the calculating technique of GM for accuracy investigation can be applied on real components without the need to produce a dedicated test part. This depends upon the geometry of the real part.

The implementation of the Grid Method in combination with the basic concept of calculating the specification limits of processes was therefore shown to provide a fast, economical and effective way to calculate and assign the design tolerances and quality control parameters in processes and process chains. This approach was verified in practical cases and was implemented for benchmarking some MNT processes and to evaluate and predict possible process chains.

FURTHER WORK

Further work could be done in two main directions

- improvement of the GM methodology;
- implementation of the GM for accuracy investigation of differnt processes and material.

The improvement of the GM could be focused on the measuring and calculation procedures. More particularly the utilisation of different measuring systems; automation of the processes; and elaboration of recommendations for the test piece geometry are some of the possible direction for further development.

Investigations and comparison (benchmarking) of different processes, materials and platforms in terms of accuracy is also a feasible target taking advantage of the methodology ability to describe the process uncertainties throughout the whole build volume quickly and cost-effectively.

Future investigation of the factors affecting part accuracy in different RP methods is promising. More specifically it is important to study and distinguish the influence of the factors affecting part deformation in SLS such as: gravity induced shrinkage; overcompensation of the layers; temperature distribution; energy delivered for processing. Comprehensive experiment set up could make a foundation for mathematical model of the process-material accuracy interaction.

APPENDIXES

Appendix 1 Program code for automatic CMM measurement control

```
Declare Sub QVBlock_2
' Declare Sub QVBlock_1
Declare Sub KBP_T_1
Declare Sub QVBlock_0
Declare Sub Write_Array_2_File
Declare Sub Write_Arrays_in_File_R
Declare Sub startup
Declare Sub Change_Row_Col
' Declare Sub Load_Points
Option Explicit
dim PointX
dim PointY
dim PointEndX
dim PointEndY
dim PointStartY
dim CoaxValue as Double
dim StageValue as Double
Dim STEP_X
Dim STEP_Y
DIM X_Focus
DIM ZEROs
DIM X_Align
dim TESTY
Dim XT() as Double
Dim YT() as double
' 04/06/2010
Dim RT() as double
' 04/06/2010
Dim Row_T() as Integer
Dim Col_T() as Integer
dim CN as Integer
dim MaxROW as Integer
dim MaxCOL as Integer
DIM C_Row as Integer
DIM C_Col as Integer
DIM CurrP as Integer
Dim Ave_Dist
Dim Answer
Dim CEN_Name as string
Dim msgtext as String
Dim R2_1
Dim Step_M
Dim KBP_Err
Dim III
Dim MEASURED_X_ACTUAL
Dim OLD_X_ACTUAL
Dim Stage_My
Dim MyCoax_V
Dim LensNomMag_KBP
'*** HERE SET ALL CONSTANTS**********YOU CAN CHANGE HERE***BIGGER VALUE - MORE LIGHT**********
' IN OLD is -->                    CONST MyCoax_V = 0.21      '  0.25 there are some white "spots!!!
```

```
'****************************************YOU CAN CHANGE HERE****0.xx is xx% LIGHT*****************************
dim C_Rad                           'EXTERNAL RADIUS
' IN OLD is --> const Stage_My = 0.19   '0.23   'STAGE LIGHT
'****************************************

sub startup '==========================
'  *** Display Format ***
DistanceUnits = MM
CoordinateMode = CART
ResolutionMode = DECIMALS_4
AngleRange = ZERO_TO_360
AngleUnits = DECIMAL_DEGREES_3

'  *** Lens in Use ***
Lens.Select Label:="1X (QV Objective)"

'  *** Results Formatting ***
Results.ShowColumnLabels = TRUE
Results.ShowFeatureTypeInHdr = TRUE
Results.ShowFeatureLabelInHdr = TRUE
Results.ShowFeatureIDInHdr = TRUE
Results.ShowNumOfPointsInHdr = TRUE
Results.FormatColumns     ELEMENT, ACTUAL, NOMINAL, DEVIATION, UPTOL, LOWTOL, PASSFAIL

'  *** Results Messages ***
Results.ShowAlignmentMsg = FALSE
Results.ShowUnitsChangeMsg = FALSE
Results.ShowConstructionMsg = FALSE
Results.ShowErrorMsg = TRUE   'FALSE - PRINT IN MESSAGE FILE

'  *** Results Data Reporting ***
Results.ReportLevel = ALLDATA

'  *** Results Logging ***
Results.LogToFile = FALSE
Results.LogToCOM1 = FALSE
Results.LogToCOM2 = FALSE

'  *** Restore MCS ***
PCS.RestoreMCS

'  *** Reference Plane ***
ReferencePlane = XY_PLANE

'  *** Measuring Device ***
MeasuringDevice = QV_VIDEO

'  *** Touch Probe Context Properties ***
TouchProbe.ApproachDist = 6.0000000
TouchProbe.SearchDist = 10.0000000
TouchProbe.CNCMeasureSpeed = 3.0000000
TouchProbe.CNCMotionSpeed = 50.0000000
TouchProbe.CNCMeasureAccel = 490.0000000
TouchProbe.CNCMotionAccel = 490.0000000
TouchProbe.CNCMeasureDecel = 490.0000000
TouchProbe.CNCMotionDecel = 490.0000000

end sub   'startup==========================
```

```
'************************************************
Sub Load_Points  '================================
end sub   'Load_Points==============================


'************************************************
Sub Change_Row_Col   '===========================

  CEN_Name = "CEN_"
  CEN_Name = CEN_Name + str(Format(C_Row,"0"))
  CEN_Name = CEN_Name + "_"
  CEN_Name = CEN_Name + str(Format(C_Col,"0"))
end sub   'Change_Row_Col==========================

'************************************************
sub Main    'start of MAIN subroutine============
Dim I
DIM II
'******************** TO READ IT *****************
' NEW - 19/03/2010
  Stage_My = InputBox("Enter STAGE Light Intensity (0.2-1)    :")
  MyCoax_V = InputBox("Enter COAX (TOP) Light Intensity (0.2-1):")
  if MyCoax_V < 0.21 then
    MyCoax_V = 0.21
  end if
  LensNomMag_KBP = InputBox("Enter Magnification (1, 2 or 6)     :")
  if LensNomMag_KBP >= 6 then
    LensNomMag_KBP = 6
  else
    if LensNomMag_KBP  >= 2 then
      LensNomMag_KBP  = 2
    else
      LensNomMag_KBP = 1
    end if
  end if
  MaxROW = InputBox("Enter Number of the Rows             :")
  MaxCOL = InputBox("Enter Number of the Columns ( <= 21)  :")
  if MaxCOL > 21 then
    MaxCOL = 21
  end if
  PointX=0
  PointY=0
  C_Rad = 2.2 / LensNomMag_KBP
  C_Row = 1
  C_Col = 1
  CurrP = 1
  Ave_Dist = 0
' ****************  NEW 4 Z Limit*****************
'************************REDim Arrays*********************************
  CN=MaxROW * MaxCol
ReDim XT(1 to CN)
ReDim YT(1 to CN)
' 04/06/2010
ReDim RT(1 to CN)
' 04/06/2010
ReDim Row_T(1 to CN)
ReDim Col_T(1 to CN)
'************************REDim Arrays*********************************
'   Stage.ClearZSafetyLimit
```

```
    call startup

  STEP_X = InputBox("Enter STEP IN X Axis    :")
  X_Focus = PointX + C_Rad

  Lens.NomMag = LensNomMag_KBP     ' OLD is --> 1.000000
'  CoaxValue  = (Lens.NomMag/20 + MyCoax_V)
  CoaxValue  = MyCoax_V
  if CoaxValue > 1 then
    CoaxValue =1
  end if
'  StageValue = (Lens.NomMag/20+0.29)
  StageValue = Stage_My
  if StageValue > 1 then
    StageValue =1
  end if

    Call   QVBlock_0
  PointY = 0
  OLD_X_ACTUAL = 0
'*********** CYCLE FOR a ROW ****************************************************
  For C_Row= 1 to MaxRow
    For C_Col= 1 to MaxCol
      Call   QVBlock_2
      if C_Col = 1 then
        if C_Row = 1 then
          STEP_Y = STEP_X
        else
          II =  ((C_Row - 1) * MaxCol + 1)
          if YT(II) > 0 then
            if  YT(II - MaxCol) > 0 then
              STEP_Y =  (YT(II) -  YT(II - MaxCol)) ' * 0.995
            else
             STEP_Y = STEP_X
            end if
          end if
            Answer = InputBox("Is Positioning in Y OK (Row=" + str(C_Row) + "   (0  -  NO  /  1-
YES) :" +" STEP_Y = " + str(Step_Y))
            if Answer = 0 then
              Measure.Point Label:="NEW_Y" + CEN_Name
              Light.PRL.SetAll     Coax:=CoaxValue,  Stage:=Stage_My  ,  Back:=0.00,  Front:=0.00,
Right:=0.00, Left:=0.00, Angle:=0.00, Color:=qvIgnore
'*************************************************************************************
***************
              ManualTool.Run, Prompt:="Click ON the RIGHT Y - Circle CENTER..."
            Measure.EndMeas
              STEP_Y = featureDB.item("NEW_Y" + CEN_Name).Y.actual - YT(II - MaxCol)
              if abs(STEP_Y - STEP_X) > 1.2 then
                  STEP_Y = STEP_X
'                   msgbox " STEP_Y = " + str(Step_Y) + " PointY = " + str(PointY) + " STEP_X = " +
str(Step_X) + " PointX = " + str(PointX) + " X_Focus = " + str(X_Focus)
              end if
            end if
        end IF
      end if
    NEXT C_Col
    PointY = PointY + STEP_Y
    PointX = 0
    X_Focus = PointX + C_Rad
```

```
  NEXT C_Row
'********** CYCLE END FOR a ROW ***********************************************

  Call Write_Array_2_File
  Call Write_Arrays_in_File_R

'***************Turn OFF the lights************************************************

Light.PRL.SetAll   Coax:=0.0, Stage:=0, Back:=0.0, Front:=0.0, Right:=0.0, Left:=0.0, Angle:=0.00
Stage.MoveTo   X:=0, Y:=PointY, Z:=0
Stage.MoveTo   X:=0, Y:=0, Z:=0

end sub   'Main====================================

'**************************************************
' END MAIN PROGRAM *********************************
'**************************************************
' 04/06/2010
'         Adding RT() in new file
'
Sub Write_Arrays_in_File_R  '============================
dim I
Dim F_Name as string
I=0
F_Name = "D:\Second_XYZR_" +str(Format(I,"0")) +".TXT"
FileLoop:   open F_Name for Input as #1
            on Error GoTo NewFile
            I=I+1
            F_Name = "D:\Second_XYZR_" +str(Format(I,"0")) +".TXT"
            Close #1
  GoTo FileLoop
NewFile:   open F_Name for OutPut as #1
  print #1, "Rows=" & Chr$(9) & MaxRow & Chr$(9) & "Columns=" & Chr$(9) & MaxCol
  print #1, "Row" & Chr$(9) & "Column" & Chr$(9) & "X" & Chr$(9) & "Y" & Chr$(9) & "R"
  for I = 1 to CN
'     if XT(I) = 0 then
'        XT(I) = (XT(I-1) + XT(I+1))/2
'     end if
'     if YT(I) = 0 then
'        YT(I) = (YT(I-1) + YT(I+1))/2
'     end if
 print #1, Row_T(I) & Chr$(9) & Col_T(I) & Chr$(9) & Format(XT(I),"0.000000") & Chr$(9) &
Format(YT(I),"0.000000") & Chr$(9) & Format(RT(I),"0.000000")
'                   print    #1,    Format(Row_T(I),"0"),Format(Col_T(I),"0"),Format(XT(I),"0.000000"),"
",Format(YT(I),"0.000000")
  Next I
  Close #1
end sub   'Write_Arrays_in_File_R ======================

'**************************************************
' 04/06/2010

Sub Write_Array_2_File  '============================
dim I
Dim F_Name as string
I=0
F_Name = "D:\Second_XYZ_" +str(Format(I,"0")) +".TXT"
FileLoop:   open F_Name for Input as #1
            on Error GoTo NewFile
            I=I+1
```

```
            F_Name = "D:\Second_XYZ_" +str(Format(I,"0")) +".TXT"
            Close #1
  GoTo FileLoop
NewFile:   open F_Name for OutPut as #1
  print #1, "Rows=" & Chr$(9) & MaxRow & Chr$(9) & "Columns=" & Chr$(9) & MaxCol
  print #1, "Row" & Chr$(9) & "Column" & Chr$(9) & "X" & Chr$(9) & "Y"
  for I = 1 to CN
'     if XT(I) = 0 then
'        XT(I) = (XT(I-1) + XT(I+1))/2
'     end if
'     if YT(I) = 0 then
'        YT(I) = (YT(I-1) + YT(I+1))/2
'     end if
     print #1, Row_T(I) & Chr$(9) & Col_T(I) & Chr$(9) & Format(XT(I),"0.000000") & Chr$(9) &
Format(YT(I),"0.000000")
'                  print   #1,   Format(Row_T(I),"0"),Format(Col_T(I),"0"),Format(XT(I),"0.000000"),"
",Format(YT(I),"0.000000")
  Next I
  Close #1
end sub   'Write_Array_2_File ======================

'*****************************************************

Private Sub QVBlock_0   '============================
Dim Far_Point
'=====22/03/2010=======
dim Square_Focus_Size
Square_Focus_Size = 0.9858766 / LensNomMag_KBP

'=====22/03/2010=======
Light.PRL.SetAll      Coax:=CoaxValue,  Stage:=0,  Back:=0.0,  Front:=0.0,  Right:=0.0,  Left:=0.0,
Angle:=0.00
'***************** NEW FOR REZERO*********************
  Measure.Point Label:="ZEROs"
    Light.PRL.SetAll   Coax:=CoaxValue, Stage:=Stage_My , Back:=0.00, Front:=0.00, Right:=0.00,
Left:=0.00, Angle:=0.00, Color:=qvIgnore
'***************************
   ManualTool.Run,  Prompt:="Click  ON  the  ZERO-ROUGHLY  NEAREST  LEFT  Circle
CENTER..."
  Measure.EndMeas
  ZEROs=featureDB.item("ZEROs").X.actual
  PCS.AlignOrigin   Axes:=ALL_AXES, Tag:="ZEROs"

'********RESTORE Zeros + RE FOCUS ******************
    Stage.MoveTo   X:=0, Y:=0, Z:=0
    Stage.MoveTo   X:=C_Rad, Y:=0, Z:=0
    Light.Color = qvWhite
    Light.PRL.SetAll     Coax:=(CoaxValue  +  0.05),  Stage:=Stage_My  ,  Back:=0.00,  Front:=0.00,
Right:=0.00, Left:=0.00, Angle:=0.00, Color:=qvIgnore
    FocusTool.SetMode   FocusType:=SURFACE, Speed:=FAST, Range:=4.2314050
    FocusTool.Focus   X:=C_Rad, Y:=0, Z:=0, W:=Square_Focus_Size , H:=Square_Focus_Size
    Stage.MoveTo   X:=0, Y:=0, Z:=0
'*****************************************************
    if MaxCOL <= 9 then
        Far_Point = (MaxCOL - 1)
      else
        Far_Point = (MaxCOL - 3)
    end if
    Far_Point = STEP_X * Far_Point
    if Far_Point > 258 then
```

```
        Far_Point = 258
    end if
    Stage.MoveTo   X:=Far_Point, Y:=0, Z:=0
'*****************************************************
'***************** NEW FOR SETTING X-Axis ***********
  Measure.Point Label:="X_Align"
    Light.PRL.SetAll   Coax:=CoaxValue, Stage:=Stage_My , Back:=0.00, Front:=0.00, Right:=0.00,
Left:=0.00, Angle:=0.00, Color:=qvIgnore
'*********************************
   ManualTool.Run, Prompt:="Click ON the SECOND X-Axis Point - ROUGHLY NEAR CIRCLE
CENTER..."
  Measure.EndMeas
'*****************SET X AXIS (and others)*****************
  PCS.AlignAxis      AlignmentAxis:=X_AXIS,      RotationAxis:=Z_AXIS,      Offset:=0.0000000,
Direction:=POS, Tag:="X_Align"
    Stage.MoveTo   X:=0, Y:=0, Z:=0
'*****************************************************

End Sub   'QVBlock_0  ================================
'*****************************************************
'*********************  KBP_T_1   ***********************
'*****************************************************
Private Sub KBP_T_1
  KBP_Err = 0       ' ********** NO ERROR *************
  III = CurrP MOD MaxCOL
  if III > 1 then
'     Step_M = abs(FeatureDB.Item(Tag:=CEN_Name).X.Actual - XT(CurrP - 1))
    MEASURED_X_ACTUAL = FeatureDB.Item(Tag:=CEN_Name).X.Actual
    Step_M = MEASURED_X_ACTUAL
    if abs(Step_M) <  0.01 then
'          msgbox "IN ERROR PART: STEP_M = " + str(Step_M) + " STEP_X = " + str(Step_X)
         Step_M = STEP_X
         KBP_Err = 1       ' ******** ERROR *******
    else
      Step_M = abs(Step_M - OLD_X_ACTUAL)      ' WAS --> XT(CurrP - 1))
      if abs(Step_M - STEP_X) > 1.75 then
'                    msgbox  str(CurrP)  +  "  MOD  =  "  +  str(III)  +  "  OLD_X_ACTUAL  =  "  +
str(OLD_X_ACTUAL) + " STEP_M = " + str(Step_M) + " WILL BE CHANGED to " + str(Step_X)
        Step_M = STEP_X  '*****************************TO SEE AGAIN*****************
      end if
      OLD_X_ACTUAL = PointX
    end if
  else
    Step_M = STEP_X
    MEASURED_X_ACTUAL = FeatureDB.Item(Tag:=CEN_Name).X.Actual
' on 02/09/2009 --> BECAUSE the 1st-X value is the last one
    OLD_X_ACTUAL = PointX
  end if      'END IF III > 1
End Sub   'KBP_T_1   ================================
'*****************************************************
'*********************  QVBlock_2 ***********************
'*****************************************************
Private Sub QVBlock_2   '============================
'********************* NEXT Position ********************
  Call Change_Row_Col
'*********************MOVE TO...************************
if PointX > 299 then
  ' STOP PROGRAM
  msgtext="Error " & Err & ": " & Error$ & " STOP (2) THE PROGRAMM !!!! X is: " & PointX
  MsgBox msgtext
```

```
   ' exit sub
end if
      Stage.MoveTo   X:=PointX, Y:=PointY, Z:=0
'      Stage.MoveTo   X:=X_Focus, Y:=PointY, Z:=0
'      Light.Color = qvWhite
'      Light.PRL.SetAll   Coax:=CoaxValue, Stage:=Stage_My , Back:=0.00, Front:=0.00, Right:=0.00,
Left:=0.00, Angle:=0.00, Color:=qvIgnore
'      FocusTool.SetMode   FocusType:=SURFACE, Speed:=FAST, Range:=4.2314050
'      FocusTool.Focus   X:=X_Focus, Y:=PointY, Z:=0, W:=0.9, H:=0.9
'      Stage.MoveTo   X:=PointX, Y:=PointY, Z:=0
'****************** NEW MEASURE ************************
   Measure.Circle Label:=CEN_Name
   Light.Color = qvWhite
   Light.PRL.SetAll    Coax:=CoaxValue, Stage:=Stage_My , Back:=0.00, Front:=0.00, Right:=0.00,
Left:=0.00, Angle:=0.00, Color:=qvIgnore
   CircleTool.ScanInt = 20
'                CircleTool.SetFilter                Alg:=DYNAMIC_THRESH,      EdgeSlope:=FALLING,
EdgeQuality:=STRONG, Outlier:=0, TH:=221.094340, THR:=0.434906, THS:=19.000000
   CircleTool.SetFilter    Alg:=DYNAMIC_THRESH, EdgeSlope:=FALLING, EdgeQuality:=WEAK,
Outlier:=0, TH:=221.094340, THR:=0.434906, THS:=19.000000
   CircleTool.Run   X:=PointX, Y:=PointY, Z:=0, R1:=0.064578, R2:= C_Rad
   Measure.EndMeas
   Results.ReportFeature   Show:=X_ and Y_ and Z_ and D_, Tag:=CEN_Name
'
      CALL KBP_T_1
'
' ********** MEASURE ERROR *************
   if KBP_Err = 1 then
      XT(CurrP)  = 0   ' PointX
      YT(CurrP)  = 0   ' PointY is ZERO...
   else
      XT(CurrP)  = MEASURED_X_ACTUAL      ' FeatureDB.Item(Tag:=CEN_Name).X.Actual
      YT(CurrP)  = FeatureDB.Item(Tag:=CEN_Name).Y.Actual   ' PointY is ZERO...
' 04/06/2010.....................
      RT(CurrP)  = FeatureDB.Item(Tag:=CEN_Name).RD.Actual   ' Saving Radius Value...
' 04/06/2010.....................

   end if
' ********** MEASURE ERROR *************
   Row_T(CurrP)  = C_Row
   Col_T(CurrP)  = C_Col
'   msgbox str(CurrP) + " MOD = " + str(III) + " IN QVBLOCK_2 => Point_X BEFORE ADDING
Step_M is ( " + str(pointX) + ")     Step_M is = ( " + str(Step_M) + " )"
   PointX = PointX + Step_M
      if PointX > 316 then
        ' STOP PROGRAM
        msgtext="Error " & Err & ": " & Error$ & " STOP (1) THE PROGRAMM !!!!  X is: " &
PointX
        MsgBox msgtext
        ' exit sub
      end if
   X_Focus = PointX + C_Rad
   CurrP = CurrP + 1
End Sub   'QVBlock_2
```

Appendix 2 Results for scaling calculations of SLS Castform

1. Coordinates of reference points (hole centres) measured by optical CMM

Row	Column	X	Y
1	1	-0.028441	0.002927
1	2	14.758026	-0.062340
1	3	29.593672	-0.060080
1	4	44.455400	-0.068964
1	5	59.328571	-0.063281
1	6	74.152018	-0.009096
1	7	89.025381	0.018581
1	8	103.934091	-0.033793
1	9	118.710436	0.077051
1	10	133.576640	-0.012410
1	11	148.446826	-0.108760
1	12	163.304722	-0.062361
1	13	178.108382	-0.001173
1	14	192.929748	-0.054534
1	15	207.635431	-0.037598
2	1	-0.080063	14.857845
2	2	14.767538	14.807908
2	3	29.581392	14.792087
2	4	44.404574	14.773611
2	5	59.280214	14.860377
2	6	74.119765	14.840508
2	7	89.002376	14.861855
2	8	103.861315	14.894177
2	9	118.698697	14.861266
2	10	133.546062	14.844221
2	11	148.397385	14.858307
2	12	163.216137	14.846251
2	13	178.134649	14.737465
2	14	192.898764	14.799640
2	15	207.641081	14.826931
3	1	-0.083501	29.694971
3	2	14.747614	29.643182
3	3	29.555633	29.661406
3	4	44.391172	29.614729
3	5	59.241547	29.683399
3	6	74.109628	29.612412
3	7	88.994694	29.659608
3	8	103.845557	29.689029
3	9	118.698908	29.642347
3	10	133.542104	29.630420
3	11	148.362177	29.654560
3	12	163.220709	29.632335
3	13	178.056877	29.490394
3	14	192.891140	29.579730
3	15	207.637578	29.631124
4	1	-0.045933	44.563628
4	2	14.754809	44.478677
4	3	29.568164	44.476677
4	4	44.400708	44.472527
4	5	59.252969	44.490380
4	6	74.124394	44.443610

4	7	89.006439	44.467310
4	8	103.848958	44.479273
4	9	118.706800	44.444173
4	10	133.537466	44.416436
4	11	148.372382	44.423013
4	12	163.252105	44.440665
4	13	178.074873	44.419654
4	14	192.907337	44.423226
4	15	207.650886	44.470550
5	1	0.010775	59.329588
5	2	14.823542	59.248382
5	3	29.614073	59.244379
5	4	44.494184	59.224351
5	5	59.300428	59.224672
5	6	74.143034	59.208172
5	7	89.044616	59.145616
5	8	103.885340	59.161164
5	9	118.714056	59.137351
5	10	133.542872	59.166119
5	11	148.444142	59.146719
5	12	163.232216	59.184580
5	13	178.054624	59.165408
5	14	192.923932	59.168877
5	15	207.655418	59.221177
6	1	0.002970	74.276118
6	2	14.837392	74.192730
6	3	29.638084	74.133953
6	4	44.478203	74.121880
6	5	59.337553	74.077679
6	6	74.167269	74.052489
6	7	88.991073	74.026154
6	8	103.867472	73.984291
6	9	118.736736	73.973925
6	10	133.599378	73.959384
6	11	148.420570	73.966616
6	12	163.261171	74.011370
6	13	178.027492	74.030036
6	14	192.893945	74.057555
6	15	207.619727	74.078198
7	1	0.029116	89.158048
7	2	14.873580	89.027353
7	3	29.641057	88.961195
7	4	44.495212	88.978109
7	5	59.335171	88.886120
7	6	74.209805	88.877499
7	7	89.045962	88.866474
7	8	103.825887	88.787241
7	9	118.686504	88.829104
7	10	133.561478	88.797543
7	11	148.382852	88.797500
7	12	163.181366	88.835176
7	13	178.055116	88.904964
7	14	192.857938	88.908928
7	15	207.578909	88.968290
8	1	0.102181	104.087085
8	2	14.892325	103.944218
8	3	29.718105	103.882299

8	4	44.541078	103.823684
8	5	59.337858	103.778944
8	6	74.195706	103.715878
8	7	89.048414	103.702077
8	8	103.905891	103.744436
8	9	118.698259	103.715523
8	10	133.523312	103.700386
8	11	148.374193	103.688890
8	12	163.180624	103.713558
8	13	177.949244	103.749933
8	14	192.785780	103.775389
8	15	207.528498	103.854059
9	1	0.132174	119.038709
9	2	14.918740	118.916322
9	3	29.745636	118.844254
9	4	44.559711	118.775070
9	5	59.366684	118.709767
9	6	74.235859	118.659836
9	7	89.045127	118.658006
9	8	103.924427	118.604801
9	9	118.639345	118.533118
9	10	133.539272	118.621196
9	11	148.356696	118.625903
9	12	163.186973	118.621567
9	13	177.901556	118.672214
9	14	192.740651	118.743500
9	15	207.495081	118.795109
10	1	0.180847	133.972675
10	2	15.002974	133.846257
10	3	29.822607	133.799655
10	4	44.611934	133.738463
10	5	59.420059	133.675910
10	6	74.231031	133.648852
10	7	89.130957	133.590282
10	8	103.787519	133.554680
10	9	118.703463	133.537116
10	10	133.541389	133.480466
10	11	148.360177	133.490241
10	12	163.192090	133.536770
10	13	177.909061	133.621820
10	14	192.735803	133.596377
10	15	207.439091	133.744617
11	1	0.182842	149.055770
11	2	14.977656	148.918907
11	3	29.795175	148.892542
11	4	44.587631	148.853694
11	5	59.514974	148.846088
11	6	74.283498	148.745621
11	7	89.035236	148.760653
11	8	103.847391	148.813714
11	9	118.598772	148.737463
11	10	133.481820	148.721197
11	11	148.364884	148.683420
11	12	163.166756	148.744756
11	13	177.946189	148.804648
11	14	192.696294	148.787152
11	15	207.433573	148.868844

2. Graphical representation of distributions of ε_x and ε_z in plate that was used for scaling calculations

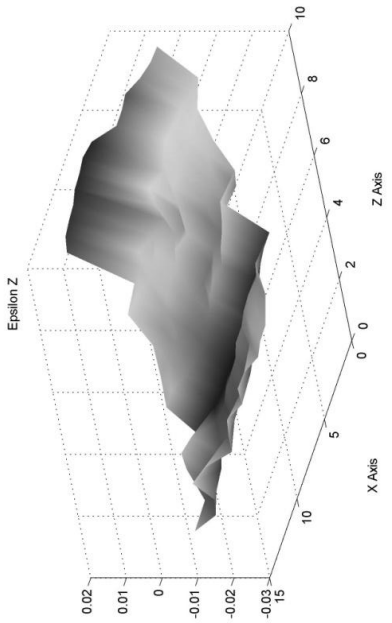

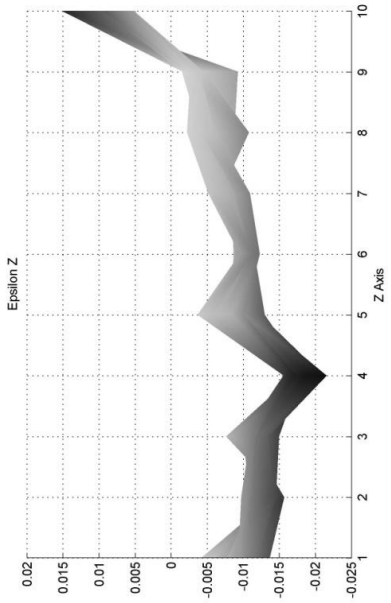

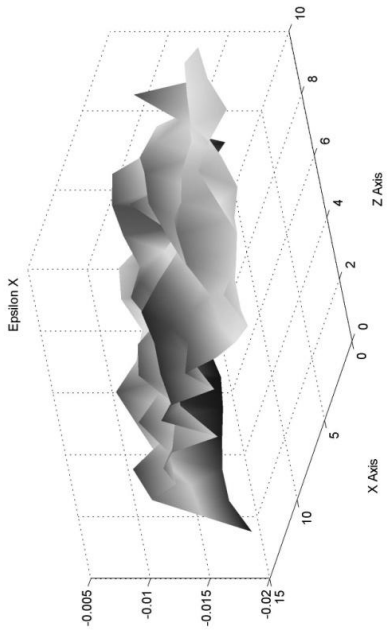

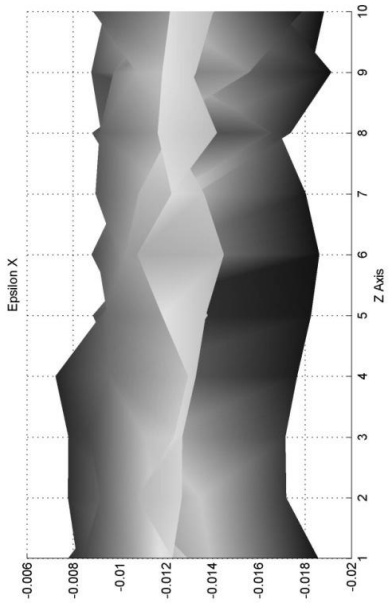

3. Distribution of deviation in sizes from nominal in *x* and z direction (ε_x and ε_z)

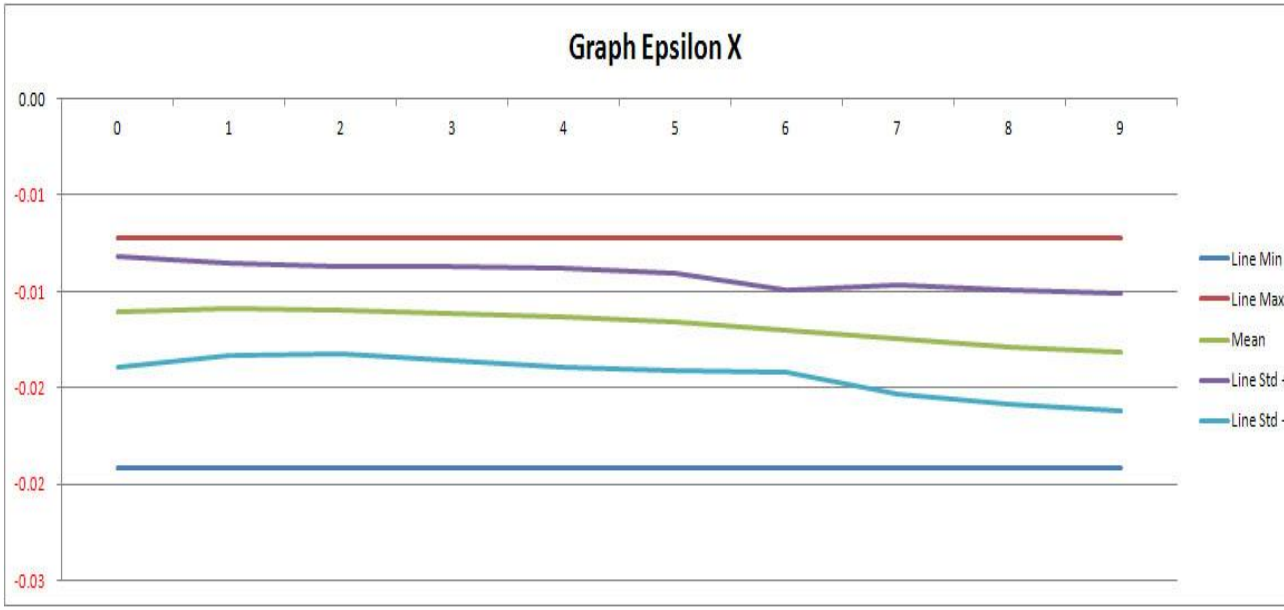

Distribution of deviation of sizes from nominal in n *x* direction for Castform

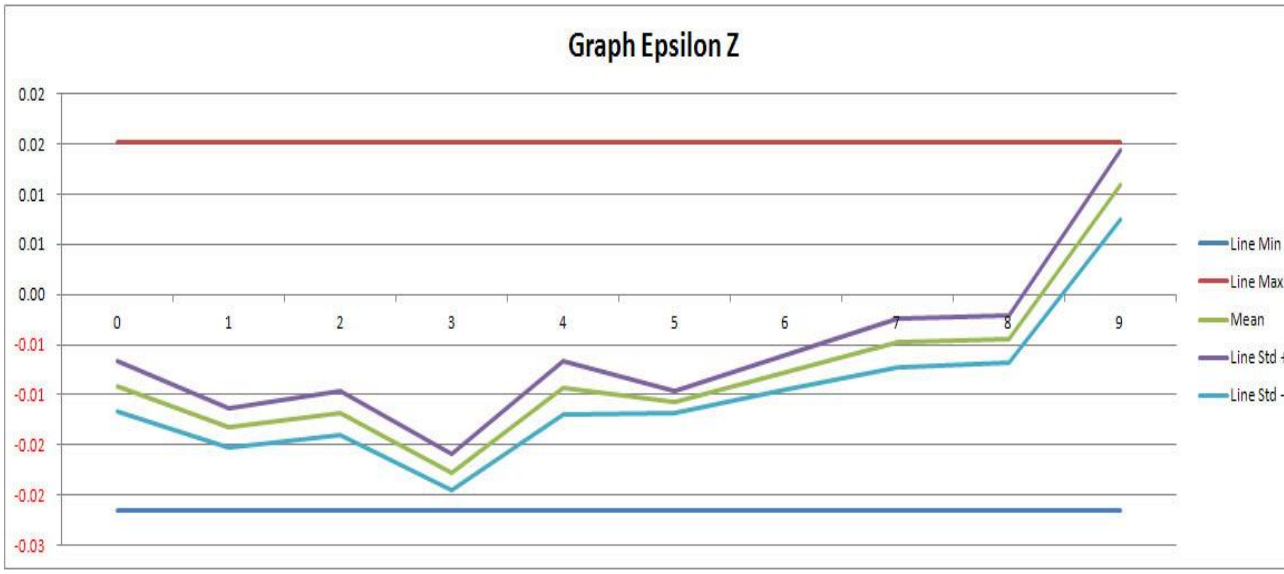

Distribution of deviation of sizes from nominal in n *z* direction for Castform

4. Matrix of calculated ε_z

Matrix εZ

X/Z	0	1	2	3	4	5	6	7	8	9
0	-0.0092	-0.0110	-0.0099	-0.0156	-0.0036	-0.0095	-0.0051	-0.0025	-0.0045	0.0052
1	-0.0093	-0.0099	-0.0117	-0.0155	-0.0055	-0.0113	-0.0054	-0.0022	-0.0038	0.0055
2	-0.0102	-0.0097	-0.0110	-0.0161	-0.0071	-0.0106	-0.0078	-0.0029	-0.0027	0.0069
3	-0.0078	-0.0113	-0.0112	-0.0173	-0.0083	-0.0112	-0.0088	-0.0039	-0.0023	0.0095
4	-0.0076	-0.0136	-0.0121	-0.0168	-0.0101	-0.0123	-0.0090	-0.0042	-0.0015	0.0089
5	-0.0103	-0.0144	-0.0121	-0.0187	-0.0092	-0.0112	-0.0109	-0.0033	-0.0026	0.0089
6	-0.0077	-0.0137	-0.0135	-0.0216	-0.0099	-0.0120	-0.0069	-0.0061	-0.0039	0.0142
7	-0.0096	-0.0142	-0.0137	-0.0210	-0.0114	-0.0115	-0.0052	-0.0108	-0.0015	0.0152
8	-0.0120	-0.0145	-0.0138	-0.0187	-0.0124	-0.0103	-0.0071	-0.0088	-0.0046	0.0146
9	-0.0059	-0.0140	-0.0150	-0.0177	-0.0130	-0.0111	-0.0069	-0.0048	-0.0093	0.0144
10	-0.0041	-0.0140	-0.0142	-0.0179	-0.0118	-0.0116	-0.0077	-0.0052	-0.0074	0.0133
11	-0.0118	-0.0155	-0.0088	-0.0172	-0.0103	-0.0101	-0.0093	-0.0057	-0.0045	0.0129
12	-0.0137	-0.0157	-0.0076	-0.0171	-0.0083	-0.0092	-0.0097	-0.0037	-0.0066	0.0124
13	-0.0094	-0.0140	-0.0106	-0.0169	-0.0085	-0.0087	-0.0083	-0.0030	-0.0066	0.0105

5. Graphs for comparison and illustration of scaling scenarios in x and z direction

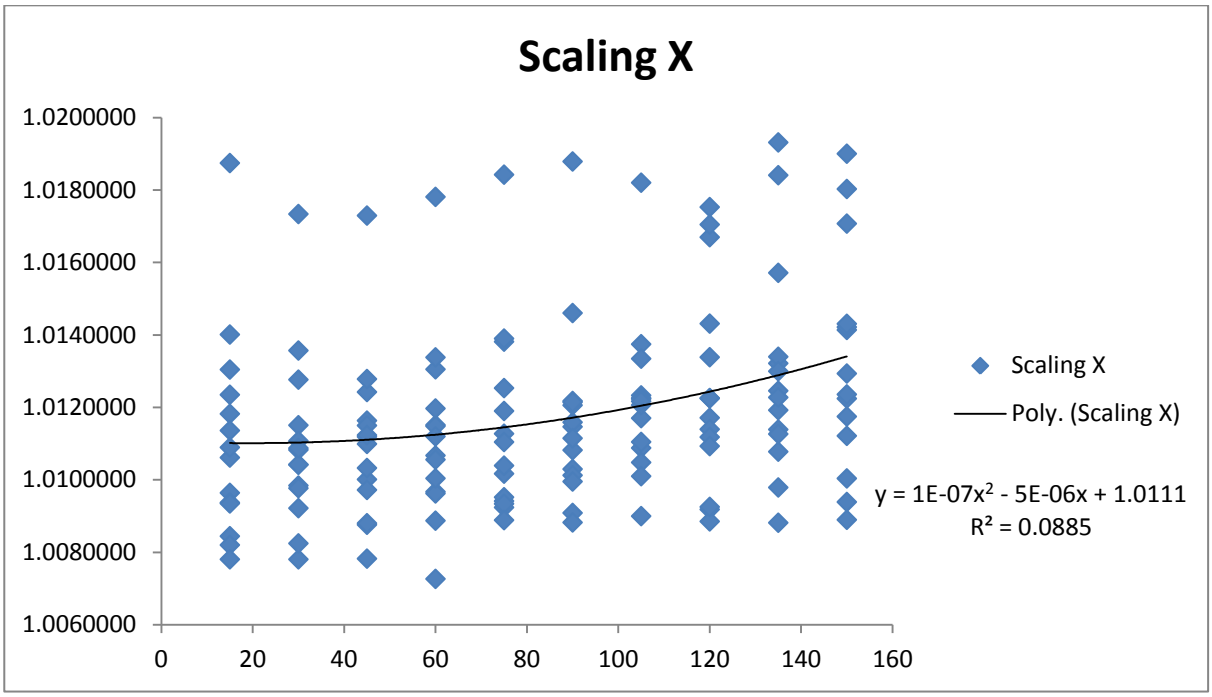

Results from experiment that illustrate scenario on Figure 5.13(a)

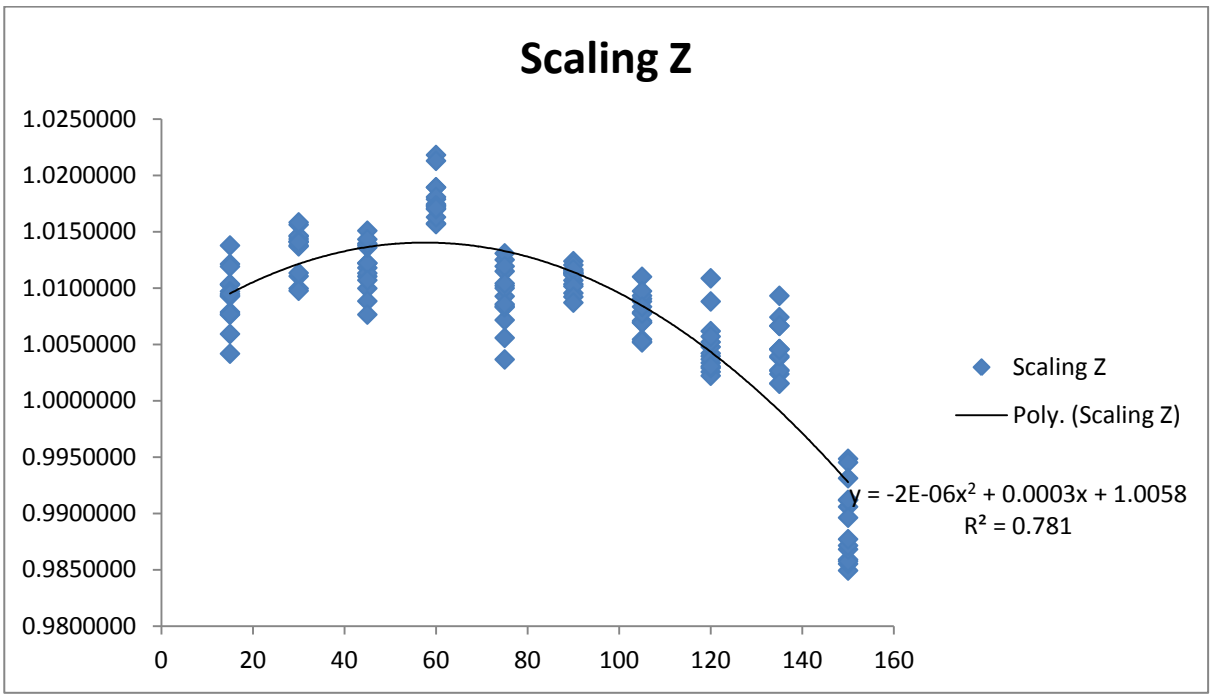

Results from experiment that illustrate scenario on Figure 5.13(d)

REFERENCES

Bae, S. W., Kim, D. S., Choi, K. H. 2007. Development of new laser algorithm in the SFF system using a SLS process. *International Conference on Control, Automation and Systems*. COEX, 17-20 October, 2007. Seoul, Korea, pp. 2583-2586.

Banerjee, P. S. 2004. Investigation on accuracy of CAD sliced data for rapid prototyping application. *Proceeding of the National Conference on Advanced Manufacturing & Robotics*. 2004. Central Mechanical Engineering Research Institute, Durgapur, pp. 370-382. ISBN: 81-7764-671-0.

Bastech, Inc. 2011. Ohio, USA, Available at: http://bastech.com/sla/techtips/STLfiles.asp [Accessed: November 2011].

Bertsch, A., Bernhard, P., Vogt, C., Renaud, P. 2000. Rapid prototyping of small size objects. *Rapid Prototyping Journal*, 6 (4), pp. 259–266.

Berzin, M., Childs, T., Dalgarno, K., Ryder, G., Stein, G. 1995. Densification and distortion in selective laser sintering of polycarbonate parts. *Proceedings of the Solid Freeform Fabrication Symposium*. The University of Texas at Austin, Austin, Texas, pp. 196-203.

Bibb, R., Eggbeer, D., Evans, P. 2010. Rapid prototyping technologies in soft tissue. *Rapid Prototyping Journal*, 16 (2), pp.130–137.

Bicheno, J., Catherwood, P. 2005. Six sigma and the quality toolbox. Picsie Books, ISBN-13: 978-0-9541244-2-7.

Bigot, S., Dimov, S., Minev, R. 2010. Function and length scale integration study in emerging MST-based products. In: Ratchev, S. ed. *Precision Assembly Technologies and Systems*. Boston: Springer, pp.337-342. ISBN:978-3-642-11597-4, DOI:10.1007/978-3-642-11598-1_39.

Bigot, S., Minev, R., Dobrev, T., Dimov, S., Matthews, C. 2009. Functional and length scale integration in micro/nano manufacturing. *Proceedings of 4M Conference in Karlsruhe*. Professional Engineering Publishing, pp147-152. DOI: 10.1243/17547164C0012009025.

Brajlih, T., Valentan, B., Balic, J., Drstvensek, I. 2011. Speed and accuracy evaluation of additive manufacturing machines. *Rapid Prototyping Journal*, 17 (1), pp. 64–75.

Bredeau, S., Bancillon, J. 2011. Opportunities and challenges in room temperature embossing/punching for ceramic green tapes. In: Kuck, H., Reinecke, H., Dimov, S. eds. *Proceedings of the 8th International Conference on Multi-Material Micro Manufacture.* 8-10 November, 2011. Stuttgart, Germany. Singapore: Research Publishing.

Bredendick, F. 1967. Zur ermittlung von deformationen an verzerrten gittern. *Wiss. Technical University Dresden*, v. 16, pp. 1473-1481.

Bredendick, F. 1969. Methoden der deformationsermittlung an verzerrten gittern. *Wiss. Zeitschrift der Technical University Dresden,* v. 18, Heft 2, pp. 531-538.

Brooks, H. L., Rennie, A. E. W., Abram, T. N., McGovern, J., Caron F. 2012. Variable fused deposition modelling - analysis of benefits, concept design and tool path generation. *Proceedings of the 5th International Conference on Advanced Research and Rapid Prototyping*, 28 September - 1 October 2011, Liera, Portugal, pp. 511-517.

Byun, H. S., Lee, K. H. 2006. Determination of optimal build direction in rapid prototyping with variable slicing. *International Journal of Advanced Manufacturing and Technology,* (28), pp. 307–313.

Callister, W. D. 2010. *Materials science and engineering*. John Wiley & Son, 8th Edition, ISBN-10: 0470505869.

Chandrupatla, T. R. 2009 *Quality and reliability in engineering*. New York: Cambridge University Press, ISBN: 978-0-521-51522.

Childs, T. H. C., Tontowi, A. E. 2001. Selective laser sintering of a cristalline and glass-filled crystalline polymer: experiments and simulations. *Proceedings of the Institution of Mechanical Engineers, Part B: Journal of Engineering Manufacture, v. 215,* pp. 1481-1495.

Choi, J. W., Wicker, B., Cho, S.H., Lee, H. C. S., Seok-Hee. 2009. Cure depth control for complex 3D microstructure fabrication in dynamic mask projection microstereolithography. *Rapid Prototyping Journal*, 15 (1), pp.59 –70.

Chua, C. K., Feng, C., Lee, C.W., Ang, G.Q. 2005. Rapid investment casting: direct and indirect approaches via model maker II. *International Journal of Advanced Manufacturing Technology, (25),* pp. 26-32.

Chua, C. K., Leong, K. F., Lim, C.S. 2010. *Rapid prototyping: Principles and applications*, Singapore: World Scientific Publishing Co., pp. 43-45; pp. 466-469.

Clijsters, S., Craeghs, T., Kruth, J. P. 2012. A priori process parameter adjustment for SLM process optimization. *Proceedings of the 5th International Conference on Advanced Research and Rapid Prototyping.* Liera, Portugal, 28 September - 1 October, 2011, pp. 553-560.

Cooke, W., Tomlinson, R.A., Burguete, R., Johns, D., Vanard, G.L. 2011. Anisotropy, homogeneity and ageing in an SLS polymer. *Rapid Prototyping Journal, 17 (4),* pp. 269 –279.

Craig, G., Neil, D., Williams, B. 2005. *Six Sigma for Dummies.* Hoboken, NJ: Wiley Publishing Inc., ISBN 0-7645-6798-5.

Danckert, J., Wanheim, T. 1979. The use of a square grid as an alternative to a circular grid in the determination of strains. *Journal of Mechanical Working Technology,* (*3),* pp. 5-15.

Danjou, S., Herbst, M., Koehler, P. 2010. Improving part quality and process efficiency in layer manufacturing by adaptive slicing. *Proceedings of Eleventh National Conference on Rapid Design, Prototyping & Manufacturing*, 2010 Lancaster University, Lancanster, pp. 63-70.

Dean, Al. Envisiontec Perfactory. 2004. Available at: http://www.docstoc.com/docs/71758335/Envisiontec-Perfactory [Accessed 04 May 2011].

Deckard, C., Miller, D. 1995. Improved energy delivery for selective laser sintering, *Freeform Fabrication Symposium*, Austin, Texas, 1995, pp.151-158.

Deckers, J., Khuram, S., Vleugels, J., Kruth, J. P., Boury, S. 2012. Production of alumina parts through selective laser sintering of alumina-polyamide composite powder. *Proceedings of the 5th International Conference on Advanced Research and Rapid Prototyping*, 28 September - 1 October , 2011. Liera, Portugal, pp.319-327.

Diatlov, A., Buchbinder, D., Meiners, W., Wisssenbach, K., Bultmann, J., 2012. Towards surface topography: quantification of selective laser melting (SLM) built parts. *Proceedings of the 5th International Conference on Advanced Research and Rapid Prototyping*, 28 September - 1 October, 2011. Liera, Portugal, pp.595-602.

Dieter, G. E. 1998. Mechanical Metallurgy. McGraw-Hill Book Company. ISBN: 0-07-100406-8.

Diller, T. T., Yuan, M. M., Bourell, D. L., Beaman, J. J. 2012. Thermal characterisation of laser sintering of nylon-12. *Proceedings of the 5th International Conference on Advanced Research and Rapid Prototyping*, 28 September - 1 October, 2011. Liera, Portugal, pp. 369-373.

Dolenc A., Mäkelä I. 1994. Slicing procedures for layered manufacturing techniques. *Computer Aided Design*, vol. 26, no. 2, pp. 119-126.

Dotchev, K. D., Dimov, S. S., Pham, D. T., Ivanov, A.I. 2007. Accuracy issues in rapid manufacturing CastForm patterns. *Proceedings of the Institution of Mechanical Engineers, Part B: Journal of Engineering Manufacture, v. 221,* pp.53–67.

Dotchev, K., Soe, S. 2006. Rapid manufacturing of patterns for investment casting: improvement of quality and success rate. *Rapid Prototyping Journal,* 12 (3), pp.156–164.

DTM Corporation, 1997. The Sinterstation System, Guide to Materials: DuraForm Polyamide. DCN: 8001-10014.

DTM Corporation, 1998. The Sinterstation System, Guide to Materials: Copper Polyamide. DCN: 8001-10022.

DTM Corporation, 1999. The Sinterstation System, Guide to Materials: CastForm PS. DCN: 8002-10006.

DTM Sinterstation System, 2000. Guide to Materials. DTM Corporation, 1611 Headway Circle, Austin, Texas 78754.

Edwards, L., Endean, M. 1995. *Manufacturing with materials*, New York: Butterworth-Heinemann Ltd. ISBN-10: 0750627549.

El-Katatny, I., Masood, S.H., Morsi, Y.S. 2010. Error analysis of FDM fabricated medical replicas. *Rapid Prototyping Journal,* 16 (1), pp.36–43.

Envisiontec, Available at: http://www.envisiontec.de [Accessed October 2011].

EOS GmbH, Training manual, 2003, EOSINT P700, Munich.

EUMINAfab. Available at: http://www.euminafab.eu [Accessed May 24, 2010].

Gagov, V., Feschiev, N., Minev, E., Tomov, B. 1995. Experimental investigations on the deformability of sheet metals. *Proceedings of Conference on Advances in Materials and Processing Technologies*, 1995 Dublin, Ireland, Hashmi, M. S. J. Eds.; Dublin City University, Ireland, v III, pp. 1389-1395.

Giannatsis, J., Sofos, K., Canellidid, V., Karalekas, D., Dedoussis, V. 2012. Investigating the influence of build parameters on the mechanical properties of FDM parts. *Proceedings of the 5th International Conference on Advanced Research and Rapid Prototyping*, 28 September - 1 October, 2011, Liera, Portugal, pp.525-529.

Gibson, I., Shi, D. 1997. Material properties and fabrication parameters in selective laser sintering process. *Rapid Prototyping Journal*, 3 (4), pp.129–136.

Hansen, H. 2007. Dimensional metrology in micro manufacturing, In: Fillon, B., Khan-Malek, C., Dimov, S. eds., *Proceedings of the 4M 2007 Conference*, October 3-5, 2007 Borovets, Bulgaria, pp.29-35.

Hideaki, I., Miyoshi, H., Takaya, T., Hayashi, Y. T. 2005. Micro-stereolithography of dot shapes for light-guide using LCD greyscale mask, *Proceedings of the Japan Society of Precision Engineering*, 2005, Japan, JSPE Autumn Meeting.

Ho, H. C. H., Cheung, W. L., Gibson, I. 2003. Morphology and properties of selective laser sintered bisphenol a polycarbonate. *Industrial & Engineering Chemistry Research*, 42, pp.1850-1862.

Ho, H. C. H., Gibson, I., Cheung, W. L. 1999. Effects of energy density on morphology and properties of selective laser sintered polycarbonate. *Journal of Materials Processing Technology,* (89–90), pp.204–210.

Hopkinson, N., Sercombe, T. B. 2008. Process repeatability and sources of error in indirect SLS of aluminium. *Rapid Prototyping Journal*, 14 (2), pp.108–113.

Hosford, W. F, Caddell, R. M. 1983. *Metal Forming: Mechanics and Metallurgy*. New Jersey: Prentice-Hall Inc., ISBN: 0-13-577700-3.

Ilkgun, Ö. 2005. *Effects of Production Parameters on Porosity and Hole Properties in Laser Sintering Rapid Prototyping Process*, Master of Science Thesis, Middle East Technical University.

Imahori, H., Miyoshi, T., Takaya, Y., Hayashi, T., Lee, D. K. 2005. Micro-stereolithography of dot shapes for lightguide using LCD grayscale mask. *Proceedings of JSPE Semestrial Meeting*. The Japan Society of Precision Engineering.

Jacobs, P. F. 1992. *Rapid Prototyping & Manufacturing. Fundamentals of StereoLithography*, Society of Manufacturing Engineering. ISBN: 0-87263-425-6.

Jacobs P. 2000. The effects of random noise shrinkage on rapid tooling accuracy. *Materials and Design,* (21), pp.127-136.

Jain, P. K., Pulak, M., Pandey, A., Rao, P.V.M. 2008. Experimental investigations for improving part strength in selective laser sinterin. *Virtual and Physical Prototyping*, 3 (3), pp.177–188.

Jamal, N. M. 2001. *Finite Element Analysis of Curl Development in the Selective Laser Sintering Process*. PhD Thesis, University of Leeds.

Jiang Cho-Pei. 2011. Development of a novel two-laser beam stereolithography system. *Rapid Prototyping Journal*, 17 (2), pp.148–155.

John, D., Williams, J. D., Deckard, C.R. 1998. Advances in modelling the effects of selected parameters on the SLS process. *Rapid Prototyping Journal*, 4 (2), pp.90–100.

Kautt, M. 2009. Facilitating open innovation in micro and nano technology by providing open access to a pan-European toolbox called EUMINAfab. In: Saile, V.; Ehmann, K.; Dimov, S., Eds. *Proceedings of 4M/ICOMM 2009 Conference*, September 23-25, 2009, Karlsruhe, Germany, 4M Association, UK, pp.11-24.

Kennedy, B. July 6th 2009. *New developments increase rapid prototyping of micro-scale features, Micro Manufacturing*. Available at: http://www.micromanufacturing.com/showthread.php?t=630 [Accessed May 24, 2010].

Kim, G. D., Oh, Y. T. 2008. A benchmark study on rapid prototyping processes and machines: quantitative comparisons of mechanical properties, accuracy, roughness, speed, and material cost. *Proceedings of the Institution of Mechanical Engineers, Part B: Journal of Engineering Manufacture v. 222*, pp.201-215.

Krajewski, L. J**.,** Ritzman, L. P., Malhotra, M. K. 2010. *Operations management*, New York, Person, pp.208-219. ISBN-10: 0-13-245891-7.

Kruth, J. P., Mercelis, P., Froyen, L., Rombouts, M. 2004. Binding mechanisms in selective laser sintering and selective laser melting. *Proceedings of 15th Solid Freeform Fabrication Symposium*, 2004, Austin, Texas, pp.26-36.

Kruth, J. P., Vandenbroucke, B., Van Vaerenbergh, J., Mercelis, P. 2005. Benchmarking of different SLS/SLM processes as rapid manufacturing techniques. *International Conference of Polymers & Moulds Innovations (PMI)*. April 20-23, 2005, Gent, Belgium, pp.1-7.

Kruth, J. P., Wang, X., Laoui, T., Froyen, L. 2003. Lasers and materials in selective laser sintering. *Assembly Automation*, 23 (4), pp.357–371.

Lee, B. H., Abdullah, J., Khan, Z. A. 2005. Optimization of rapid prototyping parameters for production of flexible ABS object. *Journal of Materials Processing Technology*, 169 (1), pp.54-61.

Lee, C. W., Chua, C. K., Cheah, C. M., Tan, L. H., Feng, C. 2004. Rapid investment casting: direct and indirect approaches via fused deposition modelling. *International Journal of Advanced Manufacturing and Technology*, (23), pp.93–101.

Lee, I. H., Dong-Woo Cho. 2003. Micro-stereolithography photopolymer solidification patterns for various laser beam exposure conditions. *International Journal of Advanced Manufacturing and Technology*, 22, pp.410–416.

Liao, H. T., Shie, R. 2007. Optimization on selective laser sintering of metallic powder via design of experiments method. *Rapid Prototyping Journal*, 13 (3), pp.156-162.

Mahesh, M. 2005. *Rapid Prototyping and Manufacturing Benchmarking*. PhD Thesis. National University of Singapore.

Mahesh, M., Wong, Y. S., Fuh, J. Y. H., Loh, H. T. 2004. Benchmarking for comparative evaluation of RP systems and processes. *Rapid Prototyping Journal*, 10 (2), pp.123–135.

Mahesh, M., Wong, Y. S., Fuh, J. Y. H., Loh, H. T., 2006. A Six-sigma approach for benchmarking of RP&M processes. *International Journal of Advanced Manufacturing and Technology*, (31), pp.374–387.

Manetsberger, K., Shen, J., Muellers, J. 2001. Compensation of non-linear shrinkage of polymer materials in selective laser sintering. *Proceedings of Solid Freedom Fabrication Symposium*, 2001, Austin, Texas, pp.346-356.

Masood, S. H., Soo, A. 2002. A rule based expert system for rapid prototyping system selection. *Robotics and Computer Integrated Manufacturing*, 18, pp.267–274.

Melchels, F. P. M., Feijen, J., Grijpma, D. W. 2010. A review on stereolithography and its applications in biomedical engineering. *Biomaterials*, 31(24) pp. 6121-6130.

Mercelis, P., Kruth, J. P. 2006. Residual stresses in selective laser sintering and selective laser melting. *Rapid Prototyping Journal*, 12 (5), pp.254–265.

Mielnik, E. M. 1991. *Metalworking Science and Engineering*. New York: McGraw-Hill, Inc. ISBN: 0-07-041904-3.

Miller, D., Deckard, C., Williams, J. 1997. Variable beam size SLS workstation and enhanced SLS model. *Rapid Prototyping Journal*, 3 (1), pp.4–11.

Minev, R., Vella, P., Brousseau, E., Dimov, S., Minev, E., Matthews, C., (a). 2010. Methodology for Capability Maturity Assessment of MNT chains, *Proceedings of 4M Conference*, 17th - 19th Nov, 2010, Oyonnax, France, pp.249-252. ISBN:978-981-08-6555-9

Minev, R., Vella, P., Brousseau, E., Dimov, S., Scholz, S., Matthews, C., (b). 2010. Capability Maturity Study of the Horizontal and Vertical Integration of Structuring, Patterning and Characterization MNTs, *Proceedings of 4M Conference*, 17th - 19th Nov 2010 Oyonnax, France, pp.253-256. ISBN:978-981-08-6555-9

Minev, E., Popov, K., Minev, R., Dimov, S., Gagov, V. 2011. Grid method for accuracy study of micro parts manufacturing. *Micro and Nanosystems (MNS)*, 3 (3), pp.263-269. ISSN: 1876-4029.

Moesen, M., Craeghs, T., Kruth, J. P., Schrooten, J. 2011. Robust beam compensation for laser-based additive manufacturing. *Computer-Aided Design*, 43, pp.876–888.

Montgomery, D. 2004. *Introduction to Statistical Quality Control*. New York: John Wiley & Sons.

Morton, W., Green, S., Rennie, A. E. W., Abram, T. N. 2012. Surface finishing for SLM manufactured stainless steel 316L components. *Proceedings of the 5th*

International Conference on Advanced Research and Rapid Prototyping, 28 September - 1 October, 2011, Liera, Portugal, pp.503-509.

Nagahanumaiah, B. R., Mukherjee, N. P. 2004. Shrinkage prediction in rapid tooling (RPT) process chain. *Proceedings of the National Conference on Advanced Manufacturing & Robotics*, Central Mechanical Engineering Research Institute, Durgapur, 2004, pp.382–390. ISBN: 81-7764-671-0.

Nelson, J. C. 1993. *Selective Laser Sintering: A Definition of the Process and an Empirical Sintering Model*, PhD Thesis, University of Texas at Austin.

Nelson, J. C., McAlea, K., Gray, D. (a). 1995. Improvement in SLS part accuracy, *Proceedings of Solid Freedom Fabrication Symposium*, 1995, Austin, Texas, pp.159-169.

Nelson, J. C., Neal, K. V., Barlow, J. W., Beaman, J. J., Bourell, D. L., Marcuss, H. L. (b). 1995. Selective laser sintering of polymer-coated silicon carbide powders. *Industrial & Engineering Chemistry Research*, (34), pp.1641–1651.

Nelson, J. C., Vail, N. K., Barlow, J. W. 1993. Laser sintering model for composite materials. *Proceedings of Solid Freeform Fabrication Symposium*, 1993, Austin, Texas, pp.360-369.

Nezhad, A. S., Vatani, M., Barazandeh, F., Rahimi, A. 2010. Build time estimator for determining optimal part orientation. *Proceedings of the Institution of Mechanical Engineers, Part B: Journal of Engineering Manufacture, v. 224*, pp.1905–1913.

Nickel, A., Barnett, D., Link, G., Prinz, F. 1999. Residual stresses in layered manufacturing, *Solid Freeform Fabrication Symposium*, 1999, Austin, Texas.

Panda, S. K., Padhee, S., Sood, A. K., Mahapatra, S. S. 2009. Optimization of fused deposition modelling (FDM) process parameters using bacterial foraging technique. *Intelligent Information Management*, (1), pp.89-97.

Pandey, P. M., Reddy, N. V., Dhande, S. G. 2003. Real time adaptive slicing for fused deposition modelling. *International Journal of Machine Tools & Manufacture*, 43, pp.61–71.

Patri, K., Venuvinod – Weiyin, Ma. 2004. *Rapid Prototyping - Laser-based and Other Technologies*. Kluwer Academic Publisher, ISBN: 1-4020-7577-4.

Pennington, R. C., Hoekstra, N. L., Newcomer, J. L. 2005. Significant factors in the dimensional accuracy of fused deposition modelling. *Proceedings of the Institution of Mechanical Engineers, Part E: Journal of Process Mechanical Engineering, Vol. 219*, pp. 89-92.

Pham, D. T., Dimov, S. S., Lacan, F. 1999. Selective laser sintering: Application and technological capabilities. *Proceedings of the Institution of Mechanical Engineers, Part B: Journal of Engineering Manufacture, Vol. 213*, pp.435-449.

Pham, D. T., Dimov, S. S., Lacan, F. 2000. The RapidTool process: technical capabilities and applications. *Proceedings of the Institution of Mechanical Engineers, Part B: Journal of Engineering Manufacture, Vol. 214*, pp.107-116.

Pham, D. T., Dotchev, K. D., Yusoff, W. A. Y. 2008. Deterioration of polyamide powder properties in the laser sintering process. *Proceedings of the Institution of Mechanical Engineers, Part C: Journal of Mechanical Engineering Science, Vol. 222*, pp. 2163-2176.

Raghunath, N., Pandey, P. M. 2007. Improving accuracy through shrinkage modelling by using Taguchi method in selective laser sintering. *International Journal of Machine Tools & Manufacture*, 47, pp.985–995.

Sabourin, E., Houser, S. A., Bøhn, J. H. 1997. Accurate exterior, fast interior layered manufacturing. *Rapid Prototyping Journal*, 3(2), pp. 44-52.

Salmoria, G. V., Leite, J. L., Ahrens, C. H., Lago, A., Pires, A. T. N. 2007. Rapid manufacturing of PA/HDPE blend specimens by selective laser sintering: Microstructural characterization. *Polymer Testing*, (26), pp.361–368.

Schultz, J. P. 2003. *Modelling Heat Transfer and Densification during Laser Sintering of Viscoelastic Polymers.* PhD Thesis. Virginia Polytechnic Institute and State University.

Senthilkumaran, K., Pandey, P. M., Pulak, M., Rao, P. V. M. 2009. New model for shrinkage compensation in selective laser sintering. *Virtual and Physical Prototyping*, 4 (2), pp.49–62.

Senthilkumaran, K., Pandey, P. M., Rao, P. V. M. 2009. Influence of building strategies on the accuracy of parts in selective laser sintering. *Materials and Design*, 30, pp.2946–2954.

Sercombe, T. B., Hopkinson, N. 2006. Process shrinkage and accuracy during indirect laser sintering of aluminium. *Advanced Engineering Materials*, 8 (4), pp.260-264.

Shakeri, M., Habibi, M., Shahmohammadi, H. 2007. A prototype SLA apparatus with a new algorithm for CAD model slicing. *Proceedings of 2nd Teheran International Congress on Manufacturing Engineering (TICME2007)*.

Shen, J., Steinberger, J., Göpfert, J., Gerner, R., Daiber, F., Manetsberger, K., Ferstl, S. 2000. Inhomogeneous shrinkage of polymer materials in selective laser sintering. *Proceedings of Solid Freedom Fabrication Symposium*, 2000, Austin, Texas, pp.298-305.

Shi, Y., Chen, J., Wang, Y., Li, Z., Huang, S. 2007. Study of the selective laser sintering of polycarbonate and postprocess for parts reinforcement. *Proceedings of the Institution of Mechanical Engineers, Part L: Journal of Materials: Design and Applications, Vol. 221,* pp.37-42.

Singhal, S. K., Prashant, K. J., Pandey, P. M. 2008. Adaptive slicing for SLS prototyping. *Computer-Aided Design & Applications*, 5 (1-4), pp.412–423.

Smith, W. F., Hashemi, J. 2009. *Foundations of Materials Science and Engineering.* New York: McGraw-Hill Higher Education, ISBN-10: 0073529249.

Strano, G., Hao, L., Everson, R. M., Evans, K. E. 2012. Surface roughness analysis in selective laser melting. *Proceedings of the 5th International Conference on*

Advanced Research and Rapid Prototyping, 28 September – 1 October, 2011, Liera, Portugal, pp.561-565.

Sun, C., Fang, N., Wu, D. M., Zhang, X. 2005. Projection micro-stereolithography using digital micro-mirror dynamic mask. *Sensors and Actuators*, A 121, pp.113-120.

Tang, Y., Loh, H. T., Fuh, J. Y. H., Wong, Y. S., Lu, L., Ning, Y., Wang, X. 2004. Accuracy analysis and improvement for direct laser sintering, *Innovation in Manufacturing Systems and Technology (IMST)* 01, Available at: http://hdl.handle.net/1721.1/3898 [Accessed 21 December 2011].

Tobolsky, A. V. 1967. *Properties and Structure of Polymers*, New York: John Wiley & Son.

Tontowi, A. E., Childs, T. H. C. 2001. Density prediction of crystalline polymer sintered parts at various powder bed temperatures. *Rapid Prototyping Journal*, 7 (3), pp.180-184.

Townsend, P. H., Barnett, D. M., Brunner, T. A. 1987. Elastic relationships in layered composite media with approximation for the case of thin films on a thick substrate. *Journal of Applied Physics*, 62 (11), pp.4438-4444.

Tyberg, J. T. 1998. *Local Adaptive Slicing for Layered Manufacturing*. Master of Science Thesis, Virginia Polytechnic Institute and State University, Blacksburg.

Tyberg, J., Bøhn, J. H. 1998. Local adaptive slicing. *Rapid Prototyping Journal*, 4 (3), pp.118–127.

Ulbrich, C. B. L., Zavaglia, C. A. C., Neto, P. I., Oliveira, M. F., Silva J. V. L. 2012. Comparison of five rapid prototype techniques (SLS/FDM/DLP/3DP/Polyjet). *Proceedings of the 5th International Conference on Advanced Research and Rapid Pprototyping*, 28 September – 1 October, 2011, Liera, Portugal, pp.573-580.

Upcraft, S., Fletcher, R. 2003. The rapid prototyping technologies (Tutorial). *Assembly Automation*, 23 (4), pp.318–330.

Vail, N. K., Barlow, J. W., Marcus, H. L. 1993. Silicon carbide preforms for metal infiltration by selective laser sintering of polymer encapsulated powders. *Solid Freeform Fabrication Symposium*, 1993, Austin, Texas, pp.204-214.

Vella, P., Brousseau, E., Minev, R., Dimov, S. 2010. A methodology for maturity assessment of micro and nano manufacturing process chains, *Proceedings ICOM*, 2010 Wisconsin, USA, pp. 327-334.

Wang, T. M., Jun-Tong Xi, Ye Jin. 2007. A model research for prototype warp deformation in the FDM process. *International Journal of Advanced Manufacturing Technologies*, (33), pp.1087–1096.

Wang, X., 1999. Calibration of shrinkage and beam offset in SLS process. *Rapid Prototyping Journal*, 5 (3), pp.129-133.

Wang, Y., Shi, Y., Huang, S. 2005. Selective laser sintering of polyamide–rectorite Composite. *Proceedings of the Institution of Mechanical Engineers, Part L: Journal of Materials: Design and Applications, Vol. 219*, pp.11–15.

Weiyin, M., Peiren, H. 1999. An adaptive slicing and selective hatching strategy for layered manufacturing. *Journal of Materials Processing Technology*, (89-90), pp.191–197.

Wikipedia. Available at: http://en.wikipedia.org/wiki/Deformation_%28mechanics%29 [Accessed December 2011].

Williams, J., Miller, D., Deckard, C. 1996. Selective laser sintering part strength as a function of andrew number, scan rate and spot size. *Freeform Fabrication Symposium*, 1996, Austin, Texas, pp.549-558.

Yang, H. J., Hwang, P. J., Lee, S. H. 2002. A study on shrinkage compensation of the SLS process by using the Taguchi method. *Internationl Journal of Machine Tool & Manufacture*, (42), pp.1203-1212.

Yang, H., Ratchev, S., Turitto, M., Segal, J. 2009. Rapid manufacturing of non-assembly complex micro-devices by microstereolithography. *Tsinghua Science and Technology*, v.14, Supplement 1, pp.164-167.

Zhang, S. J., Raja, V. H., Fernandes, K. J., Ryall, C., Wimpenny, D. 2003. Rapid prototyping models and their quality evaluation using reverse engineering. *Proceedings of the Institution of Mechanical Engineers, Part C: Journal of Mechanical Engineering Science, Vol. 217*, pp.81-96.

Zhang, X., Jiang, X. N., Sun, C., 1999. Micro-stereolithography of polymeric and ceramic microstructures. *Sensors and Actuators*, 77 (2), pp.149-156.

Zhu, H. H., Lu, L., Fuh, J. Y. H. 2006. Study on shrinkage behaviour of direct laser sintering metallic powder. *Proceedings of the Institution of Mechanical Engineers, Part B: Journal of Engineering Manufacture, Vol. 220*, pp.183–190.